THE
PHYSICAL REVIEW

A journal of experimental and theoretical physics established by E. L. Nichols in 1893

VOL. 61, NOS. 1 AND 2 JANUARY 1 AND 15, 1942 SECOND SERIES

On the Separation of Nuclear Isomers

EUGENE P. COOPER*
Department of Physics, University of California, Berkeley, California
(Received November 10, 1941)

The fact that nuclear isomers can be separated chemically cannot be explained on the basis of the recoils involved. However, with K capture, or with internal conversion accompanying the isomeric transition, there is a mechanism for the separation. The positive charge built up by the Auger effect during the electronic readjustment is enough to cause molecular dissociation. To illustrate this, the probabilities for Auger effect and for x-rays for all shells of the Br atom were calculated and compared, and they show that the excess charge in this case becomes as high as $4.7e$. The effect on homopolar binding is examined by using a hydrogen molecule model. It is found that excess charges considerably less than $4.7e$ should cause dissociation in the Br case.

1. INTRODUCTION

FOR the study of artificial radioactivities it is a fortunate experimental fact that two nuclear isomers can be separated chemically.[1] However, since no transmutation of elements is involved in the isomeric transition, the mechanism of the separation is not at once clear. Evidently molecular dissociation must accompany the transition; that is, the emission of a gamma-ray must in some way rupture chemical bonds. It has been suggested of course that the recoil given the nucleus by the gamma-ray supplies such a mechanism. The momentum imparted to the nucleus is $h\nu/c$, where $h\nu$ is the energy of the gamma-ray, c the velocity of light. Thus the kinetic energy of recoil is $2.5\times10^5(m/M)(h\nu/mc^2)^2$, where M is the mass of the nucleus, m the mass of the electron. For $M\sim100$ and rather high energy gamma-rays, i.e., $h\nu\sim mc^2$, this gives a few volts (the order of magnitude of chemical binding energies) for the recoil. However, it is just characteristic of nuclear isomerism that the gamma-rays usually have low energies ~100 kev. A typical and thoroughly investigated activity is that of Br^{80},[1-4] whose daughter isomer emits a beta-ray with half-life of 18 min. The bromine is usually in soluble organic form, and the 18-min. activity may be separated from the 4.5 hr. with simple reagents, for example with water. The energy of the gamma-ray in the isomeric transition is less than 50 kev ($\sim mc^2/10$) and m/M $\sim7\times10^{-6}$. The nuclear recoil, ~0.02 ev, is very small compared to chemical binding and cannot be responsible for an appreciable separation.

The amount of chemical separation is usually large. For Br it is at least 85 percent. Now, since the long lifetimes of gamma-rays in nuclear isomerism are, in many cases, probably due to

* Now at the University of North Carolina, Chapel Hill, North Carolina.

[1] E. Segrè, R. S. Halford, and G. T. Seaborg, Phys. Rev. **55**, 322 (1939).

[2] F. Fairbrother, Nature **145**, 307 (1940).

[3] D. DeVault and W. F. Libby, Phys. Rev. **58**, 688 (1940).

[4] J. E. Willard, J. Am. Chem. Soc. **62**, 256 (1940).

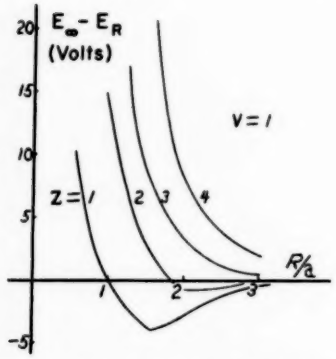

FIG. 1. Franck-Condon curves for a hypothetical molecule.

angular momentum changes of several units, most of the gamma-rays are then internally converted, which suggests that the internal conversion is connected with the separation as has, in fact, been experimentally established, particularly in experiments in which Zn and Te isomers were subjected to similar chemical conditions. No separation was attained for the Zn isomers where the gamma-rays are unconverted, but with the large internal conversion of the Te gamma-rays was associated a large separation.[5,6] In any case the conversion is accompanied by another and, for low energy gamma-rays, more energetic recoil. The electron on leaving, say, the K shell gives the atom the momentum $(2mh\nu)^{\frac{1}{2}}$ or energy $(h\nu)m/M$. This differs from the direct recoil by a factor $mc^2/2h\nu$. For Br this factor is ~ 5 and the recoil is thus ~ 0.01 ev, still small compared to chemical bonds. This example illustrates the necessity of abandoning the idea of recoil as a general primary explanation of the separation. (In Te^{127} the conversion recoil is ~ 0.1 ev. There are, however, cases in which it is of the order of chemical binding, *viz.*, Sc^{44} and In^{113}.)

We have found that internal conversion, independent of the recoil it allows, is responsible for a very efficient mechanism leading to dissociation. What is of importance here is the hole, left in an inner shell, that induces serious subsequent electronic and molecular readjustments. Even for low energy conversions the time for complete ejection of the electron is short compared with that for any electronic transitions to the hole. Thus the atom becomes a positive ion of charge $+e$ and its chemical properties are temporarily altered. The outer electrons, responsible for molecular binding, move in a new field to which the wave functions are readjusted in times short compared to molecular periods. Thus the unchanged configuration of atoms in the molecule no longer necessarily represents minimum potential energy and, since the atoms will move along their new potential curves, dissociation may occur as in other examples of the Franck-Condon principle.

Now, since it is very unlikely that the atom return to its ground state solely by the emission of x-rays, the excess charge does not remain $+e$ but increases due to the Auger effect. With each Auger process the increase is $+e$ and another Franck-Condon process occurs. The molecular states will tend to become more and more repulsive since the excess charge will tend to distribute equally over the molecule. If, as a result, the molecule becomes unstable by several volts there will be ample time for dissociation before the excited atom returns to the ground state by electron capture.

It is clear that, for a quantitative discussion, two questions are involved: (1) How much charge builds up by the competition of Auger effect with x-ray emission, and (2) how do the Franck-Condon curves shift with the charge. We have investigated (1) for the special case of the bromine atom with a hole initially in the K shell by calculating, from the individual x-ray and Auger transitions, the probabilities of the many possible series of states, and from these made estimates of the average charges and average times for their accumulation as shown in Table I. For (2) actual molecules like C_2H_5Br

TABLE I. Average charges and times for their accumulation.

Condition of Br atom	Average excess charge	Average time between conditions
Hole in K shell	$+1.0e$	$480\ h/mc^2\alpha^2$
K shell filled	$+1.5$	800
L shell filled	$+2.4$	6500
M shell filled	$+4.7$	

[5] J. W. Kennedy, G. T. Seaborg, and E. Segrè, Phys. Rev. **56**, 1095 (1939).
[6] G. T. Seaborg, G. Friedlaender, and J. W. Kennedy, J. Am. Chem. Soc. **62**, 1309 (1940).

were not considered directly, because of mathematical complexities, but, since homopolar bonds are usually involved, the hydrogen molecule was, for simplicity, taken as a model, and an Auger process idealized by increasing the charge on one proton and leaving the molecule unaltered by any other causes. Energy calculations (Heitler-London) even with this model are rough, but reasonable estimates show that, even for molecules in question, excess charges less than are actually built up by Auger effect must cause dissociation. In Fig. 1 are shown Franck-Condon curves for this hypothetical molecule for various charges Z on one proton, the other having $Z=1$. In spite of the rough nature of the calculations we believe they indicate that the mechanism we have considered is responsible for the chemical separation. (See Part 3 for the meaning of $\nu=1$.) However, it should be remarked that there is also an even more potent mechanism which would operate, were the molecule to remain undissociated in spite of the excess positive charge. This is the actual loss by Auger effect of some of the bonding electrons themselves. An examination of Table I shows that such loss will most certainly occur, but not until times of approximately $10^3-10^4 h/mc^2\alpha^2$ after ample positive charge has been built up for dissociation by the Franck-Condon principle, and in such times two atoms in a molecule unstable by a few volts will separate by several atomic radii.

Molecular dissociation may also accompany radioactive transitions involving K capture. (Of course it would usually occur anyway because of the atomic transmutation, but not until the completion of processes of the type we are considering, i.e., the outer (valence) shell would not be characteristic of the new element until the completion of electronic readjustments in the inner shells, the probability for these readjustments being greater than for those in the valence shell.) Here the bonding wave functions are little perturbed by the transition since it corresponds merely to the transfer of a charge in the atomic interior. But the charge built up by the subsequent Auger processes, although always one unit less than it would be for the corresponding internal conversion, should again be sufficient to cause dissociation. Recently individual atoms in

TABLE II. Probable transitions (units of $mc^2\alpha^2/h$).

Transition to K shell		to L shell		to M shell	
$2s-1s$	2.8×10^{-3}	$3s-2s$	4×10^{-3}	$4s-3s$	5×10^{-4}
$2p-\infty$		$3p-\infty$		$4s-\infty$	
$2p-1s$	6.5×10^{-3}	$3p-2s$	7×10^{-3}	$4p-3s$	1.8×10^{-3}
$2p-\infty$		$3p-\infty$		$4p-\infty$	
$2p-1s$	2.0×10^{-3}	$3s-2p$	3.5×10^{-3}	$4p-3d$	6×10^{-4}
$3p-\infty$		$3p-\infty$		$4p-\infty$	
$3p-1s$	3.9×10^{-3}	$3p-2p$	7.8×10^{-3}		
$3p-\infty$		$3p-\infty$			
$3p-1s$	1.8×10^{-3}	$3p-2p$	4.0×10^{-3}	to N shell (for Te)	
$3d-\infty$		$3d-\infty$			
		$3d-2p$	4.2×10^{-3}	$5p-4s$	2×10^{-4}
		$3d-\infty$		$5p-\infty$	

K capture have been observed.[7] Cd^{107} which decays to Ag^{107} was electroplated on a filament and Ag atoms were collected in a Geiger counter. It was hoped that such an experiment would be direct evidence for neutrino recoil. However the calculations made in this paper show an effect so definite that we believe similar calculations for the perturbations on the periodic potential in a metal surface by the K capture would show them to be enough to overcome the work function and eject individual atoms. Further theoretical work is needed here.

An earlier attempt to show direct neutrino recoil was made by observing Cl^{38} beta-rays in a cloud chamber.[8] Small clusters of ions were always found at the beginning of the tracks. These were attributed to the ionization produced by the nuclear recoil from beta-ray and neutrino. However, quite aside from the fact that such drop-counting technique is very difficult and subject to large errors, the recoil velocities involved are so low that no appreciable ionization is to be expected from this source,[9] and the

[7] B. T. Wright, Ph.D. Thesis, University of California (1941).

[8] H. R. Crane and J. Halpern, Phys. Rev. **56**, 232 (1939).

[9] It is true that the recoil Cl nucleus may have ~5 Mev kinetic energy, but this corresponds to a velocity which is only a small fraction of orbital electronic velocities. Most of the energy loss to a gas atom will contribute to the kinetic energy of the atom as a whole rather than to its individual electrons. Hence the efficiency of ionization

TABLE III. Transition probabilities for Br.

Initial state	Final state 1s	2s	3s
2p	3.7×10^{-2}		
3p	1.1×10^{-2}	1.2×10^{-3}	
4p	0.7×10^{-2}	0.5×10^{-3}	5.7×10^{-5}
		2p	3p
3s		3.6×10^{-4}	
4s		1.4×10^{-4}	3.4×10^{-5}
3d		8.5×10^{-4}	

ionization actually observed may here again be largely attributed to Auger processes dissipating electronic excitation energy.

2. THE AUGER EFFECT

In order to show how Auger effect competes with x-ray emission in building up positive charge in the radioactive atom it is necessary to compare the individual transition probabilities for both processes. We have made no attempt to do this generally for all Z since for low Z the Auger effect is more important for individual transitions whereas for high Z more Auger transitions corresponding to a given x-ray are allowed, so that we should expect the competition not to change markedly with Z.

We have calculated individual Auger probabilities after the methods of Burhop[10] and Pincherle,[11] using screened hydrogen-like wave functions (Slater's constants) for the bound states but, instead of exact Coulomb functions, a plane wave for the ejected electron. The transition probabilities agree, at least in order of magnitude, with those calculated with the Coulomb functions, which are, in any case, rough because of the absence of a true Coulomb field and the approximate nature of the bound wave functions. The expression for the transition probability reduces to:

$$\sum_{\nu=0}^{\infty} a_\nu \left| 2\pi \int_0^\infty \int_0^\infty R_0(r_1) R_f(r_1) R_0(r_2) \frac{J_{\frac{1}{2}}(\kappa r_2)}{(r_2)^{\frac{1}{2}}} r_1^2 r_2^2 \times \left(\frac{r_<}{r_>}\right)^\nu dr_1 dr_2 \right|^2 \frac{mc^2\alpha^2}{h},$$

where $R_0(r_1)$, $R_f(r_1)$ and $R_0(r_2)$ are the radial hydrogen-like functions for the initial and final state of electron 1 and the initial state of electron 2; κ is the momentum of the ejected electron in atomic units. The a_ν's are numbers of order unity only a very few of which are nonvanishing. The r_1 integration is elementary and the final integration was done graphically. The most probable transitions are shown in Table II.

The probabilities for x-ray emission were found from the formula for electric dipole radiation. Experimental frequencies were used. The matrix element of the dipole moment, which takes the form $\int r^3 R_0(r) R_f(r) dr$ was again integrated graphically by using screened hydrogen-like functions for initial and final radial wave functions, $R_0(r)$ and $R_f(r)$. The transition probabilities for Br are shown in Table III.

A comparison of Tables II and III shows that in the outer shells Auger effect will occur exclusively. In Table IV the condition of the Br atom after the K shell has been filled is indicated. (Here we have used not only our own values for the more probable transitions as shown in Table II but also the values for the less probable transitions as given by Burhop and Pincherle.) By tracing the many possible series of events and finding the corresponding distributions after the L and M shells have been filled the averages in Table I were obtained.

TABLE IV.

Holes	2p	3p	4p	2s and 2s or 2p	2p and 2p or 3d or 4s	2p and 3p or 3s	3p and 3p or 3d or 4s
Prob.	0.33	0.10	0.05	0.10	0.23	0.09	0.10

3. THE HYDROGEN MOLECULE MODEL

To draw Franck-Condon curves one must calculate the total energy of the molecule at atomic separation R (diatomic molecule) and subtract off the energy at infinite separation. We have used the method of Heitler and London[12]

TABLE V.

Z	$E\left(\substack{\lambda=0\\ \nu=1}\right)$	λ	$E(\nu=1)$	$E\left(\nu=1+\frac{Z-1}{4}\right)$
1	−3.3 ev	0.16	−4.0 ev	−4.0 ev
2	+6.7	0.75	+3.2	+3.8
3	+16.6	1.2	+11.5	+13.7
4	+28.8	1.9	+19.4	+25.0

will not compare with that for high speed ions and the assumption, made by Crane and Halpern, of one ion pair for 30 volts kinetic energy is untenable, cf. N. Bohr, Phys. Rev. 59, 270 (1941).

[10] E. H. S. Burhop, Proc. Roy. Soc. 148, 272 (1935).

[11] L. Pincherle, Nouvo Cimento 12, 81 (1935).

as modified by Slater and Pauling.[13] Our hypothetical molecule has two protons with charges $+Ze$ and $+e$. The distances of electron 1 from $+Ze$ and $+e$ are r_1 and R_1, respectively. The corresponding distances of electron 2 are R_2 and r_2. We define:

$$\Psi_1=(\nu^3/\pi a^3)\exp(-\nu r_1/a),$$
$$\Psi_2=(\nu^3/\pi a^3)\exp(-\nu R_2/a),$$
$$\varphi_1=(1/\pi a^3)\exp(-R_1/a),$$
$$\varphi_2=(1/\pi a^3)\exp(-r_2/a),$$

where $a=h^2/4\pi^2me^2$. For $z=1$ a good zero-order wave function is:[12,13]

$$\Psi(R)=\Psi_1\varphi_2+\Psi_2\varphi_1+\lambda(\Psi_1\Psi_2+\varphi_1\varphi_2) \quad \text{for } \nu=1,$$

where λ is a constant depending on R and so chosen as to give minimum energy. We are interested in changes of Z of several units, but in atoms like Br the wave functions will contract with increasing Z far less than for the case of the hydrogen atom where $\Psi_1(\nu=1)$ is a correct atomic wave function. Therefore, to make our model correspond more closely to a molecule in question like, say, HBr where we are interested in different charges on the Br atom, we use atomic functions of the form Ψ_1 etc. but with $\nu-1$ only a fraction of $Z-1$. We have used for the fraction $\frac{1}{4}$ and zero. However, in the Hamiltonian we do not modify Z:

$$H=(-h^2/8\pi^2m)(\Delta_1+\Delta_2)$$
$$+e^2(Z/R+1/r_{12}-Z/r_1-Z/R_2-1/R_1-1/r_2).$$

Also in the zero-order wave function we drop the term $\lambda\varphi_1\varphi_2$ since it corresponds to the configuration in which both electrons are on the proton with lesser charge (except for $Z=1$ where the term is included in the standard calculations[13]). With these modifications we have calculated the energy by: $\Psi(R)\cdot H\Psi(R)$ and subtracted off the energy of an atom in the state $\Psi_1(\nu)$ in the field of the charge Ze plus the energy of a normal hydrogen atom. All the integrals were evaluated in closed form except for

$$\int \frac{1}{r_{12}}\Psi_1\varphi_1\Psi_2\varphi_2 dV_1 dV_2$$

for $\nu-1$ not zero, but for this integral a good approximation was found. Each point on the curve (Fig. 1) is calculated for the minimum in λ. Table V shows values of E and λ for $R/a=\frac{3}{2}$ (the equilibrium separation of normal H_2) and also E for $\lambda=0$ thus illustrating the effect of ionic terms in reducing the energy. Our hypothetical molecule, even for the case $\nu=1+(Z-1)/4$, is roughly the size of a normal hydrogen molecule. For larger molecules the displacement of the curves (Fig. 1) from the normal curve ($Z=\nu=1$) will be reduced by a factor roughly the ratio of the diameter of the molecule to that of the H_2 molecule. Even then the shift is still considerable for charges of at least two so that with the charges which are built up by Auger effect dissociation should certainly occur. Also, for conversion in the L shell, a high enough charge, ~ 3, will be built up.

ACKNOWLEDGMENTS

The author wishes to express his sincere gratitude to Professor J. R. Oppenheimer who suggested this problem and whose continued helpful guidance was invaluable. He also wishes to thank Professor Willard F. Libby for interesting discussions on the experimental side, and Dr. Emilio Segrè for suggestions in the preparation of the manuscript. He is grateful to Miss Marjorie Cameron for assistance with the integrations.

[12] W. Heitler and F. London, Zeits. f. Physik **44**, 455 (1927).
[13] J. H. VanVleck and A. Sherman, Rev. Mod. Phys. **7**, 184 (1935).

On the Electrical and Anomalous Scattering of Mesotrons

RALPH P. SHUTT
The Bartol Research Foundation of the Franklin Institute, Swarthmore, Pennsylvania
(Received November 3, 1941)

Photographs obtained without a magnetic field in a large counter-controlled cloud chamber containing lead plates of two different thicknesses have been analyzed in regard to the scattering of the mesotrons in lead. The theory of scattering developed by E. J. Williams has been used. The mathematical form of this theory makes it possible to eliminate the energy distribution of the mesotrons in comparing the observed scattering intensity in two lead thicknesses. The scattering in a 5-cm lead plate into angles greater than 4°, when compared to that in a 1-cm lead plate, is more than would have been expected on the basis of Williams' theory. The average cross section calculated for this anomalous large angle scattering agrees with the results obtained by Code but it is somewhat larger than that previously reported by Wilson. It is also noted that this cross section is in agreement with the interaction between mesotrons and nuclei computed by Marshak and Weisskopf when a spin of ½ for the mesotrons and an energy distribution such as that computed by Hartree are assumed. Although these experiments are perhaps not yet able to distinguish between the scatterings to be expected from a mesotron spin of ½ and that from a spin of 0, a spin of 1 seems to be definitely excluded since for this value of the spin the theory indicates a cross section of about 1000 times more than that found. It is noted that a possibility for an explanation of the observed anomaly still might be found in electromagnetic effects such as those leading to burst production by mesotrons or in attributing the anomaly to nuclear scattering of the proton component instead of mesotrons.

INTRODUCTION

THE scattering of mesotrons by matter is of interest because of its dependence on the forces between mesotrons and nuclear particles. Williams[1] has developed a theory for the scattering of cosmic-ray particles by the atomic electric fields and some experimental studies of the scattering of mesotrons in various thicknesses of different materials have been made by Vargus,[2] by Wilson,[3] and by Code.[4] Although the results of these investigations are still meager, all have found angular distributions in approximate agreement with Williams' theory in the case of mesotrons scattered up to ~5° in thicknesses to an equivalent of ~6 cm of lead; but a few improbable cases in which high energy particles are scattered into angles greater than ~5° have also been found, and these indicate the possible existence of another type of scattering force.

Williams has shown that the electrical scattering in lead is always multiple if the scattering plate is more than 1 cm thick and if the velocity of the scattered particle is not very much less than that of light, a condition which may be considered fulfilled for mesotron energies as low as 20 Mev.

[1] E. J. Williams, Proc. Roy. Soc. **A169**, 531 (1939).
[2] J. A. Vargus, Jr., Phys. Rev. **56**, 480 (1939).
[3] J. G. Wilson, Proc. Roy. Soc. **A174**, 73 (1940).
[4] F. L. Code, Phys. Rev. **59**, 229 (1941).

Suppose $P(\alpha, t, E_k)d\alpha$ is the probability that a particle of kinetic energy E_k is scattered into an angular range $d\alpha$ at the angle α while traversing a plate of thickness t. Then Williams shows that

$$P(\alpha, t, E_k)d\alpha=\frac{2}{\pi\bar{\alpha}}\exp\left(-\frac{\alpha^2}{\pi\bar{\alpha}^2}\right)d\alpha \qquad (1)$$

with

$$\bar{\alpha}=(19.5-3.1\log_{10}Z)^{\frac{1}{2}}\frac{600Ze(Nt)^{\frac{1}{2}}}{\beta^2E}, \qquad (2a)$$

where $\bar{\alpha}$ is the arithmetic mean of the angles of the multiple scatterings in a material of N atoms of atomic number Z per cm³, when the particles have charge e, mass m, velocity βc, kinetic energy E_k and total energy $E=E_k+mc^2$. The approximations involved are good up to scattering angles of about 25°. The expression (2a) takes into account the relativistic effect, the Coulomb shielding of the nucleus by the atomic electrons, and the finite size of the nucleus, the latter of which prevents single electrical scattering into large angles. For lead (2a) reduces to

$$\bar{\alpha}=0.90\times10^9\times t^{\frac{1}{2}}/\beta^2E, \qquad (2b)$$

where t is measured in cm and E in electron volts. Williams has shown that the effect of a mesotron spin of ½ on the electrical scattering would be completely negligible for the energy and angular ranges with which we are here concerned. Al-

though this theory does not consider the possibility of spin 1 for the mesotron, the good agreement between experiment and theory shows that whatever the spin of the mesotron its contribution to the small angle electrical scattering must be very small.

For very close collisions we have to assume that forces other than those of the electrical type prevail, and here the effect of the spin may be all important. Theories for the scattering of mesotrons by the non-electric short range nuclear forces have been developed by several authors. All of those theories based upon a mesotron spin of 1 predict a nuclear scattering cross section per neutron or proton between 10^{-25} and 10^{-26} cm^2, values 100–1000 times too large to agree with the experiments, and of such a magnitude that in a lead plate of thickness between 0.3 and 3 cm the nuclear scattering of a beam of mesotrons of spin 1 would be complete. As Williams and others have shown, because of their intensity and short range, the nuclear forces must scatter into large angles considerably wider than those given by the electrical theory, and this type of scattering would, therefore, be easily recognized. For mesotrons of spin 0 Bhabha[5] has shown that the non-electric scattering cross section is almost of the right order of magnitude to agree with the experiments although it is perhaps somewhat too small, and he predicts a decreasing cross section for higher energies. Assuming a spin $\frac{1}{2}$ for the mesotron, Marshak and Weisskopf[6] have given a theory which agrees with the results of scattering experiments, but quite recently Weinberg[7] has given a new theory for the nuclear scattering of mesotrons of spin $\frac{1}{2}$ which yields a cross section about 100 times too large. Weinberg's treatment, however, has the satisfactory feature, in common with the theory of Bhabha, but in contrast with that of Marshak and Weisskopf, of predicting a decreasing cross section after reaching a maximum as the energy increases, a feature in harmony with the known hardening of cosmic rays as the depth increases.

TABLE I. Experimental results.

Projected angle α	Number of scattered particles observed: Upper plate $t=1$ cm	Center plate $t=5$ cm	Lower plate $t=1$ cm	Upper and lower plates $t=1$ cm
0°– 2°	5380	3783	3057	8437
2°– 4°	138	462	144	282
4°– 6°	77	188	47	124
6°– 8°	48	119	18	66
8°–10°	7	53	3	10
10°–12°	15	34	6	21
12°–14°	8	27	2	10
14°–16°	3	13	2	5
16°–18°	7	10	2	9
18°–20°	3	6	0	3
20°–22°	3	8	0	3
22°–24°	2	5	1	3
24°–26°	0	3	4	4
26°–28°	3	5	0	3
28°–30°	0	1	0	0
>30°	9	4	0	9
0°–90°	5703	4721	3286	8989
4°–90°	185	476	85	270

[5] H. J. Bhabha, Phys. Rev. **59**, 100 (1941).

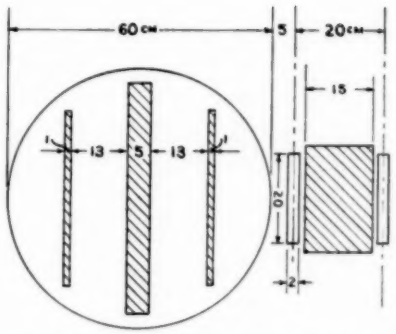

FIG. 1. Cloud chamber containing 3 lead plates, 1, 5, and 1 cm thick, respectively. Control by two counters above the chamber with 15 cm of interposed lead.

EXPERIMENTS

In view of the conflicting theories it seemed important to make more extensive studies of the scattering of mesotrons in matter. The large Wilson cloud chamber used in these experiments was 60 cm in diameter, 8 cm illuminated depth, and it contained three lead plates having thicknesses of 1 cm, 5 cm and 1 cm, respectively, spaced at distances of 13 cm from each other. Expansions were controlled by two counters in coincidence, both of which were above the chamber with 15 cm of lead interposed between them, as shown in Fig. 1. The chamber was located in a basement room with concrete equivalent of about 10 cm of lead above it. A short description of this chamber has already been given[8] and more details will be published elsewhere. The chamber was filled with 1.3 atmos. of

[6] R. E. Marshak and V. K. Weisskopf, Phys. Rev. **59**, 130 (1941).
[7] J. W. Weinberg, Phys. Rev. **59**, 776 (1941).
[8] T. H. Johnson, J. G. Barry, and R. P. Shutt, Phys. Rev. **59**, 470 (1941).

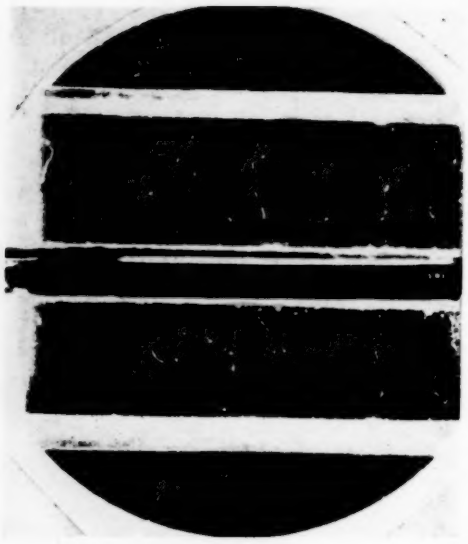

FIG. 2. Track of a mesotron scattered in lead. The difference of the density in the two upper compartments from that in the two lower ones is due to technical circumstances and not to a difference in ionization.

argon, saturated with a mixture of water and *n*-propyl alcohol vapors; the resulting volume expansion ratio was 1.07. Although magnetic field coils have recently been added, these were not used in the present experiments.

The present report covers the analysis of 8345 pictures, 7537 of which were stereoscopic. In all 5703 traversals through the upper 1-cm lead plate, 4721 through the 5-cm lead plate and 3286 through the lower 1-cm lead plate were observed. For each traversal the projection on the central plane of the chamber of the scattering angle of the particles traversing the lead plates was measured. In order to exclude from the analysis the electrons and penetrating rays incident obliquely, only rays which could have passed through the counters and the interposed lead were taken into consideration. Rays which appeared heavily ionizing after emerging from the lead were also excluded. The number of particles scattered by the lead plates into various angles α is given in Table I. The angles were measured with an accuracy of $\pm 0.5°$. A typical example of a track of a scattered mesotron is shown in Fig. 2.

DEDUCTION OF AVERAGE NUCLEAR SCATTERING CROSS SECTION

The observed scattering, recorded in Table I, is assumed to have resulted from two effects, the electrical scattering and the scattering due to nuclear forces. If we knew the energy distribution of the incident mesotrons, it would be possible to calculate from Williams' theory the scattering due to electrical forces and then to subtract this from the total to find the nuclear scattering, but the energy distribution in our chamber is affected by the distribution of absorbing material above the chamber and is not precisely known. It is therefore necessary to resort to an indirect method which makes use of the scattering observed in the two thicknesses of lead.

The cross section for the nuclear scattering, as mentioned above, must be small compared with that for the electrical scattering. Consequently the nuclear scattering in our lead plates will be single, and the number of particles scattered by the nuclear forces into a given angular range must be proportional to the first power of the thickness of the material. If we assume that the large angle scattering is nuclear, our 5-cm plate should show five times as much large angle scattering as that occurring in the 1-cm plate. On the other hand, the dependence of the multiple scattering on the thickness is different from that of the single scattering because the former obeys a law involving the thickness in a different and a comparatively complicated way. Suppose $I(\alpha, t)d\alpha$ represents the multiple scattering intensity. Its theoretical value may be represented by

$$I(\alpha, t)d\alpha = \int_{E_k=\bar{E}_{k0}}^{\infty} i(E_k)P(\alpha, t, E_k)dE_k d\alpha, \quad (3)$$

where $P(\alpha, t, E_k)d\alpha$ is the scattering probability given by (1), $i(E_k)dE_k$ is the number of rays in the energy range from E_k to E_k+dE_k, and $\bar{E}_{k0}$ is a certain average lower limit of the kinetic energy E_k determined by the experimental conditions.

The special mathematical form of (1) enables us to apply a direct method for the determination of the electrically scattered intensity without bringing the energy distribution into the calculation, for if instead of calculating the distribution with respect to α we transform to a new variable $u=\alpha t^{-\frac{1}{2}}$ the distribution with respect to u will be given by

$$f(u) = I(\alpha, t)(\partial\alpha/\partial u) = I(\alpha, t)t^{\frac{1}{2}}, \quad (4)$$

where $f(u)du$ is the number of particles in the

range u to $u+du$, and using (1), (2b) and (3) we find

$$f(u)=\frac{2}{\sqrt{\pi}}\int_{\bar{E}_{k0}}^{\infty} i(E_k)z\exp(-z^2u^2)dE_k, \quad (5)$$

where $z=\beta^2E/k$ and $k=1.59\times10^9$ ev. The important feature of this transformation is that the distribution in u is independent of t so that if the scattering is entirely electrical the function $f(u)$ should be the same for all thicknesses of scattering material, and the product $I(\alpha, t)t^{\frac{1}{2}}$ plotted as a function of u must lie on one uniform curve independent of t. If the functions $f(u)$ obtained from the observations with different thicknesses of scattering material are not equal, the difference must be due to a disturbance by a nuclear force whose variation with distance from the center is different from and not proportional to the Coulomb force.[9] Actually $\bar{E}_{k0}$ depends upon t so that these last statements are not completely accurate, but in the range of α and E_k with which we are concerned this effect is only one of a second order correction.

Columns 1 and 2 of Table II show the experimental results for the two thicknesses of lead expressed in percent of the total number of traversals observed in each, and in Table III these values have been reduced to $f(u)$.

If the scattering were produced by Coulomb forces alone the $f(u)$ values in columns 1 and 2 of Table III would be identical except for statistical fluctuations resulting from the finite number of tracks observed. In making this comparison the sums of the $f(u)$ numbers in the range of u from 2 to 12 have been used in place of the individual values because of their greater statistical weights; but, instead of an equality, we find a value for the 5-cm thickness greater than that for the 1-cm thickness by

$$\delta=9.04-5.64=3.40. \quad (6)$$

The corresponding difference in the number of particles scattered in the 5-cm thickness over that of the particles scattered in the 1 cm of lead is

$$\Delta_1=\delta/\sqrt{t}=3.4/\sqrt{5}=(1.5\pm0.5)\text{ percent} \quad (7)$$

of the total intensity, or (15 ± 5) percent of the number of scattered rays. This represents the excess of rays scattered in the 5-cm block into angles between 4.5° and 26°, or between $u=2$ and 12, over those we should have expected to be scattered there on the basis of the theory of electrical scattering, taking into account the number actually observed to have been scattered in the 1-cm block. The standard error of Δ_1 indicated above was found by first determining the standard errors for each of the two thicknesses, considering all particles between $u=2$ and 12 and then adding these two errors geometrically. In this calculation the standard error is taken as the square root of the number of particles scattered.

In order to find a cross section for this anomalous large angle scattering we have to apply some corrections to the above result. First, our observations concern the projections into the cloud-chamber plane of the actual angles in three dimensions. These are the angles dealt with in the Williams theory; but in the case of nuclear scattering this fact must also be taken into

TABLE II. Relative intensities of the total scattering for different thicknesses of lead.

	$I(\alpha, t)$, experimental results				$I(\alpha, t)$ computed from Hartree's energy distribution at sea level	
	1		2		3	4
α	$t=1$ cm %	Stand. error ±%	$t=5$ cm %	Stand. error ±%	$t=1$ cm %	$t=5$ cm %
0°–2°	93.80	1.02	80.10	1.30	92.30	81.30
2°–4°	3.16	0.19	9.79	0.46	4.77	9.95
4°–6°	1.39	0.12	3.98	0.29	1.50	3.79
6°–8°	0.74	0.09	2.52	0.23	0.65	1.89
8°–10°	0.11	0.04	1.12	0.15	0.32	1.08
10°–12°	0.24	0.05	0.72	0.12	0.18	0.65
12°–14°	0.11	0.04	0.57	0.11	0.13	0.45
14°–16°	0.06	0.02	0.28	0.08	0.08	0.30
16°–18°	0.10	0.03	0.21	0.07	0.04	0.22
18°–20°	0.03	0.02	0.13	0.05	0.03	0.16
20°–22°	0.03	0.02	0.17	0.06	0.03	0.12
22°–24°	0.03	0.02	0.11	0.05	0.02	0.10
24°–26°	0.04	0.02	0.06	0.04	0.02	0.08
26°–28°	0.03	0.02	0.11	0.05	0.02	0.06
28°–30°	0.00	—	0.02	0.02		0.05
>30°	0.11	0.04	0.08	0.04		0.10
4°–90°	3.02	0.19	10.08	0.47	2.95	9.05

[9] The electrical single scattering, $I_{se}(\alpha, t)$, although of negligible magnitude, is proportional to t/α^3 at not too large angles, see reference 1, and $I_{se}(\alpha, t)t^{\frac{1}{2}}$ is proportional to $1/u^3$. Hence the combined multiple and single electrical scattering can also be transformed to a function of u alone

$$[I(\alpha, t)+I_{se}(\alpha, t)]t^{\frac{1}{2}}=f_1(u).$$

consideration. For this reason it is estimated that a correction of 30 percent should be added to Δ_1. Secondly, since Δ_1 is the *difference* between the nuclear scattering in 5 cm and that in 1 cm of lead, the total nuclear scattering in the 5-cm plate is ~ 25 percent greater than Δ_1. Taking both corrections into account we have an excess

$$\Delta = 2.3 \pm 0.8 \text{ percent} \qquad (8)$$

of the total number of traversals to be accounted for by nuclear scattering. A further small correction might be made in consideration of the fact that the effective thickness of a plate for the scattering is somewhat larger than the geometrical thickness t, but an estimate of this effect gives a correction which is wholly negligible in view of the other rather large experimental uncertainties.

If we attribute this anomaly to non-electric nuclear forces, we can now determine an average cross section σ per neutron or proton for the non-electric nuclear scattering. This cross section may be defined by

$$\sigma = \Delta / tN, \qquad (9)$$

where N is the number of neutrons and protons in 1 cm^3, t is the thickness of the lead, and Δ, as already noted, is the fraction of the rays scattered by other than electrical forces. Inserting values in (9) we find

$$\sigma = 6.5 \times 10^{-28} \text{ cm}^2 \pm 35 \text{ percent per neutron or proton.} \qquad (10)$$

In the above calculation the energy distribution has not been used explicitly and it has only been necessary to assume that the distribution is the same for the particles incident upon the lead plates of both thicknesses.

Although the energy distribution is affected by the absorbing matter above our chamber, and is therefore not necessarily the same as that for cosmic rays in the free atmosphere at sea level, it is perhaps of interest to calculate the scattering to be expected in our lead plates with a normal sea-level energy distribution. For the purpose of such a calculation we have chosen the distribution cited by Rossi[10] as having been computed by Hartree on the basis of the Bethe-Bloch ionization energy losses by taking into account the radioactive decay of the mesotrons during their passage through the atmosphere. This distribution has been used in Eq. (3) together with the scattering probability function given by Eq. (1) and a lower energy limit $\bar{E}_{k0}$ determined in the following way. As mentioned, rays which appeared to ionize heavily have been excluded in our statistics. We define the energy loss by ionization of a ray which begins to ionize heavily as twice the energy loss at high energy and with this assumption we can calculate from the Bethe-Bloch formula a corresponding kinetic energy $E_{k01} = 16$ Mev; (we assume $m = 200$). $\bar{E}_{k0}$ lies between E_{k01} and the sum, E_{k02}, of E_{k01} plus the total energy loss in t. Actually the final result is not sensitive to the choice of $\bar{E}_{k0}$ and the approximation $\bar{E}_{k0} = (E_{k01}E_{k02})^{\frac{1}{2}}$ should be satisfactory as this gives more weight to E_{k01} in accordance with the large weight low energies have for large angles in regard to the expression (3). We find for $t = 1$ cm, $E_{k02} = 40$ Mev and $\bar{E}_{k0} = (16 \times 40)^{\frac{1}{2}} = 25$ Mev, and for $t = 5$ cm, $E_{k02} = 99$ Mev and $\bar{E}_{k0} = (16 \times 99)^{\frac{1}{2}} = 40$ Mev. With this limit the integration of Eq. (3) has been made graphically, and the scattering distribution computed in this way for the two thicknesses of our lead plates is shown in columns 3 and 4 in Table II. In comparing the calculated percentage scattered into angles greater than 4° with that observed, we find only an indication of a discrepancy in the case of the 5-cm plate and a satisfactory agreement in the case of the 1-cm plate. Thus there is little explicit evidence here to indicate the presence of non-electric nuclear scattering, although the Hartree distribution probably contains a larger percentage of low energy particles than were present in our chamber, and therefore predictions based upon it should lead to a broader

TABLE III. Values of Table II reduced to $f(u)$.

$u = \alpha/t^{\frac{1}{2}}$	$I(\alpha, t)t^{\frac{1}{2}} = f(u)$	
	1 $t = 1$ cm	2 $t = 5$ cm
Degrees $\times$cm$^{-\frac{1}{2}}$	% $\times$cm$^{\frac{1}{2}}$	% $\times$cm$^{\frac{1}{2}}$
2–4	3.16	6.20
4–6	1.39	1.67
6–8	0.74	0.64
8–10	0.11	0.33
10–12	0.24	0.20
2–12	5.64	9.04

[10] B. Rossi, Rev. Mod. Phys. **11**, 296 (1939).

scattering pattern than would result from the actual energy distribution. If the figures are taken as they stand, the actual scattering into angles of more than 4° exceeds the electrical scattering predicted from the Hartree distribution by

$$\Delta_2 = (10.08 - 9.05) \text{ percent} \pm 0.5 \text{ percent} = (1.0 \pm 0.5) \text{ percent} \quad (11)$$

of the total intensity. Putting this value into expression (9) and correcting, we find a cross section per neutron or proton for the electrical nuclear scattering of

$$\sigma = 4.5 \times 10^{-28} \text{ cm}^2 \pm 50 \text{ percent}. \quad (12)$$

However it must be pointed out that this expression involves the uncertainties connected with the energy distribution in addition to our experimental errors, a fact which makes it less reliable than the expression (10).

DISCUSSION AND CONCLUSION

Other experiments with which our results may be compared include those of Code, Vargus, and Wilson. From an analysis of 451 tracks of measured energy traversing 3.8 cm of tungsten, Code[4] found a Gaussian distribution with respect to the product $\bar{E}\alpha$, where $\bar{E}$ is the average energy of a ray while traversing the scattering metal plate, in the range up to 8×10^9 ev×degrees. The average value of $\bar{E}\alpha$ was in close agreement with that predicted by Williams; but Code found 10 rays having a value $\bar{E}\alpha$ greater than 8×10^9 ev×degrees whereas only 1.5 were expected. If this excess of large angle scattering is attributed to non-electric nuclear scattering, the estimated cross section per neutron or proton is

$$\sigma = 5.7 \times 10^{-28} \text{ cm}^2 \pm 35 \text{ percent}. \quad (13)$$

In Wilson's experiments[3] 185 rays of measured energy were scattered in plates of lead, copper, or gold. Out of a total path of these rays, equivalent to 4 meters of lead there was only one indication of a nuclear collision, and from this Wilson infers that the cross section per neutron or proton is of the order of

$$\sigma = 4.0 \times 10^{-28} \text{ cm}^2. \quad (14)$$

Out of a larger number of traversals for which the total path was of the order of 50 meters of lead equivalent, there occurred only one collision resulting in a *nuclear disintegration*. Wilson estimated the cross section per neutron or proton for events of this type to be of the order of

$$\sigma = 0.3 \times 10^{-28} \text{ cm}^2. \quad (15)$$

From an analysis of 55 tracks of measured energy and 670 tracks of energies too high for measurements traversing one cm of platinum in the chamber of Anderson and Neddermeyer, and by using Anderson and Neddermeyer's and Blackett's energy distributions for the 670 tracks of high energy, Vargus[2] found that the scattering was in accord with the theory of Williams and no evidence could be obtained from the scattering alone of forces other than that of the Coulomb field, although, of course, Anderson and Neddermeyer have observed a number of examples of nuclear disintegrations induced by cosmic rays. Perhaps the most extensive analysis of such nuclear disintegrations resulting from cosmic-ray impacts is that of Brode and Starr[11] from which Wilson[3] has estimated a cross section per neutron or proton of

$$\sigma = 0.1 \times 10^{-28} \text{ cm}^2 \pm 60 \text{ percent}. \quad (16)$$

Comparing Code's result, (13), with ours, (10), we find good agreement considering the rather large experimental errors. This agreement is significant because of the difference of the two methods, Code's energies having been determined by the magnetic method while our method compares the scattering in two different thicknesses of material. Comparison with the cross section given by Wilson, (14), shows agreement at least in the order of magnitude. Wilson points out that the number of large angle scatterings observed depends partially on the geometry of the apparatus. It seems that the arrangements of Code and ourselves are more alike and suitable for detecting large angle scattering since both arrangements have all coincidence counters either above or inside the chamber.

As a final comparison we can average the theoretical expression for σ as function of E given by Marshak and Weisskopf over Hartree's energy distribution. The resulting theoretical *average* cross section per neutron or proton in a

[11] R. B. Brode and M. A. Starr, Phys. Rev. **53**, 3 (1938).

nucleus is

$$\bar{\sigma}_{th}=3.8\times10^{-28}\ \text{cm}^2. \quad (17)$$

To give an angular distribution of the anomalous scattering which could be compared with theory is not possible with the experimental data obtained thus far.

Comparing the theoretical average cross section with the experimental values we find agreement at least within the order of magnitude. Since $\bar{\sigma}_{th}$ for mesotrons of spin 0 would be about 10–20 times smaller than that for spin $\frac{1}{2}$ (Bhabha)[5] our experiments and those of Code would indicate a spin of $\frac{1}{2}$, assuming that the theory of Marshak and Weisskopf is correct, while Wilson's estimates from nuclear disintegration tend to show a spin of 0.

It has to be mentioned that by attributing a magnetic moment to the mesotron in addition to the spin some authors[12–13] have calculated the probability of burst production by mesotrons in a Coulomb field. The theoretical result when spin 0 or $\frac{1}{2}$ is assumed is of the order of that observed whereas theories based upon spin 1 seem to be definitely excluded. The scattering cross section for mesotrons has not yet been calculated under these new assumptions, and thus it is not impossible that the anomaly found experimentally can still be explained by some kind of electromagnetic interaction.

In the foregoing discussion it has been assumed that all of the rays involved in the experiments were mesotrons. Other types of rays, especially electrons and protons, are also present in the cosmic radiation at sea level, and we should estimate to what extent these might have affected our results. Considering first the electrons, there are three types which might have been included in our statistics. Electrons normally present at sea level with sufficient energy to pass through the 25-cm lead shield above the chamber would have multiplied and given rise to a cascade shower in the chamber so that these electrons would not have been counted. Knock-on electrons produced by the penetrating component would in general have been accompanied by the primary mesotron and would thus have been identified as electrons and would not have been included in the count. Finally electrons created by mesotron decay in the gas or in the lead plates of the chamber might have been present, and these might be expected to show some rather large changes in direction from that of the primary mesotron. An upper limit for the number of mesotrons decaying in the gas can be estimated by assuming a lifetime of $\tau_0=2.7\times10^{-6}$ sec. and a lower limit of $\beta=\frac{1}{2}$ for the mesotrons. The latter value of β we assume because particles slower than that ionize heavily and thus are excluded. The probability p for a mesotron decay within the range of height of about $H=60$ cm included in the cloud chamber will be

$$p=H(1-\beta^2)^{\frac{1}{2}}/\tau_0\beta c=1.3\times10^{-3}\approx0.1 \text{ percent}.$$

Mesotrons which enter the lead plates with $\beta c\geqq\frac{1}{2}c$ but are slowed down to velocities $\beta c<\frac{1}{2}c$ would have an increased probability of a decay, and some of the resulting electrons might emerge from the lead at almost any angle with respect to the direction of the primary mesotron. This would contribute to the large angle scatterings included in the count but the number of such events would be negligibly small. From the energy distribution we expect about 1 or 2 percent of the total intensity to be stopped in our lead thicknesses. This estimate agrees well with the number of particles actually observed in these experiments as having been stopped. It is also noted that Rasetti[14] has found a mesotron decay in iron, and from his results we should expect about 0.1–0.2 percent of the total intensity of mesotrons to be decay electrons emerging from a 10-cm iron plate, and a somewhat smaller percentage under lead. We can thus consider the 0.2 percent as an upper limit for this effect, and adding the two effects inside the cloud chamber we find an upper limit of 0.3 percent for the number of decay electrons. As we see, this value constitutes the total number of electrons which could not easily be identified as such and might have been included in our counts. The number lies well within our statistical error and need not be further considered.

The percentage of protons in the cosmic radia-

[12] H. C. Corben and J. Schwinger, Phys. Rev. **58**, 953 (1940).
[13] R. F. Christy and S. Kusaka, Phys. Rev. **59**, 414 (1941).
[14] F. Rasetti, Phys. Rev. **59**, 706 (1941).

tion is not well known. From the number of slow protons which can be identified as such and with reasonable assumptions as to the proton energy distribution it has been estimated[15] that the total number of protons is of the order of 2 percent of the total penetrating component. As Wilson[3] has shown, a component of this order would not be evident as regards its effect upon the multiple electrical scattering. *However the possibility cannot be excluded that a great fraction or even the total of the anomalous large angle scattering observed is associated with the proton component and not with the mesotron component.* The observed number of tracks scattered in an anomalous way amounts to about 2 percent and is of the same order as the estimates of the proton component. If the cross sections for the proton-proton and proton-neutron scattering at cosmic-ray energies were about 100 times larger ($\sim 10^{-26}$ cm^2) than that calculated here for mesotrons, we could attribute the whole effect to the proton component. A further indication that we might have to seek for an explanation of the anomalous scattering in the proton component rather than in the mesotron component is the abnormally high energy loss of protons in lead reported by Wilson.[16]

The author wishes to express his deepest appreciation to Dr. Thomas H. Johnson whose permanent interest, advice, and inspiring guidance have made this work possible.

Acknowledgment is also made of extensive support given to this work by the Carnegie Institution of Washington.

[15] T. H. Johnson, J. G. Barry, and R. P. Shutt, Phys. Rev. **57**, 1047 (1940).

[16] J. G. Wilson, Proc. Roy. Soc. **A172**, 517 (1939).

JANUARY 1 AND 15, 1942 PHYSICAL REVIEW VOLUME 61

Scattering of Protons by Deuterium

R. F. TASCHEK*
Department of Physics, University of Wisconsin, Madison, Wisconsin
(Received December 1, 1941)

The scattering of protons by deuterium has been studied in the energy interval between 200 kev and 300 kev and as a function of angle between 20° and 90°. The ratio of observed scattering to that expected on the basis of Rutherford's formula is found to differ appreciably from unity and increase, both with increasing energy and angle.

THE work of Tuve, Heydenburg and Hafstad[1] has shown that at proton energies near 800 kev the scattering of protons from deuterium does not obey Rutherford's formula. They find a slow increase in the ratio of observed to Rutherford scattering between the angles 20° and 75°. Beyond 75° the ratio increases extremely rapidly. Primakoff[2] and Ochiai[3] have investigated proton-deuteron scattering theoretically, making use of calculated neutron-deuteron cross sections but find difficulty in fitting the observed data at large angles. It is useful to determine the energy and angular dependence of the protons scattered from deuterium since it may lead to information about the proton-proton and proton-neutron interactions.

The scattering of protons from deuterium has been observed in the energy interval between 200 kev and 300 kev, from the scattering chamber-proportional counter system described in a previous article.[4] The source of high potential[5] and the differential pumping system[6] have also been previously described. The collision products were detected by three proportional counters,

* Now at Oldbury Electro-Chemical Company, Niagara Falls, New York.

[1] M. A. Tuve, N. P. Heydenburg, and L. R. Hafstad, Phys. Rev. **50**, 806 (1936).

[2] H. Primakoff, Phys. Rev. **52**, 1000 (1937).

[3] K. Ochiai, Phys. Rev. **52**, 1221 (1937).

[4] G. L. Ragan, W. R. Kanne, and R. F. Taschek, Phys. Rev. **60**, 628 (1941).

[5] L. J. Hayworth, L. D. P. King, G. T. Zahn and N. P. Heydenburg, Rev. Sci. Inst. **8**, 486 (1937).

[6] W. R. Kanne, R. F. Taschek, and G. L. Ragan, Phys. Rev. **58**, 693 (1940).

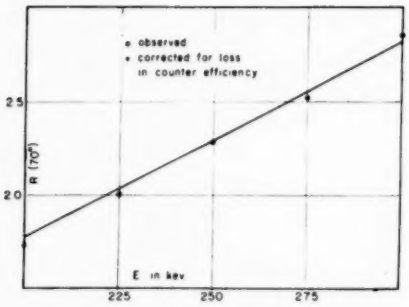

FIG. 1. Energy dependence of $R(70°)$.

one rotatable, and the other two fixed at 15° to each side of the incident beam. The dimensions of the detecting slits of the counters and other quantities which determine the geometry factor are as follows, in the notation of Breit, Thaxton, and Eisenbud:[7]

Rotatable counter	$2b=$ 0.0868 cm, $2a=$ 0.2009 cm, $\underset{\sim}{h}$ = 4.0 cm, $R_0=$ 7.0 cm.
15° counters	$2b=$ 0.0106 cm and 0.0100 cm, $2a=$ 0.1028 cm and 0.1018 cm, $\underset{\sim}{h}$ = 4.0 cm, $R_0=$ 19.0 cm.

The geometrical factor is $4\pi ba^2/R_0\underset{\sim}{h}$ and the ratio of the factor for both 15° counters to the factor for the rotatable counter was 44.4. The counters were kept filled with palladium purified hydrogen to a pressure of about 40 mm of mercury.

Deuterium gas (obtained from the Stuart Oxygen Company and labeled 95+percent pure, dried with liquid air), was continuously passed through palladium tubes and kept the scattering chamber at a pressure of about 1.3 mm of mercury, measured with an oil manometer. The Pd tubes were heated in a vacuum for about thirty minutes before passing deuterium through them. Since there was always a very slow leakage of hydrogen from the counters into the scattering chamber through the thin collodion foils, and since the impurities in the deuterium were probably principally hydrogen, the principal contaminating gas was hydrogen.

The observation of proton-deuteron scattering is complicated by the fact that the energy of a deuteron recoiling at angles less than about 50° from a proton of incident energy greater than 250 kev, should be sufficient to produce a pulse in the counter. The efficiency of the rotating counter decreased rapidly if the energy of a proton incident on it was less than about 100 kev[4] so that for angles greater than 50° only protons scattered from deuterium had sufficient energy to give a countable pulse, but near 90° the energy again became too low for reliable counting. At small angles it was found impossible to distinguish clearly on the oscilloscope between pulses due to scattered protons and pulses from recoil deuterons, for pressures in the counters ranging from 30 mm to 65 mm of mercury.

The data taken consisted of observations of the number of protons scattered into the rotatable counter at some angle in a given time interval and the simultaneous determination of the number of particles entering one or both of the fixed monitor counters at 15°. The monitor counters received protons scattered from deuterium, from contaminating gases (especially hydrogen) and recoil deuterons. The number of recoil deuterons at 15° is practically negligible compared to the number of scattered protons, since the recoils arise from protons scattered at about 125°.

A calculation was made to find out how large an effect the scattering from contaminating

TABLE I. Energy dependence of $R(70)$. The value of R in parenthesis is corrected for loss in counter efficiency by use of the efficiency curve in reference 4.

Proton energy in kev	θ	No. of protons	$\left[\frac{Y(\theta)}{Y(15)}\right]_{obs}$	$\left[\frac{Y(\theta)}{Y(15)}\right]_{calc}$	R
200	290°	A16 33,568 B4 1,804	0.0539	0.0311	1.730 (1.781)
225	290°	A16 40,672 B4 2,636	0.0624	0.0311	2.01
250	70°	A16 37,104 B4 2,644			
250	290°	A16 30,144 B4 2,148	0.0711	0.0311	2.29
275	70°	A16 23,024 B4 1,804			
	290°	A16 24,816 B4 1,976	0.0785	0.0311	2.52
300	290°	A16 20,000 B4 1,776	0.0889	0.0311	2.858

[7] G. Breit, H. M. Thaxton and L. Eisenbud, Phys. Rev. **55**, 1018 (1939).

hydrogen would have. It was found that if the pressure of the hydrogen were as large as 0.15 mm of mercury, i.e., 10 percent or more of the total pressure in the scattering chamber, a constant correction of 8 percent *of* the ratio $[Y(\theta)/Y(15)]_{obs}$ would have to be added *to* this ratio. This correction is constant only for angles at which no protons scattered from hydrogen are detected by the rotatable counter, i.e., the angles at which most of the data were taken. Whatever contaminating gases were present, remained constant in amount since the data taken from day to day with varying pressures of hydrogen in the counters and of deuterium in the scattering chamber were comparable within limits of error set by other factors. No correction for the amount of contamination present was made.

The experimental values obtained consisted of the ratio of the number of protons scattered into the rotatable counter at an angle θ, to the total number of protons and deuterons entering the 15° monitors during the same time interval. The ratio is expressed as $[Y(\theta)/Y(15)]_{obs}$; the same ratio was calculated for the known counter geometry on the basis of Rutherford's formula, and the quantity

$$R=[Y(\theta)/Y(15)]_{obs}/[Y(\theta)/Y(15)]_{calc}$$

was used to express any observed deviation from classical scattering. The quantity R is the ratio of the observed proton-deuteron cross section to the Rutherford cross section for scattering at an angle θ if the scattering at 15° is Rutherfordian.

Since only a small amount of deuterium was available and that which passed through the differential pumping system was not recovered, a greatly detailed study of proton-deuteron scattering was not possible. The energy dependence of $R(70°)$ is shown in Fig. 1, the data obtained are given in Table I. The letters A and B refer, respectively, to the monitors and to the rotatable counter, while the numbers 4 and 16 refer to the factor of the scaling circuit used in each case. It will be seen that corresponding data on opposite sides of the beam have been obtained in only a few cases, but the chamber was known to be accurately aligned from the detailed work on proton-proton scattering.[4] No corrections have been applied to the data except for counter efficiency at 200 kev.

Tables IIa and III list the angular distribution data obtained at 250 kev and 275 kev in the

TABLE IIa. Angular distribution of protons scattered from deuterium at 250 kev. The values of R in parenthesis are corrected for loss in counter efficiency by use of the efficiency curve in reference 4.

θ	No. of protons	$\left[\frac{Y(\theta)}{Y(15)}\right]_{obs}$	$\left[\frac{Y(\theta)}{Y(15)}\right]_{calc}$	R
45°	A16 11,296 B4 3,536	0.3201	0.2293	1.362
50°	A16 9,632 B4 1,936	0.2010	0.1361	1.475
55°	A16 13,296 B4 1,848	0.1388	0.0877	1.581
60°	A16 21,232 B4 2,348	0.1105	0.0595	1.860
65°	A16 18,320 B4 1,616	0.0882	0.0423	2.083
70°	A16 37,104 B4 2,644			
290°	A16 30,144 B4 2,148	0.0711	0.0311	2.29
75°	A16 29,616 B4 1,748	0.0589	0.02333	2.522
80°	A16 32,688 B4 1,628	0.0498	0.01782	2.792
85°	A16 42,256 B4 1,636	0.0387	0.01421	2.718 (2.895)
90°	A16 42,320 B4 1,328	0.0314	0.01143	2.742 (3.078)

TABLE IIb. Small angle values of R at 250 kev, obtained by correcting the observed data for the number of recoil deuterons.

θ	No. of protons	$\left[\frac{Y(\theta)}{Y(15)}\right]_{obs}$	$\left[\frac{Y(\theta)}{Y(15)}\right]_{corr}$	$\left[\frac{Y(\theta)}{Y(15)}\right]_{calc}$	R
20°	A4 1,216 B16 27,360	22.5	22.2	20.65	1.072
25°	A4 2,256 B6 17,760	7.89	7.54	6.88	1.094
30°	A4 1,512 B16 5,632	3.73	3.25	2.84	1.146
35°	A4 2,212 B16 4,704	2.125	1.558	1.361	1.141
40°	A16 684 B4 7,984	0.731	0.477	0.382	1.250
45°	A16 832 B4 7,024	0.528	0.285	0.229	1.241

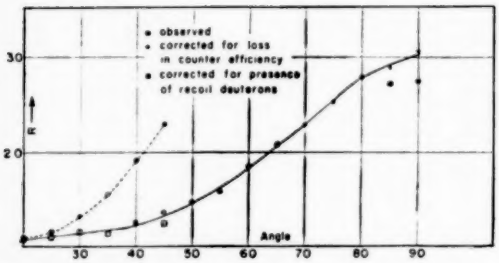

FIG. 2. Angular dependence of R at 250 kev.

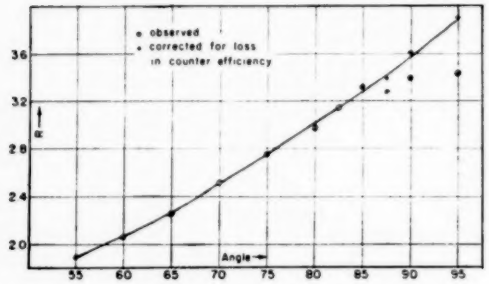

FIG. 3. Angular dependence of R at 275 kev.

angular range where only protons scattered from deuterium were counted. The values of $[Y(\theta)/Y(15)]_{obs}$ and $[Y(\theta)/Y(15)]_{calc}$ are given for each angle together with their ratio R.

In the data of Table IIa the counter pulses obtained at angles larger than 45° arise only from deuterium scattered protons. In order to obtain approximate values of R for smaller angles, the scaling circuit bias for the rotatable counter was set to count all particles entering the counter, the particles other than scattered protons being almost entirely recoil deuterons. Since the recoil deuterons arose from protons scattered at large angles the equation

$$\frac{d\Omega(\Theta)}{d\Omega(\theta)}=4\frac{\sin\Theta\cos^2\Theta\cos^2\theta}{\sin\theta\cos^2 3\theta}(1+2\sin^2\theta),$$

relating the solid angle $d\Omega(\Theta)$ into which protons are scattered by the deuterons which recoil into the solid angle $d\Omega(\theta)$ was used to obtain corrected values of R. Θ and θ are, respectively, the angles of a scattered proton and its recoil deuteron. Since the scattering volumes at the angles Θ and θ were also different, the true value of $Y(\theta)/Y(15)$ at angles less than 45° was obtained from

$$\left[\frac{Y(\theta)}{Y(15)}\right]_{cor}=\left[\frac{Y(\theta)}{Y(15)}\right]_{obs}-\frac{d\Omega(\Theta)}{d\Omega(\theta)}\frac{\sin\Theta}{\sin\theta}\left[\frac{Y\Theta}{Y(15)}\right]_{obs},$$

where the last term is the contribution to the ratio at the angle θ due to recoil deuterons which arise from protons scattered at Θ, and where $[Y(\Theta)/Y(15)]_{obs}$ is obtained from the large angle data. Only a small amount of data was obtained between 20° and 45° and these are listed in Table IIb.

The angular dependence of R at 250 kev and 275 kev is shown in Figs. 2 and 3. In Fig. 2 for angles smaller than 45°, the dashed curve represents the observed value of R before application of the above correction for recoil deuterons. It is seen that the corrected values join fairly smoothly

TABLE III. Angular distribution of protons scattered from deuterium at 275 kev. The values of R in parenthesis are corrected for loss in counter efficiency by use of the efficiency curve in reference 4.

θ	No. of protons	$\left[\frac{Y(\theta)}{Y(15)}\right]_{obs}$	$\left[\frac{Y(\theta)}{Y(15)}\right]_{calc}$	R
55°	A16 13,216 B4 2,204	0.1658	0.0877	1.89
60°	A16 6,672 B4 832	0.1228	0.0595	2.065
65°	A16 20,000 B4 1,940	0.0959	0.0423	2.265
70°	A16 23,024 B4 1,804			
290°	A16 24,816 B4 1,976	0.0785	0.0311	2.521
75°	A16 26,544 B4 1,720			
285°	A16 8,032 B4 524	0.0643	0.02333	2.758
80°	A16 54,992 B4 2,968			
280°	A16 7,840 B4 404	0.0531	0.01782	2.976
82.5°	A16 82,432 B4 4,184	0.0505	0.01608	3.139
85°	A16 89,216 B4 4,256	0.0473	0.01421	3.325
87.5°	A16 84,112 B4 3,548	0.0418	0.01275	3.275 (3.39)
90°	A16 58,912 B4 2,208	0.0389	0.01143	3.397 (3.605)
95°	A16 38,080 B4 1,256	0.0325	0.00946	3.439 (3.915)

on to the data for angles greater than 45° where no recoil deuterons were present, and approach unity for the smallest angles. The low angle portion of the curve, due to the small amount of data taken and the method of applying the correction, is to be taken merely as indicative of the trend of R. More accurate data would have allowed an evaluation of the amount of contamination present if it is correct to assume that R should be unity at the smallest angles.

The curves show that the deviation from Rutherford scattering increases both with energy and angle, as might be expected. The angular dependence is in qualitative agreement with calculations based on Primakoff's formula with the "one body" theory combined with a theoretical cross section for neutron-deuteron scattering given by Ochiai, but is smaller by almost a factor of two in magnitude. At the largest angles considerable corrections for reduced counter efficiency must be made so these values of R cannot be expected to be very good.

The writer wishes to express his thanks and appreciation to Professor G. Breit for much helpful discussion and correspondence concerning this problem.

JANUARY 1 AND 15, 1942 PHYSICAL REVIEW VOLUME 61

Magnetic Scattering of Neutrons

M. HAMERMESH
Department of Physics, Stanford University, Palo Alto, California

(Received October 30, 1941)

The problem of magnetic scattering of neutrons has been reconsidered. The possible sources of error in the previous estimate are discussed. The form factor of the 3*d* shell of iron has been recalculated, with Hartree functions for Fe. This results in removal of the discrepancy between theory and experiment. Some predicted results of measurements with monoenergetic neutrons are given.

A RECENT theoretical evaluation[1] of neutron polarization experiments has indicated a marked discrepancy between theory and experiment. The calculated values are consistently too low by more than a factor two.

There appear to be three possible causes for this disagreement:

1. Since experimentally only the gyromagnetic ratio is measured, the possibility of neutron spin $=\frac{3}{2}$ might be considered. This suggestion, which would result in an increase in the theoretical estimate, has been made by Halpern and Johnson.[2] However, it is well known to be irreconcilable with our present understanding of the structure of light nuclei.[3]

2. The velocity distribution of the neutrons is not very accurately known. H. H. J. (reference 1) used the data of Dunning, etc.[4] obtained by use of a mechanical velocity selector. Though these results may contain considerable error, the theoretical estimate is not very sensitive to change in the distribution.

3. The calculated values of polarization effect are extremely sensitive to changes in the form-factor of the magnetically active 3*d* shell. H. H. J.

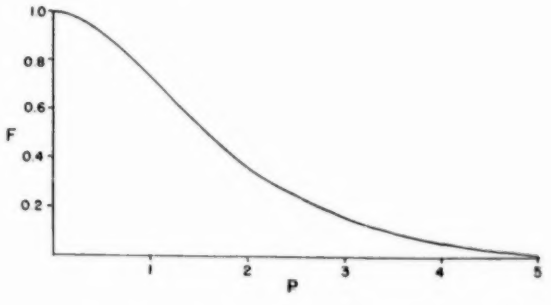

FIG. 1. Form factor for the 3*d* shell as a function of P.

[1] O. Halpern, M. Hamermesh, and M. H. Johnson. Phys. Rev. **59**, 981 (1941). In what follows, this is referred to as H.H.J. and similar notation is used.
[2] O. Halpern and M. H. Johnson, Phys. Rev. **57**, 160 (1940).
[3] See also J. Schwinger, Phys. Rev. **52**, 1250 (1937).
[4] Dunning, Pegram, Fink, Mitchell, and Segrè, Phys. Rev. **48**, 704 (1935).

TABLE I. Values of $w(x)$.

$\lvert l\rvert^2$	$A=\frac{1}{1+\frac{\lvert l\rvert^2\lambda^2}{4a^2}}$	F	$f_0(v)$ $f(\lvert l\rvert)$	fFA	$f_1(v)$ $f(\lvert l\rvert)$	fFA	$f_2(v)$ $f(\lvert l\rvert)$	fFA	$f_3(v)$ $f(\lvert l\rvert)$	fFA	$f_4(v)$ $f(\lvert l\rvert)$	fFA
2	1.14	0.48	0.281	0.154	0.252	0.138	0.231	0.126	0.207	0.113	0.193	0.106
4	1.29	0.28	0.076	0.028	0.071	0.026	0.068	0.025	0.063	0.023	0.061	0.022
6	1.43	0.19	0.183	0.050	0.181	0.049	0.178	0.048	0.171	0.047	0.170	0.046
8	1.57	0.12	0.061	0.012	0.062	0.012	0.062	0.012	0.061	0.012	0.062	0.012
10	1.71	0.08	0.086	0.012	0.089	0.012	0.092	0.013	0.092	0.013	0.095	0.013
12	1.86	0.053	0.021	0.002	0.022	0.002	0.023	0.002	0.023	0.002	0.024	0.002
14	2.00	0.035	0.094	0.007	0.098	0.007	0.106	0.007	0.109	0.008	0.115	0.008
		Remainder		0.002		0.004		0.004		0.004		0.004
		Total =		0.267		0.250		0.237		0.222		0.213
		$w(x)=$		0.090		0.084		0.080		0.075		0.072

determined the form-factor by using Hartree functions for Cu, adjusting to fit the case of iron by expanding the radius of the shell in the inverse ratio of the effective charges. This procedure would be exact for hydrogenic functions. Since, however, the $3d$ wave functions are not hydrogenic, and since the form factor is strongly dependent on the exact shape of the charge distribution, this procedure might lead to a considerable error.

Fortunately the Hartree functions for Fe have been computed by Manning and Goldberg.[5] The form factor for the $3d$ shell has been calculated by numerical integration and is plotted in Fig. 1 as a function of $p=4\pi a_0/\lambda\cdot\sin\theta/2$ where $a_0=$Bohr radius, $\lambda=$neutron wave-length, and θ is the angle of scattering. This form factor is throughout larger than that obtained by H. H. J.

By following the procedure of H. H. J., the quantity $w(x)$ has been computed. Table I corresponds to their Table II.

From the values of $w(x)$, the polarization effect has been calculated, and is compared in Table II to various experimental results. (This replaces Table III of H. H. J.)

The new values for the form factor considerably improve the agreement. Whereas in the first three cases there still remains a discrepancy of unknown origin by about a factor three, the agreement in the last case[6] may be considered satisfactory.

[5] M. F. Manning and L. Goldberg, Phys. Rev. **53**, 662 (1938).
[6] L. W. Alvarez and F. Bloch, Phys. Rev. **57**, 111 (1940).

The lack of sensitivity of the theoretical estimate to changes in the velocity distribution

TABLE II.

Thickness	0.8	1.3	1.95	4.0
% Effect	0.23	0.63	1.38	5.1
Experimental	0.76	1.78	3.32	6.0

can be seen from Table I. The distribution in the initial beam leads to $w=0.090$, while that for a beam filtered through 1 cm gives $w=0.084$. The filtering can be described roughly as a decrease of the number of neutrons in the low velocity range (say up to 1.5 km/sec.) by 35 percent, as compared to the rest of the distribution. Yet this change in distribution would lead to only a 15 percent change in the final answer. Changes of this order would be sufficient to secure complete agreement with the Bloch-Alvarez case.

The change in form-factor also increases the calculated polarization for monochromatic beams. Some predicted results are given in Table III.

TABLE III.

			% Effect for:	
λ(A)	w	Temp. (°K)	1 cm	4 cm
3	0.25	75	3.0	15.5
4	0.55	42	54.	367.

For $\lambda>4.04$A the effect should disappear entirely, since the crystal becomes transparent. Experiments in this low velocity range should give a crucial test of the correctness of our theory.

I wish to thank Professor F. Bloch for discussion and suggestions concerning this problem.

On the Photodisintegration of Beryllium and Deuterium

F. E. MYERS* AND L. C. VAN ATTA†
Physics Department, Massachusetts Institute of Technology, Cambridge, Massachusetts
(Received November 14, 1941)

High voltage x-rays have been used to redetermine the thresholds for the photodisintegration of beryllium and deuterium nuclei, giving 1.627±0.010 Mv and 2.183±0.012 Mv, respectively. The ratio of the two cross sections (σ_{Be}/σ_D) at 15 kv above the threshold voltage is approximately 10. The angular distribution of the neutrons from the photodisintegration of deuterium has been investigated, with x-rays of 2.43 Mev maximum energy, and found to be approximately isotropic. On the basis of these data, the value of the ratio of the photomagnetic to photoelectric cross section is estimated to be 6 to 1.

THE most direct method of determining the binding energy of the deuterium and beryllium nuclei is to measure the voltage threshold for the photodisintegration process. Previous measurements of these thresholds give values ranging from 2.17 to 2.25 Mv for deuterium[1] and from 1.55 to 1.63 Mv for beryllium.[2] These values have been redetermined in the present research under conditions which provide good sensitivity and give a direct measure of the threshold voltage.

The essential features of the experiment are the use of high voltage x-rays[3] to produce the disintegrations and a boron-trifluoride filled proportional counter to detect the resulting neutrons. The arrangement of the apparatus (Fig. 1) provides good sensitivity by locating the target material in the region of maximum x-ray intensity and close to the neutron counter. The obvious disadvantage is that the neutron counter is also exposed to intense radiation, and it is of some interest that a proportional counter can be operated under these conditions. The height of the pulses increases steadily and the amplitude of the background disturbance decreases as the x-ray intensity is reduced. Thus for reliable counting it is only necessary to introduce sufficient lead shielding to bring the pulses well above background for the highest x-ray intensity to be used. Since the counter sensitivity depends on the x-ray intensity, it is also necessary to calibrate the counter with a standard neutron source (Ra-Be) as a function of tube voltage and current. For the range of voltages used in this experiment the maximum change in counter sensitivity was approximately 30 percent. The background counting rate was shown to be

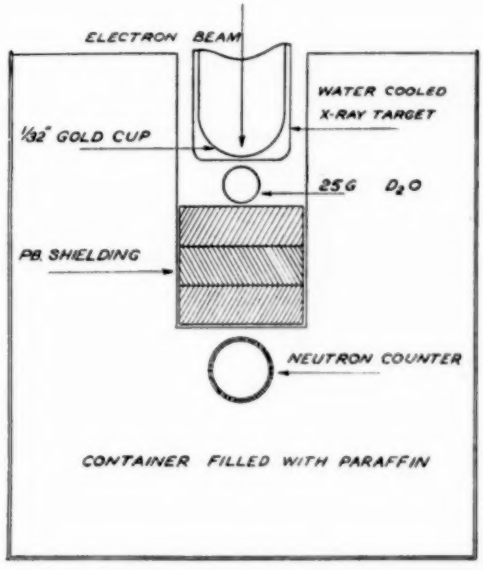

FIG. 1. Schematic diagram of the apparatus used for determining the threshold voltages. The scale of the drawing is indicated by the total thickness (3″) of the lead shielding.

* On leave of absence from New York University, and now at Frankford Arsenal, Philadelphia, Pennsylvania.
† Now with the Department of Electrical Engineering, Massachusetts Institute of Technology.
[1] J. Chadwick, N. Feather, and E. Bretscher, Proc. Roy. Soc. **A163**, 366 (1937); J. R. Richardson and L. Emo, Phys. Rev. **53**, 234 (1938); H. A. Bethe, Phys. Rev. **53**, 313 (1938); G. Stetter and W. Jentschke, Zeits. f. Physik **110**, 214 (1938); F. T. Rogers and M. M. Rogers, Phys. Rev. **55**, 263 (1939); K. Kimura, Kyoto Coll. Sci. Mem. **22**, 237 (1940).
[2] G. B. Collins, B. Waldman, and E. Guth, Phys. Rev. **56**, 876 (1939); M. Korsumskij, N. Nikolaevskaja, and M. Bakh, J. Exper. and Theor. Phys. U.S.S.R. **9**, 517 (1939); L. S. Skaggs, Phys. Rev. **56**, 22 (1939).
[3] Details of the x-ray source and x-ray tube have been published: L. C. Van Atta, D. L. Northrup, R. J. Van de Graaff, and C. M. Van Atta, Rev. Sci. Inst. **12**, 534 (1941).

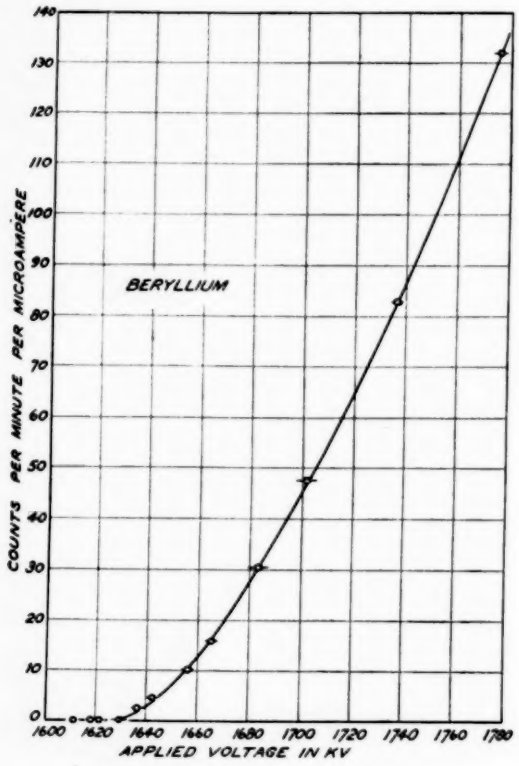

FIG. 2. Neutron counting rate *versus* tube voltage for beryllium. The length of the horizontal line through each point represents the average value of the voltage fluctuation. Corresponding vertical lines representing the expected statistical fluctuations in the counting rate have been omitted, since they would fit within the small circles representing the data points.

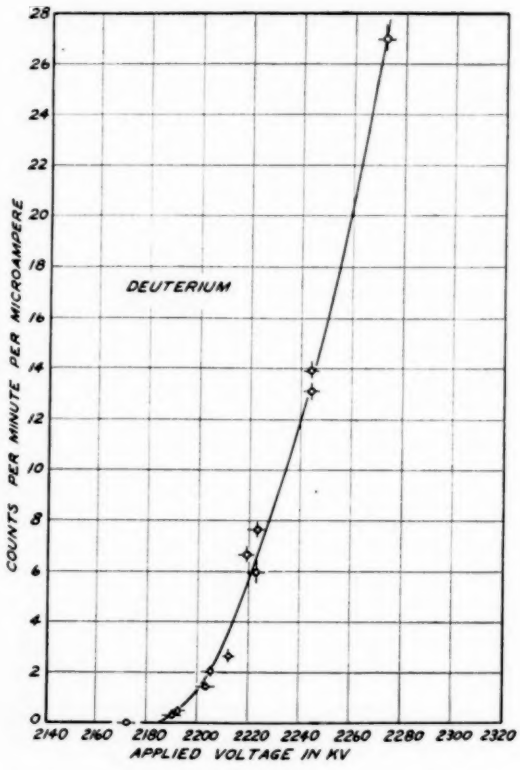

FIG. 3. Neutron counting rate *versus* applied voltage for deuterium. The horizontal and vertical lines through the data points represent, respectively, the average voltage fluctuations and the expected statistical error in the counting rate.

negligible by operating below threshold with the target material in place, and above threshold with the target material removed.

Results obtained with this apparatus are shown in Figs. 2 and 3, in which the counting rate, reduced to unit electron current and corrected for counter sensitivity, is plotted against tube voltage. If these data are plotted in double logarithmic form as shown in Figs. 4 and 5, straight lines are obtained for assumed values of threshold indistinguishably near those read from Figs. 2 and 3. Since the straightness of these lines is sensitive to the value assumed, this procedure has been used to define the threshold. The values obtained in this way are 1.627 ± 0.010 Mv for beryllium on the basis of one determination and 2.183 ± 0.012 Mv for deuterium on the basis of four determinations. The probable errors on a relative scale being independent of the voltage calibration,[4] are about one-half as large as those indicated.

For a comparison of the cross section for the two processes it is convenient to use the analytic expressions for the curves shown in Figs. 2 and 3. Over the limited range of voltage used the experimental points are reasonably well fitted by the expressions $Y_B=0.075(V-V_B)^{1.5}$ for beryllium and $Y_D=0.005(V-V_D)^{1.9}$ for deuterium where the voltages are expressed in kilovolts. Whereas the numerical values of the constants may be affected by the apparatus, their relative values should be significant. The larger multiplying constant and smaller exponent in the case of beryllium indicate a cross section which is larger initially but which increases more slowly than in the case of deuterium. By allowing for the

[4] It should be noted that the voltage scale has not been checked against other reactions, so it is impossible to assign precise limits to the voltage uncertainty. The figures cited are based on extensive tests on the performance of the generating voltmeter.

increase of efficiency of x-ray production with voltage,[5] and taking the relative amounts of target material into consideration (40 g Be, 25 g D_2O), it becomes possible to estimate the ratio of the two cross sections. At 15 kv above the respective thresholds, where the analytic expressions still fit the experimental points, the ratio $\sigma_B/\sigma_D \approx 10$. This agrees as closely as can be expected with the value of 13 for the ratio as found by Kimura,[1] who used 2.198-Mev γ-rays from radium for his determination.

In view of the interest in the angular distribution of neutrons from the photodisintegration of deuterium,[6] the numbers of neutrons emitted in the forward direction and at right angles to the incident x-rays were measured at a voltage near the threshold. The apparatus (Fig. 6) consisted of a small flask of D_2O, 7.5 cm from the x-ray target in the forward direction, a sheet of silver located 10 cm from the D_2O, either in the forward direction or at right angles, and a beta-ray counter and recording circuit for measuring the silver activity. For the angular comparison the x-ray tube was operated at an average of 2.43 Mv and 60 microamperes. While this gives a maximum quantum energy of 0.25 Mev above threshold, the major part of the intensity lies within 0.10 Mev of threshold. The thin walled glass flask holding the heavy water was spherical and only 0.5 cm in radius to avoid appreciable neutron scattering. The size of the silver sheet, 6.6 cm by 4.6 cm, represented a compromise between good geometry and high intensity. Again for the sake of intensity the silver was enclosed between sheets of paraffin, as shown in the figure. The G-M beta-ray counter operated a recording counting rate meter[7] which considerably simplified the labor of analyzing the results. The silver was regularly activated for 3.75 minutes, and then as quickly as possible, it was rolled into a cylinder and placed in a standard position around the G-M counter. The resultant

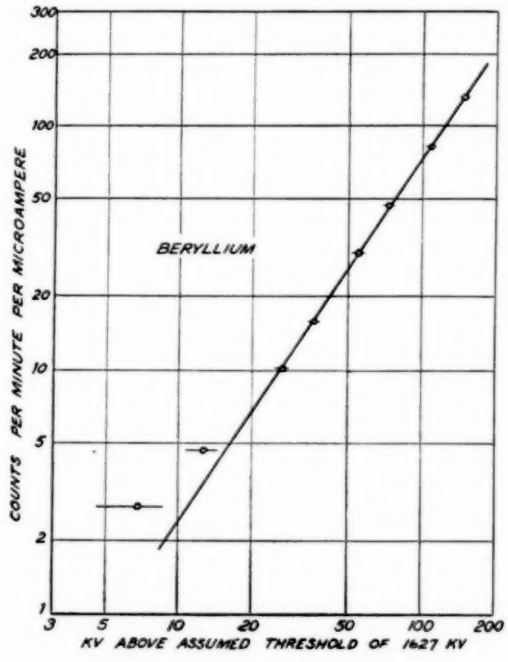

FIG. 4. Log-log plot of the neutron counting rate *versus* voltage above threshold for beryllium. Note that the apparent fluctuations at the lower voltages are exaggerated by the scale used. Due to the rapid increase in counting rate with voltage, the first points are expected to lie to the left of the curve, but the possibility that the curve undergoes a slight change in slope is not excluded.

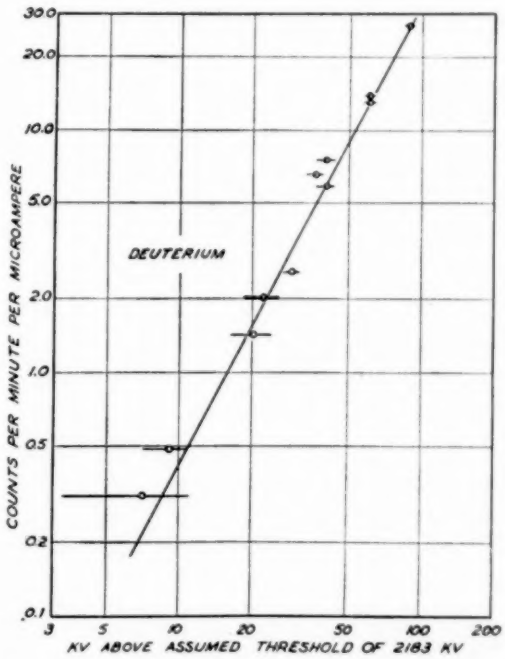

FIG. 5. Log-log plot of the neutron counting rate *versus* voltage above threshold for deuterium. Note that the average voltage fluctuation for the first point is only ± 5 kv.

[5] A. A. Petrauskas, F. E. Myers, and L. C. Van Atta, Phys. Rev. **59**, 688A (1941).

[6] H. A. Bethe and R. F. Bacher, Rev. Mod. Phys. **8**, 122 (1936); J. Chadwick, N. Feather and E. Bretscher, Proc. Roy. Soc. **A163**, 366 (1937); J. R. Richardson and L. Emo, Phys. Rev. **53**, 234 (1938); H. Von Halban, Nature **141**, 644 (1938); B. Peters and C. Richman, Phys. Rev. **59**, 804 (1941).

[7] We are indebted to Dr. Arthur Roberts for the use of this counting rate meter.

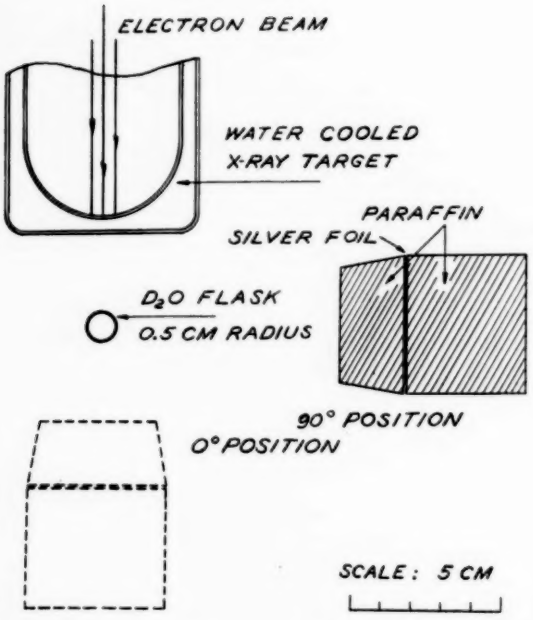

FIG. 6. Schematic diagram of the equipment used for measuring the ratio of the number of photo-neutrons ejected at 90° to that at 0° to the incident x-rays.

decay curve plotted by the recorder was of course, subject to statistical fluctuations. To minimize errors from this cause, a smooth curve fitting the data was drawn in free hand, and the counting rate was read from it 3.75 minutes after the irradiation ceased. The background of the counter was measured at frequent intervals and subtracted from the total counting rate to get the true activity of the foil. The interval of 3.75 minutes was chosen because it represents the distance between adjacent time lines on the recorder paper, and because it is long enough to prevent appreciable errors due to the time constant of the counting rate meter circuit.

Several tests were made to establish the proper functioning of the apparatus. When the x-ray tube was operated at 2.10 Mv with the D_2O in place and at 2.43 Mv with the D_2O removed, no measurable activity was observed in the silver, so that the possibility of stray neutrons from other parts of the apparatus was eliminated. When the distance between the silver and the D_2O was varied from 7 cm to 20 cm (both in the forward direction and at right angles) the activity followed the inverse square law to within expected statistical fluctuations, and indicated a constant background equal to 10 percent of the activity at the 7 cm distance.

The mean of seven measurements taken at 2.43 Mev and alternately at 0° and 90° gave 1.15 ± 0.10 as the ratio of the foil activity at 90° to that at 0° after correction for neutron background and for the slight variations in x-ray intensity caused by fluctuations in electron current and accelerating voltage. The probable error cited is twice that indicated by the internal consistency of the data. This has been arbitrarily increased to allow for the uncertainties due to geometry and neutron scattering. From these data it appears that the angular distribution of the neutrons from deuterium is approximately isotropic at voltages near threshold. This result is not necessarily in diagreement with the results of other experiments which used homogeneous radiation of much higher effective voltage.

The photo-disintegration of deuterium is usually ascribed to a "photomagnetic" and a "photoelectric" process.[8] The former is expected to predominate at voltages near threshold and to result in an isotropic neutron distribution. The latter is expected to predominate at high voltages and to result in a neutron intensity proportional to $\sin^2\theta$, where θ is measured from the forward direction of the incident quanta. A rough value for the ratio of the photomagnetic to photoelectric cross sections obtained from these data with allowance for the effect of the geometry is approximately 6. It should be emphasized that this ratio represents an average for quantum energies ranging from 0 to 0.25 Mev above threshold, with the number of quanta increasing rapidly as the threshold voltage is approached. With even less precision it is possible to estimate the order of magnitude of the total cross section: reasonable guesses as to the effective number of quanta and the sensitivity of neutron detection lead to a value of about 10^{-28} cm^2.

We are pleased to acknowledge the cooperation of the other members of the high voltage group, and in particular we wish to express our appreciation to Dr. A. A. Petrauskas who constructed the neutron counter and its associated equipment.

[8] See, e.g., first reference under 7.

Thermal Scattering of X-Rays in Crystals

J. WEIGLE,* *University of Geneva, Geneva, Switzerland*

AND

CHARLES S. SMITH, *University of Pittsburgh, Pittsburgh, Pennsylvania*

(Received October 27, 1941)

The reciprocal lattice of a crystal with heat waves is calculated under simplifying assumptions. The resulting representation exhibits in a simple manner the principal facts concerning observed diffuse scattering maxima. The assumptions used are justified and the problem of scattering from waves of large amplitude is considered.

I. INTRODUCTION

THE effect of thermal motion of the atoms in crystals on the scattering of x-rays has been studied by numerous authors[1] but it seems to us that the point of view adopted in this paper presents the facts in a slightly different and perhaps simpler fashion.

It is well known that the problems of scattering by crystals are best considered in the reciprocal space, the space in which wave vectors are drawn, because the scattering is due to the interaction of two systems of waves (a) the electromagnetic waves and (b) the material waves (which are usually frozen in, not propagating and are called the reticular planes). Thus the first thing to do in considering a problem of this type is to obtain a reciprocal representation of the crystal, that is, the collection of all the material, frozen in, waves which by superposition reconstruct the distribution of scattering matter of the crystal. In other words one must obtain the Fourier analysis of the electronic density. The different wave vectors, traced in reciprocal space, define what has been called the reciprocal lattice and this lattice in turn determines the geometry of scattering, that is, the directions in which scattering is possible. The amplitudes of the material waves, which one can consider as the weights attached to the points of the reciprocal lattice, determine the intensity of scattering; they are in fact proportional to the structure factors of the reticular planes. If we call $F_{n_1n_2n_3}$ the structure factor of the plane whose Miller's indices are $(n_1n_2n_3)$ and $\rho_{n_1n_2n_3}$ the Fourier coefficient[2] of the electronic density ρ (number of electrons per unit volume), we have

$$F_{n_1n_2n_3} = -\frac{\epsilon^2}{m(2\pi\nu)^2}\rho_{n_1n_2n_3}$$

in which ϵ and m are the charge and mass of the electron and ν the frequency of the electromagnetic waves being scattered. The factor

$$F_{000} = -\frac{\epsilon^2}{m(2\pi\nu)^2}N,$$

with N, the average number of electrons per unit volume in the crystal, determines the index of refraction $n = 1 + \frac{1}{2}F_{000}$.

In the problem of diffuse scattering we shall have to find the distribution of matter in the crystal in the presence of heat waves. These waves (of very small amplitude) are not frozen in as the material waves describing the unperturbed crystal, but their frequencies are so small compared to those of x-rays that we will be able to show that they can also be considered as frozen in. Then our whole problem becomes that of finding how the reciprocal lattice of the unperturbed crystal is changed by the presence of heat waves and we can expect that the changes thus brought about will be of two sorts: New points will appear in the reciprocal lattice (new reticular planes) and new weights (new structure factors) will be attached to the points.

* Visiting Professor of Physics at the University of Pittsburgh during the Physics of Metals Summer Session, 1941.

[1] See G. D. Preston, Nature **147**, 467 (1941) or Proc. Roy. Soc. (Aug. 29, 1941) for a bibliography.

[2] We shall also call the Fourier coefficients simply the structure factors.

II. RECIPROCAL LATTICE OF A CUBIC CRYSTAL WITH HEAT WAVES

In order to reduce to its essential physical part the mathematical problem of calculating this reciprocal lattice we shall make the following assumption which will be justified later.

(a) The crystal is cubic with atoms at

$$r=a(p_1i+p_2j+p_3k), \tag{1}$$

where a is the periodicity, i, j, k are unit vectors in the directions x, y, z, and the p_i are integers.

(b) The atoms have the form of cubes, the electronic density being constant in the atomic regions ($p_1a\pm\frac{1}{2}\Delta$, $p_2a\pm\frac{1}{2}\Delta$, $p_3a\pm\frac{1}{2}\Delta$) and zero elsewhere. If we let Δ^3 tend towards zero and ρ towards infinity in such a way that $\Delta^3\rho$ remains constant and finite, we obtain point atoms.

(c) There is a single standing heat wave.

(d) The amplitude ξ of the atomic displacements due to this wave is very small compared to a.

(e) The heat waves are subject to the boundary condition of Born, Kármán

$$\xi(p_1p_2p_3)=\xi(p_1+N_1,\ p_2+N_2,\ p_3+N_3), \tag{2}$$

N_1a, N_2a, N_3a being the dimensions of the crystal in the direction xyz, respectively, and thus a standing wave has the form

$$\xi=\xi\sin 2\pi(\sigma\cdot r)e^{-2\pi i\omega t}, \tag{3}$$

$$\sigma=\frac{l_1}{N_1}\frac{1}{a}i+\frac{l_2}{N_2}\frac{1}{a}j+\frac{l_3}{N_3}\frac{1}{a}k. \tag{4}$$

(f) The frequency ω (order of 10^{+12}) is entirely neglected being very small in comparison with the frequency ν of the x-rays (order of 10^{18}).

Let us now calculate the Fourier expansion of the density of the crystal. The periodicities are now N_1a, N_2a, N_3a and we have

$$\rho(xyz)=\sum_{n_1}\sum_{n_2}\sum_{n_3}\rho_{n_1n_2n_3}\exp\left[2\pi i\left(\frac{n_1}{N_1a}x+\frac{n_2}{N_2a}y+\frac{n_3}{N_3a}z\right)\right] \tag{5}$$

with

$$\rho_{n_1n_2n_3}=\frac{1}{a^3N_1N_2N_3}\int_0^{N_1a}\int_0^{N_2a}\int_0^{N_3a}\rho(x,\ y,\ z)\exp\left[-2\pi i\left(\frac{n_1}{N_1a}x+\frac{n_2}{N_2a}y+\frac{n_3}{N_3a}z\right)\right]dxdydz, \tag{6}$$

which we can write

$$\rho_{n_1n_2n_3}=\frac{\rho}{a^3N_1N_2N_3}\sum_{p_1=0}^{N_1-1}\sum_{p_2=0}^{N_2-1}\sum_{p_3=0}^{N_3-1}\int_{z_1}^{z_2}dz\int_{y_1}^{y_2}dy\int_{x_1}^{x_2}dx\exp\left[-2\pi i\left(\frac{n_1}{N_1a}x+\frac{n_2}{N_2a}y+\frac{n_2}{N_3a}z\right)\right] \tag{7}$$

for the coordinates of the atoms are no more given by (1) but by

$$x=p_1a+\xi_{px};\quad y=p_2a+\xi_{py};\quad z=p_3a+\xi_{pz};\quad \text{with}\quad x_1,\ x_2=p_1a+\xi_{px}\pm\tfrac{1}{2}\Delta. \tag{8}$$

If we write $\xi_{px}=\xi_0\alpha M$,
α, β, γ being the direction cosines of the displacement ξ and

$$M=\sin 2\pi\left(\frac{l_1p_1}{N_1}+\frac{l_2p_2}{N_2}+\frac{l_3p_3}{N_3}\right)$$

we obtain

$$\rho_{n_1n_2n_3}=\Gamma\sum_{p_1p_2p_3}\exp\left[-2\pi i\left(\frac{n_1p_1}{N_1}+\frac{n_2p_2}{N_2}+\frac{n_3p_3}{N_3}\right)\right]\cdot\exp\left[-2\pi iM\frac{\xi_0}{a}\left(\frac{n_1}{N_1}\alpha+\frac{n_2}{N_2}\beta+\frac{n_3}{N_3}\gamma\right)\right] \tag{9}$$

with

$$\Gamma=\frac{\rho}{\pi^3 n_1 n_2 n_3}\sin\frac{\pi n_1\Delta}{N_1 a}\sin\frac{\pi n_2\Delta}{N_2 a}\sin\frac{\pi n_3\Delta}{N_3 a}. \tag{10}$$

As ξ_0/a is very small we can write the second exponential as

$$1+\frac{\pi\xi_0}{a}\left(\frac{n_1}{N_1}\alpha+\frac{n_2}{N_2}\beta+\frac{n_3}{N_3}\gamma\right)\left(\exp\left[-2\pi i\left(\frac{l_1p_1}{N_1}+\frac{l_2p_2}{N_2}+\frac{l_3p_3}{N_3}\right)\right]-\exp\left[2\pi i\left(\frac{l_1p_1}{N_1}+\frac{l_2p_2}{N_2}+\frac{l_3p_3}{N_3}\right)\right]\right) \tag{11}$$

and the final expression for the Fourier coefficients becomes

$$\begin{aligned}\rho_{n_1n_2n_3}=\Gamma\sum_{p_3=0}^{N_3-1}\sum_{p_2=0}^{N_2-1}\sum_{p_1=0}^{N_1-1}\exp\left[-2\pi i\left(\frac{n_1p_1}{N_1}+\frac{n_2p_2}{N_2}+\frac{n_3p_3}{N_3}\right)\right]\\ +\Gamma\frac{\pi\xi_0}{a}\left(\frac{n_1}{N_1}\alpha+\frac{n_2}{N_2}\beta+\frac{n_3}{N_3}\gamma\right)\sum_{p_3}\sum_{p_2}\sum_{p_1}\exp\left\{-2\pi i\left[\frac{p_1}{N_1}(l_1+n_1)+\frac{p_2}{N_2}(l_2+n_2)+\frac{p_3}{N_3}(l_3+n_3)\right]\right\}\\ -\Gamma\frac{\pi\xi_0}{a}\left(\frac{n_1}{N_1}\alpha+\frac{n_2}{N_2}\beta+\frac{n_3}{N_3}\gamma\right)\sum_{p_3}\sum_{p_2}\sum_{p_1}\exp\left\{-2\pi i\left[\frac{p_1}{N_1}(n_1-l_1)+\frac{p_2}{N_2}(n_2-l_2)+\frac{p_3}{N_3}(n_3-l_3)\right]\right\}.\end{aligned} \tag{12}$$

The first term in expression (12) is zero unless all the following relations hold:

$$n_1=hN_1,\quad n_2=kN_2,\quad n_3=lN_3. \tag{13}$$

The first term then has the value $\Gamma N_1N_2N_3$ but the second and third terms will be zero.

If the relations

$$n_1=hN_1\pm l_1,\quad n_2=kN_2\pm l_2,\quad n_3=lN_3\pm l_3 \tag{14}$$

hold, either the second or third terms of (12) will have the absolute value

$$\Gamma\frac{\pi\xi_0}{a}\left(\frac{hN_1\pm l_1}{N_1}\alpha+\frac{kN_2\pm l_2}{N_2}\beta+\frac{lN_3\pm l_3}{N_3}\gamma\right)(N_1N_2N_3)$$

but the first term will be zero.

The result may then be written as

$$\rho_{hN_1,\,kN_2,\,lN_3}=\frac{\rho}{\pi^3hkl}\sin\pi h\frac{\Delta}{a}\sin\pi k\frac{\Delta}{a}\sin\pi l\frac{\Delta}{a} \tag{15}$$

and

$$\begin{aligned}\rho_{hN_1\pm l_1,\,kN_2\pm l_2,\,lN_3\pm l_3}=\mp\left[\frac{\rho N_1N_2N_3\pi\xi_0/a}{\pi^3(hN_1\pm l_1)(kN_2\pm l_2)(lN_3\pm l_3)}\right]\left[\frac{hN_1\pm l_1}{N_1}\alpha+\frac{kN_2\pm l_2}{N_2}\beta+\frac{lN_3\pm l_3}{N_3}\gamma\right]\\ \times\left[\sin\frac{\pi(hN_1\pm l_1)}{N_1}\frac{\Delta}{a}\sin\frac{\pi(kN_2\pm l_2}{N_2}\frac{\Delta}{a}\sin\frac{\pi(lN_3\pm l_3}{N_3}\frac{\Delta}{a}\right]\end{aligned} \tag{16}$$

and all other $\rho_{n_1n_2n_3}=0$.

If we let Δ tend towards zero and let ρ increase in such a way that $\rho\Delta^3$ remains finite and equal to the number A of electrons per atom we obtain the structure factors for point atoms:

$$\rho_{hN_1,\,kN_2,\,lN_3}=A/a^3, \tag{17}$$

$$\rho_{hN_1\pm l_1,\,kN_2\pm l_2,\,lN_3\pm l_3}=\mp\frac{\pi\xi_0}{a}\frac{A}{a^3}\left[\frac{hN_1\pm l_1}{N_1}\alpha+\frac{kN_2\pm l_2}{N_2}\beta+\frac{lN_3\pm l_3}{N_3}\gamma\right]. \tag{18}$$

These two sets of Fourier coefficients show that the structure factors of the unperturbed crystal are not changed by the presence of a single heat wave. The effect of this disturbance is to bring in new points in the reciprocal lattice, new material planes from which x-rays can be "reflected," and it is these which will be discussed in the next section. Later we will consider the effect of all the heat waves together and we will find that (17) which is obtained as a first approximation does depend on the heat waves giving what has been called the Debye temperature factor.

III. GEOMETRY OF RECIPROCAL LATTICE AND FORM OF THE SCATTERING POLES

We have represented in Fig. 1 the *hk*0 layer of the reciprocal lattice resulting from the calculations of the last section. The new points introduced into the reciprocal lattice by the sinusoidal heat wave represent the terms that have to be added to the Fourier series in order to obtain the new distribution of matter. The vectors radiating from the point (000) to each of these new points represent material frozen in waves, the superposition of which, added to the former waves describing the unperturbed distribution of matter, recreates the crystal. We can easily understand why so many new points appear in spite of the sinusoidal nature of the disturbance by comparing our results with the ones we would have obtained for a heat wave in a continuous medium. In this case the Fourier series is made of the three terms only

$$\rho_0+\rho_1\exp[2\pi ix/\lambda]+\rho_{-1}\exp[-2\pi ix/\lambda]\ \rho_1=\rho_{-1} \quad (19)$$

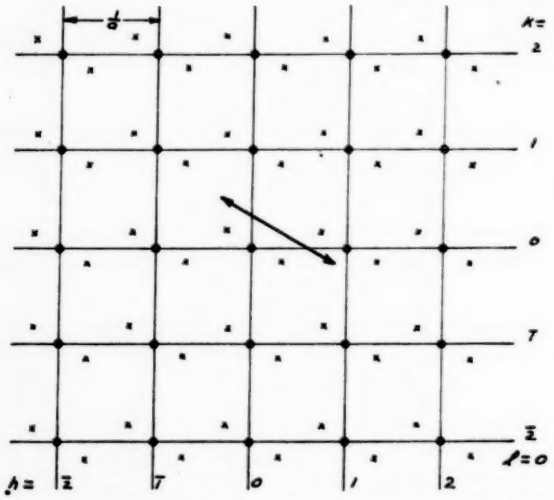

FIG. 1. Reciprocal lattice of a crystal perturbed by a heat wave. The heat wave (standing wave) has the direction of propagation indicated by the double arrow. Without heat waves the crystal would have consisted of points marked 0 only. The heat wave introduces new points marked x at a distance from the points 0 given by $1/\lambda$ where λ is the wave-length of the heat wave.

and the reciprocal lattice is made of three points only with the structure factors ρ_0, ρ_1 and ρ_{-1} (Fig. 2a). If, however, the heat wave goes through a chain of atoms whose reciprocal lattice was that represented in Fig. 2b, the reciprocal lattice becomes that of Fig. 2c. And we see that waves of wave vectors $n/a\pm 1/\lambda$ appear. These waves have the same frequency as the original heat wave and they are well known in the theory of specific heats where it is shown that waves of different wave-lengths can represent the same distribution of atoms (Fig. 3). The relation between the different wave-lengths is exactly what we have written above. In a crystal in which three periodicities appear the points are more numerous but the same explanation obtains.

The structure factors of the new points of the reciprocal lattice are in general very small and as they are proportional to the amplitude ξ_0 of the heat waves they decrease as the wave-length of the heat waves decrease, or, as the new points recede from the old ones. Recent diffuse scattering experiments show maxima only in the immediate neighborhood of Bragg reflections and thus we will restrict our considerations to regions in the reciprocal space close to the points marked (*hkl*) in Fig. 1. The heat waves with which we have to deal have their wave-lengths between L, the dimension of the crystal ($\sim$1 cm, and 100A ($\sim 10^{-6}$ cm). Thus the numbers l_i which appear in (4) and which give the wave-length λ_l of the heat wave l, $\lambda_l=L/l$ are always small compared to N_i, the number of atoms in the dimension L_i. The largest value of l_i, that for the shortest waves ($\lambda\leqq 10^{-6}$ cm) considered, is of the order of 10^6 when N is of the order of 10^8. We will thus neglect l/N and our formulas for the structure factors become

$$\rho_{hN_1\pm l_1,\ kN_2\pm l_2,\ lN_3\pm l_3}=\mp\rho_{hN_1,\ kN_2,\ lN_3}\frac{\pi\xi_0}{a}[h\alpha+k\beta+l\gamma]. \quad (20)$$

We need now to calculate ξ_0 as a function of the temperature and the wave-length. The frequency of these rather long heat waves is such as to make $h\nu$ small with respect to kT ($T\sim 300°$) and thus equipartition of energy gives the result that each wave carries an energy kT. Now the energy density of a wave of velocity v frequency ω and amplitude ξ_0 in a medium of density ρ is

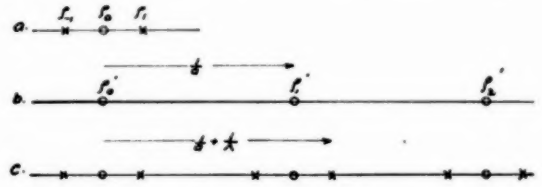

FIG. 2. Reciprocal lattice of: (a) a continuous medium with a sinusoidal wave; (b) a chain of atoms; (c) a chain of atoms with a sinusoidal wave.

given by

$$\tfrac{1}{2}\rho(2\pi\omega\xi_0)^2 = kT/V \quad V \text{ volume of the crystal}$$

or

$$\xi_0^2 = \frac{kT}{2\pi^2\omega^2\rho V} = \frac{kT}{2\pi^2\rho V}\frac{\lambda^2}{v^2}. \tag{21}$$

For these relatively long waves the velocity is very nearly independent of λ and we thus find for KCl to which our considerations apply (cubic crystal) that $\xi_0/a \sim 10^{-4}\lambda$. We see that even for very long wave-lengths of the order of the dimensions of the crystal ξ_0/a is very small and this justifies the approximations we have employed.

It is remarkable that transverse and longitudinal waves of the same wave-length and same direction give the same points in the reciprocal lattice. However their structure factors are different, because we have, for waves moving in the x direction, for instance,

$$\rho_{hN_1,\, kN_2\, lN_3}\frac{\pi\xi_0}{a}h \text{ longitudinal} \tag{22}$$

$$\left.\begin{aligned}\rho_{hN_1,\, kN_2,\, lN_3}\frac{\pi\xi_0}{a}k &\quad \text{polarized in } y \text{ direction}\\ \rho_{hN_1,\, kN_2,\, lN_3}\frac{\pi\xi_0}{a}l &\quad \text{polarized in } z \text{ direction.}\end{aligned}\right\}\text{transverse}$$

Thus, even if the amplitude of these waves were equal (they are not equal in general because the velocities are different) the structure factors would be different. But, as one can see, that is not true for all the associated (hkl) planes. For instance, the (111) plane has its thermal structure factors equal for longitudinal and transverse waves but the (100) plane has a structure factor equal to zero for transverse waves, as we should expect, since under the influence of such waves the atoms move in the plane (100) itself and thus no change in the distribution of scattering matter affecting the reflection of x-rays takes place.

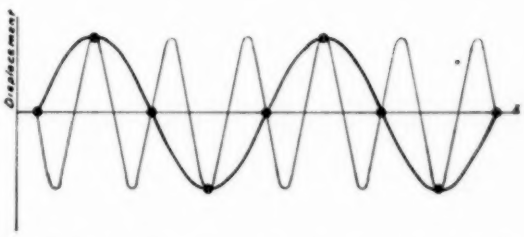

FIG. 3. Two different wave-lengths may represent the same periodic displacement of atoms.

We have represented in Fig. 4 a few of the "scattering poles" for a crystal of the KCl type. We call scattering poles the contour lines of equal intensities of scattering. These intensities are proportional to the sum of the squares of the structure factors for the transverse and the longitudinal waves of wave-length corresponding to the position considered in reciprocal space. The variations of the structure factors with direction coming from the appearance of the direction cosines α, β, γ of the atomic displacements due to the waves, and from the variations of the velocity of these waves are not the only ones. The structure factors decrease around each point (hkl) of the reciprocal lattice, since they are proportional to the wave-length of the heat waves. They vary thus inversely as the distance between the point (hkl) and the point at which they are measured. If we restrict ourselves to the layer ($hk0$) of Fig. 4 we can write for the intensities I

$$I(r,\theta) = \frac{K}{r^2}\rho^2_{hk0}\left[\frac{R_t^2(\theta)}{v_t^2(\theta)} + \frac{R_l^2(\theta)}{v_l^2(\theta)}\right], \tag{23}$$

$$R_t(\theta) = k\cos\theta - h\sin\theta, \quad R_l(\theta) = h\cos\theta + k\sin\theta,$$

where θ and r are the polar coordinates around the point ($hk0$) of the point at which the in-

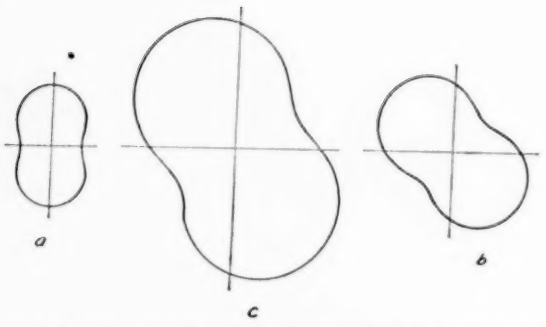

FIG. 4. Scattering poles of a few reticular planes (h k o) of KCl: (a) (100); (b) (110); (c) (210).

tensity is measured, K a constant, and v_t and v_l the velocities of the transverse and longitudinal waves, respectively. In (23) we have assumed that the transverse waves are decomposed into two directions of vibration, one perpendicular to the layer ($hk0$) and the other contained in this plane. In Fig. 4 we have neglected the variations of the velocities with direction, since for KCl these variations are at most of the order of 25 percent, but we have assumed that longitudinal waves travel with a velocity twice as large as that of transverse waves. Besides, if a, b, and c, of Fig. 4 are supposed to be drawn in the same scale, the different structure factors ρ_{hkl} are equal, or in other words we have to deal with point atoms: the atomic structure factor plays no part in these pictures.

Figure 5 in which we have drawn different contour lines of equal intensities (decreasing from the center in steps of a factor of $\frac{1}{2}$) can be used to determine the intensity of the scattered x-rays. With x-rays incident in one fixed direction (towards point 0) off the Bragg angle by an amount Δ the circle of reflection cuts the contour lines. From the center of the circle of reflection the rays arriving in each of these points of intersection have an intensity proportional to the value marked on the contour line. And thus without rotating the crystal or changing the direction of incidence of the x-rays we see that thermal scattering will take place in the form of a broad beam with a distribution of intensity showing a flat maximum and not necessarily symmetrical.

In order to obtain an approximate formula for the intensity of the x-rays diffracted by the thermal waves we shall assume that Fig. 4 degenerates into spheres. Then we can draw in reciprocal space in the vicinity of a point (hkl) the contours of equal magnitude of the structure factors in the form of circles. (Fig. 6).

A reflection circle (intersection of the sphere of propagation with the layer plane of the reciprocal lattice represented) is shown passing near but not through the point (100) corresponding to the reflection of x-rays near the Bragg angle for (100). The reflection circle cutting the contours shows that there will be a broad maximum of diffuse thermal scattering. The maximum obviously occurs in the direction of the intersection of the reflection circle with the contour of largest structure factor, that is, in the direction of the line joining the center of the circle of reflection with the point (100). We find then for the angle of maximum reflection θ_m,

$$\theta_m = \theta_B + \Delta \sin^2\theta_B, \tag{24}$$

where θ_B is the Bragg angle for (100) and Δ is the angular displacement from this Bragg angle at which the crystal is set. This formula has been given by Zachariasen.[3,4]

Zachariasen[3] has also given

$$J = \frac{K}{(\Delta \sin 2\theta_B)^2 + x^2}, \tag{25}$$

as the form of the maximum of the diffuse scattering. K is a constant and x the angle measured in the equatorial plane relative to the maximum. The geometry of Fig. 6 leads,

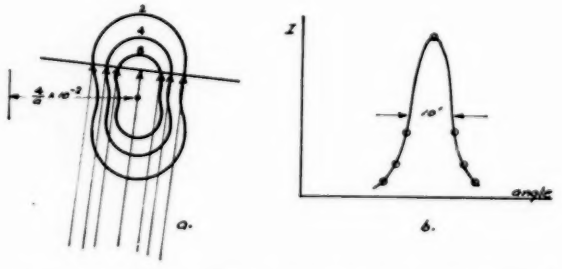

FIG. 5. (a) The diffuse scattering of x-rays from the (100) pole of KCl in the (h k o) layer. The wave-length of the x-rays is 0.71A and the crystal is set at an angle of $\theta_{B_{100}}+1°$ with respect to the primary beam. (b) Angular distribution of scattered intensity drawn from (a).

[3] W. H. Zachariasen, Phys. Rev. **57**, 597 (1940).
[4] W. H. Zachariasen and S. Siegel, Phys. Rev. **57**, 795 (1940).

however to

$$J=\frac{K}{(\frac{1}{2}\Delta \sin 2\theta_B)^2+x^2}, \tag{26}$$

if we consider the variations of the structure factors along the circle of reflection.

As regards the value of the intensity diffusely scattered compared to the intensity of the associated reflection on the point (*hkl*), we find that this value will depend, with monochromatic x-rays, on the divergence of the incident beam. With acceptable values of this divergence and of the natural width of the x-rays lines we find that, at about 1° off the Bragg angle, the ratio of these intensities is of the order of 10^{-2} or 10^{-3}.

IV. REAL ATOMS

We have assumed so far that the atoms of our crystal were "cubic" atoms. This was necessary to simplify our calculations. However it is easy to show that in the case of real atoms for which the distribution of scattering matter is known our results still hold. Let us consider a crystal having only one periodicity a, whose electronic density $\rho'(x)$ in the absence of heat waves is known and given by

$$\rho'(x)=\sum_m \rho'_m e^{2\pi imbx}, \quad b=1/a. \tag{27}$$

In addition let us suppose that the atoms are placed at points $x=pa$ ($p_i=0, 1\cdots N-1$), the pth atom extending from $pa-a/2$ to $pa+a/2$. When a longitudinal standing heat wave goes through the crystal the pth atom is displaced *as a whole* by an amount

$$\xi_p=\xi_0 \sin\frac{2\pi qp}{N}, \quad q \text{ integer} < N. \tag{28}$$

To find the Fourier expansion of the new distribution of matter we assume that the period is equal to the length of the crystal $N\,a$ and we have

$$\rho(x)=\sum_n \rho_n \exp\left[\frac{2\pi in}{Na}x\right], \tag{29}$$

$$\rho_n=\frac{1}{Na}\int_{-\frac{1}{2}a}^{Na-\frac{1}{2}a}\rho(x)\exp\left[-\frac{2\pi in}{Na}x\right]dx. \tag{30}$$

Carrying the integration over each atom separately we write

$$\rho_n=\frac{1}{Na}\sum_{p=0}^{N-1}\int_{pa-\frac{1}{2}a+\xi_p}^{pa+\frac{1}{2}a+\xi_p}\rho'(x-\xi_p)\exp\left[-\frac{2\pi in}{Na}x\right]dx \tag{31}$$

or

$$\rho_n=\frac{1}{Na}\sum_{p=0}^{N-1}\exp\left[-\frac{2\pi in}{Na}\xi_p\right]\int_{pa-\frac{1}{2}a}^{pa+\frac{1}{2}a}\rho'(y)\exp\left[-\frac{2\pi in}{Na}y\right]dy, \tag{32}$$

which on introducing (27) gives

$$\rho_n=\left\{\sum_{p=0}^{N-1}\exp\left[-\frac{2\pi in}{N}(p+\xi_p/a)\right]\right\}\left\{\sum_m \rho'_m\frac{\sin(\pi/N)(mN-n)}{\pi(mN-n)}\right\}. \tag{33}$$

As $\xi_p/a \ll 1$ we have

$$\exp\left[-\frac{2\pi in}{Na}\xi_p\right]=1-\frac{\pi n\xi}{Na}\left(\exp\left[\frac{2\pi iqp}{N}\right]-\exp\left[-\frac{2\pi iqp}{N}\right]\right) \tag{34}$$

and finally

$$\rho_n=\left\{\sum_m \rho'_m \frac{\sin(\pi/N)(mN-n)}{\pi(mN-n)}\right\}\left\{\sum_p \exp\left[-\frac{2\pi inp}{N}\right]\right.$$
$$\left.-\frac{\pi n\xi}{Na}\sum_p\left(\exp\left[\frac{2\pi ip}{N}(q-n)\right]-\exp\left[-\frac{2\pi ip}{N}(q+n)\right]\right)\right\}. \quad (35)$$

For $n=sN$, $s=$integer positive or negative, the first summation on p gives N and the others zero. Then we find

$$\rho_{sN}=\rho'_s \quad (36)$$

or in other words the structure factors of the unperturbed lattice are not changed by the presence of one heat wave. But there are new points in the reciprocal lattice, those for which

$$n\pm q=sN \quad s \text{ integer} \quad (37)$$

for in this case one or the other of the second summations over p is equal to N, the others being equal to zero. We have then

$$\rho_{sN\pm q}=\frac{\xi}{a}\sum_r \rho'_{r+s}\frac{sN\pm q}{rN\mp q}\sin\frac{\pi q}{N}(-1)^r, \quad (38)$$

which gives

$$\rho_{\pm q}=\frac{\xi}{a}\sin\frac{\pi q}{N}\left[\cdots\pm\rho'_{-1}\frac{q}{N\pm q}-\rho'_0\mp\rho'_1\frac{q}{N\mp q}+\cdots\right] \quad (39)$$

and

$$\rho_{N\pm q}=\frac{\xi}{a}\sin\frac{\pi q}{N}\left[-\rho'_{-1}\frac{N\pm q}{2N\pm q}+\rho'_0\mp\rho'_1\frac{N\pm q}{q}-\rho'_2\frac{N\pm q}{N\mp q}+\cdots\right] \quad (40)$$

or if $q\ll N$

$$\rho_{\pm q}=\mp\frac{\xi}{a}\frac{\pi q}{N}\rho'_0 \quad (41)$$

and

$$\rho_{N\pm q}=-\frac{\xi}{a}\pi\rho'_1. \quad (42)$$

Thus we see that the structure factors of the additional points of the reciprocal lattice depend on the relative amplitude ξ/a of the heat waves and on the structure factor ρ'_n of the plane (n) with which they are associated. That obviously is only true because we have taken $q\ll N$ which restricts us to new points of the reciprocal lattice which are very near the unperturbed points sN. For very short heat waves ($q=N/2$ for instance) the new point of the reciprocal lattice is no longer near one of the points of the undisturbed lattice (it is half way between two of these) and we would find

$$\rho_{N+N/2}=3\xi/a\left[\cdots+\rho'_{-2}\frac{1}{7}-\rho'_{-1}\frac{1}{5}+\rho'_0\frac{1}{3}-\rho'_1-\rho'_2+\rho'_3\frac{1}{3}-\rho_4\frac{1}{5}+\cdots\right], \quad (43)$$

which shows that its structure factor depends mostly on the structure factor of the two nearest points ρ'_1 and ρ'_2 but also on all the others. If we compare these results with those obtained for point atoms, i.e.,

$$\rho_{hN_1\pm l_1,\,kN_2\pm l_2,\,lN_3\pm l_3}=-\frac{\rho\Delta^3}{a^3}\frac{\pi\xi_0}{a}(h\alpha+k\beta+l\gamma) \quad (44)$$

we see that the introduction of the known structure factors does not change our conclusions. The term $\rho\Delta^3/a^3$, constant for all points of the reciprocal lattice for point atoms, is simply the ρ_N of the formulas of this paragraph.

V. SUPERPOSITION OF ALL THE HEAT WAVES

We have so far considered separately the different heat waves going through the crystal and have assumed that these waves are frozen in, that is to say, we have neglected the effects of their propagation. These two assumptions can be easily justified by means of the dynamical theory of x-rays. If the frequency of heat wave is ω_l and the frequency of the incident x-rays is ν, one finds that the frequency of the x-rays "reflected" from the plane of structure factor $\rho_{N\pm l}$ is $\nu\pm\omega_l$. As ω_l is at most of the order of 10^{13} and as ν is of the order of 10^{18}, ω_l is negligible in the equations determining the wave field of x-rays.

To understand the reason for the independence of the different heat waves let us consider the sphere of propagation in the reciprocal lattice. It is well known that this sphere of radius $k=1/\lambda$, λ being the wave-length of x-rays, does not have to be such as to go through a point of the reciprocal lattice in order to give a "reflection." If the point is near the sphere there will be x-ray energy in this direction because of the finite width of the reflections. If many points of the reciprocal lattice are near the sphere, the type of reflection becomes that which obtains in the diffraction of light by ultrasonic waves and one can no longer calculate the energy diffracted by each point independently. The theory gives for the order of magnitude of the angular width of the reflection on a plane whose structure factor is ρ_n, the value $\rho_n/\sin\theta$, θ being the angle of scattering. This width multiplied by k determines the distance which the point of the reciprocal lattice can be from the sphere and still give rise to reflection.

In the case of heat waves the reciprocal lattice points are very close together but the ρ_n are very small. The distance between the points is of the order of the inverse of the dimensions of the crystal (of the order of 1 cm^{-1}) and $\rho_n k/\sin\theta$ is of the order of 10^{-6}. Thus the reflections due to the different points do not encroach upon one another, the energy diffracted in the direction of one of the points is not diffracted again in the direction of another, or in other words, these diffractions are independent. We were then justified in assuming that the presence of one heat wave does not affect the scattering of the others, their effects being simply cumulative.

We have found that a single heat wave in the first approximation leaves the structure factors of points of the unperturbed lattice unchanged. Although each heat wave gives different and independent new points in the reciprocal lattice, all the heat waves act together on the unperturbed points and the neglected second-order terms become important, giving rise to a decrease

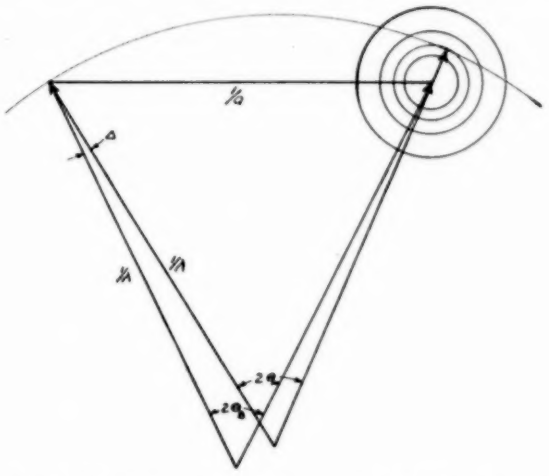

FIG. 6. The reciprocal lattice geometry of diffuse scattering. The contours of Figs. 4 and 5 have been assumed to degenerate into spheres.

of the structure factor. The simple considerations which follow are meant to show the order of magnitude of this effect without being precise.

We show in the next section that for waves of any amplitude we have

$$\rho_{hN}=\rho_h' J_0(2\pi h\xi_0/a), \tag{45}$$

which in the case of small ξ_0/a gives

$$\rho_{hN}=\rho'_h\left(1-\frac{4\pi^2\xi_0^2h^2}{a^2}\right). \tag{46}$$

In the first approximation we can consider that each wave contributes a term $4\pi^2h^2\xi_0^2/a^2$, and taking $\xi_{0l}^2=(kT/\rho V)(\lambda_l^2/2\pi^2v^2)$ we find a correction term

$$h^2kT/\rho V(2/a^2v^2)\sum_l\lambda_l^2. \tag{47}$$

The number of waves having wave vectors between b and $b+db$ ($\lambda^2=1/b^2$) is $n4\pi b^2db$, where n is the density of points in the reciprocal space

which we can obtain from

$$n\int_0^{\frac{1}{2}(1/a)} 4\pi b^2 db = 3N$$

since we know that there are $3N$ waves, N being the number of atoms in the crystal. We thus get

$$\sum_l \lambda_l^2 = 12\pi N a^2 \tag{48}$$

and

$$\rho_{hN} = \rho'_h\left(1-\frac{kTh^2}{mv^2}\cdot 24\pi\right), \tag{49}$$

m being the mass of an atom.

This form of the temperature correction factor compares with that of Ewald[5] and also has the right order of magnitude. The form of the correction factor does not compare with that of Debye because we have neglected the fact that the short wave-lengths, which predominate in number, do not have the energy kT but an energy given by quantum distribution laws, and also because we have neglected the difference in velocity of the transverse and longitudinal waves.

VI. WAVES OF LARGE AMPLITUDES

The heat waves at ordinary temperatures are of extremely small amplitudes (relative to interatomic distances). This fact allowed certain simplifications in our calculations and we found, for instance, that in the reciprocal lattice the presence of one heat wave introduced only two new points around each of the points of the unperturbed lattice. The relation between the sinusoidal nature of these waves and their representation in the reciprocal lattice was thus well marked. If, however, the amplitudes of the waves had been large compared to interatomic distances, this would not be true. Inasmuch as the theory of the diffraction effects of these waves is very similar to that of the preceding, it seemed worth while to investigate this phenomenon. We might thus be able to offer an explanation of the experimental results concerning ultrasonic waves and x-ray diffraction which have already been published,[6] for if waves of large amplitudes never appear in thermal excitation they can be realized experimentally by means of piezoelectric or ultrasonic excitations.

We start then with

$$\rho_n = \sum_m \rho'_m \frac{\sin(\pi/N)(mN-n)}{\pi(mN-n)} \sum_{p=0}^{N-1} \exp\left[-\frac{2\pi i}{N}\left(\frac{n\xi p}{a}+p(n)\right)\right]. \tag{50}$$

Now, assuming that the wave has the thickness of the crystal as wave-length, we have

$$\xi_p = \xi_0 \sin\frac{2\pi p}{N}. \tag{51}$$

With

$$\exp\left[-\frac{2\pi i n}{Na}\xi_0 \sin\frac{2\pi p}{N}\right] = \sum_{l=-\infty}^{+\infty} J_l\left(\frac{2\pi n\xi}{Na}\right)\exp\left[-\frac{2\pi i p l}{N}\right], \tag{52}$$

where J_l is the Bessel function of the first kind of order l, we find

$$\rho_n = \sum_m \rho'_m \frac{\sin(\pi/N)(mN-n)}{\pi(mN-n)} \sum_l J_l\left(\frac{2\pi n\xi}{Na}\right) \sum_p \exp\left[-2\pi i\frac{p}{N}(l+n)\right]. \tag{53}$$

The last summation will have values different from zero only if $l+n=rN$, r being an integer positive or negative and thus l can take only the values $l=rN-n$

$$\rho_n = \left\{\sum \rho'_m \frac{\sin\pi[m-(n/N)]}{\pi[m-(n/N)]}\right\}\left\{\sum_r J_{rN-n}\left(\frac{2\pi n\xi}{Na}\right)\right\}. \tag{54}$$

[5] P. P. Ewald, *Handbuch der Physik*, Vol. XXIV, p. 271.
[6] G. W. Fox and D. S. Stebbins, Phys. Rev. **55**, 405 (1939).

We find then

$$\rho_0 = \rho'_0, \tag{55}$$

which means that the index of refraction has not changed, a result which we had to expect.

As N is a large number we find further

$$\rho_1 = \rho_0 \{ \cdots J_{-(2N+1)} + J_{-(N+1)} + J_{-1}(2\pi\xi/Na) + J_{N-1} + J_{2N-1} + \cdots \}. \tag{56}$$

However, as ξ is of the order of 10^{-5} or 10^{-6} cm J_{-1} only has a non-negligible value,

$$J_{-1}(2\pi\xi/Na) = \pi\xi/Na,$$

of about 10^{-4}. But for ρ_2 we would find $\rho_0(\pi^2\xi^2/4N^2a^2)$, which is negligible. All the other ρ_n are also negligible except when n takes a value approaching N. Thus the disturbance does not affect the reciprocal lattice near the point 0. However, around the point N we find

$$\rho_N = \rho'_1[\cdots J_{-2N} + J_{-N} + J_0(2\pi\xi/a) + J_N + J_{2N} + \cdots]. \tag{57}$$

As $N \gg 2\pi\xi_0/a$, all these terms are negligible except J_0; we have then

$$\rho_N = \rho'_1 \frac{\cos[(2\pi\xi/a) - (\pi/4)]}{\pi} \left(\frac{a}{\xi}\right)^{\frac{1}{2}},$$

$l \ll N$ (58)

$$\rho_{N+l} = \rho'_1[\cdots + J_{-N-l} + J_{-l}(2\pi\xi/a) + J_{N-l} + \cdots].$$

Again the only non-negligible term is

$$J_{-l}(2\pi\xi/a)$$

and if l is of the order of $2\pi\xi/a$ this has a value of the order of 0.05. If however l is slightly larger than $2\pi\xi/a$ the Bessel function rapidly decreases to zero. In fact if $2\pi\xi/a$ has a value of 1000 we find that for $l = 1050$, J_{1050} is smaller than 0.001. For values of l smaller than $2\pi\xi/a$ the values of the Bessel functions oscillate, having slightly larger values than J_0. Thus without looking at the fine structure of the reciprocal lattice around the points, we obtain for the square of the structure factors a distribution represented approximately on Fig. 7. For the higher order we have

$$J_{hN+l} = \rho'_h J_{-l}\left(\frac{2\pi\xi}{a}h\right), \tag{59}$$

which shows that non-negligible structure factors extend from

$$l \leqq -\frac{2\pi\xi}{a}h \quad \text{to} \quad l \leqq +\frac{2\pi\xi}{a}h.$$

Figure 7 explains the experimental results which show that the transmitted beam (in the direction of the point 0) in an oscillating crystal remains as sharp as in a non-oscillating one.

The spreading of the structure factors around the points of the reciprocal lattice explain the "fuzziness" of the Laue spots and their larger intensities. As the angular width of this spreading can, in favorable cases, attain a value of several minutes of arc, it should be possible to analyze it experimentally. The experimental work in this field has, so far, been concerned with Laue spots and thus has remained qualitative; spectrographic methods would yield interesting results.

VII. CONCLUSIONS

We have shown, for a cubic monatomic crystal, how the heat waves, which describe the thermal motion of the atoms, affect the diffraction of x-rays. And we have given a simple representation, in the reciprocal lattice, of these effects. These results are not new, they are contained in the papers of Faxen, Waller, and Zachariasen, but their simpler representation given here allows an easy interpretation of the experimental data. This theory could immediately be extended to crystals which are not cubic or monatomic if the spectrum of their heat waves was known. It is however difficult to calculate this spectrum especially when the crystal is composed of different atoms or ions, for with a given wave-length a number of waves of different frequencies may be associated (optical and acoustic waves). It seems thus that the experimental study of the diffuse thermal scattering of x-rays will give us an analysis of the spectrum of heat waves in crystals for a range of wave-lengths extending from the dimensions of the crystal to about 300A. (The amplitudes of the shorter waves being in general too small to affect the diffraction of x-rays.) The intensity of the x-rays scattered in a given direction is directly proportional to the square of the amplitude of the heat waves whose wave-length can be obtained directly from the direction of scattering and the direction of the incident rays if the wave-length of the x-rays is known. If the amplitude and the wave-length are known the equipartition of energy determines the frequency or the velocity of the waves. However for a given wave-length different heat waves (longitudinal and transverse) contribute to the scattering. But it is easy to see that the study of the scattering poles around different associated reflections allows one to separate the scattering due to longitudinal and to transverse waves, respectively. In fact, for the layer (*hko*) we found in the expression of the structure factors a term which depended on the direction of vibration of the waves, *viz.*,

$$\alpha h+\beta k= \begin{cases} h\cos\theta+k\sin\theta & \text{Longitudinal wave} \\ -h\sin\theta+k\cos\theta & \text{Transverse wave} \end{cases} \quad \text{in layer } (hko).$$

θ being the angle between the x axis and the direction of propagation of the heat wave.

Thus if

$$h\cos\theta+k\sin\theta=0 \quad \text{or} \quad h/k=-\tan\theta \qquad (60)$$

the points of the scattering poles in the direction θ will be due entirely to the transverse wave.

If on the other hand

$$-h\sin\theta+k\cos\theta=0, \quad \text{or} \quad k/h=\tan\theta' \qquad (61)$$

the points in the direction θ' (at right angle to the direction θ) will be due entirely to the longitudinal wave.

As θ varies with h/k the experimental study of the diffuse thermal scattering in well-defined directions around a series of associated points (*hko*) will determine separately the velocities of the longitudinal and transverse waves in all directions. Figure 8 shows approximately the directions in which the scattering poles should be measured to obtain this information.

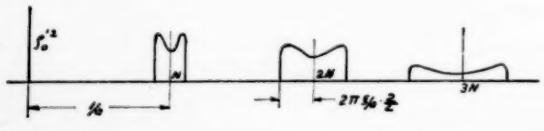

FIG. 7. Distribution of the structure factors squared in the reciprocal space for a sinusoidal wave of large amplitude. The disturbing wave has a wave-length L (the thickness of the crystal), its amplitude is ξ and the distance between atomic planes perpendicular to which the wave travels is a.

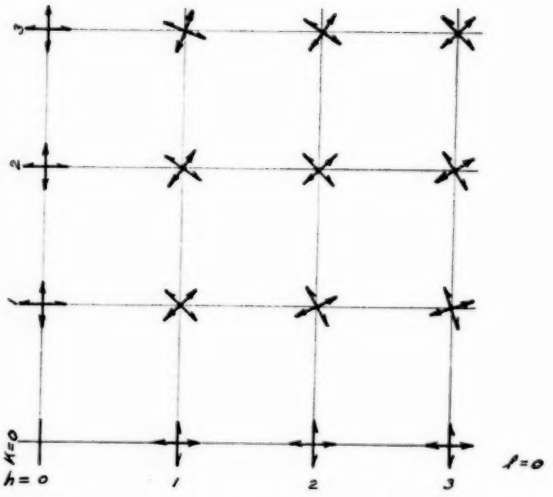

FIG. 8. Directions in which the scattering poles depend only on longitudinal waves (↔) or on transverse waves (⌒).

Scattering of Polarized X-Rays by Ferromagnetic Substances

ERIC RODGERS
University of Alabama, University, Alabama

(Received November 12, 1941)

It is shown that if high frequency polarized x-rays are scattered by some substance, the total intensity of the scattered rays should be altered by anything leading to special orientations of the electron spins of the scattering electrons. Some experiments are described in which attempts were made to detect the effect on intensity due to changes in spin orientations in ferromagnetic substances when these substances are magnetized. No effects were observed. It is shown that an attempt to reconcile the results of these experiments with those of gyromagnetic experiments leads to orientations of the spin giving the spin magnetic quantum numbers $+1/2$ and $-1/2$.

INTRODUCTION

SEVERAL attempts have been made to detect some effect of an applied magnetic field on reflections of x-rays by ferromagnetic substances.[1] These experiments have not been successful. No changes have been observed in position or intensity of the diffraction maxima. A change should have been observed if magnetization results in special orientations of the planes of the orbital electrons, but not if magnetization is caused by electron spin. The fact that gyromagnetic experiments on ferromagnetics always yield a value of approximately 2 for the Landé g factor indicates that ferromagnetism is associated with the spin. The present paper deals with the problem from a new approach in which polarized x-rays were used, and a phenomenon was used that should be sensitive to spin orientations.

It is well known that Thomson's classical theory of x-ray scattering predicts complete polarization for x-rays scattered at 90° to the primary beam by free electrons. This theory was modified by the quantum-mechanical treatment of Klein and Nishina in 1928. Nishina[2] showed that there should be an unpolarized component, the relative intensity of which varies approximately as the square of the frequency of the primary x-rays. The existence of an unpolarized component of the order of magnitude predicted has been shown experimentally.[3]

By taking electron spin into account, A. H. Compton[4] has shown that classical electrodynamics also predicts an unpolarized component that is proportional to ν^2. The unpolarized, or magnetic, scattering arises in classical theory from a precessional acceleration of the spin magnetic moment vector due to the torque on it of the magnetic vector of the x-ray wave. If γ is the magnetic moment of the electron and H the magnetic vector of the x-ray wave, this torque is

$$T=\gamma\times H. \tag{1}$$

If the Y axis be taken as the direction of propagation of the primary wave and the YZ plane be chosen to include OP, the direction of the scattered ray, Compton showed that the classical magnetic scattering of an electron is

$$I_s'=I_0\frac{4\pi^2\nu^2\gamma^4}{r^2c^4p^2}\sin^2\xi\sin^2\theta, \tag{2}$$

where I_0 is the intensity and ν the frequency of the primary wave, p is the angular momentum of the electron, ξ is the angle between γ and H, and θ is the angle between OP $(=r)$ and T. Averaging this expression over all possible orientations of the spin vector gave

$$I_s=I_0\frac{4}{3}\frac{\pi^2\nu^2\gamma^4}{r^2c^4p^2}[1+\sin^2\varphi\cos^2\alpha], \tag{3}$$

where φ is the angle between OP and the Y axis and α is the angle between H and the Z axis.

[1] M. de Broglie, Le Radium **10**, 186 (1913); K. T. Compton and E. A. Trousdale, Phys. Rev. **5**, 315 (1915); A. H. Compton and O. Rognley, Phys. Rev. **16**, 464 (1920); J. C. Stearns, Phys. Rev. **35**, 1 (1930).
[2] Y. Nishina, Zeits. f. Physik **52**, 869 (1928).
[3] E. Rodgers, Phys. Rev. **50**, 875 (1936).
[4] A. H. Compton, Phys. Rev. **50**, 878 (1936).

The appearance of $\sin^2\xi$ and $\sin^2\theta$ in (2) shows that the magnetic scattering by a single electron depends sharply on the orientation of the spin vector. Equation (3) would not be expected to apply if the spins were not oriented at random, but were oriented so as to have a strong component in some definite direction. Gyromagnetic experiments indicate that magnetization of ferromagnetic bodies may result in just such orientations. Some experiments have recently been done by the writer with the purpose of attempting to determine whether magnetic scattering of polarized x-rays by ferromagnetic substances is influenced by an applied magnetic field.

EXPERIMENTAL PROCEDURE

The conventional experimental procedure was used to produce and study the polarized x-rays. The primary rays were directed toward a block of carbon and a beam of rays scattered by it at 90° to the primary beam was again scattered, this time by the ferromagnetic substance under investigation. Intensity measurements of the tertiary rays were made at a point P in a direction at 90° to both the primary and secondary rays. According to the classical theory of Thomson, the intensity in this direction ought to be zero. Actually there are three reasons why it is not zero. The first reason is geometrical in nature. Since the scattering substances do not have zero dimensions, some rays that have not been scattered at exactly 90° will arrive at P. Secondly, some rays will be scattered more than once in each scatterer, and some of the multiply scattered rays will reach P. In the third place some magnetically scattered rays that are unpolarized will reach P. The magnetic scattering is negligible when the x-ray tube is operated at low voltages but becomes appreciable at voltages of 200 kilovolts or higher.

The relative intensities of the three types of scattering to P can be estimated roughly. The "geometrical" scattering can be calculated from the dimensions of the apparatus. Such a calculation for the apparatus used shows that this scattering should be about 0.012 I' where I' is the intensity of the tertiary rays at a point P' ($OP' = OP$) in a direction at 90° to the secondary rays but parallel to the primary rays. The intensity due to multiple scattering can only be estimated experimentally. Following a method used by Compton and Hagenow,[5] this was done by using different thicknesses of the scattering substances and noting the effect on the polarization obtained. The results obtained indicated that the intensity reaching P by multiple scattering was about 0.036 I'. The magnetic scattering to P can be calculated from either Compton's or Nishina's formula if the wave-length of the primary x-rays is known. Throughout all the experiments the x-ray tube was operated at 220 kilovolts and the primary rays filtered through 0.7 mm of copper and 0.5 mm of aluminum. Under such circumstances, it would seem reasonable to assume that the effective wave-length is about 0.10 angstrom. If this value be used in Nishina's formula, we get for the magnetic scattering to P the intensity 0.038 I'. A result of the same order of magnitude would be obtained if Compton's formula were used. If we add the intensities for the three types of scattering, we see that the magnetic scattering accounts for about 44 percent of the total that should reach P.

The ferromagnetic substance being studied was cut into a thin slab and mounted so that each of its ends was in contact with one of the pole pieces of a powerful electromagnet. Lead was used to shield the pole pieces from the x-rays. The substances studied consisted of several samples of iron and permalloy. A Geiger-Müller counter was used to determine the relative intensities of the tertiary rays with the magnet off and then on.

It was found in all the experiments that magnetizing the sample did not make the slightest detectable difference in the intensity of the rays scattered to P. This was true regardless of whether the sample was magnetized parallel or perpendicular to the magnetic vector of the polarized x-rays. No high degree of accuracy can be claimed for the intensity measurements, but it is believed that a change of 2 or 3 percent in intensity would not have escaped detection.

[5] A. H. Compton and C. F. Hagenow, J. Opt. Soc. Am. and Rev. Sci. Inst. **8**, 487 (1924).

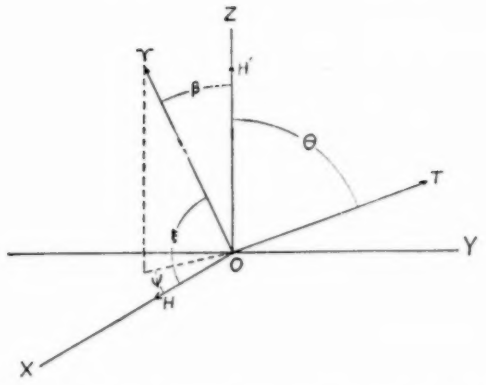

FIG. 1. Orientation of x-ray beam, sample, and applied field.

DISCUSSION OF THE RESULTS

When the sample is magnetized parallel to the magnetic vector of the x-rays, the magnetic scattering ought to vanish if all electron spins should be oriented parallel to the field. This, as we have seen, would cause a reduction of about 44 percent in the intensity at P. When the sample is magnetized perpendicular to the magnetic vector, a calculation based on Compton's results shows that orientation of the spins parallel to the field should cause the total intensity at P to be practically doubled. Such ideal orientations were, of course, not expected. It would seem reasonable, however, to expect some change in intensity if ferromagnetism is associated with special spin orientations as indicated by gyromagnetic experiments.

Assuming that the scattering electrons of ferromagnetic substances do take up special orientations when the sample is magnetized, we shall now inquire as to whether any such orientations are possible for which the scattering is the same as for random orientations. We shall indicate by β any angle that the spin axes may assume with the field such that the scattering is unaltered, and then determine what values β may have. The computations will be carried out for the case in which the applied field is perpendicular to the magnetic vector of the x-rays. The same values of β are obtained when computations are made for the field parallel to the magnetic vector.

In Fig. 1 the polarized x-rays are considered to move along the Y axis with the magnetic vector in the XY plane. The sample is at the origin and the applied field H' is along the Z axis which is also the direction of observation of the scattered rays. The spin vector γ is assumed to make a constant angle β with the applied magnetic field. The angles ξ and θ of (2) are shown in the figure. Since T is perpendicular to both γ and H, it lies in the YZ plane. In order to compute the scattering for a constant value of β, we must compute the average value of $\sin^2\xi$ $\sin^2\theta$ in Eq. (2) for this value of β. This may be done in the following manner.

The direction cosines of T are

$$0,\ \sin\theta,\ \cos\theta,$$

and those of γ are

$$\cos\xi,\ \pm(1-\cos^2\xi-\cos^2\beta)^{\frac{1}{2}},\ \cos\beta.$$

Since T is perpendicular to γ

$$\pm\sin\theta\ (\sin^2\xi-\cos^2\beta)^{\frac{1}{2}}+\cos\theta\ \cos\beta=0.$$

This gives

$$\sin^2\theta\ \sin^2\xi-\sin^2\theta\ \cos^2\beta=\cos^2\theta\ \cos^2\beta$$
$$=\cos^2\beta-\sin^2\theta\ \cos^2\beta,$$

or

$$\sin^2\theta\sin^2\xi=\cos^2\beta.$$

Thus we see that $\sin^2\theta\ \sin^2\xi$ has the constant value $\cos^2\beta$.

To get the scattering for this orientation of the spin we simply substitute $\cos^2\beta$ for $\sin^2\xi\ \sin^2\theta$ in (2). We shall write the result as

$$I_s'=4K\cos^2\beta, \tag{4}$$

where K represents a constant factor.

To compute the scattering in the Z direction of the polarized rays for random orientations, we can either use Eq. (3) by noting that $\alpha=90°$ and $\varphi=90°$, or we can average (4) for all values of β. We could do the latter by evaluating the following integral

$$I_s=\frac{1}{4\pi}\int_0^{\pi}\int_0^{2\pi}4K\ \sin\beta\ \cos^2\beta d\psi d\beta.$$

Either method gives

$$I_s=\frac{4}{3}K. \tag{5}$$

We now obtain the possible values of β by equat-

ing the scattering from (4) and (5) which leads to the expression

$$\cos\beta = \pm\tfrac{1}{3}\sqrt{3}. \qquad (6)$$

We thus see that there are two orientations of the spins which give the same scattering as random orientations. These values of β are of special interest because they are just the angles necessary to give the spin magnetic quantum numbers $+\frac{1}{2}$ and $-\frac{1}{2}$ that are demanded by the theory of spectra. It is of further interest to note that they are arrived at here by classical electrodynamics in an attempt to reconcile experimental results.

JANUARY 1 AND 15, 1942 PHYSICAL REVIEW VOLUME 61

The Discharge Mechanism of Fast G-M Counters from the Deadtime Experiment

H. G. STEVER*
California Institute of Technology, Pasadena, California
(Received November 15, 1941)

The deadtime of a self-quenching counter is an insensitive time, of the order of 10^{-4} second, which occurs between the time when a counter registers a count and the time at which it has recovered sufficiently to register another count. A simple method of measurement of this time is shown. From a theory developed to explain this deadtime phenomenon it is possible to compute times associated with the deadtime. The check between theory and experiment is very good. The theory involves the formation of a positive ion space charge sheath about the wire of the counter, this sheath expanding to the cylinder. Not only is it possible to show the internal action of a counter by the deadtime experiment, but also it is possible to study the lengthwise spread of that discharge. It was found that the discharge spread throughout the length of the counter, but the spread could be stopped by a small glass bead on the wire. This discovery led to the construction of a directional Geiger counter.

I. INTRODUCTION

A. Historical

SINCE the publication of the original works on G-M counters in 1928 and 1929 by Geiger and Müller,[1] there have been numerous articles concerned with construction techniques, operating properties and theories of discharge of G-M counters. In 1936 the value of the G-M counter as a laboratory instrument was greatly increased by the design of the Neher-Harper[2] extinguishing circuit. Around 1935 and 1936, independently in several laboratories, the fast, or self-quenching, G-M counter was discovered and used. In construction, the fast counters differed from the usual G-M counter only in the addition of alcohol vapor or some other organic vapor to the gas. Many of the operating properties of fast counters were investigated by Trost.[3] The properties of the fast counters differed from those of the usual type G-M counter, here termed a slow counter. In 1940, based primarily on experimental measurements by Ramsey,[4] Montgomery and Montgomery[5] formulated a consistent theory of G-M counter action.

In this present investigation of fast counter action, the most illustrative experiment is that showing the deadtime phenomenon. The deadtime technique herein developed can be used to study the lengthwise spread of the discharge within the G-M counter tube.

* Now at Massachusetts Institute of Technology Electrical Engineering Department, Cambridge, Massachusetts.
[1] H. Geiger and W. Müller, Physik. Zeits. **29**, 839 (1928); *ibid.* **30**, 489 (1929).
[2] H. V. Neher and W. W. Harper, Phys. Rev. **49**, 940 (1936).
[3] A. Trost, Zeits. f. tech. Physik **16**, 407 (1935); Physik. Zeits. **36**, 801 (1935); Zeits. f. Physik **105**, 399 (1937).
[4] W. E. Ramsey, Phys. Rev. **57**, 1022 (1940).
[5] C. G. Montgomery and D. D. Montgomery, Phys. Rev. **57**, 1030 (1940).

B. Experimental Properties of Fast Counters

In the analysis by Montgomery and Montgomery,[5] the action of G-M counter discharge is pictured as the rapid formation of a positive space charge sheath about the counter wire, followed by the removal of this sheath of positive ions to the cylinder. They then point out that the difference between the action of counters with organic vapor and the action of those without is that, in the organic vapor counters, there are no secondary electrons produced during, or after, the arrival of positive ions to the cylinder, whereas, with the non-organic vapor counters, there are formed secondary electrons which continue the discharge unless the voltage is dropped below threshold, when the positive ions arrive at the cylinder. Although this is not the only difference, as will be shown later, it is still sufficient to necessitate the use of different circuit constants with these two type counters. The action of the organic vapor counter circuit is faster than that of the other type; hence, the names fast and slow counters.

In discussing the experimental properties of a G-M counter, or in comparing different types of counters, it is best to refer to the properties exhibited by the counter when operated in the fundamental G-M counter circuit, shown in Fig. 1, lest the action of a more complicated circuit mask, or change, the properties of the counter. The fundamental circuit consists of the counter, a voltage source and a resistance R in series. There is included a capacity C across the resistance R; this capacity represents the sum of the capacity-to-ground of the counter wire and leads, plus the capacity-to-ground of

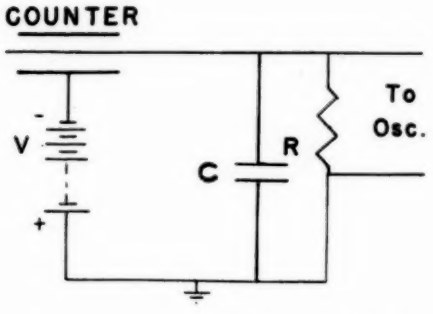

FIG. 1. The fundamental G-M counter circuit. In this circuit which is used in the deadtime experiment, a fast counter will quench with any value of R and C.

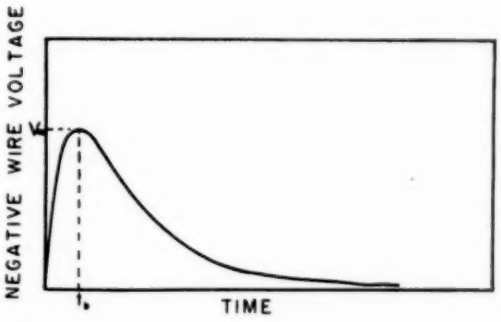

FIG. 2. A typical voltage pulse from a fast counter. As viewed on an oscilloscope with a linear sweep, the voltage across R during a pulse is shown here.

the input of the oscilloscope, or recording circuit, which is being used.

The results of experiments performed in the earlier portion of this investigation enhance previous experimental evidence for certain properties of counters. The results are summarized:

1. Fast counters quench in the fundamental circuit independently of the magnitude of the series resistance R. A fast counter was operated with several values of resistance from 10^9 ohms down to 10^2 ohms. Even with zero series resistance, the fast counter did not go into continuous discharge.

2. The amount of charge which flows in a single pulse in a given fast counter is practically independent of the circuit constants, other than voltage.

3. The voltage across the fast counter does not drop necessarily to the threshold voltage in a pulse. The voltage change may vary anywhere from zero voltage to a value considerably more than the overvoltage which is defined as the voltage above threshold at which the counter is operated. Since the charge is independent of circuit constants, the voltage change in a single discharge should vary inversely as the value of C. This was found to be true if both R and C were varied to keep the product RC constant.

4. The *sine qua non* of fast counter action is the organic vapor present in the gas. Of course, treatment of cylinder walls, choice of material, etc. determines the quality of the counter but, regardless of other treatment, if a counter has organic vapor in it and if it functions at all, it functions as a fast counter.

II. THE DISCHARGE MECHANISM FROM THE DEADTIME THEORY

A. The Deadtime Phenomenon

The phenomenon of the deadtime of a fast G-M counter was found in the course of experiments to measure directly the voltage-time characteristics of a single fast counter pulse. Figure 2 is a drawing of a typical fast counter pulse as estimated from random pulses viewed on an oscilloscope screen. The counter is operated in the fundamental circuit. The breakdown time t_b is extremely short, of the order of 10^{-5} second. Since the writing speeds on an oscilloscope screen, which were necessary for a reasonable size pulse, were greater than those which can be photographed, it was not possible to photograph the single pulses. However, this difficulty was surmounted by using the fact that the pulses from a fast counter are identical in size and shape. An electronic circuit was devised so that many pulses could be superimposed on an oscilloscope screen, thus making the pattern intense enough to photograph. A discussion of the circuit and the experimental procedure will be discussed later.

In the deadtime experiment, the fundamental circuit is used. The vertical plates of an oscilloscope are connected across the resistance R so that the voltage change on the wire during a pulse is delivered to the vertical plates. A small portion of the first part of a voltage pulse is used to trigger off the electronic circuit which then delivers a linear sweep voltage to the horizontal deflecting plates of the scope. The beam is normally at rest at the side of the screen. When an ionizing particle triggers off the counter, the beam traces over the voltage *versus* time curve. This, of course, presupposes that the sweep starts rapidly enough so that the vertical deflection is not very great before the sweep starts. After tracing over a pulse the beam returns to its normal position and awaits another triggering pulse. With a high counting rate, due to a suitably placed radioactive source, the pulse will be traced over and over. With the high intensity of the pattern on the screen due to the superposition of many pulses, the shape can be photographed.

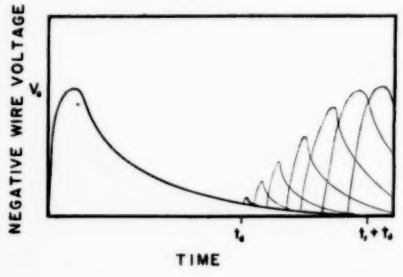

FIG. 3. Drawing of oscilloscope pattern of the result of the deadline experiment. This shows the deadtime t_d and the recovery time t_r. The time (t_d+t_r) corresponds to the arrival of the positive ion sheath at the cylinder. The time t_d corresponds to the point in the transit of the positive ions at which the field about the wire has returned to threshold field.

At a high counting rate there will be numerous pulses from the G-M counter, which arrive after the beam has started to trace over the pattern but before it has returned to its original position. These pulses register on the vertical plates but in no way affect the horizontal sweep. These pulses are expected to occur at random all across the horizontal sweep if the counter is sensitive all the time. *Experimentally, this is not the case.* Figure 3 is a drawing of the actual pattern as viewed on the oscilloscope screen. It is seen that the G-M counter is insensitive for a time t_d, the deadtime of the counter. This deadtime, measured experimentally, is of the order of 10^{-4} second. Moreover, when the counter does regain its sensitivity to ionizing particles, it is not capable of registering a full voltage pulse but regains that ability in the time t_r which is the time from t_d to the appearance of full size pulses. This time t_r is also of the order of 10^{-4} second.

The single traces occurring in increasing size from t_d to (t_r+t_d) cannot be photographed due to their low intensity. However, Fig. 4 is a time exposure taken of the oscilloscope screen, showing clearly the integrated effect of the following pulses as they build up in size from t_d to t_r+t_d. Note that the RC time constant of the fundamental circuit is smaller in the case of the photograph than in the case represented by the drawing; hence the sharp, short pulse in the photograph.

It is wise to examine what this deadtime implies as to the limits of the use of fast counters. It does not imply that fast counters cannot be used in highly resolving coincidence circuits

for that use depends on the speed of breakdown. It does however fix the limit on numbers of particles counted per second since the closest together two pulses may occur is of the order of 10^{-4} second. This closest spacing is constant regardless of the shortness of the RC constant.

B. Postulated Mechanism of Fast Counter Action

The deadtime phenomenon is of importance because of the conclusive evidence it presents for a postulated discharge mechanism of fast counters. With the experimental evidence presented above, and former knowledge of fast counter behavior, this postulated mechanism must account for: (1) the very rapid breakdown time of 10^{-5} second or faster; (2) the deadtime, or insensitive time; (3) the building up in pulse size from the deadtime to the recovery time.

Consider a fast G-M counter in the fundamental circuit. When an ionizing particle passes through the counter, in order to be detected, it must form at least one ion pair consisting of a positive ion and an electron, or else knock a photoelectron out from the walls. The electron, or electrons, formed anywhere within the volume of the counter, is accelerated toward the wire. In the region about the wire, cumulative ionization takes place. By some process, as yet unspecified, the discharge spreads along the wire throughout the entire sensitive length of the counter, so that, in the neighborhood of the wire, along its entire length, there is an ion sheath consisting of positive ions, electrons, and probably some negative ions formed by electron capture by neutral atoms. This whole action is assumed to take place in a very short time. Since the ionization took place in the immediate neighborhood of the wire, the electrons and negative ions have but a short distance to be moved by the electric field before they are collected on the wire. This leaves a positive ion space charge sheath around the wire. Of course, this positive space charge would have moved a short distance toward the cylinder while the negatives were being collected on the wire. By this separation of charge the field between the wire and the positive space charge sheath is so reduced that no more ionization can take place. It is interesting and important to note that the charge collected in a single pulse sometime exceeds that necessary for charging the counter to its operating voltage.

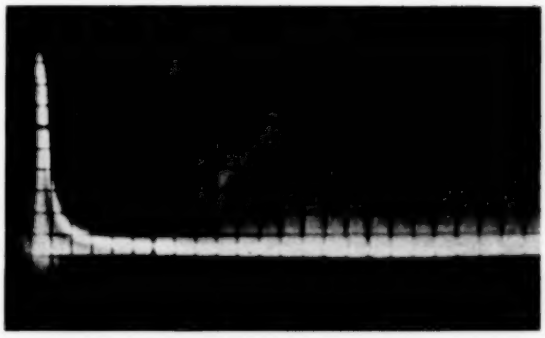

FIG. 4. Time exposure of oscilloscope pattern of the results of the deadtime. This is a one-minute time exposure of the pattern drawn in Fig. 3. Note the envelope of the follow pulses as they build up from t_d to (t_d+t_r).

In this analysis, the fact that the G-M counter is in the fundamental circuit must not be overlooked. Only fast counters are considered here, so the value of the series resistance R may be low. The separation of the positive and negative charges causes the voltage on the wire to drop. This lowering of the wire voltage would continue as the positive ions moved out from the wire region if it were not for the relatively low resistance (10^5). The negative charge collected on the wire leaks off the wire at a rate determined by the RC time constant, so that the voltage V is reapplied across the counter before the positive ion sheath moves very far. The shape of the voltage pulse on the wire is that shown in Fig. 2.

The action of the external circuit is to reapply the working voltage across the counter. This may be accomplished in a very short time, of the order of 10^{-5} second, depending on RC. Even though the voltage is returned to working voltage, the presence of the positive ion space charge sheath lowers the amount of positive charge on the wire, which is necessary for the working voltage to be reapplied. Hence, the field in the region between the wire and the positive ion sheath is so lowered that no more ionization can take place. Even though an ionizing particle passed through the counter, there would be no cumulative ionization about the wire due to the field lowering by the positive ion sheath. This accounts for the internal quench-

ing of a fast counter. It also accounts for the deadtime. As the positive ion space charge sheath moves toward the cylinder, the field about the wire increases since the positive charge on the wire increases in order to keep the voltage across the counter at working voltage. When the space charge sheath has reached a critical distance R, the field about the wire has just returned to threshold counting field, at which time counts may again be recorded. Threshold counting field is defined as that field which exists when the counter is at threshold voltage, with no positive ion space charge sheath present. As the positive ion sheath continues to move to the cylinder, the field builds up from threshold field to the operating field, the latter being reached when the positive ions arrive at the cylinder. Any ionizing particle which goes through the counter would cause a smaller pulse than normal on the oscilloscope if the field were between threshold field and operating field. This is due to the fact that the amount of charge which flows in a single counter pulse depends on the voltage, hence, the field, above threshold at which the counter is being operated.

This picture accounts qualitatively for the observed phenomena. Many observers have postulated the quenching of the ionization by space charge lowering of the field. Some observers[3, 6, 7] have credited an insensitive time to the removal of positive ions. All of their methods were indirect and all of their arguments were qualitative, merely indicating that the order of magnitude of the time was that of positive ion migration. It is to be noticed that the formation and removal of a positive ion sheath postulated above is identical with the mechanism postulated by Montgomery and Montgomery.[5]

C. Deadtime Theory Developed Electrically

The electrical analysis of the mechanism postulated above is to be carried out as a two-dimensional problem, in which end effects are neglected. Figure 5 is a cross-sectional diagram which shows: the wire, of radius a, with a positive charge, Q per unit length; the positive ion space charge, q per unit length at a distance r_0 from the center; and the cylinder of radius b with a negative charge, $-(Q+q)$ per unit length. Assume that there is a potential V across the counter at this time.

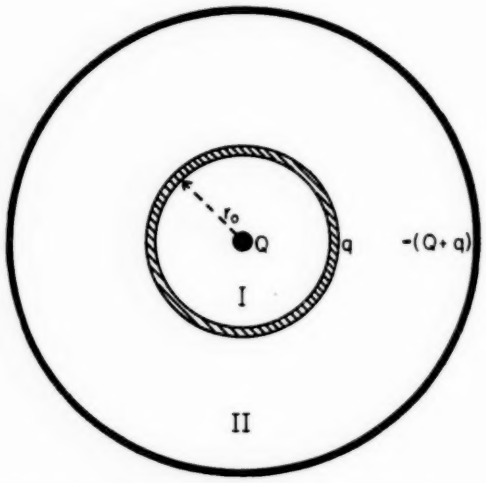

FIG. 5. Cross-sectional view of counter. This shows the positive ion space charge sheath at a point r_0 from the center of the counter.

The field in region I, between the positive ion space charge and the wire, is

$$E_{\mathrm{I}}=2Q/r, \tag{1}$$

where r is the variable distance. In region II the field is

$$E_{\mathrm{II}}=2(Q+q)/r. \tag{2}$$

Since the potential across the counter is V,

$$-V=\int_a^{r_0} E_{\mathrm{I}}dr+\int_{r_0}^{b} E_{\mathrm{II}}dr, \tag{3}$$

and by (1) and (2)

$$-V=\int_a^{r_0}\frac{2Q}{r}dr+\int_{r_0}^{b}\frac{2(Q+q)}{r}dr. \tag{4}$$

Integrating, we have

$$-V=2Q\log(b/a)+2q\log(b/r_0). \tag{5}$$

The charge Q which is necessary for a voltage V, with the other conditions as outlined, is

$$Q=\frac{-1}{2\log(b/a)}\left[V+2q\log\frac{b}{r_0}\right]. \tag{6}$$

[6] H. Aoki, A. Narimatu, and M. Siotani, Proc. Phys. Math. Soc. Jap. **22**, 746 (1940).
[7] L. B. Loeb, *Fundamental Processes of Electrical Discharge in Gases* (John Wiley and Sons, New York, 1939).

The negative integral of E_1 across the counter is now defined as an effective voltage V_e. This effective voltage is the apparent voltage across the counter with reference to counting action, for, when this voltage is above threshold voltage, the field in the sensitive region around the wire is above threshold field so that the counter will count ionizing particles.

$$-V_e=\int_a^b \frac{2Q}{r}\,dr$$

$$=\frac{-1}{\log(b/a)}\int_a^b \frac{[V+2q\log(b/r_0)]}{r}dr. \quad (7)$$

Integrating,

$$V_e=V+2q\log(b/r_0). \quad (8)$$

From the postulated mechanism, when V_e equals the threshold voltage V_t, the counter just begins to count, so that then r_0 is the critical distance R. Hence

$$V_t-V=2q\log(b/R). \quad (9)$$

Since both V and V_t are negative voltages, for simplicity, drop the negative sign and consider only the absolute difference. Then

$$R=b\exp[-(V-V_t)/2q]. \quad (10)$$

The critical distance R defining the deadtime is found.

In the experiments to measure deadtime and to check this theory, the wire capacity was relatively high (around 10^{-10} farad), and the resistance relatively low (around 10^5 ohms), so that the voltage pulses were small, and the RC recharging time was short. Then, throughout the entire pulse, V varied very little from V_0. To a very good approximation

$$R=b\exp[-(V_0-V_t)/2q]. \quad (11)$$

The quantity, V_0-V_t, is now termed the overvoltage V_u, or the voltage above threshold at which the counter is operated. Hence, for the experiments to check the theory

$$R=b\exp[-V_u/2q]. \quad (12)$$

D. Ion Mobilities

The experiment described in Section II, A furnishes a method to measure t_d the deadtime and t_r the recovery time, directly. In order to check the theory developed above in Section II, C, an expression for either t_d or t_r in terms of R and other constants of the counter is needed. For this, an understanding of gas ion mobilities is necessary. Loeb[7, 8] discusses the subject both from a theoretical and experimental point of view. Due to the great complexity of the field of gas ion mobilities, it is possible, for the purposes of this work, to examine only those factors directly affecting the ion mobilities in a G-M counter.

The mobility constant is the ratio of the velocity of the ion in question to the field strength:

$$k=\frac{dr}{dt}\Big/E_r \quad (13)$$

usually expressed in cm/sec./volt/cm. Theoretically, the mobility constant should vary inversely as the number of molecules per unit volume, as measured by the pressure. Loeb[7] states that this law has been verified for pressures from 0.1 mm to 60 atmospheres, so that in the G-M counter work, with pressures ranging from several millimeters to 25 or 30 cm, the law will hold;

$$k=Kp/p_0, \quad (14)$$

where K is the mobility at atmospheric pressure, and p/p_0 is the ratio of the pressure in the G-M counter to normal pressure. The slight temperature dependence of the mobility constant plays no role in the counter experiments for these experiments are carried out at room temperature where most mobility measurements are made.

In self-quenching G-M counters the gas filling is a mixture of, say, a noble gas such as argon and an organic vapor such as alcohol, xylol, or petroleum ether. The simple theoretical expression for the mobility constant of a mixture of gases A and B is

$$k=K_AK_B/(C_AK_B+C_BK_A), \quad (15)$$

where K_A and K_B are the respective mobilities of the pure gases, and the constants C_A and C_B are the partial pressures of the respective

[8] L. B. Loeb, *Kinetic Theory of Gases* (McGraw-Hill, New York, 1927).

components;

$$C_A=P_A/(P_A+P_B), \quad C_B=P_B/(P_A+P_B). \quad (16)$$

Loeb[8] has pointed out that many mixtures do not follow that law and, from his experiments, gives another law,

$$K=K_AK_B/(C_AK_B^2+C_BK_A^2)^{\frac{1}{2}}. \quad (17)$$

It is safe to say that, unless data are taken on the mobility of the particular gas mixture used, one cannot be certain of the true mobility. However expressions (15) and (17) are the first approximations.

After a time of the order of 10^{-2} second has elapsed following the formation of the positive ions, their mobilities become smaller probably due to attachment of neutral atoms, resulting in a higher effective mass for the ions. Since the ions migrate to the cylinder in a time less than a tenth of that, the values for newly formed positive ions must be used. These values usually are the same as for negative ions.

In the use of mobility constants, a very critical matter is their dependence on field strengths. At the surface of the wire there is a field higher than 10^4 volts per cm. At the surface of the cathode the fields are considerably reduced, to around 10^2 volts per cm or less, depending on the radius of the cylinder. Loeb[7] and Druyvesteyn and Penning[9] point out that the ratio E/p, usually expressed in volts/cm/mm, is the essential criterion for the energy which ions acquire between collisions. The variation of K with that ratio is important. For a counter with 10-cm pressure, the E/p ratio is around 100 volts/cm/mm at the wire, and at the cylinder it is about 1 volt/cm/mm. Loeb[7] lists, for various gases, the critical ratio below which the mobility constant does not vary with E/p. These critical ratios vary from about 5 volts/cm/mm to about 80 volts/cm/mm. For argon the value is about 5 volts/cm/mm.

Above the critical ratio the mobility constant is no longer constant with a variation of E/p. As E/p is increased, the mobility increases first and then decreases. The functional relationship of this is not known and, moreover, it varies considerably from gas to gas. Hence, an accurate analysis of the deadtime problem is not possible in the region of the wire. However, the recovery time was indicated as that time which the ions needed to migrate from the critical distance to the cylinder. This region is the low field region. The value of the ratio of E/p is below the critical value so that the expression for the recovery time is calculable using the mobility constant as truly a constant.

[9] M. J. Druyvesteyn and F. M. Penning, Rev. Mod. Phys. **12**, 87 (1940).

E. Expression for Recovery Time

The expression for the recovery time is derived rather simply. From (13) the element of time taken for the positive ion sheath to move a distance dr is

$$dt=dr/kE. \quad (18)$$

In this expression E is the field acting on the positive ion sheath. This field is

$$E=E_I+(q/r). \quad (19)$$

The q/r is due to the fact that the force on a surface charge density σ, due to the field of the rest of the surface charge, is $\frac{1}{2}E\sigma$. Hence

$$E=\frac{2Q_0}{r}+\frac{2q}{r}\left[\frac{1}{2}-\frac{\log(b/r_0)}{\log(b/a)}\right], \quad (20)$$

where Q_0 is the charge on the counter when a potential V_0 is across the counter. Note that the second term in the brackets is small compared with $\frac{1}{2}$ for $r_0=R$, so that it may be neglected. R, experimentally, is from $\frac{1}{3}$ to $\frac{2}{3}$ of the radius of the cylinder. With this analysis it is seen that the positive space charge is moving in a field equivalent to that from $Q_0+\frac{1}{2}q$ on the wire. Hence, the effective potential across the counter is

$$V=V_0+q\log(b/a). \quad (21)$$

The field in (1) is

$$E=\frac{V}{\log(b/a)r}, \quad (22)$$

so that (18) becomes

$$dt=\frac{r\log(b/a)dr}{kV}. \quad (23)$$

The recovery time t_r is obtained by integrating this from R to b.

$$t_r=\frac{(b^2-R^2)\log(b/a)}{2kV}. \tag{24}$$

With the pressure dependence of k substituted in,

$$t_r=\frac{(b^2-R^2)(p/p_0)\log(b/a)}{2KV}. \tag{25}$$

If the mobility constant could be correctly assumed constant or if an expression of its variation with field strength were known, the deadtime could also be calculated by integration of (23) from a to R. By assuming the former, we have

$$t_d=\frac{(p/p_0)(R^2-a^2)\log(b/a)}{2KV}. \tag{26}$$

This will be shown to give erroneous results.

III. EXPERIMENTAL VERIFICATION OF THE DEADTIME THEORY

A. Measured Quantities

From the postulated mechanism of G-M counter discharge presented in Part II B, there was derived (25), the expression for the recovery time where R is given by (12) and V is given by (21). In order to verify the postulated theory, the recovery time is measured, and compared to the recovery time as calculated from (25). That t_r may be calculated from (25) is seen in an examination of the quantities which appear in the expression. The radii of the wire and cylinder, the pressure, the operating voltage, and the voltage above threshold, are all directly measurable. If the composition of the gas is known, the mobility constant is calculable in a very good first approximation from the expressions given in Part II D. This leaves only the charge per unit length in the positive ion space charge sheath. The total charge which flows in a single pulse is measured quite simply. The voltage source is replaced by a low leakage condenser which is charged to operating voltage. Care is taken to reduce the leakage between the counter wire and cylinder to a minimum. If one then measures a small change in voltage ΔV which takes place in a time t, the total charge which flows in a single pulse is

$$q_l=C\Delta V/st.$$

s is the counting rate of the counter, and C is the capacity of the condenser which is charged to operating voltage. Since it was assumed that the counter breaks down along its whole length, so that the charge in the space charge sheath is uniform along the length of the counter, the charge per unit length in the space charge sheath is found by dividing q_l by the length of the counter.

Experimentally, it was found that q varied approximately linearly with overvoltage, for a given counter and a particular gas mixture. This linear relationship held for different pressures and different threshold voltages, if the same mixture were kept in the counter. From (12), this linear relationship fixes the critical distance R as a constant for a given counter. There is no theoretical significance placed on this linear relationship. In fact, since there was some indication that it broke down for high values of V_u, it is shown that it does not hold in all cases. Nevertheless, when it does hold, it simplifies calculation, and enables one to speak of a particular critical distance, characteristic of a given counter. In the calculation of V for different conditions, each separate value of q must be substituted.

B. Experimental Measurement of the Recovery Time

In Part II A, it was pointed out that the deadtime phenomenon was discovered in the course of experiments to measure the voltage-time characteristics of the G-M counter pulse. A writing speed of about 10^5 inches per second on the oscilloscope screen is needed to get a pattern of the fast breakdown of the G-M counter. From data given in a commercial cathode-ray tube catalog,[10] this is about 10 times as fast as it is possible to photograph in a single trace. For that reason a superimposition of pulses was required. Several methods were tried. Since two of the methods can be used in the deadtime work, they will be discussed.

[10] Catalog B, Allen B. Dumont Laboratories, Inc. Passaic, New Jersey.

In most oscilloscopes the linear sweep on the horizontal is furnished by the sawtooth voltage pulses from a gas discharge, relaxation oscillator, which employs a Type 885 gas triode tube. Single sweeps are obtained by biasing the gas tube sufficiently high that the ratio of plate voltage to negative grid voltage does not exceed the firing ratio which is in general about 10. To trigger the single sweep, a positive pulse is fed onto the grid. When fired, the tube discharges a condenser in the plate circuit till the plate voltage drops sufficiently for the grid to take control again. Then the first part of the *RC* exponential recharging of the condenser is used as the linear sweep. Since the time of firing the gas tube is about 10^{-5} second it is impossible to get the breakdown portion of the G-M counter pulse on the linear sweep. However, it is possible to measure the deadtime and recovery time since they are of the order of 10^{-4} second. For the work here reported, an RCA 155 oscilloscope was made to work as a single sweep instrument by increasing the bias on the 884 relaxation oscillator tube. In practice it was not possible to get away from a non-linear return sweep but the return sweep was calibrated with a sine wave oscillator so the difficulty was surmounted.

A more convenient method of getting the deadtime pattern also originated in attempts to measure the breakdown characteristics. It has several advantages over the method described above. In it, a different circuit is used to obtain the single horizontal sweep. When triggered, the circuit starts the electron beam of the oscilloscope across the screen in a linear sweep at the end of which it returns it rapidly. This is a decided advantage over the relaxation oscillator which first swings the beam across the screen and returns it in an exponential sweep, for, in the latter case, part of the pulse to be measured is over before the sweep starts.

The circuit is diagramed in Fig. 6. A positive pulse is fed onto the grid of T_1 from the cylinder of the G-M tube. T_1 is an isolation stage to prevent feedback from the rest of the circuit to the fundamental circuit. This feedback would distort the characteristics of the negative pulse which is fed onto the vertical plates of the oscilloscope from the wire of the G-M counter. A negative pulse is then passed onto the grid of T_2 which, together with T_3, acts as a multivibrator biased to prevent self-oscillation. The circuit characteristics of multivibrators are discussed adequately by Neher[11] or in many electronics textbooks. Briefly, its action is described here. A negative pulse fed onto the grid of T_2 starts to cut off the current, for normally T_2 is conducting. This action passes a positive pulse through the large condenser C_6 to the grid of T_3, which normally is biased to cut off. The negative pulse which T_3 puts out is fed back onto the grid of T_2 through the condenser C_5. This causes T_2 to become even less conducting. The result of this action is that the plate of T_3 drops in voltage very rapidly. When the charge on the grid of T_2 has leaked off, the whole action is reversed. The result is a square pulse output from the plate of T_3. The natural length of this square pulse is determined by the *RC* discharge rate of the grid of T_2. The resistance R_6 is variable so that the length of the square pulse can be changed. The square pulse output from T_3 is fed onto the grid of T_4 which is normally in a conducting state. The plate is nearly at ground potential, most of the voltage drop being across the resistance R_{14}. The condenser C_{10} is charged to a voltage i_pR_{14}, where i_p is the plate current of T_4 in the conducting state. Since the plate voltage swing of T_3 is nearly the full 250 volts, T_4 is cut off completely. C_{10} begins to discharge through R_{14} and continues until T_4 again becomes conducting. If the natural length of the multivibrator pulse is shorter than the $R_{14}C_{10}$ time constant, the voltage pulse from the plate of T_4 is a nearly perfect sawtooth. This voltage pulse is fed onto the horizontal plates of the oscilloscope. The linear sweep which it causes starts with a time delay of around 10^{-6} second from the time T_1 receives the trigger pulse.

The circuit described above was used in obtaining the picture of the deadtime and the recovery time shown in Fig. 4. With it, measurements of the recovery time and the deadtime may be made. It is not necessary to photograph the pattern on the oscilloscope screen, for visual

[11] H. V. Neher, in *Procedures in Experimental Physics* by John Strong (Prentice-Hall, New York, 1928).

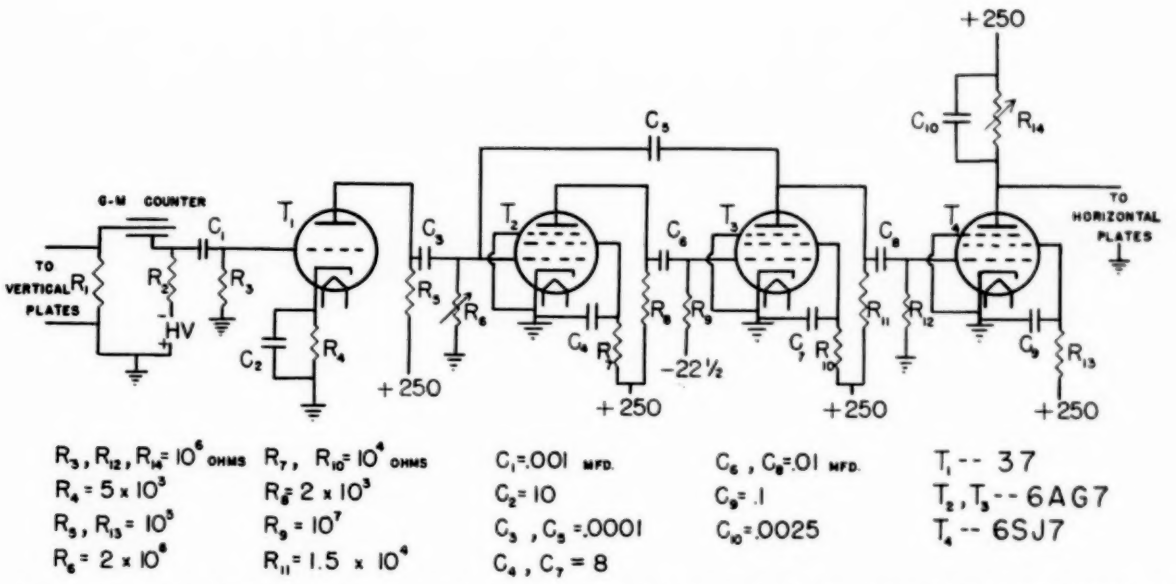

$R_3, R_{12}, R_{14} = 10^6$ OHMS $R_7, R_{10} = 10^4$ OHMS $C_1 = .001$ MFD. $C_6, C_8 = .01$ MFD. T_1 -- 37

$R_4 = 5 \times 10^3$ $R_8 = 2 \times 10^3$ $C_2 = 10$ $C_9 = .1$ T_2, T_3 -- 6AG7

$R_5, R_{13} = 10^5$ $R_9 = 10^7$ $C_3, C_5 = .0001$ $C_{10} = .0025$ T_4 -- 6SJ7

$R_6 = 2 \times 10^6$ $R_{11} = 1.5 \times 10^4$ $C_4, C_7 = 8$

FIG. 6. Circuit used in deadtime experiment. It consists of the fast counter in the fundamental circuit; T_1 which is an isolation state; T_2 and T_3, which act together as a multivibrator; T_4, which together with R_{14} and C_{10} give a sawtooth pulse when T_4 is rapidly biased to cut off.

measurements on a ruled screen are sufficiently accurate.

C. Comparison of Calculated and Observed Recovery Times

In Parts III A and III B, a description of the methods of measurement for the various quantities was given. In this section, results of those measurements are to be presented.

In (25) the quantities a, b, R, K and p_0 are constants for a particular counter. One can get a variety of different conditions by varying the pressure in the counter containing a given gas mixture. It is possible to vary the pressure of an argon-xylol, 9 to 1, mixture from about 16 cm to about 1 cm pressure and still have a good fast counter. Argon-xylol counters will work as fast counters at much higher pressures but the percentage of xylol must be lower, since the vapor pressure of xylol at room temperature is around 16 mm.

A permanent glass system with provision for changing cylinders, wire, and gas, was used in these experiments. It was far more convenient than making a new sealed-off counter for every change in the parameters.

The first counter used to test the theory was a copper cylinder counter which had been given the NO_2 treatment. This treatment consists in heating the counter cylinders in the presence of NO_2 gas, after first cleaning them with nitric acid and rinsing. A velvety black or dark brown color of the copper cylinder results. The NO_2 is then pumped out. The first counter was 15.3 cm long by 1.11 cm radius with an 0.010-cm tungsten wire. The gas filling was a 9 to 1, argon-xylol mixture. The critical distance R was calculated to be 0.65 cm. Table I gives the data taken with that counter. The pressure was varied from 13.2 cm to 5.0 cm. The threshold voltage changed from 1410 to 985 volts. The threshold voltage is given in parenthesis for each different pressure. The calculated and observed values of t_r are listed for each different set of conditions. Note the good agreement and that the variation of the observed t_r follows closely that of the calculated t_r.

The value of 0.8 for the mobility constant is the average of the values obtained from the two formulae in Part II D. The two values are 0.6 and 1.0. These are obtained with 1.8 as the mobility constant of newly formed positive argon ions and 0.2 for the mobility of xylol ions. This last value is obtained as an estimate from tables[12] listing mobilities of close relatives of

[12] *International Critical Tables*, National Research Council (McGraw-Hill, New York, 1926).

TABLE I. Calculated and observed recovery time.

$b=1.11$ cm Pressure (cm)		$a=0.010$ cm Voltage (V_0)	$K=0.8$ t_r (calc.) (sec.)	$R=0.65$ cm t_r (obs.) (sec.)
13.2		1470	2.4×10^{-4}	2.2×10^{-4}
	(1410)	1540	1.6	2.1
		1620	1.6	2.0
		1680	1.5	1.9
11.0		1380	1.9	2.0
	(1290)	1450	1.6	1.9
		1515	1.4	1.8
		1612	1.2	1.7
9.0		1270	1.7	1.7
	(1200)	1330	1.5	1.7
		1375	1.3	1.6
		1500	1.0	1.5
7.0	(1115)	1235	1.3	1.4
		1445	0.8	1.2
5.0		1045	1.1	1.2
	(985)	1140	0.9	1.1
		1215	0.8	1.0

xylol. The value of 0.8 may be in error by 30 percent but, even so, the agreement with all predictions of the theory is very good.

As a check on the above, and as further verification of the theory, a counter of different dimensions was investigated. The radius was 1.43 cm. The gas in this counter was an argon-xylol mixture but this time it was 5 percent xylol and 95 percent argon. Although the radius b was larger, the value of q was so much smaller than in the previous case that R, the critical distance, was only 0.47 cm. With the different gas mixture, the value of K was 1.0, obtained as before. In this particular experiment, a better condenser was used in the measurement of q so that the final data are expected to be more accurate. The results are given in Table II. Even though the conditions are such to give calculated recovery times more than twice those of the other counter, there is still excellent agreement between calculated and observed recovery times.

The data herein presented, along with other data on less complete runs with different counters, seem to give sufficient verification of the theory of counter discharge.

D. Comparison of Calculated and Observed Deadtimes

The deadtime may be measured by the same method as used for the recovery time. As discussed in Part II D, the simple expression for the deadtime derived in Part II E is not accurate. To show the discrepancies between the observed deadtime and the calculated deadtime, Table III tabulates the results for the counter to which Table II refers. The observed deadtime is 4 or 5 times as long as the calculated deadtime. Not only for this counter but also for other counters, this fact was observed. The apparent mobilities are much lower in the high field region. There is still observed a dependence of the deadtime on the pressure/voltage ratio.

Although the deadtime can be used only in a semi-quantitative way to prove the theory, it is still an important quantity to measure. It is the quantity which determines the maximum counting rate of fast counters. In a particular experimental set-up, the size of the voltage pulse necessary to trip the recording circuit must be known. Then the insensitive time of the set-up may be measured experimentally as that time from the beginning of a trigger pulse to the time when the follow pulses have built up to the required size. The experiment employing the RCA 155 oscilloscope takes but a short time to perform. After it is set up, the insensitive times can be measured for a large number of counters very quickly.

IV. DEADTIME TECHNIQUE APPLIED TO DISCHARGE SPREAD

A. The Spread of the Discharge

In the postulated mechanism of discharge of Part II B, it was assumed that the discharge spread throughout the full length of the counter in a time short compared with the 10^{-5} second breakdown time. The excellent agreement with experiment of the predicted action from that theory seems to justify the assumption. In fact,

TABLE II. Calculated and observed recovery time.

$b=1.43$ cm Pressure (cm)		$a=0.010$ cm Voltage (V_0)	$K=1.0$ t_r (calc.) (sec.)	$R=0.47$ cm t_r (obs.) (sec.)
13.4	(1320)	1370	4.5×10^{-4}	4.3×10^{-4}
		1480	4.5	4.3
11.0	(1185)	1235	4.2	4.3
		1360	4.3	4.2
9.0	(1080)	1145	3.7	3.7
		1230	3.6	3.1
7.0	(985)	1035	3.3	3.6
		1170	3.0	3.1

in view of the identical nature of the pulses in size and shape, it is hardly possible to assume anything but complete, and uniform, spreading of the discharge along the counter length. With the deadtime theory so convincingly supported by experiment, an examination of the spreading of the discharge was undertaken. Many of the experiments herein reported were performed before the complete theory was worked out; they contributed immeasurably to the formulation of the theory.

Some time before the deadtime technique was discovered, Professor Brode of the University of California described to the author an unpublished experiment on the spread of discharge in counters. This experiment, referred to as the Brode experiment, was performed with a double counter, i.e., a single glass tube container with two cylinders and two wires. The cylinders, end to end, were separated by a fraction of an inch. The wires were supported in the middle by an insulating glass bead. The pulse from either counter could be taken from its wire or its cylinder. Brode connected one wire to the vertical plates of an oscilloscope and the other wire to the horizontal. If one counter fired without the other the electron beam of the oscilloscope would undergo a horizontal or a vertical displacement. If both fired coincidentally, either from a true coincidence or from the spread of the discharge from one to the other, there would be a 45° deflection of the beam. This assumes equal pulses from each counter. Brode found that, if both counters were slow counters, the discharge did spread. For fast counters the discharge did not spread; most pulses were either vertical or horizontal, very few 45° deflections being observed.

In repeating the Brode experiment, the author found similar results. There is, of course, the possibility that some of the occasional coincidences observed were from discharge spreading but the number was so small that it did not indicate a uniform spreading of the discharge along the counter. This experiment was interpreted as an indication that the discharge was localized. It definitely eliminated photoelectric action on cathode and in the gas as a mechanism for discharge spread. When the deadtime technique was discovered and supported so well, this whole question of discharge spread was reexamined, for the deadtime theory demands that the discharge spread along the unobstructed wire.

TABLE III. Calculated and observed dead time.

$b=1.43$ cm Pressure (cm)	$a=0.010$ cm Voltage	$K=1$ t_d (obs.) (sec.)	$B=0.47$ cm t_d (calc.) (sec.)
13.4	1370	2.6×10^{-4}	0.65×10^{-4}
	1480	2.5	0.52
11.0	1235	2.4	0.60
	1360	2.3	0.46
9.0	1145	2.1	0.52
	1230	2.1	0.41
7.0	1035	1.8	0.43
	1170	1.7	0.32

B. Divided Cylinder, Divided Wire Counter

In order to see if the deadtime, as well as the discharge, spread in the type counter described in Part IV A, a similar counter was built. This, along with other multiple counters, is diagramed in Fig. 7. The over-all length was about 8 inches, the two cylinders being separated by about $\frac{1}{4}$ inch. The two wires were held together mechanically, but separated electrically, by a glass bead about $\frac{1}{8}$ inch in diameter. All gas fillings in the multiple counters considered in this section were 9 to 1, argon-xylol, mixture. Each counter exhibited the deadtime and, because of equal dimensions, the two deadtimes were the same.

The particular deadtime experiment performed on this and other multiple counters needs some explanation. If two counters, say A and B, are connected in parallel, then a count from either of them may act as a trigger pulse for the linear sweep in the deadtime experiment. Moreover, a count from either of them may act as a follow pulse. If the two counters are independent, as far as deadtime is concerned, there will be no definite deadtime for the combination. This is because, although the one which gave the trigger pulse, say A, is dead for a short period thereafter, the other, B, is still sensitive. The same holds true if B furnishes the trigger pulse, for then A is still sensitive. On the oscilloscope screen this shows as the customary deadtime pattern, as illustrated by Fig. 4, except there are additional pulses filling in the open space from $t=0$ to $t=t_d$.

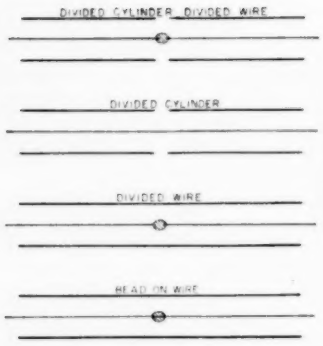

FIG. 7. Diagrams of special counters. These counters are forms used in the study of the lengthwise spreading of the discharge in fast counters.

If the two counters are not independent with respect to deadtime, then the customary deadtime picture with no modification is expected. Also, when the discharge spreads from one counter to the other, the resulting voltage pulse is the sum of the individual voltage pulses.

In order to test the spread of the deadtime in the divided wire, divided cylinder counter, the two separate counters were connected in parallel. The deadtime did not spread. There were, of course, a few double pulses from either true coincidences or occasional discharge spread.

C. Divided Cylinder Counter

The next step was to test to see if the deadtime and discharge would spread in a counter with a divided cylinder but a single wire. Again the counter, diagramed in Fig. 7, was 8 inches overall. When the pulses were taken from the cylinders individually, each of the counters exhibited the same deadtime. When the cylinders were paralleled externally it was found that the deadtime did spread. Moreover, the discharge spread too, for the voltage pulses were the sum of the voltage pulses of the individual counters. The counters acted together as a single counter. In other words, it was not the divided cylinder but the wire divided by the glass bead which prevented the spread of discharge and deadtime in the experiment of Part IV B.

One very interesting and important fact was observed in the performance of Brode's experiment on the divided cylinder counter by taking the pulses from the two cylinders. As expected from the results of the deadtime experiment, all the deflections were at 45°. However, when these deflections were examined closely, it was found that the counter which received the ionizing particle did start slightly ahead of the other. To test this, a radioactive source was moved from one end to the other. This indicated definitely that the spread of discharge does take a measurable, finite time. This time was estimated to be but a fraction of the breakdown time or around 10^{-6} second or less. This spreading of the discharge down the length of the counter in a time, short compared with the breakdown time, was assumed in the postulated theory of discharge. It is comforting to note that it is verified experimentally.

D. Divided Wire Counter

Merely as a check on the experiments of Part IV C a divided wire counter was made as diagramed in Fig. 7. The over-all length of the single cylinder was 8 inches. As was expected, neither the deadtime nor the discharge spread. These experiments were sufficient to indicate that a spread of the discharge implied a spread of the deadtime. All the experiments agree with the theory of the deadtime.

E. Bead on Wire Counter

In the deadtime experiment, performed with the divided wire counter, the two wires were externally connected electrically. Hence, it was concluded that the spread of the discharge was a surface phenomenon on the wire or some phenomenon occurring in the gas very close to the wire. To test that conclusion, a counter was constructed with a single cylinder and single wire but with a glass bead about $\frac{1}{8}$ inch in diameter and $\frac{1}{4}$ inch long on the wire in the center of the counter. This counter is diagramed in Fig. 7.

Although Brode's experiment could not be performed with this counter, there still remained two methods with which the spread of the discharge could be investigated. The experiments on the spread of the deadtime and the size of the voltage pulses were still applicable to the problem. When tested with the deadtime experiment, the counter was found to behave as two. The discharge did not spread. This was corroborated by the pulse size experiment. *A glass bead on the wire was sufficient to prevent the spread of the*

discharge. In the previous experiments, it was not the fact that either the cylinder or the wire were divided but the fact that there was a glass bead on the wire that prevented the discharge from spreading. No longer does one conclude from Brode's experiment that the discharge is localized. It spreads along the unobstructed wire; but a small glass bead is sufficient to stop it. This experiment shows that a new mechanism must be used to account for the spread of discharge, for, previous to Brode's experiments, it was thought to be photoelectric action on the cylinder and from the time of Brode's experiment to very recently, it was considered to be localized.

F. Small Bead on Wire Counter

The next step in the investigation of the discharge spread was to find the minimum bead size which would stop the spread of discharge. For that purpose an 0.022-inch diameter bead was put on an 0.008-inch diameter wire. Instead of sealing off the counter constructed with this wire, the deadtime experiment was performed at several pressures. At 10-cm pressure with an operating voltage of 1300 volts, the deadtime did not spread; the counter acted as two counters. The same held true at 6.5-cm pressure with an operating voltage of 1100 volts. However, at 3.5-cm pressure the action changed. From the threshold voltage of 790 volts to 840 volts, the deadtime did not spread. As the voltage was increased above 840 volts, more and more double sized counts appeared until all counts were double sized. Then there was a unique deadtime. The counter had changed in action from that of two apparently separate counters to that of a single counter.

A partial explanation of this phenomenon is obtained if a fact mentioned in Part II D is examined. It was there indicated that the quantity which determines the energy which an electron gains between collisions is the ratio E/p. This is obvious since E is a measure of the energy gained per unit path and $1/p$ determines the mean free path. For a particular gas, or gas mixture, there is a critical value of E/p for which the electrons gain sufficient energy between collisions for cumulative ionization to take place. As the voltage across a G-M counter is raised, the threshold voltage is reached when the critical value of E/p is obtained near the wire. As the voltage is raised above threshold, the point at which the critical value of E/p is obtained is pushed out from the wire so that the volume which is sensitive to cumulative ionization is increased. This increase in the sensitive volume probably accounts for the observed increase with overvoltage of charge flowing in a single pulse. Although this ratio of E/p has a critical value, cumulative ionization is not obtained in a limited space, such as the region of the wire, if the pressure is too low, for then there are not enough collisions for very rapid multiplication.

With this in mind the explanation of the change in action of the small beaded counter is clear. As the pressure was lowered, the operating voltage decreased but not as rapidly as the pressure. Since

$$E=\frac{V}{r\ln(b/a)}, \tag{27}$$

the value of E/p at a given radius then increased. At the pressure 3.5 cm, with an operating voltage of 840 volts, the sensitive region had been pushed out from the wire till its radius exceeded that of the bead. Then, the discharge could spread.

G. The Directional Geiger Counter

The results of Parts IV A through IV F point out the experimental basis of the discovery of the directional Geiger counter which was reported[13] earlier. The fact that a small glass bead on the wire would localize the counter discharge by preventing the spread along the wire immediately suggested the idea of separating a single counter into sections which could be used in coincident arrangement.

The behavior of the directional counter well illustrates the efficiency of the bead in preventing the discharge spread. This of course assumes that the counter cylinder has been treated to give a low photoelectric emission and a high work function. It is known that the NO_2 treatment of copper gives such a surface. Unpublished results of some photoelectric experiments show this to

[13] H. G. Stever, Phys. Rev. **59**, 765 (1941).

be true. Also, this work with beads on the wire has been tried only with organic vapor filled counters.

V. CONCLUSIONS

It is in order to examine the implications of the deadtime phenomenon with reference to the use of a G-M counter as a laboratory instrument. It is obvious that the deadtime in no way limits the use of these counters in highly resolving coincidence circuits, for the high resolution in those circuits depends upon the speed of potential fall of the wire, which is known to be fast. However, the deadtime does limit the maximum counting rate at which these counters can be used since there is an absolute minimum time, t_d, between recorded counts. This time is easily measurable and is of the order of 10^{-4} second. Even though the RC recharging time in the fundamental circuit is reduced to a minimum, the deadtime, or insensitive time, is present.

Even though there is a limit to the counting rate, the self-quenching, organic vapor filled counter still justifies the name, fast. It can be used in a circuit which reacts more rapidly than the one used with what has been termed a slow counter. Montgomery and Montgomery[5] point out that the only difference between the organic vapor filled counter and the other type is that, in the organic vapor filled counter, the positive ions do not knock out electrons when they arrive at the cylinder wall, whereas in the usual type counter they do. This implies that with the fast counter one can use a low resistance and take advantage of the maximum counting rate, limited only by the deadtime. With a slow counter the voltage across the counter must have dropped to threshold, or below, when the ions arrive at the cylinder lest the secondary electrons continue the discharge. This necessitates a larger resistance with the slow counter so that the voltage takes considerably longer to return to full operating voltage.

Besides the presentation of a clear, simple picture of the internal action of a fast G-M counter, the deadtime experiment can be applied to the problem of the discharge spread in a fast counter. It is not applicable to discharge spread in slow counters. It is seen from experiments described in Part IV of this paper that the spreading of discharge is quite localized, being confined to the region of the gas about the wire. The small-bead-on-wire counter experiment however indicates that the spreading action takes place in the gas rather than right on the surface of the wire. The lengthwise spread of the discharge may be due to a photoelectric action which is particularly selective to the gas in the region of the wire. This would imply that a function of the organic vapor is to absorb the photons emitted in the cumulative ionization region about the wire. Perhaps, on the other hand, the lengthwise spread of the discharge is due to a scattering phenomenon. This could be tested by some experiments with beads on the wire by reducing the length of the bead but keeping the diameter constant. Eventually a point might be reached where the scattered electrons would jump over the short bead. If it were a photoelectric spread, a quartz bead might allow the passage of the ultraviolet photons which were responsible whereas a glass bead would absorb them.

The author wishes to take this opportunity to thank both Professor H. V. Neher and Dr. W. H. Pickering. Throughout the entire experiment on counters their aid was always available and often sought.

Angular Distribution of Current from a Point in Hydrogen

WILLARD H. BENNETT
Electronic Research Corporation, Newark, Ohio

(Received October 14, 1941)

The angular distribution of current of electrons from a sharp point in hydrogen is measured for various currents and sizes of wire. Evidence is obtained for the critical effect of the potential drop in the ionization sheath.

IN previous articles on the corona discharge[1] from points, it has been supposed that the discharge takes place essentially forward from the point and grows backward to approach a hemispherical distribution for increasing current.

Recent measurements show this not to be the case at least in hydrogen, and the results seem to require a revision of some of the previously accepted ideas concerning the mechanisms of this form of discharge.

The tubes used in these measurements are illustrated in Fig. 1. In type 1, the collecting electrode was spherical with radius of one inch about the tip of the point except for a relatively narrow neck axial about the support for the point, as in Fig. 1. The sphere consisted of rings of equal thickness, insulated from each other with empire cloth to make possible the measurement of current to each ring insulated from the support for the point by a ground glass joint. Apiezon grease was used between surfaces and gave a vacuum tight system which was then rinsed with hydrogen and filled with hydrogen for a measurement.

In type 2 a modification was used in which all except a hemisphere was replaced with glass, down to *A* in Fig. 1. In type 3 all except nine collecting sectors are replaced with glass giving a little more than a hemisphere of collecting surface, down to *B* in Fig. 1. In all three forms, the wire tip was accurately centered and trimmed to come at the center of the spherical surface.

Since the rings all had the same thickness, the collecting surfaces of the sectors were all equal in area. The current to each ring would therefore be the same as the current to any other ring if the discharge current had uniform spherical density. A polar plot of the currents to the collecting sectors at radial directions midway between the angular extremities of the sectors represents correctly the current densities in those respective directions.

In Figs. 2 to 7 are shown some representative angular distributions of current in hydrogen at atmospheric pressure for several sizes of wire ends and tube types. It will be noted in Figs. 2 and 3 for the nearly complete sphere, at the lower currents, by far the greater part of the current moves sideways and a little backward when the glass is not obstructing such flow. The 0.0075-cm wire of Fig. 2 projects the discharge increasingly forward with increasing current, but the 0.0025-cm wire of Fig. 3 produces the largest increases in current to the

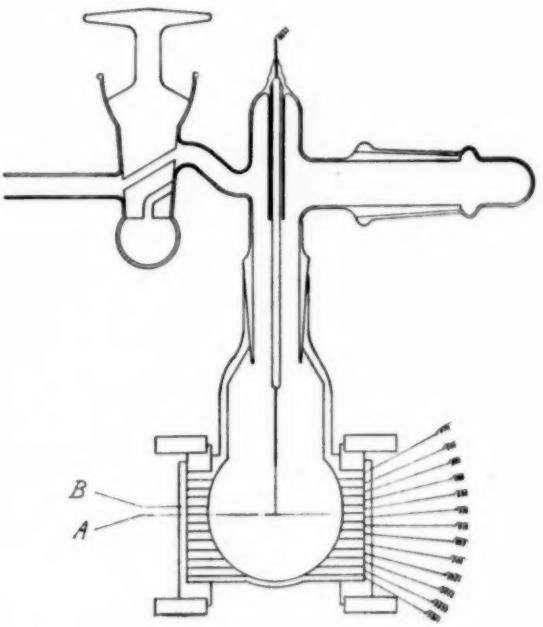

FIG. 1. Discharge tube.

[1] W. H. Otto and W. H. Bennett, J. Chem. Phys. **8**, 899 (1940); W. H. Bennett, Phys. Rev. **58**, 992 (1940). See also L. B. Loeb, *Fundamental Processes of Electrical Discharges in Gases* (Wiley, 1939), pp. 514–535.

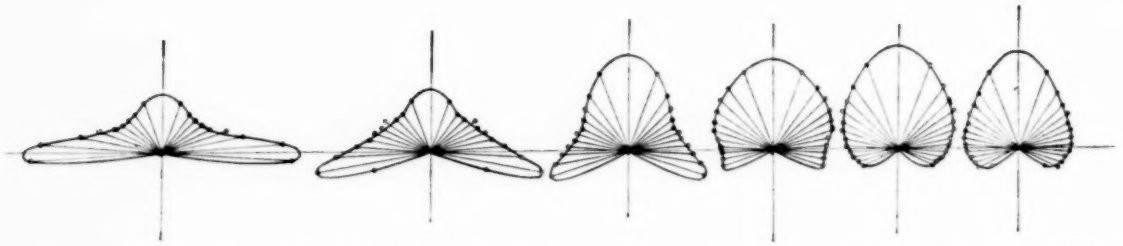

FIG. 2. Distributions from 0.0075-cm wire end in tube of type 1. Currents were, from left to right, in ma, 0.02, 0.05, 0.1, 0.2, 0.5, 1.0.

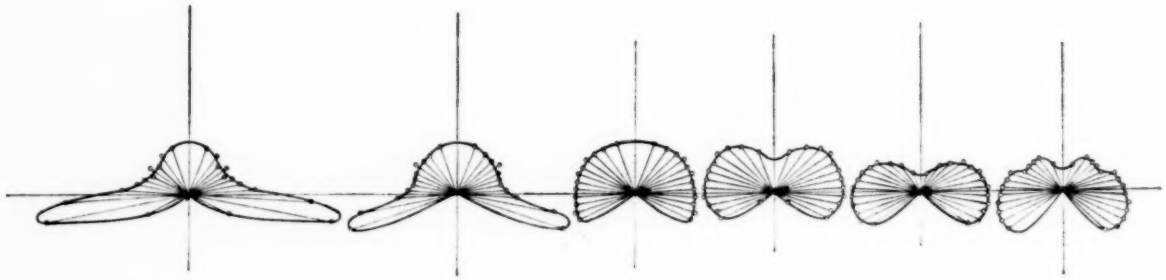

FIG. 3. Distributions from 0.0025-cm wire end in tube of type 1. Currents were, from left to right, in ma, 0.02, 0.05, 0.1, 0.2, 0.5, 1.0.

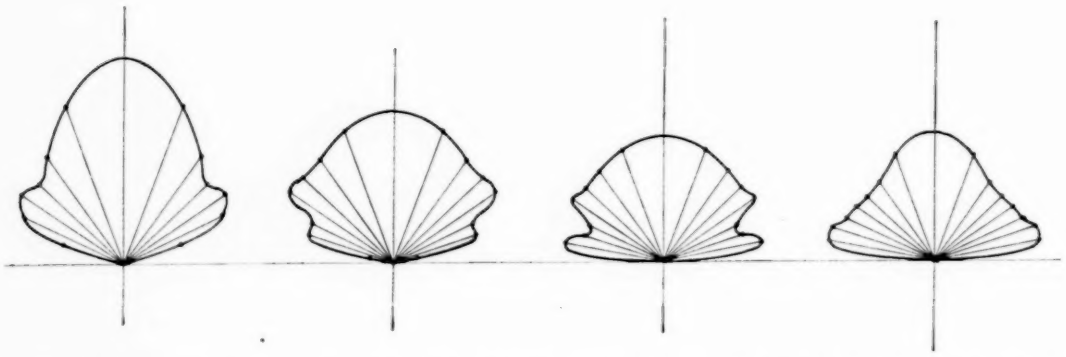

FIG. 4. Distributions from 0.0075-cm wire end in tube of type 2. Currents were, from left to right, in ma, 0.1, 0.2, 0.5, 1.0.

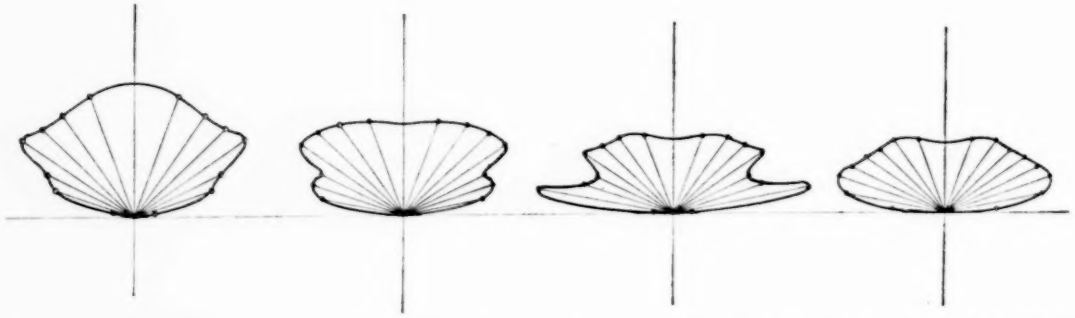

FIG. 5. Distributions from 0.0025-cm wire end in tube of type 2. Currents were, from left to right, in ma, 0.1, 0.2, 0.5, 1.0.

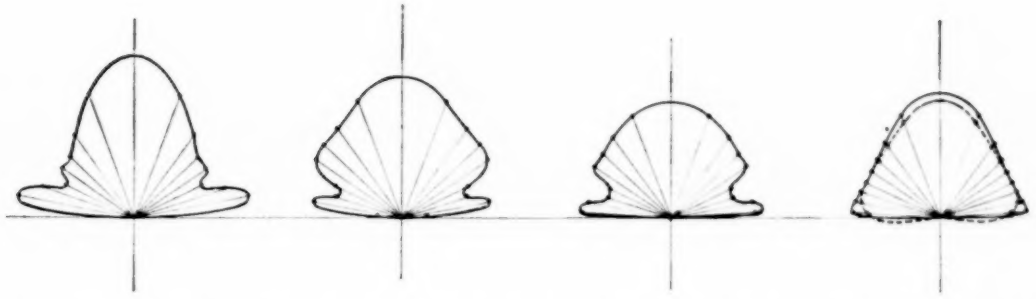

FIG. 6. Distributions from 0.0075-cm wire end in tube of type 3. Currents were, from left to right, in ma, 0.1, 0.2, 0.5, 1.0

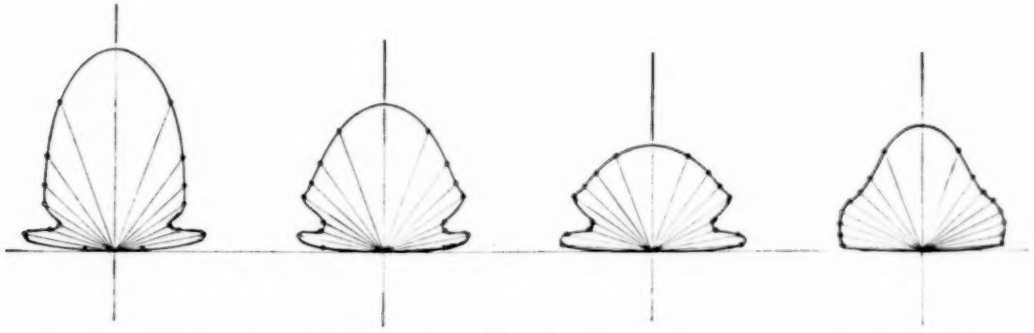

FIG. 7. Distributions from 0.0050-cm wire end in tube of type 3. Currents were, from left to right, in ma, 0.1, 0.2, 0.5, 1.0.

side and back. The increase of current from the 0.0025-cm wire from 0.5 ma to 1.0 ma is accompanied by a growth of the visible glow on the tip back along the wire for about one millimeter which probably explains the excessively large backward current from this wire at 1 ma.

The change to a hemispherical collecting electrode in Figs. 4 and 5 turns the collecting current forward without changing the relative form of the discharge distribution.

In Fig. 6, an extra ring is added and brings the discharge a little more nearly to a uniform hemispherical distribution. The dotted line shows a check run after the tube had been completely disassembled and cleaned, and a new wire end put in.

TABLE I. Variation of tube voltage with type of tube.

Tube type	Wire size	Current 0.1 ma	0.2 ma	0.5 ma	1.0 ma	Distribution
1	0.0075	1640	1760	2450	3330	Fig. 2
2	0.0075	1490	1680	2440	3360	Fig. 4
3	0.0075	1510	1650	2340	3220 3310	Fig. 6
1	0.0025	1360	1560	2160	3060	Fig. 3
2	0.0025	1350	1590	2300	3050	Fig. 5

In Fig. 7, the distribution is similar to that for 0.0075-cm wire in Fig. 6, showing that there is a change in the character of the discharge between 0.0050-cm wire and 0.0025-cm wire to result in an excessive sidewise current from the smaller wire.

As mentioned previously,[1] a tube conditions itself with the passage of current. Microscopic examination of a conditioned wire end shows that some of the material is etched away, usually leaving a conical end which is sharper than a freshly cut wire end. There are two conditioning processes which take place. The sharpening of the wire end goes on quite rapidly while the most of the electron-attaching impurities are removed from the gas. This usually takes 2 to 30 minutes in hydrogen at 1 ma, but the tube will decondition with standing unless the discharge is continued for another 30 minutes to 2 hours. It is believed that this continued passage of current is needed for elimination as permanently precipitated material of the last traces of the electron attaching impurities.

The variation in sharpness results in a small variation in the voltage required for a given current as shown in Table I, and any difference in voltage required for the current due to changing the character of collecting surface is less than this random variation between wire ends.

DISCUSSION

In a previous article[2] it was reported from point-to-plane measurements that there is an ionization sheath potential drop which remains approximately constant while the distance to the collector is varied by large amounts.

The observations being reported here show that for the finest points, the charge in front of the tip of the point reduces the field intensity more in those parts of the ionization sheath nearer that space charge in a manner to reduce the ionization current in the forward direction and thus favor the lateral current. This effect is most noticeable at the smallest values of current so it is evident that a very small reduction of field intensity produces a large percentage reduction in ionization current. At the largest values of current, the current is essentially a space charge limited current arising at the hemispherical cap over the tip, and as such the percentage change of field intensity at the tip does not vary so much with angle at the tip.

The heavier wires have dull enough ends to prevent this effect from pushing the discharge back because the field attenuates less rapidly with distance from the tip and there is a less accumulation of charge near the tip.

[2] W. H. Bennett, reference 1, pp. 995, 996.

JANUARY 1 AND 15, 1942 PHYSICAL REVIEW VOLUME 61

The Electrical Conductivity of Titanium Dioxide

MARSHALL D. EARLE
Randal Morgan Laboratory of Physics, University of Pennsylvania, Philadelphia, Pennsylvania
(Received September 25, 1941)

Experiments on titanium dioxide show that it is an electronic semi-conductor in which the the current carriers are actually free electrons, as contrasted with the hole conduction of the other type of semi-conductor. It is found that the variation with oxygen pressure is that which would be expected if the titanium dioxide decomposes in the following manner: $TiO_2 \rightarrow Ti^+ + O_2 + e^-$. The deviation of the curves at low pressures is probably due to the presence of small impurities in the samples used. It is found that the variation of conductivity with temperature is represented by the formula $\sigma = Ae^{-\epsilon/kT}$. The activation energy ϵ is about 1.7 electron volts. Transport measurements show that the ionic conductivity is less than that which can be measured in these experiments. Measurements of the Hall effect, although not very quantitative, show that the mean free path for the conduction electrons is very small.

INTRODUCTION

The Electrical Conductivity of Titanium Dioxide

RECENTLY much interest has been shown in the mechanism of electrical conduction in solid materials known as semi-conductors. These substances are characterized by the fact that they possess a room temperature resistivity lying between approximately 10^3 and 10^8 ohm-cm, which decreases with increasing temperature. They differ from metals in that their resistance is much higher and that their temperature coefficient of resistance is of the opposite sign. The current in semi-conductors is usually carried by electrons, although ions may carry a large part or all of the current. Substances in which the conduction is principally by ions are spoken of as ionic semi-conductors. Their resistance in general is slightly lower than that of the electronic semi-conductors.

There are three well-known means of distinguishing between electronic and ionic conductivity. These are: Hall effect measurements,

thermoelectric effect measurements, and measurement of ionic transport.[1]

The electronic semi-conductors can be divided into two classes. These are: reduction semi-conductors in which there is a deficiency of the electronegative element and oxidation semi-conductors in which there is an excess of the electronegative element. In the first case, the Hall constant is negative as it should be if the current carriers are negatively charged. Typical cases of reduction semi-conductors are zinc oxide whose properties have been extensively investigated by Fritsch, Baumbach, Wagner and others,[2-4] and titanium dioxide as was found in the experiments described in this paper.

The mechanism of electrical conduction in reduction semi-conductors can be explained in the following way. We can assume that the heated semi-conductor loses atoms of the electronegative element from the surface, leaving the electropositive element in excess. This type of conductivity is described by the relation

$$\sigma = kP_0^{-1/n}. \tag{1}$$

k and n are constants; P_0 = pressure of oxygen around sample; and σ = the conductivity.

These excess atoms which occupy interstitial positions can be thought of as providing additional levels from which electrons may be more easily released thermally into an allowed region for conduction.

In the case of oxidation semi-conductors, the sign of the Hall constant is positive, being opposite to that of the reduction semi-conductors. This would make it appear that the current in oxidation semi-conductors is carried by positive charges. This apparently anomalous behavior can be explained in the following way. We can assume that there is a band of quasi-continuous energy levels which are normally filled, thus preventing any net motion of electrons in either direction. If it is now assumed that there are additional levels lying a short distance above the filled band to which electrons may be excited and trapped, the conductivity can be explained by the motion of the vacancies thus produced in the previously filled band.

Semi-conductors are found to depend on the temperature according to the following equation.

$$\sigma = Ae^{-\epsilon/kT}, \tag{2}$$

where σ = the conductivity; ϵ = the activation energy for producing free electrons or free holes; T = the absolute temperature; k = Boltzmann's constant; and A = (const.) $\ln^{\frac{1}{2}} T^{\frac{1}{2}}$ ohm^{-1} cm^{-1} which is seen to be only very slightly dependent on the temperature and can thus be regarded as a constant.

Titanium dioxide is a white powder which finds extensive use today in the paint industry as a pigment as well as uses in the paper and textile industries. It exists in three allotropic forms: rutile, anatase and brookite. Rutile and anatase are the most common forms. Brookite is exceedingly rare, being very unstable.

Most of the work described in this paper was carried out on rutile, although some curves plotted from data taken on anatase are shown.

EXPERIMENTAL PROCEDURES

The samples used in these experiments were prepared by pressing 1.5 g of powdered titanium dioxide into cylindrical pellets $\frac{1}{2}''$ in diameter and about $\frac{1}{4}''$ in length at a pressure of 36,000 lb./in.^{2}. These values in weight and pressure were chosen as standards after extensive experimenting because it was found that the pellets made under these conditions were of a convenient size and of a sufficient degree of durability. The density of the pellets thus made was about 50 percent of the single crystal density of the powder. By sintering these pellets for 10 hours at 1300°C in air their density became approximately 95 percent that of the single crystal.

The press used was made from a hydraulic truck jack capable of exerting a total force of eight tons. The die in which the powder was pressed was made of hardened tool steel equipped with two hardened plungers.

In making measurements on pressed powder samples it is very difficult to get results that are constants of the material being investigated. The results are greatly influenced by the pressure under which the samples are made, the amount

[1] C. Tubandt, *Handbuch der Experimental Physik* (1932), Vol. 12, pp. 396–399.
[2] O. Fritsch, Ann. d. Physik **22**, 375 (1935).
[3] W. Schottky and C. Wagner, Zeits. f. physik. Chemie **11B**, 163 (1933).
[4] C. Wagner and H. H. von Baumbach, Zeits. f. physik. Chemie **22B**, 199 (1933).

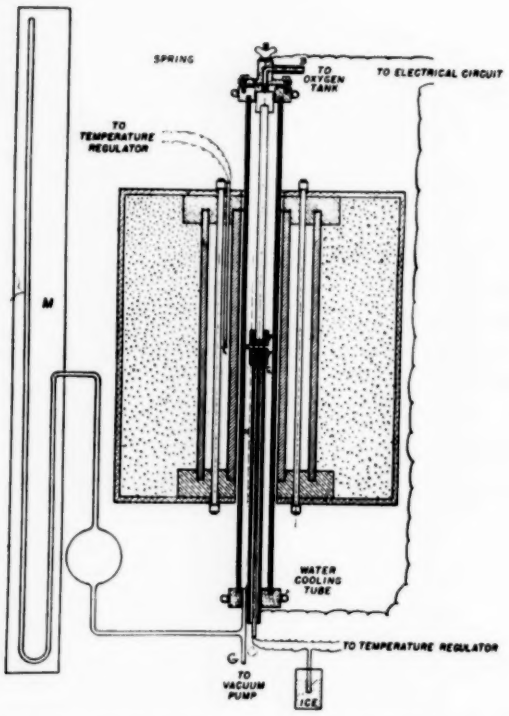

FIG. 1. Apparatus for measuring the electrical conductivity of titanium dioxide.

of sintering and the previous treatment of the sample. In making absolute measurements of a substance such as titanium dioxide it is obviously best to use a sample which has been sintered until it approaches as closely as possible the density of the single crystal. However, for making measurements in which diffusion plays an active part, such as the dependence of conductivity on oxygen pressure, it is found that much more valuable relative measurements could be obtained by using unsintered samples made under fixed conditions. It is undesirable to use highly sintered samples for this type of measurement because equilibrium is reached very slowly after a change has been made in the pressure of the vapor surrounding the sample.

This introduces a large uncertainty in the measurements because one can never be certain that the system has reached equilibrium, even after a long period of time. With the unsintered samples of approximately 50 percent single crystal density, reproducible results were obtained and the system apparently came to equilibrium within a few seconds after a change was made. This was indicated by the fact that the current through the sample very quickly reached a steady value, after a change in the pressure of the surrounding oxygen was made. With a well-sintered sample, the current drifted with time for hours or even days.

After considerable experimenting it was found that the best electrical contacts were metal films evaporated on the surface of the samples. The contacts in these experiments were made of gold evaporated on the parallel surfaces of the pellets. The samples before being placed in the vacuum chamber were carefully wrapped with aluminum foil to keep their sides free from gold.

In this work gold was found to have the following advantages over many other metals: (a) its melting point is sufficiently high (1063°C) so that it can be used at all temperatures at which these measurements were made; (b) its evaporation temperature (1445°C) is sufficiently low for easy evaporation; (c) it adheres readily to a clean tungsten filament by surface tension so that no crucible is necessary; and (d) it does not oxidize when heated in oxygen or in air.

The experimental equipment for making conductivity measurements at various pressures of the gas surrounding the sample and at various temperatures is shown in Fig. 1. The furnace proper consisted of two Alundum[5] tubes two inches and five inches in diameter and twelve inches in length, mounted concentrically. In the space between these tubes there were four

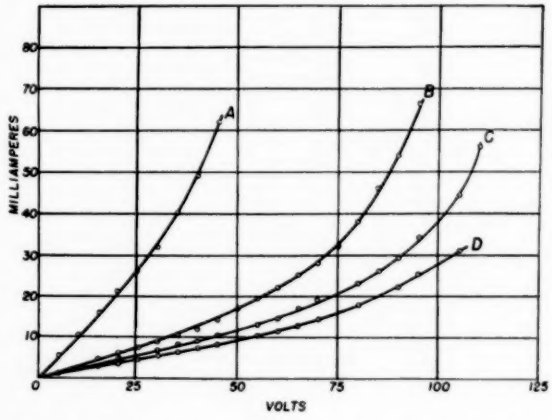

FIG. 2. Current as a function of voltage. *A*—2-mm mercury oxygen pressure; *B*—11.1-cm mercury oxygen pressure; *C*—38.8-cm mercury oxygen pressure; *D*—77.0-cm mercury oxygen pressure.

[5] Alundum is aluminum oxide. Manufactured by the Norton Company.

Globar[6] heaters. The whole furnace was encased in a transite box approximately fourteen inches on each edge and packed with crushed firebrick for insulation. In order that the composition and pressure of the atmosphere surrounding the sample might be varied at high temperatures it was necessary that the samples be placed inside a quartz tube mounted in the furnace as shown in Fig. 1. The quartz tube was two feet long and one and one-quarter inches inside diameter and was fitted with grooved end plates waxed in place and cooled with running water to prevent the softening of the wax. The sample *S*, the parallel faces of which had been coated with gold by evaporation, was placed between the platinum electrodes *P*. These electrodes were held in place by Lavite blocks *F*, whose adjacent faces were machined plane to insure uniform contact over the surface of the pellet. The lower Lavite block was supported by a small quartz tube $\frac{5}{16}$ of an inch inside diameter which was closed at the upper end. The thermocouple T_2 used for measuring the temperature of the sample, was placed in the tube from outside the furnace. In this way the thermocouple could not come in contact with the strong oxidizing atmosphere surrounding the sample during many of the measurements, thus greatly increasing its life.

The platinum wires *H* connected the platinum electrodes to the brass end plates to which the external connections were made. However, it was found necessary to take the following precaution with regard to insulation. It was noticed that if the copper cooling tubes on the top and bottom end plates were directly connected with a rubber tube to complete the water circuit, some current was bypassed due to impurities in the cooling water. When fifteen feet of glass tubing was inserted in the cooling circuit between the upper and lower end plates, the current bypassed was negligible. *B* is a small tube used to admit the oxygen into the system. *G* is the tube used for evacuating the system. A closed end mercury manometer *M* was used for measuring the pressure of the vapor surrounding the sample. The thermocouple T_1 was used to control the temperature of the furnace. The thermocouple T_2 could not be used for this purpose because the time required for it to respond to changes in the temperature of the heating elements was great enough to allow the temperature to drift badly.

[6] Globar heaters are made of silicon carbide. Manufactured by the Carborundum Company.

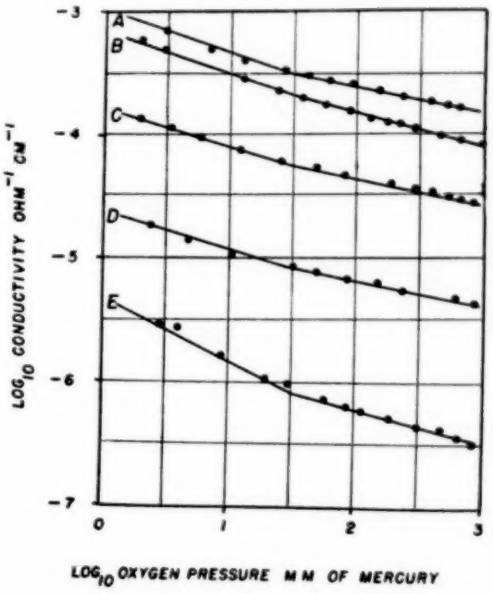

FIG. 3. Conductivity as a function of oxygen pressure. *A*—rutile, 968°C; *B*—rutile, 820°C; *C*—anatase, 861°C; *D*—rutile, 755°C; *E*—rutile, 626°C.

The conductivity was measured by the direct current fall of potential method. The advantage of this method is that it not only enables one to measure the conductivity but also to measure the current passing through the sample as a function of the voltage impressed on it. In this way one can determine to what extent Ohm's law is obeyed.

CURRENT AS A FUNCTION OF VOLTAGE

The curves in Fig. 2 show the current in milliamperes plotted as ordinate against the potential in volts plotted as abscissae. The data for each curve were taken with the pressure of the oxygen surrounding the sample maintained at a constant value. It is seen that for a short distance the variation is linear, which is as would be expected from Ohm's law. Beyond this point the curves deviate from a straight line, the current increasing more rapidly with voltage than Ohm's law predicts. In each curve it is seen that the deviation from linearity occurs when the power dissipated in the sample because

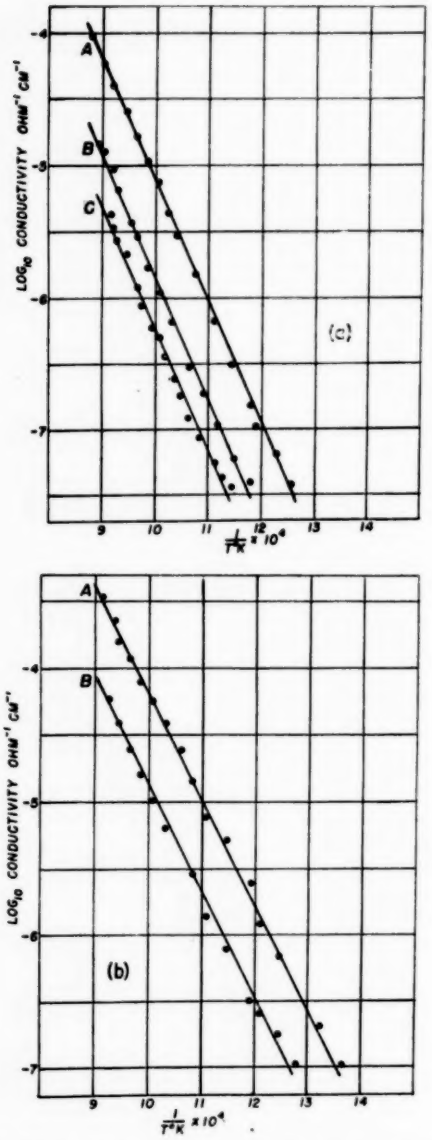

FIG. 4. Conductivity as a function of temperature. (a) Unsintered samples of rutile. *A*—0.1-mm mercury oxygen pressure; *B*—5-cm mercury oxygen pressure; *C*—79.5-cm mercury oxygen pressure. (b) Sintered samples of rutile. *A*—0.1-mm mercury oxygen pressure; *B*—14.0-cm mercury oxygen pressure.

of Joule heating is about 0.6 watt (0.95 watt/cm³). When the Joule heating is less than this value the heat is dissipated fast enough so that the specimen reaches thermal equilibrium.

CONDUCTIVITY AS A FUNCTION OF OXYGEN PRESSURE

The dependence of the conductivity of rutile on the pressure of the surrounding oxygen is shown in Fig. 3. It is seen that for oxygen pressure above 30 mm Hg all the lines have a slope of approximately $-1/4.3$. The slope at pressures lower than this varies from $-\frac{1}{2}$ at the lower temperatures to $-\frac{1}{3}$ at the higher temperatures. If it is assumed that there is one free electron for each interstitial titanium atom the decomposition of the titanium dioxide can be represented by the reaction:

$$TiO_2 \rightarrow Ti^+ + O_2 + e^-. \tag{3}$$

With this assumption the slope of the lines at oxygen pressures above 30 mm Hg can be accounted for in the following manner.

Let n = number of interstitial Ti^+ ions or the number of free electrons, N_{O_2} = number of O_2 molecules in gas surrounding sample ($N_{O_2} \gg n$), N = possible number of sites for Ti^+ ions, ϵ energy required to create a Ti^+ ion, a free electron and one molecule of gaseous oxygen, A = the free energy; then

$$A = n\epsilon + kT\left\{n \log\frac{n}{N} + n \log\frac{n}{C} + (N_{O_2}+n) \log\frac{N_{O_2}+n}{C}\right\}. \tag{4}$$

The first entropy term is that of the interstitial Ti^+ ions; the second entropy term is that of the free electrons, and the third is that of the oxygen vapor. If $N_{O_2} \gg n$ the above can be written:

$$A = n\epsilon + kT\left\{n \log\frac{n}{N} + n \log\frac{n}{C} + N_{O_2} \log\frac{N_{O_2}}{C}\right\}, \tag{5}$$

$$\frac{dA}{dn} = \epsilon + kT\left\{\log\frac{n}{N} + \log\frac{n}{C} + \log\frac{N_{O_2}}{C} + C_1\right\} = \epsilon + kT\{\log n^2 N_{O_2} + C_2\} = 0. \tag{6}$$

The conductivity at a temperature T is

$$\sigma = Ae^{-\epsilon/kT} \tag{7}$$

(where $A = 0.024 \ln^{\frac{1}{2}} T^{\frac{1}{2}}$ ohm^{-1} cm^{-1}).

It is seen that the conductivity varies as $\sqrt{n}$ where n is the number of centers present (in this case the number of interstitial Ti^+ ions).

From Eq. (6) we have $n \propto N_{O_2}^{-\frac{1}{4}}$; replacing $\sqrt{n}$ by σ we obtain $\sigma \propto \sqrt{n} \propto N_{O_2}^{-\frac{1}{4}}$. This gives very good agreement with the curves to the right of the break in Fig. 3 whose slope is seen to be about $-1/4.3$.

The increased slope of the curves at pressures lower than 30 mm Hg is probably due to small impurities. The samples were as pure as could be conveniently obtained, but contained a number of impurities as the following chemical analysis shows:

TiO_2—98.5 percent
SiO_2— 1.09
P_2O_5— 0.27
MgO— 0.11 (approx.)
Fe_2O_3— 0.012.

CONDUCTIVITY AS A FUNCTION OF TEMPERATURE

Figure 4 shows the dependence of conductivity of the rutile form of titanium dioxide on temperature. The data of Fig. 4(a) were taken on unsintered samples whose bulk density was approximately 50 percent the single crystal density. The data of Fig. 4(b) were taken on well-sintered samples with a bulk density of 93 percent that of a single crystal. These data show that the law (Eq. (2)) $\sigma = Ae^{-\epsilon/kT}$ is well obeyed in the range of temperature investigated. The slope of these curves shows that the value of the activation energy (ϵ in the equation above) required to produce free conducting electrons was 1.75 electron volts for the unsintered samples and 1.7 electron volts for the sintered samples.

Figure 5 shows curves representing the conductivity of unsintered samples of rutile as a function of temperature at 10 mm and 300 mm of Hg, respectively. These curves were compiled from data obtained from Fig. 3. They should be very reliable in that they show the temperature dependence of the conductivity of rutile at a constant pressure for a number of different samples. They also indicate that the value of ϵ is approximately 1.7 electron volts. It is to be noted that the curve for 300 mm of Hg oxygen pressure was selected from the portion of the curves that can be explained by the theory outlined previously, whereas the curve for 10 mm of Hg oxygen pressure was selected from the anomalous portions of the curves where the slope is greater than theory would predict. The change in the slope of the curves of Fig. 3 is not sufficient to make any noticeable change in the activation energy as determined from the conductivity *versus* temperature curves. This shows that a very slight change in activation energy is sufficient to cause a deviation from proportionality, $n \propto No_2^{-\frac{1}{4}}$ derived from Eq. (6).

IONIC CONDUCTIVITY

The following method was used in an effort to detect the possible ionic conductivity of rutile. Three pellets which had been sintered in air for sixteen hours at 1250°C were polished on a flat plate until their parallel faces were plane. The samples were accurately weighed and placed in the furnace with these adjacent faces in good contact. A direct current which averaged 90 milliamperes was passed through the three samples in series for five days, which corresponds to a total charge of approximately 36,000 coulombs. The furnace was kept at 850°C during the experiment. The pellets were then removed and weighed again. The weights of the pellets before and after are recorded below:

	Before	After	Change
Top	1.4013 g	1.4008 g	−0.0005 g
Middle	1.4068 g	1.4066 g	−0.0002 g
Bottom	1.3965 g	1.3965 g	0.0000 g.

These data show that the upper limit of the change in weight due to a migration of ions cannot be greater than the experimental error involved in weighing. Since the charge passed through the samples was 0.37 faraday, it

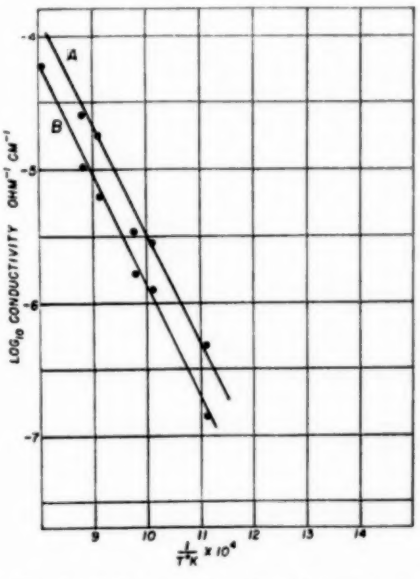

FIG. 5. Conductivity as a function of temperature. *A*—10-mm mercury oxygen pressure; *B*—30.0-cm mercury oxygen pressure.

seems conclusive that the ionic conductivity is negligible.

Inasmuch as the result of this experiment was negative, it was not necessary to employ the more elaborate means which enables one to separate the conductivities due to positive and negative ions which has been described by Tubandt.[1] One might raise the objection that the change in weight due to positive ions might exactly cancel that due to negative ions. This, however, would be extremely improbable in the case of titanium dioxide. The radius of the oxygen ion is 1.32A, while the radius of the titanium ion is 0.64A.[7] The titanium ions are therefore very much smaller and hence more mobile than the oxygen ions. As a result we should expect the positive ion transport number to be much greater than the negative ion transport number.

An attempt was made to determine the possible ionic conductivity by another method. This experiment was carried out in the following manner. A pressed strip of titanium dioxide 5 cm long and 8 mm wide was prepared and carefully balanced on the beam of an analytical balance above the knife edge. The position of the strip for balance was accurately marked by a small clip whose weight was exactly balanced by a similar one on the other side. This sample was then placed in the furnace and a charge of about 10,000 coulombs was passed through it. The sample was then accurately replaced on the beam of the balance and no change in weight could be detected. In the first method it is possible that the interfaces between separate pellets may be forming blocking layers which impede the free flow of ions. For this reason the second method was considered significant, because there are no boundaries of this type present.

HALL EFFECT MEASUREMENTS

The samples of rutile used for making Hall effect measurements were strips of pressed powder 5 cm long and 8×2 mm in cross section. As samples of titanium dioxide of these dimensions have a room temperature resistance of approximately 25×10^{12} ohms and since the equipment available could not make measurements at temperatures above 120°C, it would have been quite impossible to get a sufficiently high current density to detect a Hall e.m.f. For this reason it was necessary partially to reduce the samples to increase their conductivity by producing a deficiency of oxygen. The reduction was carried on in an atmosphere of hydrogen at a temperature of 500°C. By varying the time for reduction it was possible to bring the sample to any desired resistance. The best samples to use were those whose resistance was between 20,000 and 30,000 ohms. Gold was evaporated on the ends for making electrical contact. Near the center on opposite sides of the width were placed two small gold contacts for measuring the Hall e.m.f. Measurement of the Hall effect was very difficult, no well reproducible results being obtained.

The following equation was used to compute the Hall constant R:

$$R=-V/dIH, \tag{8}$$

where V = voltage developed in sample; d = thickness of sample; I = current; and H = field strength.

It was found that the Hall constant was of the order of magnitude of -10^{-7} volt/cm-amp.-gauss. This result is only qualitative at best. By assuming the value of the Hall constant to be -10^{-7} volt/cm-amp.-gauss the mean free path l for the conductive electrons is found to be approximately 5.1×10^{-7} cm. If R is known, the number of conducting electrons, n_f is found to be approximately 3.72×10^{9}/cm^3.[8]

These experiments are of value in that they indicate the order of magnitude of the mean free path and of the number of the conducting electrons. These Hall effect measurements do not rule out the possibility of ionic conductivity, but the transport measurements previously described show that the conductivity is almost entirely electronic.

In conclusion I would like to express my gratitude to Dr. Frederick Seitz and Dr. Park Miller for their helpful advice and criticisms, and to the Titanium Division of the Sherwin-Williams Company for part-time employment during the period in which this work was done.

[7] W. H. Bragg, *Atomic Structure of Minerals* (Cornell University Press), p. 31.

[8] The equations for making these computations are:

$$R=-\frac{\pi el}{(2\pi mkT)^{\frac{1}{2}}\sigma(Hz)}=-\frac{3\pi}{8}\frac{1}{n_f eC}.$$

See F. Seitz, *Modern Theory of Solids* (McGraw-Hill), p. 192.

Ionization of Gases by Collisions of Their Own Accelerated Atoms and Molecules

H. W. BERRY, R. N. VARNEY, AND S. NEWBERRY
Department of Physics, Washington University, Saint Louis, Missouri

(Received November 6, 1941)

Apparatus for producing fast neutral atom beams and measuring ionization caused by collisions of these atoms with others is described together with preliminary results on argon and nitrogen. The ionization of argon atoms appears to be similar to ionization by electron collisions in that the efficiency reaches a peak and falls off again with increasing speed. Ionization of nitrogen by neutral nitrogen was observed but the nature of the ionization function was not positively established.

IONIZATION of noble gases by their own fast neutral atoms has been observed by various experimenters.[1-3] In these cases the ionizing atom needed only to have an energy of 30 to 70 electron volts in order to succeed in detaching an electron from another atom during a collision. The onset energies observed were roughly only three times the ionization potentials of the respective atoms. The results indicated the desirability of further experiments for several reasons: First, no trace of ionization of other than noble gases had been observed, although at least one of the workers had looked for it. Second, the experimental velocities used were not high enough either to assure that ionization failed to occur in the low energy range or to connect the observations with the higher range sometimes described as the alpha-particle range. Finally, no theory satisfactorily explains the very low energy ionization, and hence more complete experimental information concerning what actually does occur is essential to the understanding of the process.

The apparatus was accordingly set up to permit forming a beam of neutral atoms with energies up to 8000 electron volts. (See Fig. 1.) An ion gun accelerated singly charged positive ions to the desired speed; an electrostatic velocity selector homogenized the beam; the beam then passed through a chamber containing the same gas so that the neutralization by charge exchange could occur. The beam of now neutralized ions passed through a set of electrodes charged with retarding potentials to remove any remaining ions from the beam. Finally the beam passed through a space charge type of ion detector[4] in which the ionizing collisions could be measured.

The apparatus was first tested with argon whose ionization was already known to occur. Intense ionization was observed in this case.

In order to determine even a qualitative ionization function, it is necessary to know something about the intensity of the neutral atom beam, if only that it is fairly constant at different speeds. The magnitude of the neutral atom intensity was measured by permitting the beam to pass through the detector and liberate secondary electrons from a small nickel plate placed behind the detector. These secondary electrons were repelled by a potential of 10 to 45 volts to the outside of the space charge cylinder, and the current was read on a galvanometer. Previous results indicated that about two neutrals were required per secondary electron liberated when the neutral energy was in the range used in our

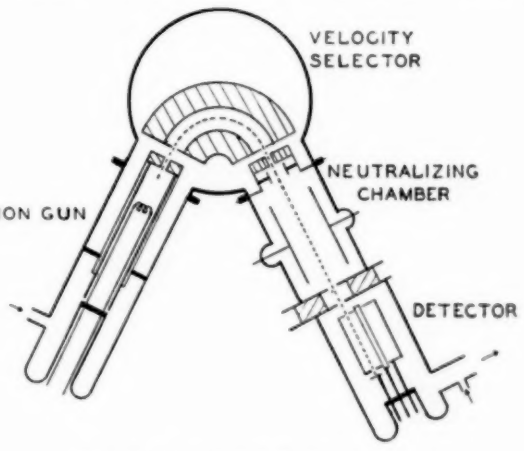

FIG. 1. Diagram of the apparatus.

[1] R. N. Varney, Phys. Rev. **50**, 159 (1936).
[2] A. Rostagni, Nuovo Cimento **11**, 34 (1934).
[3] H. Wayland, Phys. Rev. **52**, 31 (1937).
[4] R. N. Varney, Phys. Rev. **47**, 483 (1935) and **53**, 732 (1938).

experiments. This is qualitatively in agreement with the extrapolated results of Rostagni.[5] Rostagni's results further suggest that there is not a very great change in secondary emission with voltage in the range of our experiments.

A qualitative ionization function for argon neutrals in argon was obtained and is shown in Fig. 2. The ordinates indicate only the relative space charge effect per neutral atom, but they should be fairly accurate as far as neutral atom intensities are concerned. Because of the long and intricate path of the beam, adequate intensities could not be obtained with speeds under 1000 volts. The curve is seen to fall off steeply with increasing energy.

An ionization function was also obtained for nitrogen. The efficiency of ionization, even at best, was far less than in argon. The reader is warned against drawing more than qualitative conclusions concerning the relative efficiency of N_2 and A because of the qualitative nature of the data. This is the first definite evidence of ionization of nitrogen by collisions of heavier particles in the energy range lower than that of alpha-particles. It is interesting to note that it occurs at all, for the previous evidence in the 0–500 volt range indicated that it must be very

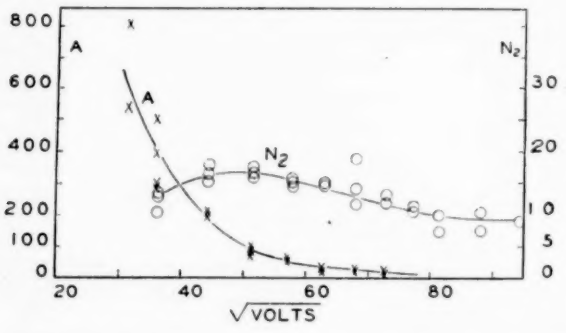

FIG. 2. Ionization functions for A and N_2 by their own neutrals. The ordinates are ratios of galvanometer readings and have no absolute significance. The numerator of the ratio is the space charge effect as shown by the galvanometer in the space charge bridge circuit. The denominator is the secondary electron current produced by the neutral beam in hitting the plate after passing through the space charge cylinder.

[5] A. Rostagni, Zeits. f. Physik **88**, 55 (1934).

feeble if it did occur. It is also of great interest to note that both argon and nitrogen ionization functions have a peak, for this is the first indication that ionization by neutral atom collisions occurs by a mechanism at least outwardly similar to ionization by electron impacts.

It must be noted here that the drop in ionizing efficiency at higher energies can conceivably be only an apparatus defect. The ionization produced by collisions is detected with a space charge type of detector which is notably dependent on the speed of the ions being detected; in fact, an ion speed of only a few volts very greatly decreases the sensitivity of the detector.

It is imaginable that in ionizing collisions between neutral atoms, the newly formed ions acquire more kinetic energy as the energy input of the collision increases. The writers are at present only able to suggest that this is not the true cause of the fall in measured efficiency at higher energies. The reason for this opinion is based on the observation that the efficiency of the detector must still be very high for argon ions produced by 1000-volt neutral atoms, and for that matter even 4000-volt atoms. If the detector efficiency is low, the space charge effect observed would correspond to a collision cross section for ionization large beyond all reason. Hence it must be concluded that in raising the speed of the ionizing argon neutrals from the onset at 48 volts to 1000 or even 4000 volts, relatively little change has occurred in the kinetic energy delivered to the newly formed argon ions. It thus seems to be unlikely that the mechanism of ionization is one involving a transfer of kinetic energy at all for there appears to be relatively little change in the kinetic energy transferred with a very great change of energy of the ionizing particle. If this conclusion in itself can be established, it will be a major addition to the knowledge of ionization mechanisms.

Preliminary results exist in helium similar to those in nitrogen. However, a more intense source is necessary to complete this work and to verify the details of the nitrogen measurements.

The Interaction Between a Molecule and a Metal Surface

E. J. R. Prosen† and R. G. Sachs*
The George Washington University, Washington, D. C.

(Received September 12, 1941)

The interaction between a molecule and a metal surface is discussed from the point of view of the perturbation theory. The interaction energy is found to be inversely proportional to the distance, R, between metal and molecule if the electron degeneracy in the metal is not taken into account and to $R^{-2}\log R$ if this degeneracy is taken into account. The application of the perturbation theory as given here is limited to values of R of the order of magnitude of the Bohr radius because of the neglect of the electron-electron interaction.

1. INTRODUCTION

THE energy of interaction of an atom or molecule with a metal surface has been calculated by Lennard-Jones[1] with the help of a semi-classical picture of the interaction process. He treated the metal classically; that is, its effect on the molecule was assumed to be given by the classical image potential acting on the electrons and nuclei in the molecule. On the other hand, the molecule was treated as a quantum-mechanical system with this image potential acting as a perturbation. The resulting interaction energy turned out to be proportional to R^{-3}, where R is the distance between the molecule and metal surface.

The limitations of this treatment have been discussed by Bardeen[2] who estimated that when the metal as well as the molecule is treated quantum mechanically the resulting interaction energy is still proportional to R^{-3} but it is about half as great as that given by Lennard-Jones. The discrepancy arises from the fact that the Lennard-Jones treatment neglects a term in the kinetic energy of the system of molecule plus metal.

The purpose of the present paper is to treat the problem of the interaction of the molecule and metal directly by means of the perturbation theory. In order to calculate the interaction energy in this way it will be necessary to make specific assumptions about the metal wave functions. In Section 2 these wave functions will be assumed to be products of plane electron waves with the result that the interaction energy is proportional to R^{-1}. Since the exclusion principle has not been taken into account, this result applies only when the density of conduction electrons in momentum space is low; that is, it applies to semiconductors and probably to metals at very high temperatures.

In Section 3 the influence of the exclusion principle is considered. The resulting interaction energy is proportional to $R^{-2}\log R$. Thus, in both cases (Sections 2 and 3) the perturbation theory leads to a smaller interaction energy than the Lennard-Jones and Bardeen treatments for small R. For large R the perturbation method as given here breaks down because of the neglect of the interactions between electrons in the metal. It will be shown in Section 4 that these interactions become important at that value of R for which the perturbation and Lennard-Jones energies become equal. Thus, taking into account the result of Bardeen, it appears that the Lennard-Jones treatment gives an upper limit to the binding energy for all values of R.

It is interesting to note that the R^{-3} dependence of energy on distance is just what would be expected for the interaction of a molecule with the surface of an insulator. The van der Waals interaction between each atom in the insulator and the external molecule is proportional to the inverse sixth power of the distance between them. If this interaction is integrated over all atoms in the insulator, the resulting total interaction is proportional to R^{-3}.

† A more detailed version of this paper was submitted by E. J. R. Prosen as a thesis to the George Washington University for the degree of Master of Arts, February, 1941.

* Now at the University of California, Berkeley, California.

[1] J. E. Lennard-Jones, Trans. Faraday Soc. **28**, 333 (1932).

[2] J. Bardeen, Phys. Rev. **58**, 727 (1940).

2. INTERACTION WITH A SEMICONDUCTOR

If the molecule is so far from the metal surface that the wave functions of the molecule and metal electrons do not overlap appreciably, the interaction between the molecule and metal may be treated as a perturbation. In first approximation, this interaction is due to the field of the instantaneous dipole moment of the molecule which acts on the electrons and positive ions in the metal. Since the average value of the dipole moment of the molecule is zero, the first-order perturbation energy vanishes and the energy of interaction of the molecule and metal will be given by the second-order term

$$W=\sum_m{}' \frac{P_{0m}P_{m0}}{E_0-E_m},$$

where $P_{0m}=P_{m0}^*$ are the matrix elements given by

$$P_{0m}=\int \psi_0^* P \psi_m d\tau.$$

ψ_0 and ψ_m are the wave functions of the system of molecule plus metal in the initial state and in the mth excited state, respectively. P is the potential energy of the interaction of the electrons and positive ions in the metal with the instantaneous dipole field of the molecule. E_0 and E_m are the energies of the states ψ_0 and ψ_m.

The potential energy P is the sum of three terms:

$$P=P^x+P^y+P^z,$$

where

$$P^x=M^xH^x, \quad P^y=M^yH^y, \quad P^z=M^zH^z.$$

M^x, M^y, and M^z are the components of the dipole moment of the molecule and H^x, H^y, and H^z are quantities depending only on the position of the center of gravity of the molecule and the positions of the electrons and positive ions in the metal. The explicit expressions for H^x, H^y, and H^z will be given below.

Since in zeroth approximation the metal and molecule are independent systems, the wave functions ψ_0 and ψ_m can be written as the product of a molecular wave function, ϕ, and a metal wave function, χ; thus

$$\psi_0=\phi_0\chi_0, \quad \psi_m=\phi_j\chi_k$$

and P_{0m}^x

$$P_{0m}^x=\int \phi_0^* M^x \phi_j d\tau \int \chi_0^* H^x \chi_k d\tau,$$

or

$$P_{0m}^x=M_{0j}^xH_{0k}^x, \quad P_{0m}^y=M_{0j}^yH_{0k}^y, \quad P_{0m}^z=M_{0j}^zH_{0k}^z.$$

Therefore

$$W=\sum_{x,j,k}{}' \frac{M_{0j}^xM_{j0}^xH_{0k}^xH_{k0}^x}{E_{00}-E_{jk}}. \tag{1}$$

$\sum_{x,j,k}$ indicates a summation over $x=x, y, z$, over all states j of the molecule, and over all states k of the metal. The prime indicates that the term $j=0$ is to be omitted.[3] By definition

$$E_{00}=E_0+E'_0, \quad E_{jk}=E_j+E'_k,$$

where E_0 and E_j refer to the energies of the ground and jth states of the molecule and E'_0, E'_k to the initial and kth states of the metal.

In Eq. (1) cross terms of the type

$$M_{0j}^xM_{j0}^yH_{0k}^xH_{k0}^y$$

do not occur as can be shown by consideration of the symmetry properties of the dipole moment with respect to reflection in planes of symmetry.

The expression $E_{00}-E_{jk}$ which occurs in the denominator of Eq. (1) is equal to $(E_0-E_j)+(E'_0-E'_k)$ where $E'_0-E'_k$ refers to an electron transition in the metal. The positive ions in the metal can also make transitions to new vibrational states but their contribution to the interaction energy can be shown to be small. Electronic transitions corresponding to large energy changes, $E'_0-E'_k$, will contribute little to the interaction energy as compared to those involving small ones because the dipole field varies slowly in the metal so that in the Fourier expansion of this field in the metal the short wave-length terms corresponding to large momentum changes for the electrons have small amplitudes. Thus, for all important terms in Eq. (1), $E'_0-E'_k$ may be neglected as compared to E_0-E_j in the energy denominator. The interaction energy can then be written

$$W=\sum_{x,j\neq 0} \frac{M_{0j}^xM_{j0}^x}{E_0-E_j}(\textstyle\sum_k H_{0k}^xH_{k0}^x).$$

[3] The terms for which $j=0, k=0$ do not occur because the diagonal elements of the dipole moment vanish.

This expression can be simplified by observing that

$$\alpha_{xx}=-2\sum'_j\frac{M^x_{0j}M^x_{j0}}{E_0-E_j},$$

$$\alpha_{yy}=-2\sum'_j\frac{M^y_{0j}M^y_{j0}}{E_0-E_j},$$

$$\alpha_{zz}=-2\sum'_j\frac{M^z_{0j}M^z_{j0}}{E_0-E_j}$$

are the diagonal elements of the polarizability tensor of the molecule. Therefore

$$W=-\tfrac{1}{2}\sum_x\alpha_{xx}(\sum_k H^x_{0k}H^x_{k0}).$$

Averaged over all orientations of the molecule, this becomes

$$W=-\tfrac{1}{2}\alpha\sum_{x,k}H^x_{0k}H^x_{k0} \qquad (2)$$

with

$$\alpha=\langle\alpha_{xx}\rangle_{Av}=\langle\alpha_{yy}\rangle_{Av}=\langle\alpha_{zz}\rangle_{Av}.$$

The quantities H^x are sums of terms corresponding to the interaction of the dipole field of the molecule with each electron and positive ion in the metal. Thus H^x can be expressed in the form

$$H^x=\sum_e H^x(e)+\sum_n H^x(n)$$

with

$$H^x(e)=\epsilon x_e/r_e^3,\quad H^x(n)=-\epsilon x_n/r_n^3, \qquad (3)$$

where $\mathbf{r}_e=(x_e, y_e, z_e)$, $\mathbf{r}_n=(x_n, y_n, z_n)$ are the distances between the molecule and the eth electron and nth positive ion, respectively. ϵ is the electronic charge. Similar equations hold for the terms in y and z. The calculation for just the x term will be carried out until further notice. The x axis is perpendicular to the surface of the metal.

We now have

$$\sum_k H^x_{0k}H^x_{k0}=\sum_k(\sum_e H^x_{0k}(e)+\sum_n H^x_{0k}(n))\times(\sum_e H^x_{k0}(e)+\sum_n H^x_{k0}(n)).$$

Since the positive ions do not undergo transitions, only those positive ion terms with $k=0$ are important. Therefore

$$\sum_k H^x_{0k}H^x_{k0}=\sum_k(\sum_e H^x_{0k}(e)+\sum_n H^x_{00}(n)\delta_{0k})\times(\sum_e H^x_{k0}(e)+\sum_n H^x_{00}(n)\delta_{k0}). \qquad (4)$$

The terms $\sum_n H^x_{00}(n)$ just cancel the sums of the electron diagonal matrix elements if we assume a smeared out charge distribution for the positive ions. If the positive ions are properly treated as discrete particles, these terms do not exactly cancel since there is a non-vanishing field outside of the metal. However this field vanishes exponentially over a distance of the order of a lattice spacing in the metal. Therefore, as long as the molecule is at a distance from the metal surface that is great compared to the lattice spacing, the difference between the terms can be neglected and Eq. (4) becomes

$$\sum_k H^x_{0k}H^x_{k0}=\sum_{k\neq 0}(\sum_e H^x_{0k}(e))(\sum_e H^x_{k0}(e)). \qquad (5)$$

It is now necessary to make some specific assumption about the wave functions of the electrons in the metal. For the present it will be assumed that these functions are products of plane waves. Thus if $u_\alpha{}^\alpha$ is the plane wave $\exp(-ik_\alpha r_\alpha)$ corresponding to the αth electron in the αth state, the wave function for the initial state will be taken to be

$$\chi_0=\prod_\alpha u_\alpha{}^\alpha. \qquad (6a)$$

The only excited states, χ_k, that will be of interest are those for which only one electron, say the βth, is excited to the state β'. The wave functions for these states are assumed to be

$$\chi_{\beta'}=u_\beta{}^{\beta'}\prod_{\alpha\neq\beta}u_\alpha{}^\alpha, \qquad (6b)$$

if

$$u_\beta{}^{\beta'}=c\exp(-ik_{\beta'}r_\beta).$$

The quantitative discussion of the effect of the Fermi degeneracy will be taken up in the next section. However if the density of electrons in momentum space is much less than two electrons per h^3/V (V is the volume of the metal), the effect of the Fermi degeneracy is negligible. Therefore the calculations in this section can be applied to semi-conductors and probably to metals at very high temperatures, since in these cases the density of conduction electrons in momentum space is small.

The interaction between electrons is neglected in both this section and next. It will be shown in Section 4 that the relative error introduced by this neglect increases with increasing distance between metal and molecule.

Making use of the wave functions (6), one finds

$$H^x_{0\beta'}(\beta)=\int u_\beta{}^{\beta*}H^x(\beta)u_\beta{}^{\beta'}d\tau_\beta \qquad (7)$$

$$H^x_{0\beta'}(\alpha)=0, \quad \alpha\neq\beta,$$

because of the orthogonality of the $u_\beta{}^{\beta*}$ and $u_\beta{}^{\beta'}$. Also because of this orthogonality, all matrix elements $H^x_{0k}(e)$ vanish for which more than one electron makes a transition since the operator $H^x(e)$ involves the coordinates of only one electron. With these results, Eq. (5) may be expressed in the form

$$\sum_k H^x_{0k}H^x_{k0}=\sum_\beta \sum_{\beta'\neq 0} H^x_{0\beta'}(\beta)H^x_{\beta' 0}(\beta). \qquad (8)$$

It can be seen that

$$\sum_{\beta'} H^x_{0\beta'}(\beta)H^x_{\beta' 0}(\beta)=(H^{x^2}(\beta))_{00}$$

or

$$\sum_{\beta'\neq 0} H^x_{0\beta'}(\beta)H^x_{\beta' 0}(\beta)=(H^{x^2}(\beta))_{00}-(H^x_{00}(\beta))^2. \qquad (9)$$

It is not difficult to show by means of Eqs. (3) and (7) that $(H^x_{00}(\beta))^2$ is proportional to L^{-1} where L is a measure of the linear dimensions of the metal. Thus, if the metal is sufficiently large, this term can be neglected and Eq. (8) becomes

$$\sum_k H^x_{0k}H^x_{k0}=\sum_\beta (H^{x^2}(\beta))_{00}. \qquad (10)$$

Now

$$(H^{x^2}(\beta))_{00}=\int u_\beta{}^{\beta*}H^{x^2}(\beta)u_\beta{}^{\beta}d\tau_\beta$$

or since $u_\beta{}^\beta=L^{-\frac{3}{2}}\exp(-ik_\beta r_\beta)$,

$$(H^{x^2}(\beta))_{00}=L^{-3}\int (H^x(\beta))^2 d\tau_\beta=\epsilon^2 L^{-3}\int\int\int \frac{x^2}{r^6}dxdydz$$

according to Eq. (3). Summing this over all electrons in the metal is equivalent to multiplying by ρL^3, where ρ is the number of electrons per unit volume in the metal, so

$$\sum_k H^x_{0k}H^x_{k0}=\rho\epsilon^2\int\int\int \frac{x^2dxdydz}{(x^2+y^2+z^2)^3}.$$

The integration is to be carried out over the volume of the metal which will be taken to be an infinite half-space.

If R is the perpendicular distance between the molecule and metal, an elementary integration yields

$$\rho\epsilon^2\int_{-\infty}^{\infty}\int_{-\infty}^{\infty}\int_R^{\infty}\frac{x^2dxdydz}{(x^2+y^2+z^2)^3}=\frac{\rho\epsilon^2\pi}{2R}.$$

The corresponding terms involving H^y and H^z are

$$\sum_k H^y_{0k}H^y_{k0}=\rho\epsilon^2\int_{-\infty}^{\infty}\int_{-\infty}^{\infty}\int_R^{\infty}\frac{y^2dxdydz}{(x^2+y^2+z^2)^3}=\frac{\rho\epsilon^2\pi}{4R}$$

and

$$\sum_k H^z_{0k}H^z_{k0}=\frac{\rho\epsilon^2\pi}{4R},$$

respectively.

Inserting these results in Eq. (2), one obtains

$$W=-\frac{\alpha}{2}\frac{\pi\rho\epsilon^2}{R}. \qquad (11)$$

It is to be noted that in the above derivation no explicit use has been made of the assumption that the electron wave functions are plane waves.

3. THE EFFECT OF ELECTRON DEGENERACY

In order to take into account the Fermi degeneracy of the electrons in the metal, it is necessary to antisymmetrize the wave functions (6). Then the electrons cannot make transitions to those states that are already occupied so the sum on the right-hand side of Eq. (8) is not carried out over a complete set of one-electron states and the completeness theorem, Eq. (9), can no longer be applied. It will therefore be necessary to calculate the sum

$$S_x(\beta)=\sum_{\beta'\neq 0} H^x_{0\beta'}(\beta)H^x_{\beta' 0}(\beta),$$

where β' runs through all values corresponding to only unoccupied states.

Since, insofar as the calculation of matrix elements is concerned, the only important part of the function $H^x(\beta)$ is that part for which the wave functions of the metal electrons do not vanish, we introduce the function $f_x(x, y, z)$ which is equal to $H^x(\beta)$ within the metal and zero outside of the metal. Thus, according to Eq. (3),

$$f_x=\epsilon x/r^3, \quad f_y=\epsilon y/r^3, \quad f_z=\epsilon z/r^3$$

for $x>R$, and

$$f_x=f_y=f_z=0$$

for $x<R$ if the x axis is perpendicular to the surface of the metal and its origin is taken to be at the molecule.

The functions f_x, f_y, and f_z can be expressed as Fourier integrals;

$$f_x=\int_{-\infty}^{\infty}\int_{-\infty}^{\infty}\int_{-\infty}^{\infty} a_x(\boldsymbol{\tau})\exp[i(\boldsymbol{\tau}\cdot\mathbf{r})]d\tau_x d\tau_y d\tau_z,$$

where the amplitudes $a_x(\boldsymbol{\tau})$ are determined by

$$a_x(\boldsymbol{\tau})=\frac{1}{2\pi^3}\int_{-\infty}^{\infty}\int_{-\infty}^{\infty}\int_{-\infty}^{\infty} f_x\exp[-i(\boldsymbol{\tau}\cdot\mathbf{r})]dxdydz.$$

With the wave functions (6), the matrix element is

$$H^x_{0\beta'}(\beta)=L^{-3}\int_{-\infty}^{\infty}\int_{-\infty}^{\infty}\int_{-\infty}^{\infty} f_x\exp[i([\mathbf{k}_\beta-\mathbf{k}_{\beta'}]\cdot\mathbf{r})]dxdydz$$

or

$$H^x_{0\beta'}(\beta)=(2\pi)^3 a_x(\boldsymbol{\tau})L^{-3} \tag{12}$$

with

$$\boldsymbol{\tau}=\mathbf{k}_{\alpha'}-\mathbf{k}_\alpha.$$

The explicit expressions for the Fourier amplitudes are

$$a_x(\boldsymbol{\tau})=\frac{\epsilon}{(2\pi)^3}\int_{-\infty}^{\infty}\int_{-\infty}^{\infty}\int_{R}^{\infty}\frac{x\exp[-i(\boldsymbol{\tau}\cdot\mathbf{r})]}{(x^2+y^2+z^2)^{\frac{5}{2}}}dxdydz.$$

In order to carry out the integration over x, consider the complex integral

$$\oint\frac{\xi\exp(-i\tau_x\xi)}{(\xi^2+a^2)^{\frac{5}{2}}}d\xi=0$$

with $\xi=x+iw$ and $a^2=y^2+z^2$. The path of integration is indicated in Fig. 1. Letting the radius bd of

the arc *cd* approach infinity, we obtain

$$\int_R^\infty \frac{x\exp(-i\tau_x x)}{(x^2+a^2)^{\frac{1}{2}}}dx = i\exp(-i\tau_x R)\int_0^{-\infty}\frac{(R+iw)\exp(\tau_x w)}{(R^2+2iRw-w^2+a^2)^{\frac{1}{2}}}dw.$$

Integration of the right-hand side of this equation by parts yields

$$\int_R^\infty \frac{x\exp(-i\tau_x x)}{(x^2+a^2)^{\frac{1}{2}}}dx = \frac{i\exp(-i\tau_x R)}{\tau_x}\left[\frac{R}{(R^2+a^2)^{\frac{1}{2}}} - \frac{i}{\tau_x}\frac{a^2-2R^2}{(R^2+a^2)^{\frac{3}{2}}}+\cdots\right]. \tag{13}$$

This expansion is valid only if the changes, τ_x, in momentum of the electron are greater than R^{-1}

If only the first term of the expansion is used,

$$a_x(\boldsymbol{\tau}) = \frac{i\exp(-i\tau_x R)}{(2\pi)^3}\frac{\epsilon}{\tau_x}\int_{-\infty}^{\infty}\int_{-\infty}^{\infty}\frac{R\exp[-i(\tau_y y+\tau_z z)]}{(R^2+y^2+z^2)^{\frac{3}{2}}}dydz. \tag{14}$$

It can be shown[4] that the integral over y and z behaves like $\exp(-[\tau_y+\tau_z]R)$, so the important amplitudes occur for those changes in momentum that are less than R. Therefore the only important changes, $\boldsymbol{\tau}$, in momentum are those vectors lying in a cylinder which is parallel to the x axis and has a radius equal to R^{-1} (cf. Fig. 2).

The expression that is to be evaluated is, according to Eq. (12)

$$S_x(\beta) = \sum_{\beta'\neq 0} H^x_{0\beta'}(\beta)H^x_{\beta' 0}(\beta) = \frac{(2\pi)^3}{L^3}\iiint |a_x(\boldsymbol{\tau})|^2 d\tau_x d\tau_y d\tau_z. \tag{15}$$

The limits of integration are to be chosen in such a way that $\boldsymbol{\tau}=\mathbf{k}_{\alpha'}-\mathbf{k}_\alpha$ corresponds to a transition from a filled to an unfilled state. According to Fig. 2, this means that, for positive τ_x, the lower limit on τ_x is equal to $k_{mx}-k_{\beta x}$, where the vector $\mathbf{k}_m$ has a magnitude given by the momentum of the electron in the highest occupied state in the metal and a direction such that its end point lies in the cylinder of allowed transitions. For negative τ_x, the upper limit is given by $-(k_{mx}+k_{\beta x})$.

The integration is to be carried out over all values of τ_y and τ_z since the lower limit on τ_x makes it certain that the transition will carry the electron out of the Fermi lake. Therefore Eq. (15) is

$$S_x(\beta) = 2\pi^3 L^{-3}\int_{-\infty}^{\infty}\int_{-\infty}^{\infty}\left[\int_{(k_{mx}-k_{\beta x})}^{\infty}|a_x|^2 d\tau_x + \int_{-\infty}^{-(k_{mx}+k_{\beta x})}|a_x|^2 d\tau_x\right]d\tau_y d\tau_z. \tag{16}$$

The integration over τ_y, τ_z can be replaced by one over y, z by means of Parseval's theorem which can be expressed in the form

$$\int_{-\infty}^{\infty}\int_{-\infty}^{\infty}|a_x(\boldsymbol{\tau})|^2 d\tau_y d\tau_z = \frac{1}{(2\pi)^4}\int_{-\infty}^{\infty}\int_{-\infty}^{\infty}\frac{\epsilon^2 R^2 dydz}{\tau_x^2(R^2+y^2+z^2)^3} = \frac{1}{4(2\pi)^3}\frac{\epsilon^2}{\tau_x^2 R^2},$$

when use is made of Eq. (14). Thus

$$S_x(\beta) = \frac{\epsilon^2}{4L^3R^2}\left[\int_{(k_{mx}-k_{\beta x})}^{\infty}\frac{d\tau_x}{\tau_x^2}+\int_{-\infty}^{-(k_{mx}+k_{\beta x})}\frac{d\tau_x}{\tau_x^2}\right] = \frac{\epsilon^2}{2L^3R^2}\frac{k_{mx}}{(k_{mx}^2-k_{\beta x}^2)}.$$

Similarly

$$S_y(\beta) = S_z(\beta) = \frac{\epsilon^2}{4L^3R^2}\frac{k_{mx}}{(k_{mx}^2-k_{\beta x}^2)}; \tag{17}$$

and finally

$$\sum_x S_x(\beta) = \frac{\epsilon^2}{L^3R^2}\frac{k_{mx}}{(k_{mx}^2-k_{\beta x}^2)}.$$

[4] Cf. E. T. Whittaker and G. N. Watson, *A Course of Modern Analysis* (Cambridge University Press, 1927), p. 384.

According to Eq. (8), this expression is to be summed over all electrons, i.e., over β. The number of electrons with momenta between $\mathbf{k}$ and $\mathbf{k}+d\mathbf{k}$ is $2(2\pi)^{-3}L^3dk_xdk_ydk_z$ hence the sum over electrons is

$$\sum_{\beta,x} S_x(\beta)=\frac{2\epsilon^2}{(2\pi)^3R^2}\int\int\int \frac{k_{mx}}{k_{mx}^2-k_x^2}dk_xdk_ydk_z.$$

Since the expansion (13) is valid only for changes, τ_x, in momentum that are greater than $1/R$, the upper limit in the integration over k_x will be taken to be $k_{mx}-1/R$. The contribution of those electrons with momenta between k_{mx} and $k_{mx}-1/R$ will be estimated below. Integration over k_x gives

$$\sum_{\beta,x} S_x(\beta)=\frac{2\epsilon^2}{(2\pi)^3R^2}\int\int \log(2Rk_{mx}-1)dk_ydk_z. \tag{18}$$

according to the definition of $\mathbf{k}_m$, $k_{mx}^2=k_m^2-(k_y^2+k_z^2)$. If this is inserted into (18), the double integral can be carried out directly by introducing polar coordinates in the k_y-k_z plane. The limits of integration are to be chosen in such a way that $1/R\leq k_{mx}\leq k_m$. The result is

$$\sum_{\beta,x} S_x(\beta)=\frac{2\epsilon^2}{(2\pi)^3}\frac{\pi k_m^2}{R^2}\log 2k_mR, \tag{19}$$

when R is chosen in such a way that $k_mR\gg 1$.

The contribution of electrons with momenta between k_{mx} and $k_{mx}-1/R$ is still to be added to (19). This contribution is certainly less than that of an equal number of free electrons. The latter can be obtained from the results of Section 2, for according to this section, if all the electrons were free the right-hand side of Eq. (19) should be replaced by $\pi\rho\epsilon^2/R$. Since the ratio of the number of electrons with momenta between k_{mx} and $k_{mx}-1/R$ to the total number is $3/k_mR$, the term that is to be added to (19) is less than $3\pi\rho\epsilon^2/R^2k_m$. By substituting $\rho=k_m^3/3\pi^2$, the ratio of the added term to the term already given is less than $1/4\pi\log 2k_mR$. This quantity is much less than one for $k_mR\gg 1$, so the additional term can be neglected and Eq. (19) is correct as it stands.

The interaction energy can now be obtained from Eq. (2) by making use of Eqs. (8) and (19) and the definition of $S_x(\beta)$. The result is

$$W=-\frac{\alpha\epsilon^2\pi k_m^2}{(2\pi)^3}\frac{\log 2k_mR}{R^2}. \tag{20}$$

The factor πk_m^2 in this expression is just the area of that cross section of the surface of maximum energy in momentum space which passes through the origin and is perpendicular to the x axis.

The assumption that the constant energy surfaces in momentum spaces are spheres is, of course, an idealized one. For a real metal, account should be taken of the true dependence of energy on momentum. However, since Eq. (20) does not depend explicitly on the mass of the electron, the more correct formula can be obtained from Eq. (20) simply by replacing the cross-sectional area πk_m^2 by the corresponding area for the actual surface of maximum energy. If it happens that the surface of maximum energy touches the surface of a Brillouin zone, the area of contact must be subtracted from the cross-sectional area.

4. THE ELECTRON-ELECTRON INTERACTION

In the two foregoing sections, use has been made of metal wave functions that are products of one-electron functions. This implies that the Coulomb interaction between electrons in the metal has been taken into account only insofar as the average effect of all electrons on a given electron in concerned.

When the molecule is near the metal, the wave function of the metal electrons is perturbed. This change in wave function implies a change in charge density near the surface of the metal, which in turn involves a change in the Coulomb interaction between electrons. An estimate of the change in Coulomb energy can be obtained by averaging the electron-electron interaction over

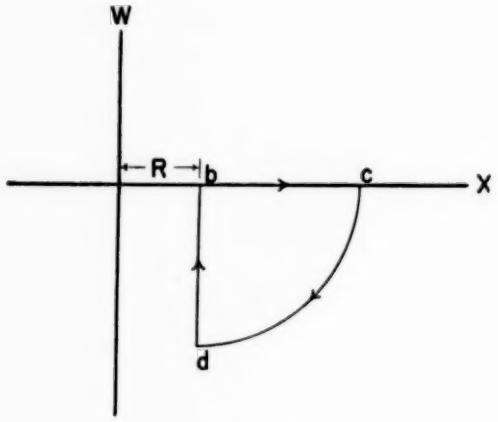

FIG. 1. Path of integration.

the perturbed wave function which is

$$\psi=\phi_0\chi_0+\sum_x\sum_{\beta'}\sum_{j\neq 0}\frac{M^x_{0j}}{E_0-E_j}H^x_{0\beta'}\phi_j\chi_{\beta'}. \quad (21)$$

The notation used here is the same as that given in Section 2.

An estimate of this average can be given for the case of the semi-conductor (Section 2) but is somewhat more difficult to obtain when the Fermi degeneracy is taken into account. In the latter case, the electron-electron interaction is somewhat smaller than in the former because the antisymmetrization of the wave function implies a greater average distance between electrons. Therefore an estimate given for the Coulomb term in the non-degenerate case is an upper limit for that term in the degenerate case, and the limits of validity to be given below for the former result (Eq. 11) are, if anything, too stringent when applied to the latter result (Eq. 20).

The average over the wave function (21) can be carried out by introducing the Fourier analysis of the interaction potential in the same way as in Section 3. When the sum in Eq. (21) is carried out over all one-electron states, the average value of the sum of the electron-electron, electron-positive ion, and positive ion-positive ion interactions is found to be

$$K=\frac{\rho^2}{2}\sum_{j\neq 0}\frac{M^x_{0j}M^x_{j0}}{(E_0-E_j)^2}\int\int\frac{\epsilon^4 x_1x_2d\tau_1d\tau_2}{r_1^3r_2^3|\mathbf{r}_1-\mathbf{r}_2|}. \quad (22)$$

The integration over both sets of variables is to be carried out over the volume of the metal so it is apparent that the integral diverges as the volume approaches infinity.

In order to eliminate this difficulty, the electron-electron interaction should be taken into account in the perturbation calculation. Since the effect of this interaction is to shield the electrons within the metal from the field of the dipole, it can be taken into account in a rough way by introducing a cut-off factor in the interaction potential between molecule and metal. For example, the potential $H^x(\beta)$ can be replaced by $H^x(\beta)\exp(-\mu\cdot\mathbf{r}_\beta)$, where μ is to be chosen large enough to guarantee that the average electron-electron interaction is small compared to the interaction between metal and molecule. It will be shown below that for sufficiently small values of R, this can be done in such a way that the energy W is still given by Eq. (11) to a very good approximation. The validity of the method is questionable for larger values of R since, then, the details of the method used in cutting off the potential become important.

Using the cut-off potential given above, the energy of interaction between metal and molecule becomes

$$W=-\frac{\alpha\rho}{2}\sum_x\int[H^x(\beta)]^2\exp[-2(\mu\cdot\mathbf{r}_\beta)]d\tau_\beta.$$

For $(\mu\cdot\mathbf{r}_\beta)<1$, the exponential can be expanded

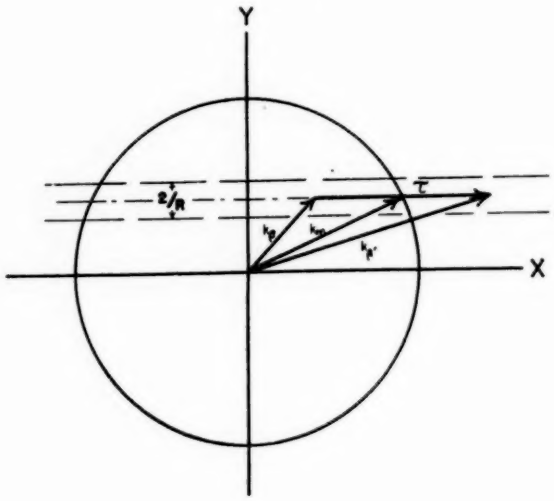

FIG. 2. Momentum vectors.

with the result

$$W=-\frac{\pi}{2}\alpha\rho\epsilon^2\left(\frac{1}{R}+\frac{2}{3}\mu\right)$$
$$+\alpha\rho\int_{(\mu\cdot\mathbf{r}_\beta)\leq 1}[II^z(\beta)]^2(\boldsymbol{\mu}\cdot\mathbf{r}_\beta)d\tau_\beta+\cdots.$$

The first term is just the value of W given by Eq. (11). It is not difficult to show that the term involving the integral becomes appreciable if

$$\mu\approx 1/R. \tag{23}$$

Thus the cut-off potential gives the same energy as the original treatment only if $\mu<1/R$.

Equation (22) is to be replaced by

$$K=\frac{\rho^2}{2}\sum_{j\neq 0}\frac{M^x_{0j}M^x_{j0}}{(E_0-E_j)^2}$$
$$\times\int\int\frac{\epsilon^4x_1x_2\exp\{-(\boldsymbol{\mu}\cdot[\mathbf{r}_1+\mathbf{r}_2])\}}{r_1^3r_2^3|\mathbf{r}_1-\mathbf{r}_2|}d\tau_1d\tau_2.$$

A rough evaluation of the integral yields

$$K\approx\frac{\pi^2\rho^2\epsilon^4}{\mu^5R^4}\sum_{j\neq 0}\frac{M^x_{0j}M^x_{j0}}{(E_0-E_j)^2}=\frac{\pi^2\rho^2\epsilon^4\alpha}{\mu^5R^4\Delta E},$$

where ΔE is some average difference in energy between levels in the molecule. The condition that K be negligible compared to W is

$$\frac{2\pi\rho\epsilon^2}{\mu^5R^3\Delta E}<1.$$

If Eq. (23) is taken into account, it follows that Eq. (11) breaks down for values of R of the order of magnitude of, or greater than $(\Delta E/2\pi\rho\epsilon^2)^{\frac{1}{3}}$. This distance is of the order of magnitude of the Bohr radius if ΔE refers to electronic transitions. The conclusion is, then, that there is, at best, a narrow region for which the Coulomb term can be neglected under the condition that the overlap between the molecular and metal wave functions is sufficiently small to justify a perturbation treatment. For semiconductors this region is much larger than for metals because of the smaller value of ρ for semiconductors.

Finally, the present method should be compared to that of Margenau and Pollard[5] which is also based on the second-order perturbation theory. They computed the interaction of the dipole field of a small element of metal with the molecule. The interaction of the molecule with a half-infinite metal body was then obtained by considering the metal to be made up of many such small elements and adding the contributions of each of them. The details of the metal wave functions were taken into account, at least in part, by introducing the experimentally measurable polarizability of the element of metal.

In order that the field of a metal element be correctly represented by a dipole field, the linear dimensions of the metal elements must be small compared to the distance, R, between the metal and molecule. Otherwise the higher multipole fields of the metal elements become important. On the other hand, the division of the metal into elements cannot be arbitrarily fine since it must be certain that each element behaves like a macroscopic piece of metal (i.e., has an experimentally measurable polarizability). This implies that the linear dimensions of the element must be very large compared to the lattice distance.

When these two conditions are taken together, it is apparent that R must be very large compared to the lattice distance. Thus the treatment of Margenau and Pollard applies for relatively great values of R, while, as we have seen before, the results given here are valid only in the region of small R. The interaction in the treatment given here will be particularly important for the calculation of heats of adsorption when much more becomes known of the repulsion potential between the molecule and metal.

The authors are indebted to Professor Teller for suggesting this problem and for many helpful discussions concerning it.

[5] H. Margenau and W. G. Pollard, Phys. Rev. **60**, 128 (1941).

The Thermal Expansion of Pure Metals. II: Molybdenum, Palladium, Silver, Tantalum, Tungsten, Platinum, and Lead

F. C. NIX AND D. MACNAIR
Bell Telephone Laboratories, New York, New York
(Received November 28, 1941)

Extremely accurate determinations of the linear thermal expansions have been made interferometrically from room temperature to the temperature of liquid nitrogen for Mo, Pd, Ag, Ta, W, Pt, and Pb. Comparisons are made with the Grueneisen theory.

THIS research is an extension of work on other metals reported in a paper of the same title.[1] It was undertaken in order to obtain much needed data on the true coefficients of thermal expansion and also to subject the well-known Grueneisen relationship to further experimental test.

The Grueneisen theory[2] expresses the true linear coefficient of thermal expansion as a function of the specific heat and two constants, Q_0 and $(M+N+3)/6$, as follows:

$$\beta=\frac{C_v}{3Q_0\left[1-\frac{M+N+3}{6}\frac{E}{Q_0}\right]^2}. \quad (1)$$

Here β is the true coefficient of thermal expansion, C_v the specific heat at constant volume, and

$$E=\int_0^T C_v dt.$$

M and n are the exponents in the attractive and repulsive terms, respectively, in the Mie equation relating the potential energy to the distance between vibrating atoms in a monatomic solid. The constant Q_0 is expressible in terms of specific heat and coefficient of thermal expansion. For further details the reader is referred to the above-mentioned paper.

In obtaining a fit of the Gueneisen curve to the data one was able in most cases to use the characteristic Debye temperature θ, found from specific heat measurements, along with values of Q_0 and $(M+N+3)/6$ obtained by fitting the curve to the data at one point.

TABLE I.

Metal	Source	Purity
Mo	Westinghouse Lamp Co.	>99.95 Wt. % Mo
Pd	International Nickel Co.	>99.99 Wt. % Pd
Ag	Handy and Harmon	99.999 Wt. % Ag
Ta	Fansteel Metallurgical Corp.	99.9 Wt. % Ta 0.01 Wt. % Fe 0.003 Wt. % C
W	Westinghouse Lamp Co.	>99.95 Wt. % W
Pt	Refined in B.T.L.	>99.99 Wt. % Pt
Pb	National Lead Co.	>99.99 Wt. % Pb

METHOD OF MEASUREMENTS

The measurements were made with an interferometric dilatometer previously described by us,[3] in the manner used in our initial work on pure metals.

EXPERIMENTAL RESULTS

The sources of the metals used in this investigation, and their degree of purity as reported by their sources are shown in Table I.

TABLE II. Molybdenum.

Temp. °C	$\Delta l/l_0\times10^4$	Temp. °C	$\Delta l/l_0\times10^4$
−187.0	−7.904	−59.5	−2.964
−182.5	−7.784	−54.7	−2.723
−172.0	−7.543	−49.0	−2.482
−165.5	−7.302	−44.5	−2.241
−156.5	−7.061	−39.5	−2.000
−149.5	−6.820	−35.0	−1.759
−143.0	−6.579	−29.9	−1.518
−136.0	−6.338	−25.0	−1.277
−129.5	−6.097	−20.0	−1.036
−123.5	−5.856	−15.6	−0.795
−117.0	−5.615	−10.7	−0.554
−111.5	−5.374	−6.8	−0.313
−107.0	−5.133	−1.5	−0.072
−100.7	−4.892	0	0
−94.8	−4.651	3.0	0.168
−90.0	−4.410	7.5	0.409
−85.0	−4.169	12.0	0.650
−80.0	−3.928	17.1	0.891
−74.9	−3.687	21.0	1.133
−69.5	−3.446	25.0	1.350
−64.0	−3.205		

[1] F. C. Nix and D. MacNair, Phys. Rev. **60**, 597 (1941).
[2] E. Grueneisen, *Handbuch der Physik*, Vol. 10, p. 1.
[3] F. C. Nix and D. MacNair, Rev. Sci. Inst. **12**, 66 (1941).

TABLE III. Palladium.

Temp. °C	$\Delta l/l_0 \times 10^4$	Temp. °C	$\Delta l/l_0 \times 10^4$
−187.0	−19.399	−65.0	−7.425
−183.0	−18.955	−61.5	−6.961
−179.0	−18.564	−57.0	−6.497
−173.0	−18.099	−52.6	−6.033
−166.5	−17.635	−48.7	−5.546
−163.5	−17.171	−44.5	−5.105
−156.0	−16.707	−40.2	−4.641
−153.0	−16.266	−36.5	−4.177
−147.0	−15.825	−32.5	−3.713
−139.8	−15.222	−28.5	−3.249
−131.0	−14.387	−24.1	−2.785
−128.0	−14.039	−20.3	−2.320
−121.2	−13.551	−16.6	−1.856
−117.0	−13.111	−12.6	−1.392
−112.0	−12.530	−8.6	−0.928
−105.5	−11.881	−4.5	−0.464
−100.0	−11.185	0	0
−95.2	−10.744	3.1	0.371
−91.0	−10.280	8.1	0.928
−86.0	−9.746	12.1	1.392
−82.3	−9.259	16.0	1.856
−78.0	−8.818	21.0	2.320
−73.0	−8.354	26.0	2.901
−70.0	−7.890		

TABLE IV. Silver.

Temp. °C	$\Delta l/l_0 \times 10^4$	Temp. °C	$\Delta l/l_0 \times 10^4$
−186.0	−31.853	−67.7	−12.519
−181.0	−31.057	−63.0	−11.680
−176.0	−30.133	−58.6	−10.841
−170.0	−29.421	−54.0	−10.003
−163.0	−28.540	−49.6	−9.164
−158.5	−27.617	−44.6	−8.325
−152.0	−26.779	−40.2	−7.528
−147.0	−25.940	−36.0	−6.647
−141.0	−25.101	−30.5	−5.809
−136.0	−24.262	−26.8	−4.970
−132.0	−23.465	−22.0	−4.131
−127.5	−22.669	−17.5	−3.292
−121.5	−21.830	−13.2	−2.453
−116.2	−20.928	−9.0	−1.615
−111.5	−20.068	−4.0	−0.775
−106.9	−19.292	0	0
−102.0	−18.475	4.8	0.901
−97.0	−17.552	8.9	1.741
−92.0	−16.713	13.5	2.579
−87.0	−15.874	18.0	3.418
−83.2	−15.098	19.8	3.838
−78.5	−14.302	21.8	4.257
−73.0	−13.358	24.5	4.697

On Tables II to VIII we give our data; the left-hand column of each table containing the temperature in degrees centigrade, the right-hand column containing the thermal expansion as $\Delta 1/l_0 \times 10^{-4}$, where $\Delta 1$ is the change in length from °C, and l_0 is the length of specimens at 0°C. From large scale plots of the data given in Tables II to VIII one obtains graphically the slope of a curve at a temperature T giving

TABLE V. Tantalum.

Temp. °C	$\Delta l/l_0 \times 10^4$	Temp. °C	$\Delta l/l_0 \times 10^4$
−181.5	−10.940	−63.0	−4.072
−172.0	−10.449	−55.7	−3.581
−162.5	−9.959	−47.3	−3.091
−154.0	−9.468	−40.0	−2.600
−144.1	−8.978	−32.0	−2.109
−136.0	−8.487	−24.5	−1.619
−127.5	−7.996	−17.0	−1.128
−119.5	−7.506	−9.1	−0.637
−111.0	−7.015	−1.0	−0.147
−102.8	−6.525	0	0
−95.0	−6.034	6.0	0.343
−87.2	−5.543	13.5	0.834
−79.4	−5.053	21.0	1.325
−71.2	−4.562	28.0	1.864

TABLE VI. Tungsten.

Temp. °C	$\Delta l/l_0 \times 10^4$	Temp. °C	$\Delta l/l_0 \times 10^4$
−171.0	−6.597	−52.5	−2.272
−162.5	−6.353	−50.0	−2.199
−154.8	−6.109	−47.0	−2.028
−146.0	−5.864	−45.0	−1.955
−139.0	−5.620	−40.8	−1.784
−132.0	−5.376	−36.0	−1.539
−125.8	−5.131	−30.0	−1.295
−118.5	−4.887	−24.1	−1.051
−112.3	−4.643	−18.7	−0.806
−106.8	−4.472	−13.2	−0.562
−105.0	−4.398	−8.0	−0.317
−99.0	−4.154	−2.1	−0.073
−94.7	−3.983	0	0
−88.0	−3.739	3.1	0.171
−82.2	−3.494	8.5	0.415
−75.7	−3.250	14.0	0.659
−70.5	−3.006	18.8	0.904
−63.5	−2.761	27.5	1.295
−58.0	−2.517		

the "true" coefficient of thermal expansion, $(1/l_0)(dl/dT)$. The dots in Figs. 1 to 7 give the true coefficients of thermal expansion β thus obtained, as a function of temperature in degrees Kelvin. The full drawn lines are Grueneisen curves obtained with the respective values for θ, Q_0 and $(M+N+3)/6$.

DISCUSSION OF RESULTS

Molybdenum

The Grueneisen curve for Mo was obtained with values of 388 degrees for θ, 365×10^3 cal. for Q_0 and 6.83 for $(M+N+3)/6$. In older work, Disch[4] reports $\Delta 1/l_0$ values at only two temperatures, 3.70×10^{-4} and 7.9×10^{-4} at −78° and −190°C, respectively. For these two points, with

[4] J. Disch, Zeits. f. Physik **5**, 173 (1921).

TABLE VII. Platinum.

Temp. °C	$\Delta l/l_0 \times 10^4$	Temp. °C	$\Delta l/l_0 \times 10^4$
−188.0	−15.301	−30.3	−2.763
−186.0	−15.208	−25.3	−2.299
−181.0	−14.860	−20.2	−1.834
−174.0	−14.373	−15.1	−1.370
−168.5	−13.908	−10.0	−0.905
−161.0	−13.467	−5.0	−0.441
−154.9	−13.003	0	0
−148.5	−12.561	2.0	0.139
−142.0	−12.051	5.9	0.487
−136.0	−11.586	10.5	0.952
−130.0	−11.122	16.0	1.416
−124.5	−10.657	21.0	1.881
−117.6	−10.193	26.2	2.345
−112.0	−9.729	28.0	2.601
−106.1	−9.264	33.0	2.993
−101.1	−8.800	38.0	3.466
−94.9	−8.336	42.9	3.930
−90.0	−7.871	48.0	4.394
−83.9	−7.409	53.0	4.858
−79.5	−6.942	58.3	5.312
−73.9	−6.478	63.0	5.776
−68.0	−6.014	68.5	6.240
−63.0	−5.549	73.5	6.704
−57.0	−5.085	78.7	7.168
−52.0	−4.621	84.0	7.632
−46.5	−4.156	89.5	8.096
−41.1	−3.692	95.0	8.560
−36.0	−3.227		

TABLE VIII. Lead.

Temp. °C	$\Delta l/l_0 \times 10^4$	Temp. °C	$\Delta l/l_0 \times 10^4$
−188.0	−50.398	−75.2	−20.833
−181.0	−49.056	−69.7	−19.666
−177.5	−48.058	−66.0	−18.437
−173.0	−46.706	−62.0	−17.300
−168.5	−45.463	−57.0	−15.978
−163.5	−44.401	−52.5	−14.749
−157.5	−43.119	−48.1	−13.520
−153.0	−41.820	−43.6	−12.291
−149.5	−40.568	−39.0	−11.062
−143.5	−39.423	−34.6	−9.833
−139.0	−38.402	−30.0	−8.604
−135.0	−36.873	−25.8	−7.375
−129.5	−35.644	−21.0	−6.146
−125.0	−34.415	−17.4	−4.916
−120.6	−33.186	−12.5	−3.687
−115.0	−31.957	−9.0	−2.458
−110.2	−30.781	−4.5	−1.229
−103.0	−28.775	0	0
−99.0	−27.669	4.2	1.229
−98.0	−27.032	8.9	2.458
−92.5	−25.842	12.2	3.687
−88.0	−24.621	17.0	4.916
−83.2	−23.353	21.2	6.146
−79.5	−22.155	25.0	7.375

an extrapolation from −187° to −190°C for the latter temperature, we obtain $\Delta l/l_0$ values of 3.90×10^{-4} and 8.0×10^{-4}, respectively. In more recent work, Erfling[5] reports only two values for the mean temperature coefficient of expansion, $\bar{\beta}$, of 5.00×10^{-6} for the interval of 0° and +20°C and 4.20×10^{-6} for 0° to −183°C compared with our values for these same intervals of 5.35×10^{-6} and 4.25×10^{-6}, respectively. From these scant data Erfling infers a θ value of 380 compared with our value of 388.

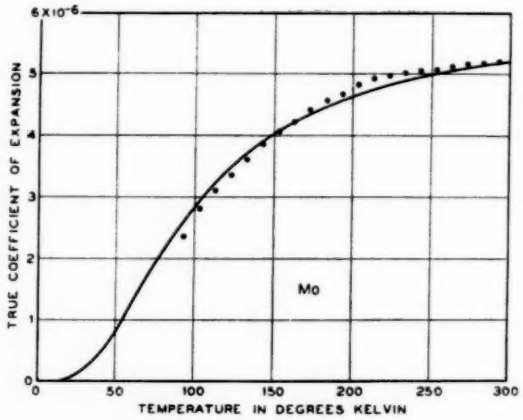

FIG. 1. True coefficient of thermal expansion *vs.* temperature for Mo. The dots are experimentally derived coefficients. The solid curve is the Grueneisen plot with $\theta=388°K$, $1/6(M+N+3)=6.83$, $Q_0=365\times10^3$ cal.

Palladium

The full drawn line of Fig. 2 is the Grueneisen curve, with a characteristic Debye temperature of 300 degrees, a $(M+N+3)/6$ value of 0.4911 and a Q_0 value of 163.7×10^3 cal. The only other study of thermal expansion of Pd at low temperatures contains data at one temperature interval only. Henning[6] reports the thermal expansion from +16° to −191°C to be 21.17×10^{-4}, in good agreement with our value, obtained by extrapolating from −187° to −191°C, of 21.31×10^{-4}.

Silver

The constants used in obtaining the Grueneisen curve for Ag given in Fig. 3 are, $\theta=215$, $Q_0=108.8\times10^3$ cal. and 2.42 for $(M+N+3)/6$.

Previous work from room temperature to the temperature of liquid nitrogen include fairly detailed studies by Buffington and Latimer[7] on silver of unknown purity, and Dorsey[8] on silver

[5] H. D. Erfling Ann. d. Physik **34**, 136 (1939).

[6] F. Henning, Ann. d. Physik **22**, 631 (1907).

[7] R. M. Buffington and W. M. Latimer, J. Am. Chem. Soc. **48**, 2305 (1926).

[8] H. G. Dorsey, Phys. Rev. **25**, 88 (1907).

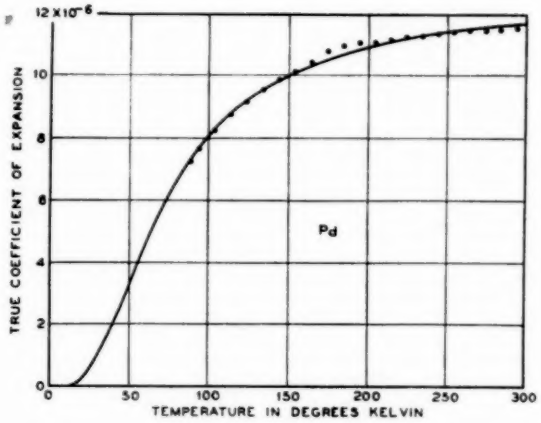

FIG. 2. True coefficient of thermal expansion *vs.* temperature for Pd. The dots are experimentally derived coefficients. The solid curve is the Grueneisen plot with $\theta = 300°K$, $1/6(M+N+3) = 0.4911$, $Q_0 = 163.7 \times 10^3$ cal.

stated to be very pure. We are only in fair agreement with these researches. Ebert[9] gives the thermal expansion from 0°C to −190°C to be 32.30×10^{-4} compared with our value, obtained by extrapolating to −190° from −186°C, of 32.35×10^{-4}. Henning[6] reports the thermal expansion from +16°C to −191°C to be 35.27×10^{-4} which compares with our value of 35.50×10^{-4}.

Tantalum

The Grueneisen curve for Ta in Fig. 4 was obtained with values of 252 for θ, 292.4×10^3 cal. for Q_0 and 0.2924 for $(M+N+3)/6$.

The only reference to similar studies in the temperature region covered in this investigation is by Disch.[4] He gives the thermal expansion, $\Delta l/l_0$, for −78°C to be 4.6×10^{-4} which is not in good agreement with our value of 5.00×10^{-4} for the same temperature.

Tungsten

The constants in the Grueneisen curve for W of Fig. 5 are 310° for θ, 471.2×10^3 cal. for Q_0 and the surprisingly large value of 30.63 for $(M+N+3)/6$.

The work of Disch[4] with tungsten of unknown purity permits a comparison to be made at −78°C. He reports a value of $\Delta l/l_0$ to be 3.3 $\times 10^{-4}$ which is identical with our value as taken from the plot of data given in Table V. Hidnert and Sweeney,[10] working with tungsten containing 99.98 percent W, report a value of 4.3×10^{-6} for

[9] H. Ebert, Zeits. f. Physik **47**, 712 (1928).

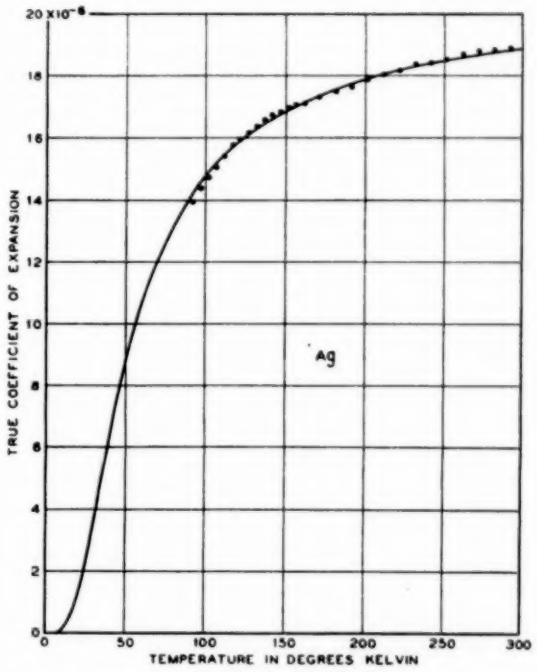

FIG. 3. True coefficient of thermal expansion *vs.* temperature for Ag. The dots are experimentally derived coefficients. The solid curve is the Grueneisen plot with $\theta = 215°K$, $1/6(M+N+3) = 2.42$, $Q_0 = 108.8 \times 10^3$ cal.

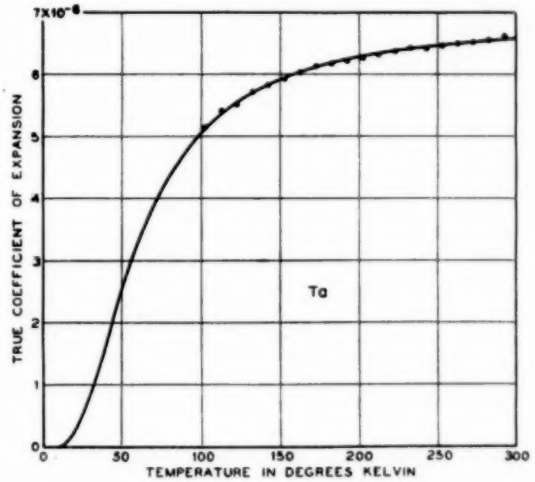

FIG. 4. True coefficient of thermal expansion *vs.* temperature for Ta. The dots are experimentally derived coefficients. The solid curve is the Grueneisen plot with $\theta = 252°K$, $1/6(M+N+3) = 0.2924$, $Q_0 = 292.4 \times 10^3$ cal.

[10] P. Hidnert and W. T. Sweeney, Sci. Pap. Bur. Stand. **20**, 483 (1925).

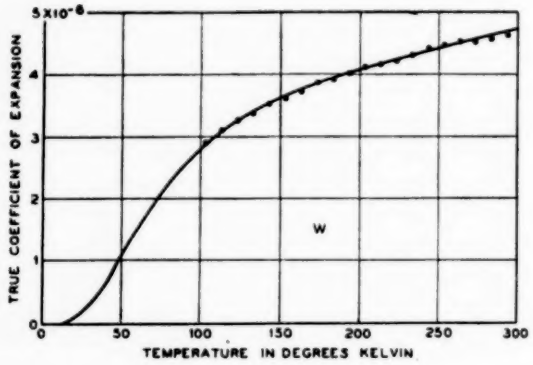

FIG. 5. True coefficient of thermal expansion *vs.* temperature for W. The dots are experimentally derived coefficients. The solid curve is the Grueneisen plot with $\theta=310°$K, $1/6(M+N+3)=30.63$, $Q_0=471.2\times10^3$ cal.

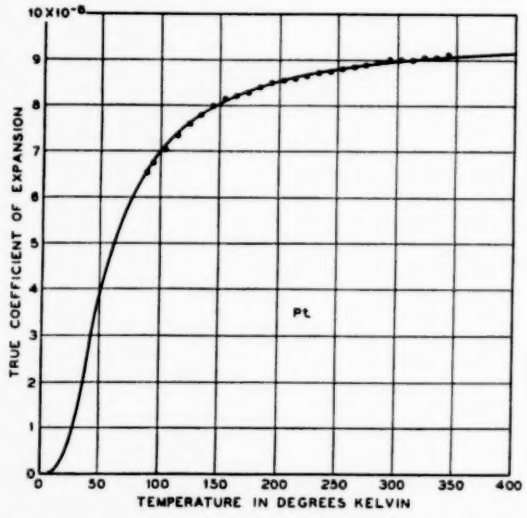

FIG. 6. True coefficient of thermal expansion *vs.* temperature for Pt. The dots are experimentally derived coefficients. The solid curve is the Grueneisen plot with $\theta=230°$K, $1/6(M+N+3)=2.21$, $Q_0=221\times10^3$ cal.

the mean temperature coefficient of expansion, $\bar{\beta}$, for the temperature interval 0° to −50°C and 4.2×10^{-6} for the temperature interval −50° to −100°C. These values compare favorably with our results of 4.39×10^{-6} and 3.96×10^{-6} for the same respective temperature intervals.

Platinum

The full drawn line of Fig. 6, the Grueneisen curve, was obtained with values of 230 for θ, 221×10^3 cal. for Q_0 and 2.21 for $(M+N+3)/6$.

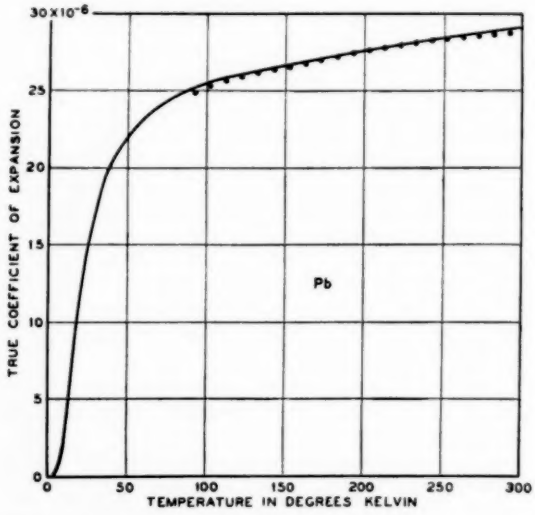

FIG. 7. True coefficient of thermal expansion *vs.* temperature for Pb. The dots are experimentally derived coefficients. The solid curve is the Grueneisen plot with $\theta=88°$K, $1/6(M+N+3)=3.19$, $Q_0=77.84\times10^3$ cal.

Our experimental values are in fair agreement with Dorsey; however, the agreement is rather poor with the results of Henning[6] and of Valentiner and Wallot.[11]

Lead

The fit between our experimental results and the Grueneisen curve was obtained with following values for the constants of the latter curve $\theta=88°$, $Q_0=77.84\times10^3$ cal., $(M+N+3)/6=3.190$. These values are in fair agreement with Ebert's[9] values of 92° for θ, 79.6×10^3 cal. for Q_0 and 3.2 for $(M+N+3)/6$ obtained from rather meager data. We are only in fair agreement with the experimental results of Ebert,[9] Grueneisen,[12] and Dorsey.[13]

The agreement between the Grueneisen theory and experiment is very good for the metals Pt, Pb and Ag with values obtained for $\frac{1}{6}(M+N+3)$ near those theoretically expected. The values of $\frac{1}{6}(M+N+3)$ for W and Mo are higher than the theory demands and much too low for the metals Ta and Pd.

[11] S. Valentiner and J. Wallot, Ann. d. Physik **46**, 837 (1915).
[12] E. Grueneisen, Ann. d. Physik **33**, 33 (1910).
[13] H. G. Dorsey, Phys. Rev. **27**, 1 (1908).

The Field of Electrets in the Presence of Gaseous Ions

ANDREW GEMANT
The Detroit Edison Company, Detroit, Michigan

(Received October 31, 1941)

It is shown by computation that the field of electrets ought to be completely shielded by the ions present in the atmosphere. Experimental evidence available at this time is in apparent contradiction with this conclusion. Some points that might help in clarifying this difficulty are discussed. In view of the fact that the electret field persists in spite of the ions present, the use of electrets in discharge tubes or in any case in high vacuum tubes is suggested. In order to achieve this purpose, the making of electrets of relatively high softening point appears to be the next necessary step in research.

SECTION 1. INTRODUCTION

ALTHOUGH some recent researches have been carried out on electrets,[1-3] one of the chief characteristics is still not understood from a physical standpoint. This is the polarity of the electret. The surface of the electret that has been in contact with, say, the positive polarizing plate is negative during the first few days only, and afterwards changes positive. This reversal is against all expectations, as both ionic and dipolar polarization should be of a sign opposite to that of the polarizing surface.

Several tentative explanations have been suggested in the published researches but none is definitely established by experimental facts. The author, for instance, thought that the final charge was not the direct result of polarization, but rather a secondary piezoelectric effect maintained by the internal stresses in the material. No experimental work has as yet been carried out in an attempt to support this idea.

It should be pointed out, however, that this circumstance did not prove a serious handicap in trying to make use of electrets in electrical appliances.[4] The situation is about the same as with permanent magnets; a thorough understanding of their physical characteristics and the application of them in machinery are two different matters.

In the following pages another question regarding electrets will be discussed, and it will be shown that, although it, too, cannot be answered satisfactorily, it immediately leads to a further suggestion concerning a new application.

This question is: How will the electric field of the electret be affected by the free ions present in the atmosphere? It will be shown that the answer to this question, as it can be derived from simple theoretical considerations, is in apparent contradiction to experimental findings. This contradictory situation is published here in order to stimulate further thought and research on electrets. Besides, considerations along these lines will lead to a discussion of the possibility of the application of electrets in discharge tubes.

SECTION 2. THEORY OF SHIELDING BY IONS

In this section a brief mathematical analysis of the field of an electret in a space of finite ion concentration will be given. The calculation is based on the type of double-layer as first conceived by Gouy[5] for electrolytic solutions. It can be applied to this case as well.

It will not be necessary to reproduce the details of the theory that are available in the original. The basic idea is that ions of a charge opposite to a given charged surface will accumulate in the neighborhood, while ions of the same charge will be repelled. When equilibrium is reached, the ions are acted upon by electrical and diffusion forces of equal magnitude and opposite direction. Thus, for a positive electret surface, negative ions will accumulate near the surface, shielding the field outside the double layer formed by the positive electret charge and the negative ionic charge.

[1] Andrew Gemant, Phil. Mag. **20**, 929 (1935).
[2] G. Groetzinger and H. Kretsch, Zeits. f. Physik **103**, 337 (1936).
[3] W. M. Good and J. D. Stranathan, Phys. Rev. **56**, 810 (1939).
[4] A. Gemant, Rev. Sci. Inst. **11**, 65 (1940).
[5] G. Gouy, J. de phys. et rad. [4] **9**, 457 (1910).

The computation for the one-dimensional case (radius of curvature of surface larger than the thickness of the double layer) yields the potential distribution φ (Fig. 1) as a function of the distance x from the surface:

$$\tanh(\alpha\varphi/4)=Ae^{-\beta x}. \tag{1}$$

Here $\alpha=z\epsilon/kT$ and $\beta=(a\alpha)^{\frac{1}{2}}$ with $a=8\pi z\epsilon n$, where z=number of elementary charge units carried by one ion (for sake of simplification assumed to be the same for both positive and negative ions), ϵ=electronic charge, k=Boltzmann constant, T=temperature in degrees K, n=number of ionic pairs per cm^3. The constant A is connected with the potential φ_0 at the electrode surface ($x=0$) by the relation

$$\tanh(\alpha\varphi_0/4)=A. \tag{2}$$

φ_0 on the other hand is a function of the specific charge, q, of the electret:

$$q=\frac{1}{2\pi}\left(\frac{a}{\alpha}\right)^{\frac{1}{2}}\sinh\frac{\alpha\varphi_0}{2}. \tag{3}$$

For numerical data,[6] n should be taken 10^4, z as unity, and q is known to be about 5 e.s.u. Then $\alpha=1.2\times10^4$, $a=1.2\times10^{-4}$ and $\varphi_0=2.2\times10^{-3}$ abs.=0.66 volt.

We now require the thickness of the double layer. The following relation gives the variation of the field intensity with x:

$$-\frac{d\varphi}{dx}=\frac{4A\beta}{\alpha}e^{-\beta x}\frac{1}{1-A^2e^{-2\beta x}} \tag{4}$$

and we now ask for that value of x (designated by δ) for which the field intensity has dropped in the ratio 1 : e. This value will be small compared with unity, as we may infer from the high field intensity (20,000 volts/cm) at the surface and the small value of the total potential (0.66 volt). Thus, the term $e^{-\beta x}$ will remain practically unity, and only the denominator in (4) will change appreciably. As to A, its value is known from (2); since the argument $\alpha\varphi_0/4=y$ has a value 6.6 and changes only very slowly even with large variations in n, the hyperbolic function can be simplified and we have for the denominator in Eq. (4):

$$1-(1-4e^{-2y})e^{-2\beta x}.$$

With the definition as given above for δ, we have the equation

$$4e^{-2y+1}=1-(1-4e^{-2y})e^{-2\beta\delta}. \tag{5}$$

Writing $1-2\beta\delta$ for the last exponential we have

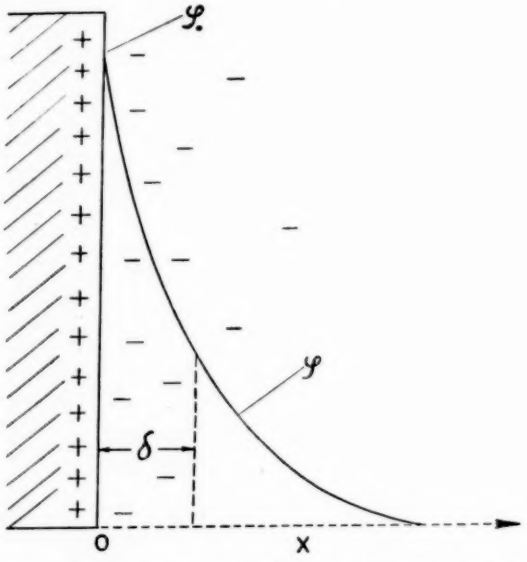

FIG. 1. Diagram of accumulation of ions near electret surface. Potential distribution curve is superimposed. Electret at the left, space charge at the right.

in good approximation

$$\delta=(1/\beta)2(e-1)e^{-2y}. \tag{6}$$

Again from Eq. (3), since the argument is larger than unity, we have

$$e^{-2y}=\frac{1}{4\pi q}\left(\frac{a}{\alpha}\right)^{\frac{1}{2}}$$

and hence from (6)

$$\delta=(e-1)/2\pi\alpha q. \tag{7}$$

It is interesting to point out that this result is entirely different from the expression usually given as the thickness of the Gouy double layer, namely $1/\beta$. Equation (6) is a more general formula from which it can be seen that δ becomes $1/\beta$ (we disregard the numerical factor) if $\alpha\varphi_0\ll1$, and the exponential is near unity.

[6] G. R. Wait and O. W. Torreson, Terr. Mag. **40**, 425 (1935).

This is the usual approximation made, but it really holds only for voltages below 50 mv.

For voltages larger than 100 mv, on the other hand, Eq. (7) will hold. The usual expression $1/\beta$ contains $1/\sqrt{n}$ as a factor, indicating an increasing thickness with decreasing number of ions; it is, however, independent of the total charge. The thickness as given by Eq. (7) is independent of n, but increases with decreasing charge q. For $q=5$, δ is 4.5×10^{-6} cm, and is thus of submicroscopic dimension.

It should be recalled that the foregoing formulas refer to the one-dimensional case. They will hold well for the center parts of an electret, but will have to be modified at the edges.

It is now possible to compare our theoretical result with experimental observations.

SECTION 3. EXPERIMENTAL FACTS ABOUT THE ELECTRET FIELD

Experience with electrets shows a behavior not in agreement with the expectations derived in the previous sections. However, considering that even the basic properties of electrets are not easily explainable at this time, one may expect to encounter other difficulties.

Briefly, the chief conclusion from the last section, as expressed by Eq. (7), is that outside of a layer of submicroscopic dimensions the electric field of an electret ought to be almost completely shielded owing to the ions present in the atmosphere. This is, however, by no means the case, as can be seen if the author's data on the application of electrets[4] are consulted. Figure 3 of the paper quoted gives the electric field as a function of the distance from the electret, and it appears that at a distance of 5 mm the field drops to about 20 percent of its surface value; thus, is quite appreciable. Besides, this drop could easily be explained on the basis that the field is by no means parallel.

One could object to the interpretation of these particular data by saying that they do not correspond to an equilibrium, a supposition underlying the deduction of Section 2. This may be true; however, for another arrangement, the vibration electrometer, conditions for an equilibrium were much more favorable. In that instrument the field between two parallel electrets in a distance of about 8 mm was about 1500 volts/cm. This intensity was maintained during several weeks; it varied with the temperature in a reversible manner.

While an explanation of the presence of high field intensities in spite of the ion content of the atmosphere cannot be given, a few points that might help to clarify the situation can be mentioned. A definitive solution of the problem will be reached only if more experimental material on this subject accumulates. For the present it should then suffice to point out the following:

(1) It is still possible that, for some reason or other, real equilibrium has not been reached in experimental cases dealing with electrets, not even in the vibration electrometer discussed above. Let us make a numerical estimate. The amount of ions required to neutralize the electret can be computed easily. The specific charge is 5 e.s.u., corresponding to $5/(4.8\times10^{-10})\sim10^{10}$ monovalent ions, and for a surface of say 10 cm^2, the total number is 10^{11}.

Now the concentration of ions in the atmosphere[7] is a varying figure. Small ions are present everywhere, as they are formed by means of a penetrating radiation. Besides, there are large ions present in rooms occupied by people, originating partly from the breath, partly from an addition of small ions to tobacco smoke particles. The number of small ions varies around 500 per cm^3, that of the large ones in rooms occupied by people varies around 10^4 per cm^3. Taking this latter figure as representative, as has been done in Section 2, we have 10^{10} ion pairs per m^3. It seems that ten m^3 of air might be easily available for the electrets, unless they were enclosed hermetically. This was not the case with the vibration electrometer, which was placed under a glass jar, but by no means under air-tight conditions.

Thus it can be concluded that conditions for reaching an equilibrium are generally favorable. Still, it might be that the process takes place slowly, and that for this reason the field remains appreciable. It also has to be considered that the spread of data in measurements of this type is of the order of 10 percent; therefore a

[7] D. H. Gish in *Physics of the Earth*, Vol. VIII (McGraw-Hill, New York, 1939).

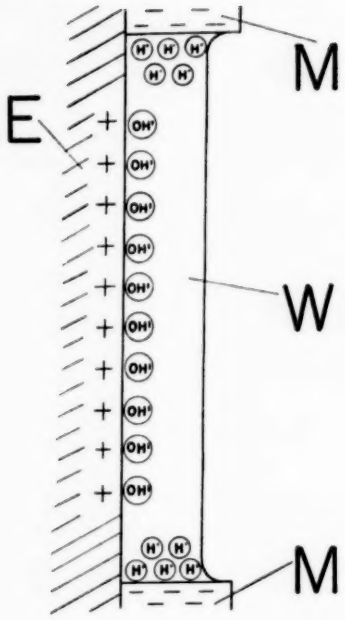

FIG. 2. Diagram of shielding effect on the electret field of adsorbed water layer.

decrease of the total charge within this limit would not be easy to detect.

(2) Another point of interest in this connection is the fact that the atmospheric ions are held near the electret surface only by electrostatic forces but not by any process that might lead to irreversible saturation of the surface. The ions that accumulate near the surface are removed easily by a suitable mechanical process. This statement is best illustrated by the effect of moisture on electrets. If an electret is brought into a room with a fairly high humidity, the field disappears very pronouncedly. Figure 2 shows diagramatically how this happens. E is the free positive electret surface, M is the nearest free edge of the metallic casing carrying an opposite charge. If a thin layer of water W deposits on the surface some of the OH^- ions will neutralize the electret charge, the corresponding H^+ ions accumulating near the metal edge. Although an adsorption of ions undoubtedly takes place in this case, yet the process is fully reversible. If the electret is placed in a dry chamber the water evaporates and removes all ions, restoring the free charge with the same intensity as before. This experiment clearly shows that the inorganic ions, even if attracted by the electric field, are not retained definitely but can be removed by a suitable process. Thus, even if neutralization according to the mechanism as outlined in Section 2 should take place, the process will be easily reversible.

(3) In case later experiments should show that the finite field intensity at a measurable distance from the electret is a true equilibrium, evidently the deduction presented in Section 2 will have to be modified, although how that will be done is not yet clear. One of the possibilities is to replace the Boltzmann statistics underlying Eq. (1) by one of the quantum statistics that might hold for the fairly high ion concentration near the surface. The order of the concentration is 10^{16} per cm^3.

Whichever explanation is established in the future, the fact of a definite charge in the presence of finite ionic concentration remains. And this fact allows certain conclusions regarding the technical applications of electrets to be drawn.

SECTION 4. USE OF ELECTRETS IN DISCHARGE TUBES

It was shown in the last section that the field of electrets is appreciable even in the presence of gaseous ions. Still it is quite likely that this field will diminish with increasing concentration of the ions. Experiments will have to establish the relation, field *vs.* ion concentration.

When this relation is known, the electret in combination with a suitable measuring device might be used as a quantitative indicator for the ion concentration of the atmosphere or any closed space. Because of the light weight of electrets such a device would be particularly suitable for upper atmospheric measurements.

Another possibility that suggests itself is the use of electrets in gas-filled or vacuum discharge tubes. Since the grid bias voltage has no work to do, and acts only on an electrostatic basis, it is generally possible to utilize electrets in tubes, wherever an electrostatic control is required. They may be used in any type of tubes, such as amplifiers, cathode-ray tubes, phototubes, electrometer tubes, and so on.

Among the conceivable advantages in this connection, simplicity of the construction and light weight may be mentioned. This latter advantage will be of particular value in devices built for airplanes or upper atmospheric record-

ing balloons. Another factor is the possibility of producing special field effects. The direction of the field depends upon the procedure followed in making the electrets and not, as with metal electrodes, upon the shape of the free surface. Thus, field distribution and shape of the surface are here independent variables.

In certain cases where the controlling field is parallel to the current it will be advisable to use perforated electrets although such an arrangement might present certain difficulties. If the two directions form a right angle, solid electrets can be used.

Recalling what has been said in the previous section, it is to be expected that the field will be shielded in the presence of a high ion concentration. If the latter is below a certain limit, the field might still persist. Even in this case the free charge of the electret surface will depend to a certain extent upon the ion concentration in its neighborhood. This would be an unusual property to be reckoned with in designing the tube. But—as generally happens in such cases—such a change in conditions is not a disadvantage; designers probably will learn very soon to make particular use of it.

It is possible, however, that in a completely closed space the conditions underlying the deduction made in Section 2 will be fulfilled, so that the field will be thoroughly shielded, even for low values of ion concentration. In this case the use of electrets will have to be restricted to high vacuum tubes in which only electrons are present and the use of negative electrets which will repel the electrons.[8]

[8] In a recent note G. E. Sheppard and J. D. Stranathan, Phys. Rev. **60**, 360 (1941), observed a decrease of the surface charge of electrets with decreasing pressure, corresponding to the breakdown strength of the gas. Thus the field of electrets will assume low values in gas discharge tubes, but high values in high vacuum tubes.

The different applications in discharge tubes are handicapped at this time by the relatively low softening point of electrets. It certainly would not be an easy matter to incorporate the electrets in the tubes and to perform the process of evacuation in the customary manner. It might be possible, of course, to devise a method by means of which this difficulty could be avoided, but it is felt that generally all applications mentioned above will be considerably promoted when electrets of a higher softening point have been found.

The next step in the development is, therefore, to attempt the making of electrets of other materials than those used today. This attempt will present many difficulties since we do not know what are the necessary conditions for a material to become an electret. Dipolar constituents seem to be necessary, also a high degree of hardness at room temperature in order that an attained orientation should not be lost too fast. Thus, it is possible to make an electret by adding carnauba wax to paraffin wax, but the life of such electrets is rather short, because of the softness of the product. However, it is not certain whether these two conditions, orientability and hardness, are sufficient, although they are certainly necessary.

Two possibilities will have to be tried. The one is the making of electrets by using some of the synthetic plastics produced today and possessing a relatively high softening point. Both thermoplastic and thermosetting plastics could be tried. The other field is that of glasses, especially those of high electrical resistivity, such as are used in the manufacture of fiber glass for electrical purposes. The technique of making the electrets will have to be adapted at least to the temperatures at which these glasses are soft, if not to temperatures at which they are fluid.

The Variation with Temperature of the Principal Elastic Moduli of NaCl near the Melting Point

LLOYD HUNTER, *Carnegie Institute of Technology, Pittsburgh, Pennsylvania*

AND

SIDNEY SIEGEL, *Westinghouse Research Laboratories, East Pittsburgh, Pennsylvania*

(Received October 31, 1941)

The principal elastic moduli of single crystal rods of NaCl were measured over the temperature range 20°C to 804°C, the melting point. The measurements were carried out by means of a tripartite piezoelectric oscillator consisting of a quartz crystal driver, an intermediate fused silica bar, and the NaCl specimen. The shear constants C_{44} and $(C_{11}-C_{12})$ decrease nearly linearly with temperature, reaching non-zero values at the melting point. The compressibility increases with temperature, but exhibits a sudden drop within a few degrees of the melting point. The results are compared with certain predictions based on Born's theory of the stability of crystal lattices.

THERE are few data in the literature on the behavior of the elastic moduli of crystals in the neighborhood of their melting point. Various suggestions dealing with this problem have been made,[1] and Born[2] has developed a theory concerning the stability of crystal lattices in which the temperature variation of the shear constants near the melting point is an important feature.

This paper is a report of a series of measurements of the elastic moduli of NaCl over the range 300°K to 1077°K, the melting temperature. Previous writers[3] have reported the variation with temperature of these quantities over the range 80°K to 480°K.

SPECIMENS

Artificial crystals, grown from the melt, were used.[4] Specimen rods of either circular or square cross section were prepared, 3 to 7 cm long, all having a lateral dimension of 0.476 cm. The square rods were prepared by grinding on a lapping plate, the round by carefully turning on a lathe. The rod axis was made to coincide with either a [100] or a [110] direction to better than 30′. Since a five degree error in orientation produces only about one percent error in modulus, the error in modulus produced by a 30′ error in orientation is seen to be negligible. In all, fourteen crystals were prepared.

EXPERIMENTAL METHOD

The experimental method is a dynamical one, making use of a composite piezoelectric oscillator.[3] Since it was necessary to make measurements at 800°C, above the $\alpha \rightarrow \beta$ transformation of quartz at 577°C, it was not feasible to use simply a two-

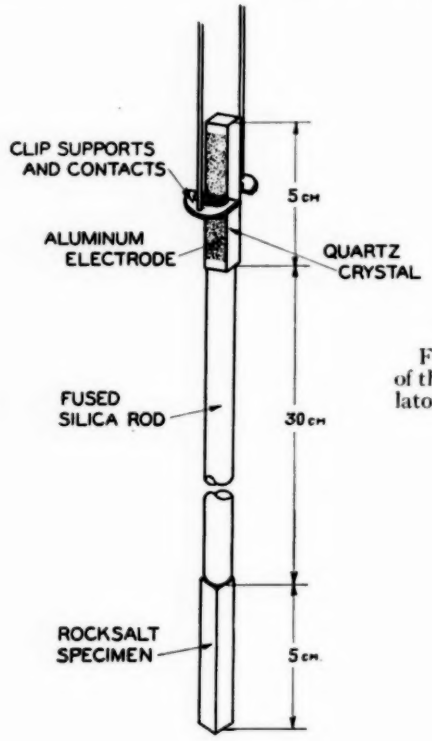

FIG. 1. Diagram of three-part oscillator.

[1] L. Brillouin, Phys. Rev. **54**, 916 (1938).
[2] M. Born, J. Chem. Phys. **7**, 591 (1939).
[3] L. Balamuth, Phys. Rev. **45**, 715 (1934); F. C. Rose, Phys. Rev. **49**, 50 (1936); M. A. Durand, Phys. Rev. **50**, 449 (1936).
[4] Obtained from the Harshaw Chemical Company.

part oscillator, in which the quartz crystal is maintained at the same temperature as the specimen. The composite oscillator in these experiments consisted of a quartz rod 5 cm long, cemented to one end of a clear fused silica rod 30 cm long; at the other end of the latter the NaCl specimen was cemented. The cement used at the quartz-silica interface was red shellac applied while molten. At the silica-NaCl interface a cement consisting of a paste of sodium silicate and finely divided calcium carbonate was used. This cement dries satisfactorily in 72 hours at room temperature.

Two types of oscillator were used—one for longitudinal, and another for torsional vibrations. In the former, both the X-cut quartz crystal and the NaCl specimen were of square section. In the latter, the Y-cut quartz rod and NaCl specimen were both round, 0.476 cm in diameter. In both cases the silica rod was circular in section, having been ground to a diameter of 0.476 ± 0.003 cm over its entire length. Figure 1 is a diagram of a typical longitudinal oscillator.

The oscillator is suspended vertically on the axis of a tube furnace 64 cm long, 4 cm bore, with the NaCl specimen at the center of the furnace, maintained at the desired elevated temperature. The quartz crystal is situated above the end of the furnace, nearly at room temperature.

The theory of such a three-part oscillator has been developed by Rose.[3] The resonance frequency f_0 of one of the normal modes of longitudinal or torsional vibration, is measured by means previously described. The resonance frequency f_3 of one of the normal modes of the NaCl specimen is obtained by means of the equation

$$f_3=f_0+(m_1/m_3)(f_0-f_1)+(m_2/m_3)(f_0-f_2), \quad (1)$$

where f_1 is the fundamental frequency of the quartz crystal, f_2 is the frequency of one of the normal modes of the silica rod, and m_1, m_2, and m_3 are the masses of the quartz, silica, and NaCl bars, respectively. This equation is an approximation, valid under the condition

$$f_0=f_1=f_2=f_3 \quad (2)$$

to about 5 percent. This condition was always fulfilled experimentally.

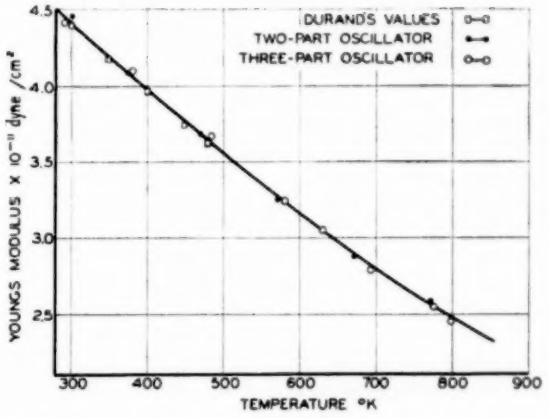

FIG. 2. Comparison of the data obtained with a two-part and a three-part oscillator with those of Durand.

From the values of f_3 obtained from Eq. (1), the appropriate elastic modulus M is obtained by means of the equation

$$M=\lambda^2 f_3^2 \rho \quad (3)$$

where ρ is the density of the specimen and λ the wave-length in the NaCl specimen. The wave-length is always $2L/n$, where L is the length of the specimen and n a small integer determined from an approximate knowledge of the modulus. The length at any temperature T°C is obtained from the room temperature length by means of the coefficient of linear expansion

$$\alpha=4.45\times10^{-5}+2.49\times10^{-8}(T-200)$$
$$+6.52\times10^{-14}(T-200)^3$$

given by Walther, *et al.*[5]

In these experiments a temperature gradient of nearly 30°C/cm may exist in the silica rod, which is therefore elastically inhomogeneous, since its elastic moduli vary with the temperature. The quantity f_2 of Eq. (1) is determined in a preliminary run in which a two-part oscillator, consisting only of the quartz crystal and the silica rod is suspended in the furnace with the silica rod occupying the identical position that it does during an actual run on a three-part oscillator. Furthermore, to ensure that the *relative spatial distribution* of vibration nodes and the temperature along the silica rod does not change appreciably during a three-part oscillator run, the length

[5] A. K. Walther, W. P. Haschkowsky, and P. G. Strelkow, Physik. Zeits. d. Sowjetunion **12**, 35 (1937).

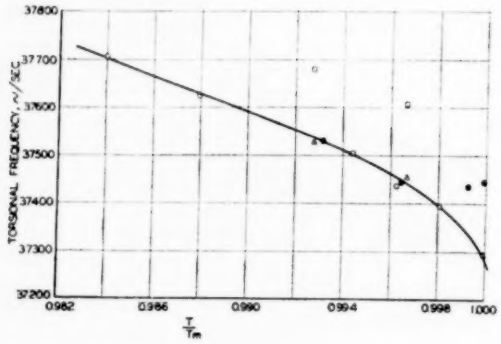

FIG. 3. Typical behavior of the natural frequency of a NaCl specimen near the melting point. Description in the text.

of the NaCl specimen is always so adjusted that condition (2) is fulfilled to 2 percent or better. This is accomplished in the following manner. The length of the NaCl specimen is first chosen so that this condition is met over the range 20°C to 200°C. Then its length is reduced successively three times, so that the condition is fulfilled over the ranges 200° to 400°, 400° to 600°, and 600° to the melting point at 804°.

Equation (1) was derived under the assumption that all parts of the oscillator are elastically homogeneous, an assumption not valid here because of the temperature gradient along the silica rod. To establish the validity of the method, Young's modulus of a [100] NaCl specimen was measured by means of a conventional two-part oscillator consisting of a quartz crystal and NaCl specimen, with the entire oscillator maintained at the elevated temperature. Data were taken from 20° to 530°C. The identical specimen was then made part of a three-part oscillator and measured over the same temperature range. Figure 2 shows the results of this experiment. The open circles are the measurements made with the three-part oscillator; the closed circles were obtained with the two-part oscillator, and the squares are results obtained by Durand.[3] The agreement establishes the validity of data obtained with the three-part oscillator in the fashion described above.

Throughout these experiments the temperature was measured with a Pt *vs.* Pt-10 percent Rd thermocouple, of which the hot junction was closely adjacent to the NaCl specimen. This couple was calibrated against the temperatures of boiling water, freezing Sn, Zn, Pb, Al, and NaCl. It was checked before and after each run against freezing NaCl, and could be checked *in situ* through the discontinuous behavior of the resonance frequency of the composite oscillator as the NaCl specimen melted.

In obtaining the data, both heating and cooling curves were taken whenever possible. In general these checked to better than 0.2 percent, but at high temperatures, within a few degrees of the melting point, the curves were not closely reproducible. In order to accurately determine the true curve in this region, several cycles of heating and cooling were carried out. Figure 3 shows the result of one such experiment. The resonance frequency of torsional vibration for one of the [100] crystals is plotted against T/T_m, the ratio of the absolute temperature to the melting point on that scale. Each measurement, represented by a point in Fig. 3, was made only after the furnace windings had been constant in temperature to better than 0.2°K for at least an hour, to ensure that the temperatures of the silica rod and the NaCl specimen were steady. The heating or cooling from one point to the vicinity of the next, prior to the establishment of thermal equilibrium at the new point, usually took only a few minutes.

The open circles represent data taken on heating, the last point on this heating cycle being

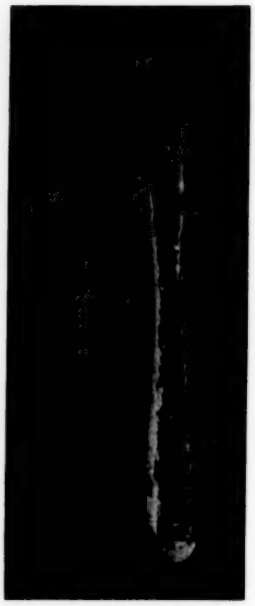

FIG. 4. Photograph of a NaCl specimen in its original condition, and one which had been held at the melting point for six hours.

at $T/T_m=0.9980$. The specimen was then cooled to $T/T_m=0.9932$, giving the closed circle there and demonstrating that the point at 0.9980 was still on a reproducible part of the curve. The remaining closed circles were obtained on heating, and the specimen cooled from $T/T_m=0.9999$ to the first square at $T/T_m=0.9927$. The specimen was heated finally to $T/T_m=0.9965$, giving the last square.

It will be observed that the two squares and the last closed circle lie on a curve parallel to the original, reproducible heating curve, but are displaced upwards from it. It is, therefore, assumed that the true position of these points is represented by the three triangles, and that the data are best represented by the curve which passes through the open circles, the first two closed circles, and the triangles. This method of determining the true curve near the melting point was employed in every set of measurements made near the melting point. The anomalous behavior of the measured frequencies is probably due to slight changes in the dimensions of the NaCl specimen due to plastic flow under its own weight near the melting point.

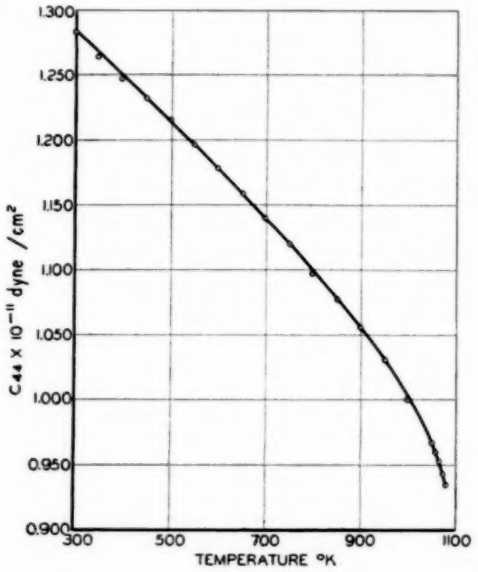

FIG. 5. The variation of C_{44} with temperature.

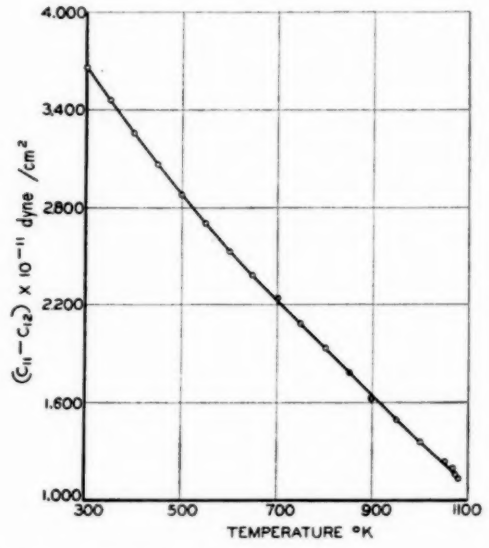

FIG. 6. The variation of $(C_{11}-C_{12})$ with temperature.

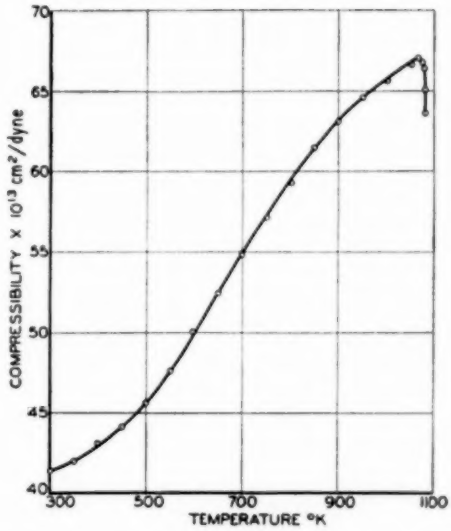

FIG. 7. The variation of the compressibility K with temperature.

The photograph of Fig. 4 shows the initial appearance of the square specimens, and the appearance of a [110] crystal which had been held at the melting point for six hours, during which time frequency measurements were made continually. As the geometrical shape of the specimen changed slowly, the frequency drifted in an erratic manner, but was never more than a few percent from its initial value. The logarithmic decrement of the NaCl specimen at the melting point was of the order of 10^{-3}. It is felt that this experiment demonstrates conclusively that the material behaves as an elastic solid right up to the melting point.

RESULTS

Four elastic moduli were measured, Young's modulus E and the rigidity modulus G, in the

TABLE I. *Adiabatic elastic moduli of* NaCl.

		Elastic Moduli $\times 10^{13}$ cm²/dyne			Elastic Constants $\times 10^{11}$ dynes/cm²		
T°K	T/T_m	S_{11}	$-S_{12}$	S_{44}	C_{44}	$C_{11}-C_{12}$	K $\times 10^{13}$ cm²/dyne
300	0.2784	22.80	4.50	78.09	1.281	3.663	41.4
350	0.3248	23.95	4.98	79.08	1.265	3.457	42.0
400	0.3712	25.23	5.46	80.14	1.248	3.258	43.1
450	0.4176	26.63	5.96	81.22	1.231	3.068	44.1
500	0.4640	28.18	6.49	82.37	1.214	2.884	45.6
550	0.5104	29.92	7.03	83.61	1.196	2.706	47.6
600	0.5568	31.85	7.58	84.87	1.178	2.536	50.1
650	0.6032	33.84	8.18	86.32	1.158	2.380	52.4
700	0.6496	35.95	8.85	87.79	1.139	2.232	54.8
750	0.6960	38.35	9.67	89.39	1.119	2.082	57.0
800	0.7424	41.14	10.68	91.08	1.098	1.930	59.3
850	0.7888	44.30	11.91	92.84	1.077	1.779	61.4
900	0.8352	47.86	13.42	94.74	1.056	1.632	63.1
950	0.8816	51.74	15.11	97.09	1.030	1.496	64.6
1000	0.9285	56.37	17.24	100.0	1.000	1.359	65.7
1050	0.9749	61.60	19.67	103.5	0.966	1.230	66.8
1055	0.9796	62.15	19.93	104.0	0.961	1.218	66.9
1060	0.9842	62.71	20.20	104.6	0.956	1.206	66.9
1065	0.9889	63.31	20.48	105.1	0.952	1.193	67.1
1067	0.9907	63.55	20.59	105.3	0.950	1.188	67.1
1070	0.9935	63.92	20.76	105.6	0.947	1.181	67.2
1072	0.9954	64.19	20.90	105.8	0.945	1.175	67.2
1073	0.9963	64.35	21.01	106.0	0.943	1.172	67.0
1074	0.9972	64.53	21.13	106.2	0.942	1.167	66.8
1075	0.9981	64.72	21.28	106.4	0.940	1.163	66.5
1076	0.9991	64.93	21.50	106.6	0.938	1.157	65.8
1077	1.0000	65.18	21.98	107.1	0.934	1.134	63.7

[100] and [110] directions. In all, twenty-five individual temperature runs were made on the fourteen crystals used. A cubic crystal has three independent elastic moduli; these are related to the measured quantities by the equations

$$\begin{aligned} 1/E_{[100]} &= S_{11}, \\ 1/E_{[110]} &= \tfrac{1}{2}(S_{11}+S_{12}+\tfrac{1}{2}S_{44}), \\ 1/G_{[100]} &= S_{44}, \\ 1/G_{[110]} &= S_{11}-S_{12}+\tfrac{1}{2}S_{44}. \end{aligned} \tag{4}$$

For each of the moduli measured, a smooth curve was drawn best fitting all of the data obtained on that modulus. At the temperatures tabulated in Table I, the best set of values of S_{ij} was computed by means of a graphical method of averaging the data obtained from the curves. These values are tabulated in the 3rd, 4th, and 5th columns of Table I. Another set of elastic constants, obtainable from the S_{ij}'s by simple linear relationships, is of primary physical significance. These are C_{44}, $(C_{11}-C_{12})$, and the compressibility K. The first two of these are pure shear constants, the last a pure dilation constant. These quantities are tabulated in the last three columns of Table I.

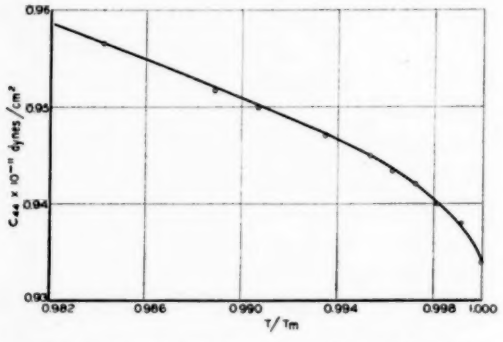

FIG. 8. The variation of C_{44} near the melting point.

In Figs. 5, 6, and 7, the elastic constants are plotted against temperature over the range 300° to 1077°K. In Figs. 8, 9, and 10, the behavior of these constants in the last 20° before the melting point is shown on a magnified scale.

The deviations among the individual runs on a single specimen averaged about 0.2 percent, except near the melting point, where the maximum deviations in the true curve, obtained by repeated cycles of heating and cooling as described before, were about 0.1 percent. The curves for different specimens agreed to better

than 0.3 percent in every case, and to better than 0.1 percent near the melting point. The moduli S_{11}, S_{12}, and S_{44} are therefore reliable, respectively, to 0.3 percent, 2.0 percent, and 0.3 percent in the main body of the curves, and to 0.1 percent, 0.4 percent, and 0.1 percent near the melting point. The shear constants C_{44} and $(C_{11}-C_{12})$ are good to 0.3 percent over most of the range, and to 0.1 percent near T_m. The compressibility K is reliable to about 2 percent over the entire range of measurement.

The present results overlap those of Durand in the interval 20°C to 230°C. The two sets of values of S_{11} check to 0.2 percent, of S_{12} to 4 percent, and of S_{44} to 1 percent. The differences may be due to the fact that his crystals were natural, these artificially prepared. The isothermal compressibility has been measured by Voigt,[6] Madelung and Fuchs,[7] Slater,[8] and Rose.[3] Their values are, respectively, 41.3, 41.2, 42.0, 41.9×10^{-13}. The present value at 20°C is 43.0×10^{-13} cm²/dyne.

DISCUSSION

The curves of Figs. 8 and 9 show clearly that the shear moduli C_{44} and $(C_{11}-C_{12})$ both have definite non-zero values at the melting point. This is probably the most important conclusion to be reached from these experiments. Born's

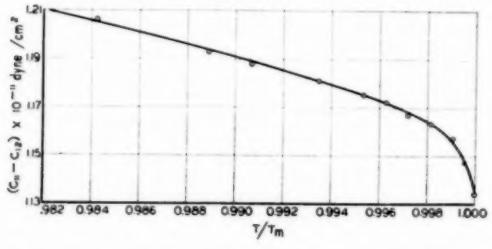

FIG. 9. The variation of $(C_{11}-C_{12})$ near the melting point.

theory cannot be compared quantitatively with these results because his calculations are for a body-centered cubic lattice, but both theory and experiment yield results for C_{44} that are qualitatively similar in form. Durand's suggestion that $(C_{11}-C_{12})$ vanishes at the melting point is seen to be erroneous.

[6] W. Voigt, *Lehrbuch der Kristallphysik*, p. 741.
[7] E. Madelung and R. Fuchs, Ann. d. Physik **65**, 289 (1921).
[8] J. C. Slater, Phys. Rev. **23**, 488 (1924).

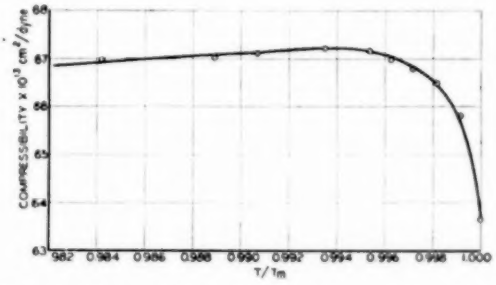

FIG. 10. The variation of K near the melting point.

Born's work has been extended by Fürth.[9] A relationship between the compressibility at the melting point, the coefficient of expansion α, and the specific volume V,

$$K/\alpha V=3.4\times10^{-9} \tag{5}$$

is obtained. The experimental value of this ratio is 7.2×10^{-9}. A further result obtained by Fürth for the b.c.c. lattice is the relation

$$\frac{C_{11}(0)-C_{11}(T_m)}{C_{11}(0)}=0.57. \tag{6}$$

With the value $C_{11}(0)=5.96\times10^{11}$ dynes/cm² given by Durand, and the present value $C_{11}(T_m)=2.34\times10^{11}$ dynes/cm², the value 0.61 is obtained for this ratio. On these two points it would appear that the theory agrees to a good approximation with experiment.

A more severe comparison is afforded by the temperature variation of the compressibility at temperatures far below the melting point. Fürth gives the relation

$$(T_m/K)(\partial K/\partial T)=1.17.$$

The experimental values of this quantity are given in Table II.

Here it is seen that the quantity $(T_m/K)\times(\partial K/\partial T)$ is not a constant at low temperatures but does become somewhat constant at intermediate temperatures.

The changes in compressibility observed in the last 10° before the melting point are considerably

TABLE II.

T°K	300	400	500	600	700	800	900	1000
$(T_m/K)(\partial K/\partial T)$	0.57	0.78	1.06	1.23	1.18	1.06	1.05	1.08

[9] R. Fürth, Proc. Camb. Phil. Soc. **37**, 34 (1941).

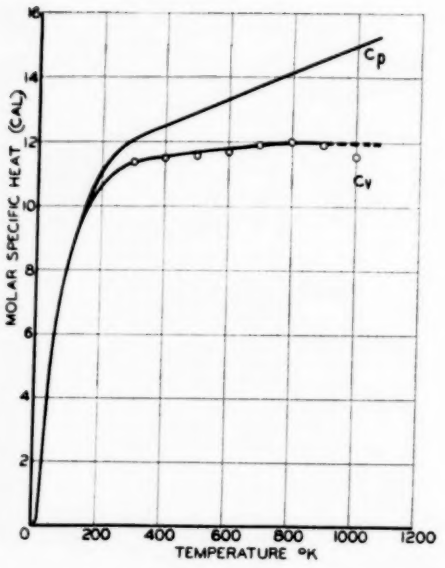

FIG. 11. The variation of C_v with temperature.

larger than the errors in the measurements, and the drop in K must be considered to be a real effect. This behavior may at first sight seem to be anomalous, implying that the lattice becomes harder to compress in the immediate neighborhood of the melting point. It should be pointed out, however, that the adiabatic compressibility is plotted in Fig. 10. The isothermal compressibility is larger by an amount $9\alpha^2VT/C_p$, and since it appears that α increases rapidly near the melting point, it is quite probable that the isothermal compressibility increases monotonically up to the melting point. The present results for the compressibility can be used to determine more reliably than has been hitherto possible the behavior of the specific heat at constant volume, at elevated temperatures. The experimental values of C_p must be corrected by a term $9\alpha^2VT/\mathrm{K}=C_p-C_v$ to yield C_v.

Eücken and Dannöhl,[10] using an extrapolated value of K, obtained an anomalously low value of C_v at high temperatures, about 2 calories per mole lower than the Dulong and Petit value. Their curve for C_v reaches 12 calories/mole at 600°K, but then drops off to 10 calories/mole at T_m.

The present data for K, together with the previously quoted values of α and data for C_p given by Kelley[11] yield results shown in Fig. 11. This curve of C_v rises to 12 calories/mole at 700°K, and as far as can be determined from the rather uncertain values of α and C_p available near the melting point, maintains the Dulong and Petit value up to the melting point.

The experimental method described here should lend itself to other problems of this kind, and the present work is being extended to other types of crystals.

One of us (Lloyd Hunter) wishes to thank the directors of the Westinghouse Research Laboratories for extending to him permission to use their facilities, and Drs. Otto Stern and O. C. Simpson of Carnegie Institute of Technology for much helpful advice and encouragement.

[10] A. Eücken and W. Dannöhl, Zeits. f. Electrochemie **40**, 789 (1934).
[11] K. K. Kelley, U. S. Bureau of Mines Bulletin, No. 371.

Absorption of Extensive Atmospheric Showers of Cosmic Rays in Air and Lead

PIERRE AUGER* AND JEAN DAUDIN
University of Paris, Paris, France
(Received December 15, 1941)

THE intensity and barometric coefficient of the large atmospheric cosmic-ray showers have been measured. These showers, referred to as "A showers" in this paper, were defined by double coincidences of two horizontal counters separated by either 3 meters or by 13 meters. Measurements were made at sea level and at 2900 m altitude.

1. BAROMETRIC COEFFICIENT AT SEA LEVEL

Four series of measurements were made at sea level under a thin aluminum roof. The counters were unshielded and had a separation of 3 meters. The duration of the experiment was eight months, and included 35,000 coincidences. Series 1 and 2 were made with counters of different cross sections, and readings were extended over different periods, so that recalculations had to be made in order to facilitate the comparison of these results with those of series 3 and 4. The latter series were made with counters of 200 cm² surface area, and results were recorded every hour.

The mean number of double coincidences per hour for different values of the pressure (the choice of which was made after close examination of the barometer curve) have been plotted on the Fig. 1 against the pressure. The statistical probable error is indicated by a vertical line as usual. The straight lines have been calculated in such a way that the sum of the squares of the distances to the experimental points is minimum, the unit being in each case the probable error. No temperature corrections were made, because the relations between barometric and thermometric variations are opposite in winter and in summer, hence compensation is automatically introduced when measurements cover both of these periods.

From these data the total barometric coefficient of A showers can be deduced: a decrease of 1 cm Hg in the atmospheric pressure gives rise to an increase of 9 percent in the number of showers. The probable error can be estimated at ± 1 percent; such a change in the coefficient would bring an increase of 10 percent in the sum of square distances. The mass absorption coefficient μ/ρ for air resulting from these measurements is equal to 0.0068 ± 0.0007 in cm² per gram.

2. INFLUENCE OF THE EXTENSION OF SHOWERS

In another series of measurements a comparison was made between the A showers of 3-m and 13-m extension with unshielded counters. The method was exactly the same, and the results are shown in Fig. 2. The straight lines which best represent the experimental points have different slopes. The coefficients are equal to 23 percent ± 5 percent for the 13-m extension showers, and 11 percent ± 2 percent for the 3-m

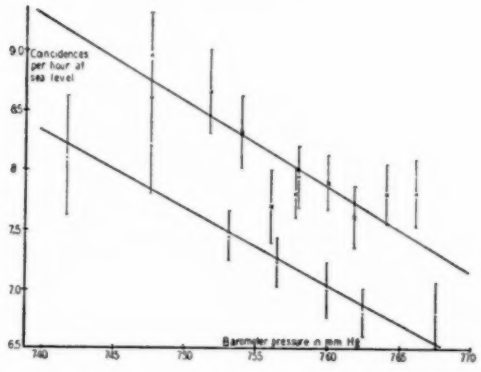

FIG. 1. Coincidences for different values of the pressure at sea level. Counter separations, 3 meters. Counters of two different cross sections were used.

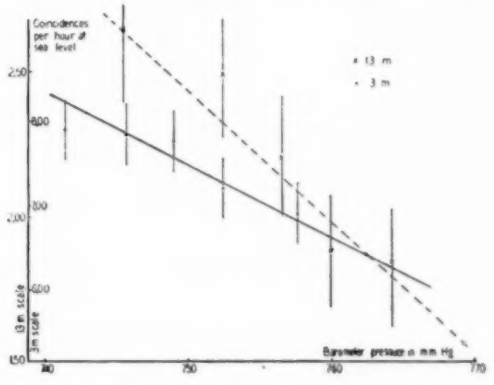

FIG. 2. Coincidences in counters 13 meters and 3 meters apart at sea level.

* Research associate at the University of Chicago.

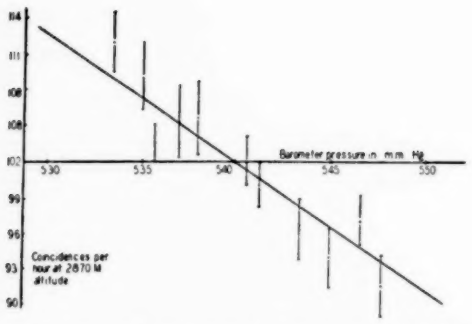

FIG. 3. Coincidences at 2870 meters in counters separated 2 meters.

extension showers (percentage variation per centimeter Hg pressure change.) The striking difference between the two coefficients is in agreement with the results published by Cosyns.[1] It suggests a difference in origin between the narrow local air showers which are mixed with portions of true *A* showers in the 3-m measurements, and these *A* showers themselves. The local air showers are probably due to decay electrons and knock-on electrons coming from mesons of high energies.

3. MEASUREMENTS IN HIGH ALTITUDE

Preliminary results of measurements of the barometric effect at 2900-m altitude (Observatoire du Pic du Midi, France) have already been published.[2] These results, were obtained with a set of two unshielded counters at two meters separation. A thorough recalculation of the data has been made in order to permit a comparison with the sea-level measurements. Because of slightly different conditions the data are separated into four series. The two best series give a coefficient equal to 11 percent$\pm$1 percent. The two other series, less reliable, lead to 10 percent and 15 percent, respectively, with probable errors of $\pm$3 percent. The adopted value, 11 percent, corresponds to a mass absorption coefficient μ/ρ equal to 0.008 ± 0.0008 cm^2 g^{-1}, not noticeably different from the value obtained at sea level (Fig. 3).

Comparison of the absolute number of counts per hour at sea level and at 2900-m altitude gives another value of the absorption coefficient in air. The precision is small, unfortunately, because of the difficulty in obtaining exactly comparable measurements at two distant laboratories. The computed value for *A* showers of 3-m extension is $\mu/\rho=0.007$ cm^2 g^{-1} in good agreement with the barometric effects at both stations.

4. ABSORPTION IN LEAD AND IN AIR

It seems difficult to bring the present results into a satisfactory agreement with those obtained in the study of the absorption of the *A* showers in lead, in terms of the cascade theory only. It has been shown[3] that in high altitude, as well as at sea level, a shield of 10 cm lead on one of the counters of a double coincidence set of 3-m distance causes a decrease of about 85 percent in the number of counts. The protection of the second counter with the same shield brings an additional reduction of the same order. Now this would mean, in the cascade theory, that a considerable fraction of the electrons in an *A* shower have energies higher than 10^{10} ev. Consequently these showers should be "young," i.e., near their maximum development. This conclusion is again difficult to reconcile with the large absorption and barometric coefficients which are only to be expected from "old" showers, definitely on their decrease, and therefore constituted principally of electrons around the critical energy for air, 10^8 ev.

Another difficulty arises from the fact that in the cascades the tracks of two electrons of high energy are never separated by large distances. Even in air two 10^{11} ev electrons have a very small probability of being found as far apart from one another as one meter, so that the coincidences between two counters shielded by 10 cm lead and separated by 3 m could scarcely be explained by this theory. Also the high counting rate with one counter shielded is difficult to account for, if the cores of the *A* showers (parts of the showers where the high energy electrons are contained) have a cross section of less than one square meter.

These considerations show that the ordinary cascade theory would have to be modified for particles of very high energy in order to explain the properties of *A* showers. The modifications would probably involve the production of mesons.

[1] Max Cosyns, Nature **145**, 668 (1940).
[2] Auger, Robley, and Pluvinage, Comptes rendus **209**, 536 (1939).
[3] Auger, Maze, and Grivet-Meyer, Comptes rendus **206**, 1721 (1938).

Letters to the Editor

PROMPT publication of brief reports of important discoveries in physics may be secured by addressing them to this department. The closing date for this department is the third of the month. Because of the late closing date for the section no proof can be shown to authors. The Board of Editors does not hold itself responsible for the opinions expressed by the correspondents. Communications should not in general exceed 600 words in length.

Order in the Alloy Cu_3Au[1]

L. H. GERMER, F. E. HAWORTH, AND J. J. LANDER
Bell Telephone Laboratories, New York, New York
December 5, 1941

FILMS of the copper-gold alloy of the composition corresponding to Cu_3Au have been investigated by electron diffraction by the transmission method. The specimens, which are about 400A thick,[2] have in some cases been prepared for examination by heating for long periods of time in an evacuated container, the treatment ending either with slow cooling or with rapid quenching from a high temperature. Other films have been heated in a high temperature furnace located within the diffraction camera, and electron-scattering patterns have been obtained from these films at various elevated temperatures.

Order, as evidenced by the appearance in the electron patterns of rings having mixed indices, is produced by heating for 16 hours at 170°C, but from diffuseness of these rings we estimate that there are anti-phase domains in the alloy crystals; patterns from films which have been heated only at 160°C do not exhibit these superstructure rings. These observations are a direct confirmation of the indirect conclusion of Nix and MacNair[3] from dilatometer measurements that the copper-gold alloy containing twenty-five atomic percent gold begins to order at a temperature somewhat below 200°C.

Stronger and sharper superstructure rings are obtained from films which have been heated at higher temperatures, and in Fig. 1 is reproduced a pattern corresponding to a degree of order which we estimate to be perfect.

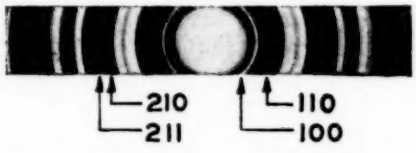

FIG. 1. Electron diffraction pattern from Cu_3Au in completely ordered condition, with designation of the four smallest superstructure rings.

FIG. 2. Pattern from Cu_3Au at 400°C showing unresolved (100) and (110) superstructure ring. Patterns which appear to be identical with this were obtained at temperatures from 370°C to 550°C.

Diffraction patterns from films which have been quenched from temperatures above 400°C are made up of sharp rings characteristic of face-centered cubic crystals of Cu_3Au without superstructure; but in addition to the sharp rings there is a very broad, ill-defined band at about the location of the (100) ring of Fig. 1. (See the pattern of Fig. 2.) If this ring is an indication of slight order in the alloy, it must either have existed at the high temperature before quench or have developed in the very short interval of time (about one second) during which the film was cooled.

Tests for order above the Curie point (380° or 390°C) have been made by obtaining patterns from films at elevated temperatures. Many series of experiments have been carried out in which films have been heated, or cooled, in the diffraction camera at a rate of about 50° per hour with electron patterns taken at frequent intervals. When an ordered specimen is heated at this rate, diffraction patterns from it, as judged from their microphotometer curves, exhibit no marked change until about 300°C is reached. Above this temperature the superstructure rings become gradually broader and less prominent, and reach finally a steady condition at about 370°C. At this temperature and at higher temperatures up to 550°C, which is the limit of our observations, the diffraction pattern is like that of Fig. 2. From the microphotometer curves one discovers that what appears as a single broad inner band on Fig. 2 is made up of (100) and (110) rings in a practically unresolvable condition.

The existence of superstructure lines above the Curie point, as an indication of short-range order, has been explicitly predicted by Peierls and implicitly by Bethe[4] and others, but as far as we are aware these lines have not been observed heretofore. From the breadths and shapes of the rings one should be able to draw significant conclusions about the nature of order above the Curie point. To do this, however, it seems to us necessary to give detailed consideration to short-range order in crystals and to the diffraction effects which could be produced.

[1] Brief accounts of part of this work have been presented at meetings of the American Physical Society, Phys. Rev. **56**, 212 (1939); **57**, 354 (1940).
[2] For the method of preparation see references 1, and L. H. Germer, Phys. Rev. **56**, 58–71 (1939).
[3] F. C. Nix and D. MacNair, Phys. Rev. **60**, 302 (1941). See Fig. 7 for the alloy Cu_3Au. C. Sykes and F. W. Jones have concluded from specific heat data that ordering begins to occur in disordered Cu_3Au at temperatures even below 100°C [Proc. Roy. Soc. **A157**, 213 (1936)].
[4] R. Peierls, Proc. Roy. Soc. **A154**, 207 (1936); H. A. Bethe, Proc. Roy. Soc. **A150**, 552 (1935).

A New Induction Accelerator Generating 20 Mev

D. W. KERST*
Research Laboratory, General Electric Company, Schenectady, New York
December 17, 1941

FOLLOWING a design similar to that used for a 2.3-Mev induction accelerator[1] a larger accelerator with a 19-inch pole face has been constructed. The new accelerator has its equilibrium orbit at a radius of approximately 19 centimeters, and the electrons reach an energy of 20 Mev. Instead of saturation of the central flux causing

the electrons to spiral inward to a target when the magnetic field approaches its maximum value, the orbits are expanded outwardly so that the electrons impinge on the tungsten injector structure which serves as a target for the production of x-rays and for the scattering of the primary electrons. This expansion is produced by a pulse of flux generated by auxiliary coils which are arranged to supply flux through the center of the orbit. These auxiliary coils are energized abruptly after the main magnetic field has reached its peak value, and the additional momentum gained by the sudden increase of central flux moves the electron orbit to larger radii.

While in operation for several months at 13 million volts the accelerator output reached 4.3 r per minute at a distance of one meter from the target as measured by an ionization chamber with thick Bakelite walls. The x-ray output measured in the same way at 20 Mev is now 16 r per minute. The radiation proceeds forward in a small cone and produces a photographic effect mainly confined within a 6° angle.

It is possible to cause the electrons to strike the target at any desired energy below the maximum of 20 Mev by controlling the phase at which the auxiliary coils are energized or by controlling the amplitude of oscillation of the main magnetic field with the auxiliary coils timed to expand the orbit at the peak of the field. The energy which the electrons reach is determined at present by measurements of the peak magnetic field.

In order to cut down bombardment of the inside of the vacuum doughnut and to improve the yield of the accelerator, electrons are injected at 15 or 20 kilovolts for only a brief interval overlapping the time when the field goes through zero. Estimates of the amount of charge which the orbit can hold show that a time average current striking the target of as much as one microampere can be expected. It is not certain that the orbit is now being completely filled.

* On leave of absence from the University of Illinois.
[1] D. W. Kerst, Phys. Rev. **60**, 47–53 (1941).

On the Function $H(m, a, x) = \exp(-ix)F(m+1-ia, 2m+2, 2ix)$

ARNOLD N. LOWAN AND WILLIAM HORENSTEIN
Mathematical Tables Project, Work Projects Administration, New York, New York
November 28, 1941

THE Mathematical Tables Project has carried out some exploratory work on the function $H(m, a, x) = \exp(-ix)F(m+1-ia, 2m+2, 2ix)$ and has computed a six-page table giving the values of $H(m, a, x)$ and of its first derivative with respect to x for the following values of the parameters: $m=0, 1, 2, 3$; $a=0, 1, 2 \ldots 10$; and $x=0, 1, 2 \ldots 10$. The project will consider extending the scope of the present short table by subtabulating for the variable x and for the parameter a provided this undertaking is warranted by the needs of the physicists. Accordingly, the project would welcome suggestions from those who have occasion to make use of the function in question. The following facts may be of importance to the readers of *The Physical Review*.

The function $H(m, a, x)$ satisfies the differential equation

$$x\frac{d^2H}{dx^2}+(2m+2)\frac{dH}{dx}+(x-2a)H=0.$$

An integral representation for $H(m, a, x)$ has been obtained in addition to several recursion formulae connecting (a) $H(m, a, x)$, $H(m+1, a, x)$ and $H(m+2, a, x)$; (b) $H(m, a, x)$ and $H(m+1, a, x)$ with their corresponding first derivatives; (c) $d/dx[H(m, a, x)]$ with $H(m, a, x)$ and $H(m+1, a, x)$; (d) $d/dx[H(m, a, x)]$ with $H(m, a, x)$ and $H(m-1, a, x)$. For the case $a=0$ there exists a simple relation between $H(m, a, x)$ and $J_{m+\frac{1}{2}}(x)$. The recursion formulae were found of great value in checking the values which had been computed from their power series expansion. They could also serve to generate the higher derivatives required in any eventual subtabulation.

The Velocity of Sound in Methyl Methacrylate Polymer

LOUIS R. WEBER AND FRANK P. GOEDER
Department of Physics, Colorado State College, Fort Collins, Colorado
December 18, 1941

IN the first report made by the authors,[1] the velocity of sound in methyl methacrylate polymer (Lucite) was determined directly by means of Kundt's tube and indirectly from elasticity measurements made by stretching several specimen rods. The rods which were 100 cm long and one cm diameter, were subjected to tensile forces from one to 20 kilograms. The velocity by the latter method was found to be at variance with that of the other methods which is to be expected.[2,3] Measurements were continued more recently,[4] with compressional forces from 500 to 4000 lb./in.[2] on specimens of various diameters and lengths. The velocity of sound through these specimens was determined from these values as shown below.

The velocity was further investigated for a number of the same rods with a modification of the electrostatic method,[5] in which resonant frequencies are excited by setting up a modulated potential of the order of 1600 volts. Iron and brass rods were excited under the same conditions and the velocity of sound through them computed to well within the experimental error. The fundamental as well as several harmonics were excited in each rod. The modification proved to be sensitive as well as selective to these frequencies. The present results indicate the velocity of sound to be as follows in methyl methyacrylate.

I. Dynamic method	
(a) Electrostatic excitation	2070 meters/sec.
(b) Kundt's tube	2090 meters/sec.
II. Static method	
(a) From Young's modulus (500 to 4000 lb./in.)	1600 meters/sec.

The stress-strain relationships from which measurements II (a) were made, were linear showing practically instant recovery so far as our instruments indicated. The strain was measured simultaneously with an optical lever and a compression micrometer. Young's modulus computed from

these measurements was found to be 3.1×10^{10} dynes/cm^2 while the value for the modulus computed from the velocity measurements in the electrostatic method gave 5.1×10^{10} dynes/cm^2 at 24.3°C. When this value is corrected for temperature, it is in fair agreement with values just published by Rinehart.[6]

These differences in the velocities come apparently from the fact that under a high stress, a cold flow occurs.[7] Froman[3] has shown an increase in Young's modulus at small stresses for metals. The authors expect to continue measurements at small loads and make a complete report later.

[1] Louis R. Weber and Frank P. Goeder, J. Colo.-Wyo. Acad. (1939).
[2] E. Gruneisen, Ann. d. Physik **22**, 801 (1907).
[3] D. K. Froman, Phys. Rev. **35**, 264 (1930).
[4] Louis R. Weber and Frank P. Goeder, J. Colo.-Wyo. Acad. (1941).
[5] John M. Ide, Rev. Sci. Inst. **6**, 296 (1935).
[6] John S. Rinehart, J. App. Phys. **12**, 811 (1941).
[7] J. Delmonte, Modern Plastics **49** (1940).

Diurnal Variation of Extensive Showers

PIERRE AUGER* AND JEAN DAUDIN
University of Paris, Paris, France
December 1, 1941

REGISTRATIONS of the number of extensive showers have been made at sea level (Paris) with a set of two unshielded coincidence counters, separated by a horizontal distance of three meters. The counts were automatically recorded every hour during a period of two and a half months, from January to April, 1940. The results are given on the curves of Fig. 1, the mean number of counts per

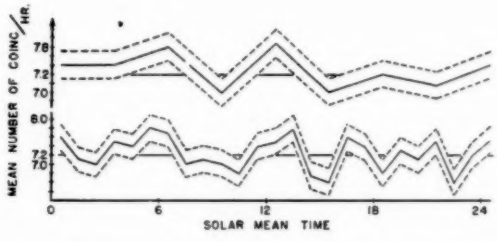

FIG. 1. Mean number of counts per hr. *vs.* solar mean time.

hour being plotted against the mean solar time. In the upper curve the means have been taken over periods of three hours. The dotted curve indicates the probable errors. All readings were corrected for barometric effect.

There is only a feeble maximum (6 percent) at noon, in agreement with the results of Kolhorster. This maximum may be due to a thermal effect. The particles responsible for the production of the big air showers, because of their high energy, are probably completely insensitive to the magnetic field of the earth and of the sun. These particles should then have an isotropic space distribution outside of the solar system. So, either the sources of the particles or the fields in which they are accelerated are uniformly distributed around us, or there must exist very strong causes of disturbance which scatter the initial directions of the particles before they reach the atmosphere.

* Research associate at the University of Chicago.

Single Scattering of Fast Electrons

E. BLEULER, P. SCHERRER, AND W. ZÜNTI
Physikalisches Institut der Eidg. Technischen Hochschule, Zürich, Switzerland
November 17, 1941

ELASTIC scattering of fast electrons (Ra B+C) by the nuclei of nitrogen, fluorine and argon is investigated with a cloud chamber (magnetic field = 450 oersteds). The length and curvature of the tracks were measured by means of stereoscopic projection. In order to avoid large errors in the determination of the energy, scattered tracks shorter than 2 cm were disregarded. Corrections were made for this and for the finite depth of the illuminated area (1 cm) in the cloud chamber.

For comparison with the Mott theory, the whole energy-range was subdivided into three groups (0.2–0.5; 0.5–1; 1–3 Mev). For each of these energy-groups angular cells were formed with the limits 15°, 20°, 30°, 45°, 60°, 90°, 180°. The total amount of scattering seems to be somewhat higher than theoretically expected. (See Table I.)

TABLE I.

Nucleus	Length of path	Number of collisions	$\frac{n_{exp}}{n_{th}}$
A	708 m	153 (>20°)	1.5
F	910 m	113 (>15°)	1.2
N	515 m	42 (>15°)	1.3

The scattering cross section as a function of energy and angle is in agreement with theoretical predictions within the limit of statistical errors. The anomalies reported for the scattering by nitrogen[1] are not confirmed. The values of the cross sections for argon and nitrogen agree well with those of Randels, Chao, and Crane.[2]

There are no measurements available to compare with our results for fluorine.

[1] Skobeltzyn and Stepanowa, Nature **137**, 456 (1936); Bosshard and Scherrer, Helv. Phys. Acta **14**, 85 (1940).
[2] Randels, Chao, and Crane, Phys. Rev. **58**, 201 (1940).

Some Discharge Characteristics of Self-Quenching Counters

W. E. RAMSEY AND EMMETT L. HUDSPETH
Bartol Research Foundation of the Franklin Institute, Swarthmore, Pennsylvania
January 2, 1942

IN a previous publication[1] it was shown that the counter discharge mechanism proposed by C. G. Montgomery and D. D. Montgomery[2] satisfactorily explains the dependence of pulse size upon counter wire capacity and counter length for a non-self-quenching gas mixture. Similar studies made with a self-quenching gas provide equally satisfactory agreement and illustrate nicely the essential difference between the two types of counter operation. As anticipated the self-quenching mixture provides no mechanism for insuring a constant pulse size (for varying capacity and length) and the total voltage swing of the wire for a given cylinder potential is simply $l\alpha/c$. Here l is the effective counter length, c is the total capacity of the wire system and α is the charge per unit length in

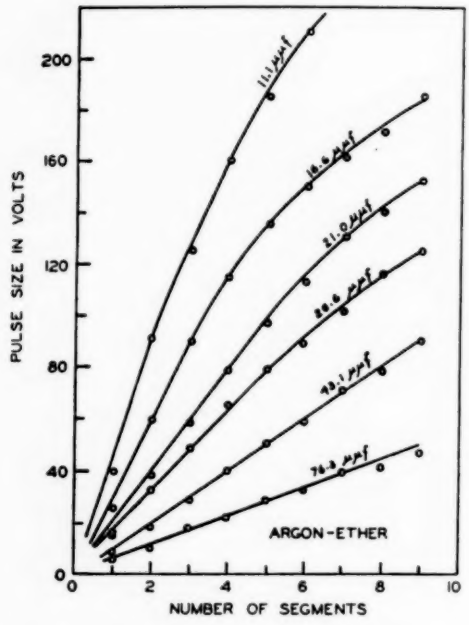

FIG. 1. Pulse size *vs.* length and capacity of counter.

the positive ion sheath which surrounds the counter wire during the discharge.

Figure 1 displays a family of curves showing the dependence of pulse size upon length and capacity while Table I gives the values of α as calculated from the slopes of the separate curves at $l=0$. For small c and large l a departure from the simple relation indicated is observed and corresponds to that found in the non-self-quenching mixture where c is small and l is large. It has been previously shown[1] that the voltage pulse can be represented best by the expression $(l/c)[\alpha-(\beta l/c)]$, where $\beta l/c$ is negligible except for a long counter with a small total wire capacity. For both types of gases the departure is to be expected if a time of the order of magnitude of 10^{-7} second is required for the discharge to spread the entire length of the tube. Such a time delay permits the potential of the wire to change while the positive ion sheath is being established in certain portions of the counter. For this reason the positive charge in the sheath is not constant over the wire length and the average value decreases as we decrease c and increase l. The theory has, with justification, assumed

TABLE I. Values of α, the charge per unit length in the positive ion sheath.

Capacity μμf	Volts / Segment	α in coulombs
11.1	40	4.4×10^{-10}
16.6	26	4.3×10^{-10}
21.0	19.5	4.1×10^{-10}
26.6	16.2	4.3×10^{-10}
32.1	13.0	4.2×10^{-10}
43.1	10.0	4.3×10^{-10}
54.2	8.2	4.4×10^{-10}
65.2	6.5	4.2×10^{-10}
76.3	5.5	4.2×10^{-10}

that, following the passage of the original ionizing particle, photons from the first electron avalanches create discharge centers throughout the counter in extremely short times. It has, therefore, naturally invoked the assumption that, for its purpose, the ionization starts instantaneously at all points along the wire. That this is not strictly true follows from the fact that the spreading process depends upon electrons moving appreciable distances through the gas. Therefore the absence, rather than the appearance, of a small correction term would occasion some surprise.

Figure 2 of reference 1 is a diagram of the counter used. In order to vary the effective counter length *without* changing the wire capacity the cylinder is made to consist of nine separately insulated segments whose voltages may be independently assigned. The number of segments at a fixed value above the starting potential determines the effective counter length. All other segments are at a given voltage well below the Geiger counter threshold. The total capacity of the wire system was varied by adding capacitors between wire and ground. The pulses were observed on an electron tube oscillograph under conditions which gave more than adequate time for the complete collection of the charge involved in the discharge process.

[1] W. E. Ramsey and Wayne L. Lees, Phys. Rev. **60**, 411 (1941).
[2] C. G. Montgomery and D. D. Montgomery, Phys. Rev. **57**, 1030 (1940).

Directional Properties of Self-Quenching Counters

W. E. RAMSEY
Bartol Research Foundation of the Franklin Institute, Swarthmore, Pennsylvania
January 2, 1942

H. G. STEVER[1] has recently reported a very interesting way in which to endow a Geiger-Mueller counter with directional properties. He finds that small beads of glass mounted on the wire of a counter filled with a self-quenching mixture effectively confines the discharge to those sections of the tube traversed by the original ionizing ray. Thus the pulse size from the wire is proportional to the number of segments traversed and is an indication of the path taken by this ray.

The ability to limit the discharge in self-quenching counters in this way is a consequence of the fact that in these counters not only is the active discharge confined to the immediate vicinity of the wire, as in all counter action, but also to the fact that no photoelectrons are formed in remote parts of the counter as a consequence of photons originating in this region. Emmett L. Hudspeth, using an arrangement employed by the author for studying the distribution of photons in time during the discharge in a non-self-quenching mixture,[2] found this absence of photoelectrons in the case of the self-quenching gas. Thus in the self-quenching mixture the *entire* ionization process is confined to the vicinity of the wire.* Started at a point (or a few points) by the passage of the ionizing ray, it must spread along the wire from this point to another very close to it. It is clear that the discharge may be confined to a desired section of the counter *by any procedure which*

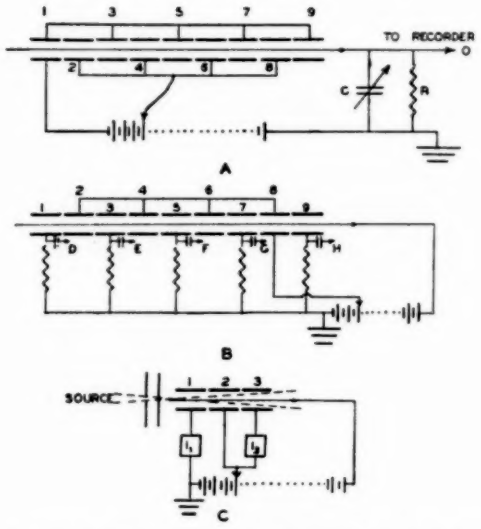

FIG. 1. Counter cylinder composed of separately insulated segments whose potentials may be independently assigned. Filled with a mixture of argon-ether.

interferes with this step-by-step process of propagation at the boundaries of the section.

In one such procedure, and one rich in possible applications, the electric field is reduced at points where it is desired to interrupt the discharge. This has been demonstrated by utilizing the segmented counter employed for other studies.[3,4] Reducing the potential of certain segments (Fig. 1*A*) below the starting potential (say for example 2, 4, 6, 8) we arbitrarily divide the counter into a series of lengths (1, 3, 5, 7, 9) which may be used in coincidence in precisely the manner described by Stever. The pulse sizes observed at 0 are proportional to the number of segments (of the group 1, 3, 5, 7, 9) traversed by the rays passing down the axis of the counter tube. The assignment of active and inactive segments is of course quite arbitrary, and one may divide the same counter into many different coincident groups.

The greatest flexibility is achieved, however, as a result of the fact that voltage pulses (Fig. 1*B*), or charges (Fig. 1*C*) may be taken from the separate segment units. Space does not permit an elucidation of these applications but Figs. 1*B*, 1*C* are suggestive. In 1*B* voltage pulses are taken from the cylinder segments (say *D*, *E*, *F*, *G*, *H*) and applied in any desired manner to the recording circuits. In 1*C* only currents (or total charges) are measured. Here, in segment 1, working in the Geiger counter region, the current to the segment is proportional to the number of ionizing particles which pass through it, while the current to segment 3, working in the proportional region, varies linearly with the product of the number of particles and the specific ionization of the particles involved. Therefore I_3/I_1 is a measure of the specific ionization of the particles of the beam. This procedure, or some obvious modification of it, can provide us with a rugged method for measuring changes of specific ionization of the particles in a beam under conditions where the number of particles does not remain constant. We may thus count particles and simultaneously measure their ionizing capacity *within the same counter.**

[1] H. G. Stever, Phys. Rev. **59**, 765 (1941).
[2] W. E. Ramsey, Phys. Rev. **58**, 476 (1940).
[3] W. E. Ramsey, Emmett L. Hudspeth, and Wayne L. Lees, Phys. Rev. **59**, 685 (1941).
[4] W. E. Ramsey, and Wayne L. Lees, Phys. Rev. **60**, 411 (1941).
* It is essential to adjust the gas mixture until each discharge, as observed on an oscillograph, consists of one single pulse. Failure to break into a continuous discharge with low resistance is not sufficient.

A Suggestion on the Detection of the Neutrino

KAN CHANG WANG
Department of Physics, National University of Chekiang Tsunyi, Kweichow, China
October 13, 1941

IT is known that the presence of the neutrino cannot be detected by its own ionization effect. It appears that the only hope of getting evidence of its existence is by measuring the recoil energy or momentum of the radioactive atom. Crane and Halpern[1] have, by measuring the momentum and energy of the emitted β-ray and the recoil atom with a cloud chamber, obtained evidence pointing toward the existence of the neutrino. However, owing to the smallness of the ionization effect of the recoil atom, it seems worth while to consider a different method of detecting it.

When a β^+-radioactive atom captures a K electron instead of emitting a positron, the recoil energy and momentum of the resulting atom will depend *solely* upon the emitted neutrino, the effect of the extra-nuclear electron being negligible. It would then be relatively simple to find the mass and energy of the emitted neutrino, by measuring the recoil energy and momentum of the resulting atom *alone*. Moreover, this recoil is now of the same amount for all atoms, since no continuous β-rays are emitted. We take for example the element Be^7 which decays in 43 days with K capture in two different processes:[2]

$$Be^7+e_K\rightarrow Li^7+\eta+(1\text{ Mev})$$

and

$$Be^7+e_K\rightarrow (Li^7)^*+\eta+(0.55\text{ Mev}),$$
$$(Li^7)^*\rightarrow Li^7+h\nu+0.45\text{ Mev}.$$

The first process is relatively large, about 10 to 1 in comparison with the second process. The recoil energy of the first process is, by assuming the mass of neutrino to be zero, about 77 ev while that of the second process is about one-third of that amount. This recoil energy would have to be detected and measured in some way, and a correction would have to be made for the disturbances due to the γ-rays and the soft x-rays (originating from the replacement of the K electrons by outer electrons). The recoil energy of certain K-capture atoms, particularly those having isomeric properties so that the K capture is followed by an α-decay, may also be possibly detected by chemical means. In this case, if the radioactive substance is prepared to form some suitable compound of non-polar type, the recoil energy of the resulting atom will break the bond and thus be detected.

[1] H. R. Crane and J. Halpern, Phys. Rev. **53**, 789 (1938); Phys. Rev. **56**, 232 (1939).
[2] R. B. Roberts, N. P. Heydenburg, and G. L. Locher, Phys. Rev. **53**, 1016 (1938); L. H. Rumbaugh, R. B. Roberts, and L. R. Hafstad, Phys. Rev. **54**, 657 (1938).

Proceedings of the Ohio Section of the American Physical Society

MEETING AT CLEVELAND, OCTOBER 10, 11, 1941

THE sixth meeting of the Ohio Section of the American Physical Society was held on October 10 and 11, 1941, at Case School of Applied Science and the General Electric Institute, Nela Park, Cleveland, Ohio. The programme was a symposium on "Light and Lighting."

The Friday afternoon session was held at the Swasey Observatory of the Case School of Applied Science. A lecture was given by Dr. J. J. Nassau, Director of the Observatory, on "The Newer Schmidt Telescopes and their Work." Astronomical movies were shown.

After a banquet Friday evening over one hundred members and guests attended a lecture on "The Mass Spectrograph" by Dr. John A. Hipple, Jr., Westinghouse Research Laboratories, East Pittsburgh, Pennsylvania.

The following papers were read at the Saturday morning session at Nela Park:

The Radiation of Mercury Vapor. B. T. BARNES, *Nela Park.*
Radiation from the Carbon Arc. H. G. MACPHERSON, *National Carbon Company.*
Home Lighting Demonstration. MISS AILEEN PAGE, *Nela Park.*
Sterilizing with Ultraviolet Radiation. ALFRED PAULUS, *Westinghouse Electric & Manufacturing Company.*
Lighting the Classroom. HENRY DATES, *Case School of Applied Science.*

RICHARD H. HOWE, *Secretary*
Denison University
Granville, Ohio

Proceedings of the New England Section of the American Physical Society

MEETING AT NORTHAMPTON, OCTOBER 11, 1941

THE eighteenth regular meeting of the New England Section of the American Physical Society was held at Smith College, Northampton, Massachusetts, on October 11, 1941. About seventy-five persons attended the meeting. The invited papers were as follows:

The Teaching and Research Programs of the Department of Physics at Smith College. GLADYS A. ANSLOW, *Smith College.*
The Native Protein, a Problem for Physics. DOROTHY WRINCH, *visiting lecturer at Smith, Mount Holyoke and Amherst Colleges.*
Stroboscopic Photographs Used in the Teaching of Mechanics. FRANCIS W. SEARS, *Massachusetts Institute of Technology.*
A Defense Training Course in Radio Techniques. WILLIS RAYTON, *Dartmouth College.*

Abstracts of the contributed papers are given below.

Members of the society were the guests of Smith College for a concert of chamber music on the evening previous to the meeting and for tea following the meeting.

At the business meeting the following officers were elected for 1942: *Chairman*, P. M. Morse; *Vice Chairman*, Gladys A. Anslow; *Secretary-Treasurer*, Alice H. Armstrong; *Members of the Program Committee*, H. Margenau and A. P. R. Wadlund.

As it does not seem feasible to hold a meeting in Cambridge during the coming winter, the program committee was given authority to suspend, for this year, the by-law requiring two meetings a year, unless the committee should decide to hold a meeting elsewhere in the spring. This is, in turn, conditional upon the schedule of national meetings of the society. The next autumn meeting will be held at Trinity College in Hartford, Connecticut, upon an October date to be announced later.

A vote of thanks was extended to the members of the Physics Department of Smith College for their generous hospitality and to the members of the Music Department for the delightful concert.

J. C. BOYCE, *Secretary-Treasurer*

ABSTRACTS OF CONTRIBUTED PAPERS

1. Measurement of the Energy of the Gamma-Radiation from Na^{24}. L. G. ELLIOTT, M. DEUTSCH, AND A. ROBERTS, *Massachusetts Institute of Technology.*—The resolution of the gamma-ray spectrometer previously described[1] has been improved and the calibration of the instrument verified by Compton electrons due to the 2.62 Mev gamma-ray from ThC″ and by means of photoelectrons produced by the 0.51-Mev annihilation radiation from Cu^{64}. No other gamma-rays were found in this copper isotope. The method has been further applied to the gamma-rays from the disintegration of Na^{24}. Two gamma-rays of energy 1.38 ± 0.02 Mev (measured by both photoelectrons and Comptons) and 2.86 ± 0.1 Mev were observed, in agreement with the values found by Kikuchi[2] and Curran, Dee, and Strothers[3] but in disagreement with results obtained by Richardson.[4] We failed to observe any other gamma-rays above 0.2 Mev. Because of the background of Compton secondaries any gamma-ray of intensity less than about $\frac{1}{4}$ of that of the 2.86-Mev radiation could not be detected in the range 1.0 Mev to 2.5 Mev. Between 2.5 and 3 Mev a gamma-ray of $\frac{1}{2}$ the intensity of the 2.86-Mev radiation might have escaped detection.

[1] M. Deutsch and A. Roberts, Phys. Rev. **60**, 362L (1941).
[2] Kikuchi et al., Proc. Phys. Math. Soc. Japan **21**, 260 (1939).
[3] S. C. Curran, P. I. Dee, and J. E. Strothers, Proc. Roy. Soc. **A174**, 546 (1940).
[4] J. R. Richardson, Phys. Rev. **53**, 124 (1938).

2. Autoradiography of Manganese Ores. CLARK GOODMAN AND DEAN C. PICTON, *Massachusetts Institute of Technology.*—By using slow neutrons from the M. I. T. cyclotron, the nuclear reaction Mn^{55} (n, γ) $*Mn^{56}$ has been employed to activate manganese ores. The locus and relative concentration of the induced radioactivity in the constituent minerals is determined from autoradiographs made by placing polished surfaces of the ore in direct contact with photographic film. The source of the effective β-radiation is ascertained from the decay rate of the activity, which in each case was predominantly the 2.6-hr. period of manganese. Petrographically interesting observations have resulted from this preliminary investigation and the method is being extended to other elements.

3. Measurements on X-Ray Production and Absorption in the Range 0.7 to 2.5 Mv. L. C. VAN ATTA, F. E. MYERS, AND A. A. PETRAUSKAS, *Massachusetts Institute of Technology.*—In the voltage range from 0.7 to 2.5 Mv, the intensity and the total mass absorption coefficient of the heterogeneous radiation produced in a thick gold target have been measured as a function of tube voltage, angle with respect to the electron beam, and thickness and material of the filter. Preliminary results have been described.[1] Curves giving the dependence of absorption coefficient on voltage are presented for lead, tin, copper, aluminum, carbon, and water as absorbers. A method is described for calculating the absorption coefficient of the heterogeneous radiation produced at a given tube voltage and subjected to a given amount of filtration, utilizing accepted values for the absorption coefficient of homogeneous radiation. Measured and calculated values of the absorption coefficients for heterogeneous radiation are in good agreement. Curves giving the dependence of intensity on angle are in qualitative agreement with approximate theory. Curves giving the dependence of absorption coefficient on angle and the dependence of intensity in the forward direction on voltage are presented. A method for calculating the efficiency of x-ray production from these data is described and used to obtain results in approximate agreement with theory.

[1] Phys. Rev. **59**, 688A (1941).

4. Smith College Generating Voltmeter. KATHLEEN KANE, *Smith College.*—A generating voltmeter of the rotating vane type,[1] employing no commutation or amplification, was constructed and calibrated for use with the Smith College electrostatic generator. Four rotor and eight stator sectors were cut from nine-inch diameter disks of Duralumin. The voltmeter is mounted opposite the generator terminal, 150 centimeters distant. It was calibrated by applying known voltages to a metal disk facing the rotor. Except for a slight deviation at low voltages, this calibration curve is linear. The output current is five microamperes per kilovolt per centimeter. A maximum voltage of 600 kilovolts on the generator terminal is obtained when operated under normal humidity conditions. When alternating current voltage is applied to the calibrating disk, the output current is found to be proportional to the voltage, but not inversely proportional to the

distance between the disk and the stator sectors. Hence, with a fixed distance between the calibrating plate and the stator, this instrument is a practical alternating current voltmeter.

[1] J. G. Trump, F. J. Safford, and R. J. Van de Graaff, Rev. Sci. Inst. 11, 54 (1940).

5. The Absorption Spectrum as a Quantitative Test for Mercury Vapor in Air. K. C. CLARK AND O. OLDENBERG, *Harvard University.*—The mercury content of the air of the laboratory is tested by photographing the absorption line 2537 over a path length of 8 m on a continuous background with a medium-size quartz spectrograph. For calibration the same absorption line is photographed, produced by a short column of air saturated with mercury vapor at various temperatures. By matching absorption lines of equal intensity, taking into account the lengths of the two absorbing paths, the mercury content of the air of the laboratory is determined. A concentration as low as 0.0075 mg/m³ can be detected by this method. This is about 1/13 of the toxic limit recently established by the National Bureau of Standards and the National Institute of Health.

6. Oriented Overgrowths of Alkali Halides on MgO. GEORGE H. VINEYARD, *Massachusetts Institute of Technology.* (*Introduced by D. C. Stockbarger.*)—From considerations of lattice similarity, NaF and LiF, of the alkali halides, when deposited on MgO might be expected to take up the orientation of the supporting crystal. Oriented overgrowths of LiF were obtained both by depositing the LiF from aqueous solution and by depositing it from the melt. NaF was found to orient when properly deposited from the melt, but orientation could neither be proved nor disproved in the case of deposition from solution. Rather exacting experimental procedures were found necessary to produce these orientations, indicating that the forces of orientation involved are weak. NaCl, which has a lattice parameter differing a little more from that of MgO than either LiF or NaF, could not be made to orient in deposition by fusion, by evaporation, or by aqueous solution. CsCl, which has a lattice parameter almost equal to that of MgO but a body-centered instead of a face-centered cubic lattice, could not be made to orient either. This confirms Royer's law of the necessity for like charged ions at corresponding points in the supporting and supported lattices. This is possibly the first reported example of orientations being artificially obtained from fusion.

7. Dielectric Absorption in Cellulose Nitrate and in Methyl Methacrylate. CATHERINE L. BURKE, *Wellesley College.* (*Introduced by Louise S. McDowell.*)—For many dielectrics the maximum absorption is smaller and the dispersion range broader than predicted by the Debye equation. Cole and Cole have demonstrated that the complex-plane locus of ϵ for many such materials is a circular arc with center below the real axis, represented by an equation which presupposes a symmetrical loss-factor *vs.* log-frequency curve. To test the applicability to plastics, measurements were made on methyl methacrylate and on cellulose nitrate in the frequency ranges 0.3 to 10 kc and 300 kc to 50 mc. For methyl methacrylate the curve is an arc as predicted by Cole's equation. For cellulose nitrate the loss-factor *vs.* log-frequency curve is asymmetrical with a secondary maximum near 1 mc and a maximum at about 30 mc. On the assumption that the asymmetry is due to the simultaneous occurrence of two types of absorption, a symmetrical dispersion curve was drawn corresponding to the 30 mc maximum and the differences between the experimentally-determined values of loss factor and the ordinates of this curve were found. The corresponding complex-plane locus consists of two intersecting circular arcs, each in good agreement with the equation. These arcs may be identified with losses due respectively to rotation of polar groups and ionic polarization within the micellae.

8. Demonstration Experiments with Tuning Forks. ERIC ROGERS, *St. Paul's School.**

* Abstracts of papers 8 and 9 are to be published in the *American Journal of Physics.*

9. Adapt the Instruction to the Student. RUSSELL S. BARTLETT, *Newark College of Engineering.**

Proceedings of the Metropolitan Section of the American Physical Society

MEETING OF OCTOBER 31, 1941

THE first meeting of the Metropolitan Section of the American Physical Society for the season 1941–1942 was held at 3 P.M. on Friday, October 31, 1941, in the Pupin Physics Laboratories of Columbia University. The following papers were presented:

Extensive Cosmic-Ray Shower Experiments in the Peruvian Andes. NORMAN HILBERRY.
Thermistors, Their Characteristics and Uses. G. L. PEARSON.
Stability and Instability Demonstrated by Soap Film Experiments. RICHARD COURANT.

W. S. GORTON
Secretary-Treasurer

Proceedings of the New York State Section of the American Physical Society

MEETING AT ALFRED, NEW YORK, NOVEMBER 1, 1941

THE Fall Meeting of the New York State Section of the American Physical Society was held at Alfred University, Alfred, New York, on Saturday, November 1. An attendance of about 130 members and visitors was recorded. The following program of invited papers was presented:

Address of Welcome. J. N. NORWOOD, *President, Alfred University.*

The Application of Polarized Light and X-Rays to the Ceramic Industry. C. R. AMBERG, *New York State College of Ceramics.*

Spectroscopy in Ceramics. LEON BASSETT, *Alfred University.*

Physical Aspects of Research in Ceramics. J. F. MCMAHON, *New York State College of Ceramics.*

What the Artists Should Know About the Science of Color. H. P. GAGE, *Corning Glass Works.*

Systems with Many Particles. EUGENE P. WIGNER, *Princeton University.*

Running a High School Science Club. WILLIAM SANFORD, *Painted Post High School.*

Some Recent Developments in Radiology. WILLIAM F. BALE, *Strong Memorial Hospital.*

Reciprocity Law Failure and Intermittency Effect in Photographic Exposure. J. H. WEBB, *Eastman Kodak Company.*

Inspection of the various laboratories of the New York State College of Ceramics proved a very interesting addition to the formal program.

PAUL R. GLEASON, *Secretary*

Proceedings of the American Physical Society

MINUTES OF THE CHICAGO, ILLINOIS, MEETING

November 21–22, 1941

THE 244th meeting of the American Physical Society was held in Chicago on November 21–22, 1941. Despite the growing diversion of physicists to national defense, the attendance upon the meeting (127 registrants) and the number of contributed papers (32, distributed over three half-day sessions) were better than fair. The University of Chicago was our host as usual; to the University, the Physics Club of Chicago, and the Local Committee (Dr. W. P. Jesse, Chairman) the thanks of the Society are due. The dinner was held on the evening of the 21st at International House, President Stewart presiding. In the course of the after-dinner programme, Professor James Franck gave many reminiscences of the history of physics during the early days of his career, Professor A. H. Compton described the National Science Fund of the National Academy of Sciences, and brief remarks were made by officials of the Physics Club and the Society.

The Council met on November 21. One hundred and sixteen new Members were elected and sixty-one Members advanced to the rank of Fellow; their names are appended. Word was received of the loss of four Fellows (Harry S. Hower, Carl E. Magnusson, Henry A. McTaggart, and Carroll F. Sparrow) and five Members (Evald Anderson, George P. Bacon, Elmer S. Imes, Leo H. Linford and Otto Rothenstein) through death. Owing to the absorption of Editor J. T. Tate in work pertaining to defense, his title is temporarily altered to "Editor on Leave" and Professor J. W. Buchta is entitled "Acting Editor."

Transferred from Membership to Fellowship: Vernon M. Albers, Paul A. Anderson, Alfred Baños, Jr., W. H. Barkas, Clarence E. Bennett,

L. V. Berkner, Francis Birch, John P. Blewett, T. W. Bonner, William E. Danforth, Lewis A. Delsasso, Charles S. Draper, Harold E. Edgerton, Walter M. Elsasser, Immanuel Estermann, Isidor Fankuchen, Eugene Feenberg, I. A. Getting, Roy W. Goranson, M. H. Hebb, Albert G. Hill, J. O. Hirschfelder, J. Warren Horton, Henry G. Houghton, Jr., Maurice L. Huggins, Curtis J. Humphreys, David R. Inglis, Ellis A. Johnson, Martin D. Kamen, George E. Kimball, Robert B. King, R. W. P. King, Harry V. Knorr, James F. Koehler, Bernhard Kurrelmeyer, Lawrence M. Langer, David B. Langmuir, L. Jackson Laslett, Humbolt W. Leverenz, Fritz London, John R. Loofbourow, Louis Malter, Maria Goeppert Mayer, Nora M. Mohler, Frank E. Myers, Chaim L. Pekeris, Boris Podolosky, Edith H. Quimby, Louis N. Ridenour, Bruno Rossi, Julian Schwinger, Emilio Segrè, Lincoln G. Smith, Joyce C. Stearns, Leo Szilard, Abraham H. Taub, Browder J. Thompson, Gregory S. Timoshenko, Edwin A. Uehling, Charles W. Ufford and Lloyd A. Young. *Elected to Membership:* Reuben E. Alley, Jr., Wallace E. Anderson, Henry S. Arms, Benjamin M. Axilrod, Eugene M. Baroody, Hilda Bass, E. Robert Beringer, G. Bernardini, John M. Blair, Léon Brillouin, Sheldon Brown, Eugene R. Brownscombe, J. H. M. Brunings, Walter H. Byers, William S. Bryan, H. M. Cave, William W. Chambers, A. Benjamin Clymer, Amador Cobas, Malcolm B. Cole, Edward Creutz, Norma L. Curtis, Charles H. Dahm, Gordon C. Danielson, Bowen C. Dees, Pierre Demers, Edward der Mateosian, Frederick P. Dickey, Sheldon H. Dike, Harry T. Drill, Henry E. Duckworth, Beverly C. Dunn, Jr., William A. Edson, G. Foster Evans, Sidney Fernbach, Charles F. Fitter, Jr., John E. Forss, William J. Fry, David H. Garber, Frederick W. Geiger, Frank N. Gillette, P. R. Gillette, Louis Goldstein, Walter A. Good, Robert S. Goodyear, James H. Green, Jr., Jack B. Greene, Bernard Hamermesh, Lucile S. Harber, Donald O. Holland, John A. Hornbeck, James N. Humphrey, G. Bowditch Hunter, Jr., Lloyd P. Hunter, Mario Iona, Jr., Herbert Jehle, Charles N. Johnson, Jr., Lawrence H. Johnston, Thomas F. Johnston, Oliver B. Keyes, Clifford C. Klick, Herman W. Koch, Joann D. Kurbatov, William J. Leas, Harry W. Lew, Robert N. Little, Jr., Alfred E. Martin, Frank J. McDonal, James F. McGee, Kenneth G. McKay, Henry L. McMurry, Robert R. Meijer, Inez K. Milbauer, John J. Miller, Walter C. Miller, Rose Mittelmann, Philip Morrison, Carl O. Muehlhause, Darragh Nagle, Morris Neustadt, Guy C. Omer, Jr., C. Harvey Palmer, Jr., David Park, Gilbert N. Plass, William Rarita, Anna J. Reardon, Lawrence J. Reimert, Theodore S. Renzema, William W. Rigrod, Clark S. Robinson, Jr., Howard J. Rowland, Robert I. Sarbacher, Richard Scalettar, Worth Seagondollar, Maurice M. Shapiro, Lenart Simons, Ralph J. Slutz, J. Gordon Stipe, Jr., John J. Stokes, Robert B. Taylor, Edward R. Thilo, Laszlo Tisza, Frank E. Towsley, Horace M. Trent, Willem van der Grinten, Delbert van Winkle, Rodman Van Wye, Peter L. Vissat, Ming-Chen Wang, Stuart E. Whitcomb, Arthur O. Williams, Jr., Robert E. Williams, John K. Wood, Jr., Don M. Yost, Gale Young, and Louis B. Young.

The abstracts of thirty-two contributed papers, of which two (Nos. 31 and 32) were read by title, are herewith appended.

KARL K. DARROW, *Secretary*
Columbia University, New York

ABSTRACTS OF CONTRIBUTED PAPERS

1. Statistical Distribution of Impedance Elements in Biological Systems. A. M. WEINBERG AND A. S. HOUSEHOLDER, *University of Chicago.*—Electric impedance measurements on systems consisting of non-uniform elements (e.g., nerve bundles, cell suspensions, imperfect dielectrics) can be interpreted if the impedance characteristics of the individuals and their impedance distribution is known. Conversely, given the observed over-all impedance, $z(p)$, the impedance distribution of the individuals is not uniquely determined in both phase angle and static capacitance. If all individual phase angles are equal, the distribution, $D(\tau)$, is the solution of Stieltjes' integral equation

$$F[z(p)]=\int_0^\infty \frac{D(\tau)d\tau}{1+p\tau},$$

F being a known function of the geometry of the system. It is shown that the phase angle of the equivalent suspension approaches that of the original suspension as the dispersion of $D(\tau)$ decreases.

2. Kinetic Theory of Mechanical Forces in Diffusion Fields. H. D. LANDAHL, *University of Chicago.*—The mechanical forces in diffusion fields are of interest in mathematical biophysics of cell division and other phenomena in metabolizing systems. Some insight into the problem may be gained by considering the force on a particle in a non-uniform, dense mixture of gases. For this reason, an expression was derived for such a force. Three types of terms arise under the assumptions made. One is due to the mass velocity of the system, one arises because of the finite sizes of the particle and molecules, and one arises because of the dependence of collision frequencies on the density, which varies in space. Each term is proportional to the density gradient if the mass velocity is due only to diffusion. The expression for the force is compared with an analogous expression arrived at by considering incompressible fluids passing through each other,[1] and obtaining the resulting force on a particle at rest suspended in the mixture.

[1] G. Young, Bull. Math. Biophysics **2**, 145 (1940).

3. Excitation of the Anode Effect. PAUL L. COPELAND AND GERALD G. CARNE, *Illinois Institute of Technology.*—The way in which charge trapped on the grid surface of an experimental triode accumulates has been observed by collecting relatively large grid currents for various short time intervals and studying the resulting changes of plate current. If the shift of the contact potential of the grid is plotted against the logarithm of the time that the grid collects current, a graph which is linear over a considerable interval results, and in this respect the curves showing the accumulation of the charge resemble those showing its decay. If the total charge collected by the grid be denoted by Q_p and the total charge trapped on the grid be denoted by Q_c, the observed results are consistent with the empirical formula $Q_c = Q_p/(A + mQ_p)$, where A and m are constants depending on experimental conditions. The charge accumulating on the grid approaches the limit $1/m$, and this quantity decreases as the grid temperature increases. A, representing the limit of the ratio of the collected charge to the trapped charge when, starting with the equilibrium state, the collected charge is made very small, also varies with the temperature of the grid.

4. Thermionic Properties of the Iron Group. H. B. WAHLIN, *University of Wisconsin.*—The pyrometer temperature scales of the iron group have been determined as a preliminary to the thermionic studies. A change in the emissivity of iron at the crystal structure transition point has been observed. This serves as a new method of determining the temperature of this charge. The work functions of the metals have been determined and the effect of certain impurities in Ni determined. A difference of 0.25 volt has been observed in the work functions of β- and γ-iron. The work function of pure Ni has been found to be 4.61 volts and that of Co 4.42 volts.

5. Theory of the Magnetron. LEON BRILLOUIN, *University of Wisconsin (Introduced by Karl K. Darrow).*—In a first paper recently published in *The Physical Review* [**60**, 385–396 (Sept. 1, 1941)] the author studied theoretically the comportment of a magnetron under steady conditions, and attempted to calculate the conditions for sustaining continuous oscillations by a magnetron with one cylindrical anode. The present paper relates to the problem of the magnetron with an even number of anodes. In order to avoid too much complication in the calculations some simplifying assumptions have been made, neglecting the radius of the filament and ignoring the role of oscillating magnetic fields; the limitations due to such simplifications are discussed, and it may be proved that they are justified in most cases. The theory shows under which condition this type of magnetron should yield a negative resistance and be able to sustain oscillations in an outer circuit.

6. An Electronic Stabilizer for 1 to 50 kv and 20 to 500 ma. J. W. TRISCHKA AND L. G. PARRATT, *Cornell University.*—An electronic stabilizer for use in the output of a high voltage d.c. power supply has been developed which is proposed as a satisfactory and economical solution of the problem of obtaining very large powers which are stable over a wide range of voltages and currents (1 to 50 kv and 20 to 500 ma in the present design). The device reduces the residual ripple and fluctuations in the load current as well as stabilizes against fluctuations in the input voltage. This stabilizer is capable of maintaining for several hours an output voltage constant within ± 0.3 percent when the input fluctuates by ± 5 percent. The largest source of output fluctuation is a slow drift. The apparatus, containing an 833-Type tube with two stages of amplification in the grid circuit, is essentially a modification of the degenerative type of stabilizer, but, taking advantage of grid current, may be adjusted to have positive, negative, or infinite, stabilization ratio.

7. X-Ray Absorption Structure in the Region of the Potassium K Edge. J. B. PLATT AND L. G. PARRATT, *Cornell University.*—Variations of the absorption coefficient of potassium near the K edge have been measured with a two-crystal vacuum spectrometer. The measurements of the transmitted beam intensity are accurate to within 1 percent of the intensity of the incident beam. The spectral region has been carefully studied from six electron volts less than the energy of the K edge to thirty electron volts greater than that of the K edge. Calcite crystals on the spectrometer gave a computed resolving power of about 12,000. Absorber "sandwiches" were prepared by evaporating a protective layer of 200Å of aluminum on a Kodapak base, evaporating 80,000Å of potassium, and finally evaporating a coating of Ceresine wax on the potassium surface to prevent oxidation when exposed to air. Results are in agreement with theoretical predictions based on the free electron approximation to the energy bands in metallic potassium.

8. Further Theoretical Studies of the Temperature Diffuse X-Ray Scattering. W. H. ZACHARIASEN, *University of Chicago.*—The general intensity formula for the temperature diffuse scattering[1] has been studied in greater

detail. In order to make exact numerical calculations for the diffraction pattern it is necessary to know the propagation velocities and the polarization directions of the proper vibrations throughout the entire vibrational spectrum. Calculations have been carried out for simple lattice models. It is found that the details of the diffuse diffraction pattern vary considerably as the elastic properties of the lattice model are changed. The calculations can be directly compared with experimental data obtained with simple crystals like rocksalt and sylvine. In all cases where such detailed comparisons have been made the agreement between theory and experiment is complete. Because the acoustical frequency branches are more important for the diffuse scattering than the optical branches calculations based upon monatomic lattice models may be used for qualitative and semi-quantitative interpretation of experimental data obtained with crystals of more complex structure. Thus theory can account for the puzzling effects reported for diamond.

[1] W. H. Zachariasen, Phys. Rev. **57**, 597 (1940).

9. On the Lattice Vibrations of the KCl Crystal. MARIO IONA, JR.,* *University of Chicago* (*Introduced by W. H. Zachariasen*).—The distribution of characteristic vibrations of the KCl crystal has been calculated following Born, v. Kármán, and Blackman under the assumption of both electrostatic and repulsive forces between the ions. The former have been calculated according to Waller following the method of Ewald. Following Ljunquist the elastic constants and the residual ray frequency have been used to determine four force constants of the repulsive forces for the interaction of 18 nearest neighbors. The distribution obtained in this way shows a relatively great number of vibrations above the residual ray frequency, a feature which has been pointed out in other works in which the electrostatic effect was considered. These higher frequencies however do not influence the specific heat, which is determined mainly by the two maxima of the distribution function. The characteristic temperature has a minimum for absolute temperatures of about 15° in accordance with the experimental results of Keesom, Clark, and Lindemann.

* Also at University of Uppsala (Sweden).

10. A Comparison Between a Geiger-Mueller Counter, a Secondary Electron Multiplier Tube, and Photographic Film for Detecting Weak X-Rays. A. EISENSTEIN AND N. S. GINGRICH, *University of Missouri*.—A Geiger-Mueller (G-M) counter and a secondary electron multiplier (S.E.M.) tube, both designed for use with x-rays, were compared for use in detecting x-rays. Each tube was used under optimum operating conditions and the x-ray intensities in the two cases were known to be approximately equivalent. The rate of counting was determined by means of an amplifier and scaling circuit. Amplified pulses from the G-M tube had a resolving time of about 10^{-3} sec., and those from the S.E.M. tube, about 8×10^{-5} sec. Both tubes were shown to respond linearly to intensity over a wide range of intensities. The relative response of the tubes (G-M to S.E.M.) at several wave-lengths was found to be: at 0.631Å, 10.71; at 0.708Å, 9.77; at 0.712Å, 9.98; at 1.39Å, 5.0; at 1.54Å, 4.92. This shows that the G-M tube is from 5 to 10 times as sensitive as the S.E.M. tube and that the S.E.M. tube sensitivity changes more rapidly with wave-length than that of the G-M tube. A qualitative comparison between the G-M tube and photographic film showed that a complete diffraction pattern of a liquid could be obtained with the G-M tube in about one-twentieth the time required in the photographic method.

11. A Two-Dimensional Phase of Peculiar Properties. WILLIAM D. HARKINS, L. E. COPELAND, AND G. E. BOYD, *University of Chicago*.—If the most condensed two-dimensional liquid (L_2) previously known is compressed isothermally, it transforms to what has been considered as a solid (S) phase, of much lower compressibility, without a latent heat of freezing (second order change). In an attempt of the senior author to discover a first order change in a two-dimensional system, a remarkable SL phase has been found. It was first noted that if the process of its formation from L_2 is freezing, this occurs by addition of heat. Then it was found that the SL phase has the extremely low compressibility of the S phase, but is a superliquid in the sense that its viscosity is very much smaller than L_2 from which it is formed. The increase of internal energy, of entropy, and the heat absorbed, when this phase expands, are excessively high. The logarithm of the viscosity of the L_2 phase normally increases linearly with the pressure, but if the LS phase instead of the S phase is to form, the viscosity decreases with extreme rapidity with the pressure. The temperature of the transformation from L_2 to SL increases about 5° per carbon atom in the molecule. With a new apparatus monolayers will be investigated from 0° to −20°C.

12. A Statistical Study of Cosmic-Ray "Star" Tracks in a Photographic Emulsion. MAURICE M. SHAPIRO, *University of Chicago* (*Introduced by Arthur H. Compton*).—To obtain data concerning the multiple nuclear disintegrations produced by the cosmic radiation, special photographic plates were left on Mt. Evans for nearly eight months. From a statistical investigation of 365 tracks in 142 "stars" found in one of these emulsions, it is estimated that more than 90 percent of the tracks were produced by protons. Most of the remaining star tracks are probably due to alpha-particles.

13. Cloud-Chamber Photographs at 14,170 Ft. Altitude. W. H. BOSTICK, *University of Chicago* (*Introduced by Arthur H. Compton*).—A cloud chamber 24 cm in diameter with a 1.3-cm lead plate in the middle was used in turn under 12.7 cm and 20 cm of lead, and was tripped with a shower arrangement to look for mesotrons in air showers at 14,170 ft. altitude. In air showers particles were found which did not produce secondaries in the 1.3-cm lead plate. These particles are classified as heavier than electrons, probably mesotrons. Out of 3041 successful expansions 172 particles are classified by their range and estimated specific ionization as either slow mesotrons or slow protons.

39 particles show a marked increase in ionization on passing through 1.3 cm of lead. 54 particles appear to be penetrating pairs and thus indicate the production of penetrating secondaries at this altitude. Some photographs give evidence of nuclear processes associated with showers. 5 photographs could possibly be explained by the theory of the disintegration of the mesotron.

14. Mass of the Meson by the Method of Momentum-Loss. RUDOLF LADENBURG AND JOHN A. WHEELER, *Princeton University.*—Observations on the curvature of the track of a meson before and after traversal of a known amount of matter allow a determination of the mass of the particle. A discussion is presented of the accuracy and advantages of this method of measuring mass, the principle of which is well known but has so far been little used. In this connection the stopping power for fast particles has been computed on the basis of recent experiments of R. R. Wilson. Curves are presented for the dependence of range on energy and momentum for swift hydrogen and helium nuclei as well as for mesons. The method of momentum loss is illustrated and values are obtained for the mass of the meson from measurements published by Anderson and Neddermeyer in 1934. The evidence available from these mass determinations and from those published by other authors shows the necessity for many more mass determinations before one can decide whether there is a distribution of masses of the meson or not.

15. Mesotron and Electron Energy Spectrum at 14,260 Feet Altitude from Absorption Measurements in Lead. DAVID B. HALL, *University of Chicago (Introduced by A. H. Compton).*—The absorption curve for lead at Mt. Evans, Colorado, was obtained for vertical cosmic rays by combining two independent sets of data of threefold and fourfold counter tube coincidence arrangements. Zero to 91 centimeters of lead were placed between the counters, and corrections for air showers were made for each thickness. For small thicknesses of lead the mesotron and electron components were distinguished by means of additional experiments in which showers arising from electrons traversing the vertical counters were detected. The intensity of the electron component was found to be less than 2 percent of the total intensity at 7.5 centimeters of lead, 10 percent at 1.5 centimeters of lead, and at 0 centimeters was estimated to be 30 percent. From this the mean energy of these electrons is seen to be approximately $5 \cdot 10^7$ ev. The lower limit of mesotron energy required for traversing the lead was calculated for each thickness and by applying this to the absorption curve an energy spectrum for mesotrons was obtained extending from 0 to 1.5×10^9 ev. A sharp maximum in the spectrum appears at a considerably lower energy than the maximum observed at sea level.

16. Production of Penetrating Particles on Mt. Evans. VICTOR H. REGENER, *University of Chicago.*—The production of penetrating particles in the cosmic radiation was investigated on Mt. Evans, Colorado (4300 m) during September, 1941. The apparatus consisted essentially of seven counter trays, each containing from 13 to 19 G-M counters of 1" and 2" diameter. The trays were arranged below 1, 5, 5, 5, 10 and 10 cm of lead or iron. For studying the cross section and multiplicity of the production process and the penetrating power of the produced particles, the counters were connected to individual neon lamps. The neon lamps were controlled by their corresponding counters only in the moment coinciding with a vertical fourfold coincidence in the apparatus. A camera, set off by the same coincidence, photographed the neon lamps on 16-mm film. A preliminary survey of the results shows multiple production of penetrating particles by a non-ionizing radiation, as one should expect from the results of former measurements.

17. The Variation of Intensity of Cosmic Rays with Zenith Angle at 14,200 Feet Altitude. MARCEL SCHEIN, DAVID B. HALL, AND JANE HAMILTON-HALL, *University of Chicago.*—The zenith angle intensities of cosmic rays at 15°, 28.5°, 44°, and 59° from the vertical were measured with four similar counter telescopes using 0, 4 and 15 centimeters of lead. Corrections were made for side showers at each angle. Changes of intensity due to barometric pressure were found to be very large for zero centimeters of lead. These variations were averaged out by repeating frequently measurements of two hours duration for each angle. The intensity for each thickness of lead decreased with increasing zenith angle θ approximately following a $\cos^2\theta$ curve, but sharpening for angles greater than 15°. The deviations for 0, 4 and 15 centimeters were, respectively, 6 percent, 8 percent, and 4 percent at $\theta = 28.5°$, and 19 percent, 22 percent, and 4 percent at $\theta = 59°$. From energy measurements at this altitude it is estimated that the particles recorded between 0 and 4 centimeters of lead consist of approximately 70 percent electrons and 30 percent mesotrons. With 4 centimeters of lead the electron component is reduced to 5 percent of the total intensity. The similarity of the zenith angle curves at 0 and 4 cm of lead indicates that at 14,200 feet altitude a large part of the electron component is in equilibrium with the mesotrons.

18. Radioactive Isotopes of Nickel. MARTIN E. NELSON, M. L. POOL, AND J. D. KURBATOV, *Ohio State University.*—The isotopic assignments of the 2.6-hr. and the 36-hr. periods in nickel are somewhat uncertain, as shown by experimental evidence and by empirical predictions. Hilger H.S. nickel metal was bombarded with 10 Mev deuterons. The 2.6-hr. activity in the separated nickel fraction was followed from 23,000 times background to one-half of background. The 36-hr. activity was not found and, if present, had an intensity less than 0.01 percent that of the 2.6-hr. period. Hilger V.P.S. cobalt metal was also activated with deuterons to test the possible $Co^{57, 59}(d,2n)Ni^{57, 59}$ reactions. A weak 2.5-hr. activity, due to a trace of nickel in the cobalt target, was found in the nickel fraction. Again the 36-hr. activity was absent and, if present, had an intensity less than one-tenth background. This is consistent with the recently reported non-existence of stable Co^{57}. Bombarding nickel with fast neutrons gave both periods, while slow neutrons gave only the 2.6-hr.

period. The presence of slow neutrons in the fast neutron radiation and vice versa was measured. The above data are best interpreted by assigning the 36-hr. period to Ni^{57} and the 2.6-hr. period to Ni^{65}.

19. Further Progress on the Study of the Radioactive Isotopes of the Nd-Il-Sm Region. J. D. KURBATOV, D. C. MACDONALD, M. L. POOL, AND L. L. QUILL, *Ohio State University.*—Since the previous report[1] on this study, the following additional data have been secured: A. The reactions, Sm+*d*, Sm+*n* (fast) and Nd+α, produce the isotopes tentatively assigned to the element samarium, as follows: (a) the isomers 21±2 min., β^- −1.8 Mev emitter and 60±6 days, γ^- emitter; and (b) a 47±1 hr., β^- low upper limit energy emitter. The short period of about 2.4 min., β^+ emitter was always present but cannot be definitely assigned as yet. B. The reactions, Nd+*d*, Nd+*n* (fast), Nd+γ, and Pr+*p*, produce the isotopes assigned to the element neodymium, as follows: (a) a 2.5 hr., β^+ 0.78 Mev emitter assigned to Nd^{141}, (b) a 41±1 hr., β^- 2.9 Mev emitter. Two additional periods, one of about 2 hr., β^- emitter, and the other a short one, are being studied. C. The reactions, Pr+α and Nd+*d*, produce an isotope >100 days, β^- emitter. The Nd+α, Nd+*d*, and Nd+γ reactions produce a β^- emitter of about 10 days half-life, and possibly two shorter period substances. Additional studies are in progress to clarify further the assignments of periods to the proper isotopes of Nd, Il, Sm.

[1] H. B. Law, M. L. Pool, J. D. Kurbatov and L. L. Quill, Phys. Rev. **59**, 936 (1941).

20. Deuteron-Tritium Reaction in Nitrogen and Fluorine. LYLE B. BORST, *University of Chicago* (*Introduced by S. K. Allison*).—The deuteron-tritium reaction has been reported for several elements including H^2, Be^9, Cu^{63}, Ag^{107}, and Sb. The following reactions have been established in nitrogen and fluorine:

$$N^{14}\,(d,H^3)\,N^{13} \qquad Q=-4.5\pm0.2 \text{ Mv}$$
$$F^{19}\,(d,H^3)\,F^{18} \qquad Q=-4.1\pm1.1 \text{ Mv}.$$

No such reactions have been found, however, in aluminum and phosphorus, using 8.2-Mv deuterons. Excitation functions have been measured and the thresholds were found to be 6.8±0.1 Mv for nitrogen; 6.6±0.2 Mv for fluorine. The percentage of the barrier height at which H^3 particles may escape is estimated to be: 58 percent for nitrogen; 66 percent for fluorine; and >76 percent for aluminum.

21. A Note on a Problem of Rayleigh. MING CHEN WANG AND G. E. UHLENBECK, *University of Michigan.*—Rayleigh (*Scientific Papers*, Vol. 3, p. 473) has considered the problem of the approach to the equilibrium distribution of a particle of mass M moving in a dilute one-dimensional gas of particles of mass m. He gave the explicit solution for the case $m/M \ll 1$; it is an illustration of the Brownian motion of a heavy particle. We have solved the problem for the case $m/M=1$; it gives an illustration of the slowing down of a neutron moving in paraffin. Pictures of the approach to the equilibrium distribution will be shown for both cases.

22. Resonance Interaction in the 2200 cm^{-1} Region in the Raman Spectra of Acetylenes. FORREST F. CLEVELAND AND M. J. MURRAY, *Illinois Institute of Technology.*—Continuing investigations of the multiplicity of lines obtained near 2200 cm^{-1} in the Raman spectra of disubstituted acetylenes, as contrasted with the single line usually observed for monosubstituted acetylenes, data (including depolarization factors) have been obtained for butyne-1, hexyne-3, octyne-4 and 1-chloro-heptyne-1. The resonance doublet 2234(6)*P*, 2312(6)*P* in butyne-2 appears at 2231(9)0.4, 2301(6)0.4 in hexyne-3, at 2234(10)0.5, 2292 (6)0.5 in octyne-4 and is replaced by a single strong line at 2242(10)0.4 in 1-chloro-heptyne-1. The disappearance of the doublet in 1-chloro-heptyne-1 suggests that its presence for dialkylacetylenes may be due to a CH_2 or CH_3 group on *each* side of the triple bond. A puzzling feature is the appearance of the strong line at 2247(8)0.4 in the spectrum of hexyne-3. This line appears with small intensity in the spectra of all the other dialkylacetylenes measured in this laboratory, with the exception of octyne-4 for which it is unexpectedly absent. It has also not been reported in the spectrum of butyne-2 which has been studied by several investigators. The spectrum of butyne-1 is interesting in that it is one of the two monosubstituted acetylenes that have been found to have *two* strong lines (2118(10), 2153(3)), rather than the usual *one*, which for monoalkylacetylenes is near 2118 cm^{-1}.

23. Raman Spectra Evidence for Hindrance of Resonance by Ortho Substitution. ROBERT H. SAUNDERS, M. J. MURRAY, AND FORREST F. CLEVELAND, *Illinois Institute of Technology.*—If two ortho methyl groups are introduced into coplanar molecules such as nitrobenzene, acetophenone, benzoyl chloride, or methyl benzoate, the Raman line characteristic of the carbonyl or nitro group is shifted to higher frequencies. This effect is apparently due to a rotation of the group about the bond connecting it to the ring, thus resulting in a minimization of the contributions of those resonating forms which, according to modern concepts, may exist only if the molecule is coplanar. The frequencies in the ortho substituted compounds approach the values for the corresponding benzyl derivatives in which the interaction between the carbonyl or nitro groups and the ring is known to be quite small. An exception to the above is benzaldehyde. In this case, substitution of two methyl groups in the ortho positions does not increase the carbonyl frequency; instead, a lowering is observed. This can be understood by supposing that the aldehyde group is small enough to lie in the plane of the ring, thus giving rise to resonance interaction despite the ortho methyl groups. The above conclusions are consistent with those drawn from dipole moment data for the same compounds.

24. Raman Spectra of *dl*- and *meso*-2,3-Dibromobutane. H. J. TAUFEN, M. J. MURRAY, AND FORREST F. CLEVELAND, *Illinois Institute of Technology.*—Raman spectra, including depolarization factors, have been obtained for *dl*- and *meso*-2,3-dibromobutane, molecules differing only in the relative spatial arrangements of the various groups.

The *dl* modification yields a greater number of Raman lines, two lines being observed for this form to one for the *meso* in regions near 470, 840, 960 and 1450 cm^{-1}. The line at 1071 cm^{-1} in the *meso* appears to have no analog in the *dl* spectrum and near 1380 the *meso* spectrum has two lines and the *dl* only one. These differences are attributed to the variant symmetry of the two diastereoisomers. A multiplicity of lines in the region attributed to vibrations involving the C-Br group indicates the presence of rotational isomers. Assuming that only "staggered" isomers exist, two rotational forms are possible for the *meso* compound, while three possibilities exist for the *dl* racemate. The spectra reveal two lines in the C-Br region for the *meso* and three such lines for the *dl* isomer. Assignment of these lines to the various rotational isomers is made on the basis of previous spectroscopic work in the field.

25. Intensity Anomalies by Collisions in Perturbed Rotational Bands. H. BEUTLER AND M. FRED, *University of Chicago.*—G. Herzberg reported in 1928 that the cyanogen bands exhibit a strong enhancement of the lines originating from $b^2\Sigma$, $v=0$, $K=4$, 7 and 15, if excited by active nitrogen. H. T. Byck confirmed this result and added that the effect decreases with rising pressure. New photographs of the bands in higher resolution reveal strong extra lines from perturbing levels, in addition to the above enhanced lines. These new lines are also apparent on pictures taken by J. U. White in absorption. Analysis shows the perturbing levels to be $^2\Pi_{\frac{1}{2}}$, $v=9$, $J=15\frac{1}{2}$ and $^2\Pi_{3/2}$, $v=9$, $J=3\frac{1}{2}$ and $7\frac{1}{2}$. The enhancement in emission can be explained by collisions of the second kind among molecules in the mutually perturbing levels for which conditions of close resonance hold. In $^2\Pi-{}^2\Sigma$ bands (red CN system) in emission, a corresponding weakening is expected. Calculations on the collision processes indicate that the enhancement of the $^2\Sigma-{}^2\Sigma$ lines is restricted to medium pressures and disappears for very low and high pressures. The enhancement is related to the ratio of the radiation lifetimes of the unperturbed $b^2\Sigma$ and $^2\Pi$ levels.—A corresponding weakening of perturbed rotational levels is known in other bands, and sometimes explained by accidental predissociation.

26. The Perturbations in the $b^2\Sigma$, $v=0$ Band of Cyanogen. A. T. WAGER, *University of Chicago.*—The (0,0) band of the blue cyanogen system has been photographed with a resolving power of 300,000. The light source was the flame of $CHCl_3$ in active nitrogen, which gives low rotational levels strongly and enhances the perturbed and perturbing levels, that have been explained as belonging to the $^2\Pi$, $v=9$ system.

The measurement of the plates revealed the positions of the perturbing levels relative to the undisplaced ones, as follows: $\Delta\nu=-0.340$ cm^{-1}, $+0.926$ cm^{-1}, and $+1.276$ cm^{-1} for $K=4$, 7, 15 respectively. The *R*- and *P*-lines up to $K=7$ are sharp and single; from $K=7$ through $K=14$ they are wider and appear to be unresolved doublets, thus confirming that the perturbing level $K=7$ is a Π state. The lines from $K=15$ to 19 are clearly resolved doublets with $\Delta\nu=0.22$ cm^{-1}, proving that the perturbation with $K=15$ is likewise a Π level. The lower components of the doublet levels lie on the continuous curve defined by the levels with $J<14$, the higher components on a parallel curve. From the fact that $^2\Pi_{\frac{1}{2}}$ with $J=15\frac{1}{2}$ is the perturbing sublevel, it follows that the perturbed level in $b^2\Sigma$ is $K=15$, $J=K+\frac{1}{2}=15\frac{1}{2}$. Hence, all the shorter wave-length components of the spin doublets for $K>15$ in the 0–0 band of cyanogen have $J'=K'+\frac{1}{2}$, the other ones $J'=K'-\frac{1}{2}$.

27. Rotational Structure of Some Bands of Chlorine Dioxide. JESSE B. COON, *University of Chicago.*—The rotational structure of four bands in the region λ4200–λ4700 has been partially analyzed. The bands correspond to the vibrational transitions[1] $(0, V_2', 0)\leftarrow(0, 0, 0)$ with the breathing vibration $V_2'=1$, 2, 3, 4. Each band has a sharp head shaded toward the red. The tails of these bands are partially resolved showing five to nine sub-bands each containing one strong branch, of which about eight members can be picked out. Term values of the form $F=BL(L+1)+CK^2\pm\frac{1}{2}\gamma_K(K^2/L)$ explain the structure reasonably well. Preliminary analysis indicates that the above lines correspond to a *qQ* branch of a prolate symmetrical top with parallel type structure showing spin doubling. The values of K for observed sub-bands range from nine to eighteen approximately. The second differences in the K structure are found to be $2(C'-C'')=1.21$ $cm^{-1}\pm0.02$. The second differences in the L structure increase approximately linearly with the vibrational quantum number varying from $2(B'-B'')=0.068$ $cm^{-1}\pm0.002$ for $V_2'=1$ to 0.077 $cm^{-1}\pm0.002$ for $V_2'=4$. $\gamma_K'-\gamma_K''$ is 0.110 cm^{-1} ±0.005. This rotational analysis is consistent with the earlier proposed vibrational analysis.[1]

[1] J. B. Coon, Phys. Rev. **58**, 926 (1940).

28. Absorption Spectrum of Sym-Trichlorobenzene Vapor. H. SPONER AND MAURICE B. HALL, *Duke University.*—The absorption spectrum of sym-trichlorobenzene in the region 2865–2620A was photographed with the Hilger spectrographs E_1 and E_2. The absorption consists of several groups of mostly diffuse bands appearing on a continuous background. The bands are degraded to the red. As in benzene the system represents a forbidden transition. It is interpreted as a transition $A_1'\rightarrow A_2'$ made possible when vibrations of type ϵ' distort the molecule. The bands at 35869 and 35073 are tentatively assigned to the $0\rightarrow1$ and $1\rightarrow0$ transitions of an ϵ' vibration, more specifically to the Raman frequency of 425 cm^{-1}. This gives a frequency value of 371 cm^{-1} for this vibration in the excited state. The interpretation is supported by the appearance of bands displaced to the red from the main bands by $425-371=54$ cm^{-1}. The forbidden 0, 0 band is calculated at 35498 cm^{-1}. Frequencies of 963 and 1122 cm^{-1} are considered as belonging to totally symmetrical carbon vibrations in the upper state. A second stronger absorption region occurs below 2250A. It may be discussed in comparison to the second benzene absorption around 2000A.

29. Nature of the Methyl Iodide Absorption System near λ2000. R. S. MULLIKEN, *University of Chicago,* AND EDWARD TELLER,* *Columbia University.*—Extensive analogies be-

tween ultraviolet transitions of several groups of molecules, especially the hydrogen and alkyl halides, indicate that B and C systems involve analogous electronic transitions in all (W. C. Price). In the hydrogen halides the band structures indicate excited states $(np\pi)^3ms\ ^{1,3}\Pi$, $m=n+1$ with coupling which varies from *jj* like for HI to nearly *LS* like for HCl. The methyl iodide B and C systems (the former near λ2000) should have upper states similar to the $^{1,3}\Pi$ of HI. These bands must be of perpendicular type even though the main B bands look like parallel bands. We can explain this appearance by an electronic angular momentum of 1 unit in the upper state persisting in spite of the C_{3v} symmetry. We further explain certain weak bands of typical but abnormally widely spaced perpendicular structure as due to "forbidden" jumps of ± 1 in the quantum number of a degenerate vibration. These are made weakly allowed by an incipient splitting of the upper electronic level due to removal of the C_{3v} symmetry under the influence of the vibration. An analysis of the observed band structures with the help of infra-red data permits evaluation of the electronic and vibrational angular momenta in the upper state, and also shows that the small moment of inertia increases by 6 percent in the upper state.

* On leave from George Washington University.

30. Spectrum of Bi I. S. Mrozowski and F. Bueso-Sanllehí, *University of Chicago.*—The line spectrum of neutral bismuth was photographed in several orders of the 30-foot Chicago grating. A hollow cathode d.c. discharge and a quartz tube with outer electrodes excited by a 4-meter oscillator were used as sources of the spectrum. The hyperfine structure in most of the lines is resolved very completely. Exact measurements of the wave-length and of separation of components were made for all the lines observed. Several new terms were identified. The very high resolving power of the grating permitted the correction of all hyperfine structure term separations previously reported by Zeeman, Back and Goudsmit (13 terms). For some terms results differing considerably from theirs were obtained. The high intensity of the spectrum in case of the short wave excitation made possible the determination of hyperfine structure separations for more than a dozen other terms.

31. The Extension of Space Group Theory to Submicroscopically Twinned Crystals and its Application to Certain Spinels. F. C. Blake, *Ohio State University.*—Space group theory has been extended by the author in the case of certain spinels to submicroscopically twinned structures and a perfect solution has been found in the case of zinc metastannate. Interesting variations of the method employed throw much light upon the correct definition of a "single crystal phase." This is offered as a substitute for the "variate atom equipoint" method of Barth and Posnjak which cannot be right in the case of zinc metastannate for it gives wrong intensity relations. It is confidently believed that submicroscopic twinning is a natural process that occurs in the manufacture of muffles made from refractories and that the two separate cubic structures are revealed when the muffle gives way due to overheating. Undoubtedly this process is an important one occurring in the proper heat treatment of many metal alloys and it must be related to grain size in certain cases at least. It is curious that to date the most important cases of submicroscopic twinning seem to be those of Cochrane [Proc. Phys. Soc. London **48**, 723 (1936)] in the case of pure nickel deposited upon a single crystal of copper and of Kirchner u. Cramer [Ann. d. Physik **33**, 138 (1938)] for gold, nickel and copper deposited upon copper or rocksalt crystals, both cases revealed by electron diffraction.

32. Spectrographic Determination of Traces of Potassium in Sodium. Stanley S. Ballard* and Carroll B. Mills, *University of Hawaii.*—The analysis of sodium acetate soil extracts for small amounts of potassium presents a difficult chemical problem. We have developed a successful spectrographic method that uses spark excitation and a one-meter replica grating spectrograph. A highly condensed spark is employed, with a large inductor and an auxiliary point-to-plane spark gap in series with the source gap. The source gap has a pure copper rod as the upper electrode and as a lower electrode, a shallow copper pan in which the solution to be analyzed has been evaporated. Uniform sparking of the salt layer is achieved by manual manipulation of the pan. Photometric measurements are made of the potassium doublet at λ4046 and the λ4102 line of indium, the internal standard element. Analyses are made by adding known amounts of potassium to the liquid samples in repeat runs. With the simple and inexpensive equipment used, the method gives results whose average error is approximately 10 percent. For amounts of potassium less than 5 micrograms, the error is larger. Samples can be analyzed in duplicate at the rate of eight to ten per man-day.

* Now at Bureau of Ordnance, Navy Department, Washington, D. C.

Author Index to Abstracts of Papers Presented at the Chicago Meeting

Ballard, Stanley S. and Carroll B. Mills—No. 32
Beutler, H. and M. Fred—No. 25
Blake, F. C.—No. 31
Borst, L. W.—No. 20
Bostick, W. H.—No. 13
Boyd, G. E.—see Harkins, W. D.
Brillouin, Leon—No. 5
Bueso-Sanllehí, F.—see Mrozowski, S.

Carne, Gerald G.—see Copeland, Paul L.
Cleveland, Forrest F. and J. J. Murray—No. 22
——— see Saunders, Robert H.
——— see Taufen, H. J.
Coon, Jesse B.—No. 27
Copeland, L. E.—see Harkins, W. D.
Copeland, Paul L. and Gerald G. Carne—No. 3

Eisenstein, A. and N. S. Gingrich—No. 10

Fred, M.—see Beutler, H.

Gingrich, N. S.—see Eisenstein, A.

Hall, David B.—No. 15
——— see Schein, M.
Hall, Maurice B.—see Sponer, H.
Hamilton-Hall, Jane—see Schein, M.
Harkins, William D., L. E. Copeland and G. E. Boyd—No. 11
Householder, A. S.—see Weinberg, A. M.

Iona, Mario, Jr.—No. 9

Kurbatov, J. D., D. C. MacDonald, M. L. Pool and L. L. Quill—No. 19
——— see Nelson, Martin E.

Ladenburg, Rudolf and John A. Wheeler—No. 14
Landahl, H. D.—No. 2

MacDonald, D. C.—see Kurbatov, J. D.
Mills, Carroll B.—see Ballard, S. S.
Mrozowski, S. and F. Bueso-Sanllehí—No. 30
Mulliken, R. S. and Edward Teller—No. 29
Murray, M. J.—see Cleveland, F. F.
——— see Saunders, Robert H.
——— see Taufen, H. J.

Nelson, Martin E., M. L. Pool and J. D. Kurbatov—No. 18

Parratt, L. G.—see Trischka, J. W.
——— see Platt, J. B.
Platt, J. B. and L. G. Parratt—No. 7
Pool, M. L.—see Nelson, M. E.
——— see Kurbatov, J. D.

Quill, L. L.—see Kurbatov, J. D.

Regener, Victor H.—No. 16

Saunders, Robert H., M. J. Murray and Forrest F. Cleveland—No. 23
Schein, Marcel, David B. Hall and Jane Hamilton-Hall—No. 17
Shapiro, Maurice M.—No. 12
Sponer, H. and Maurice B. Hall—No. 28

Taufen, H. J., M. J. Murray and Forrest F. Cleveland—No. 24
Teller, Edward—see Mulliken, R. S.
Trischka, J. W. and L. G. Parratt—No. 6

Uhlenbeck, G. E.—see Wang, Ming Chen

Wager, A. T.—No. 26
Wahlin, H. B.—No. 4
Wang, Ming Chen and G. E. Uhlenbeck—No. 21
Weinberg, A. M. and A. S. Householder—No. 1
Wheeler, John A.—see Ladenburg, R.

Zachariasen, W. H.—No. 8